

Eastman Dental Institute, UCL

Development of a Tissue Engineered Three Dimensional (3D) Gingival Model to Replicate the Native Human Gingival Tissue

Zainab Muhi Al-Fatlawi BDS, MSc

Thesis submitted to University College London in fulfilment of the requirements for the degree of Doctor of Philosophy

UCL Eastman Dental Institute

2025

Declaration

I, Zainab Muhi Al-Fatlawi confirm that the work presented in this thesis is my own. Where information has been derived from other sources, I confirm that this has been indicated in the thesis.

Signature: Date: 16th August 2025

Dedication

In dedication to memory of my dad, mom, and my sister
And to my beloved children Fatima, Abbas and to my sister Raghad...

And to my colleagues and all people who have supported me throughout my life

Thank you all.....

Acknowledgments

First and most importantly, I would like to express my sincere gratitude to my supervisors, Professor Francesco D'Aiuto, Dr David Chau, and Dr Mei Huang who supported me throughout my PhD journey with an incredible amount of guidance and motivation. Your achievements and supervision pushed me to work harder than I thought would ever be possible. And I am truly thankful for the belief you put in me and your ongoing support. None of this would be possible without you.

I would like to express my deepest gratitude to the Ministry of Higher Education and Scientific Research and to the University of Babylon/Iraq for their sponsorship, encouragement, and invaluable support throughout my studies.

My grateful to Dr Maja Sabalic-Schoener for her generous help. Sincere appreciation goes to division of Biomaterials and Tissue Engineering at the UCL Eastman Dental Institute and head of division Prof Jonathan Knowles for offering great facilities to make this research achievable. I would like to extend my gratitude to lecturer Linh T.B. Nguyen for her help, and for Dr George Georgiou, Dr Graham Palmer, Dr Nicola Mordan for their endless technical advice and being true friends during my time at the Eastman.

No research is done in isolation; therefore, I would like to thank Faisal Alotaibi for generously providing the funding for one project. I would like to thank my friends and colleagues from the Eastman: Dr. Mohammad Aljaber Dr Nazanin Owji and Dr Zalike Keskin-Erdogan, Dr. Lady Barrios Silva, and Dr. Nik Sharifulden, and Mohammad Salih. Thank to Rawan Almujaydil, Shailly Luthra, Hesham Matabdin, Syed Basit Hussain, Naiwen Tan, Yumeng Yan, Sandra Olivia Kuswandani, Rizky Aditya Irwandi, Karim Djebali, Nor Shafina Mohamed Nazari, and special thanks to Sharon Oyhanart and Robyn Macartney, who made my journey easier and were always there for me during my breakthroughs and my breakdowns.

I would like to acknowledge and show my gratitude to my closest friends who have seen me grow as a scientist and have always been there when I needed a laugh and an escape. Mrs.Naeemah Alwahib, Mrs.Hiba Kadhum Alwash, Mr.Zaid Kadhum Alwash, and Mr.Aiad Al-Shiybani, your friendships are truly invaluable. Thank you to Mrs. Fawzia AL-Khayyat, and her children Dr. Dhuha Jassim, Mr Haider Jassim, and her son in low Dr. Ghassan Jassim, and to Dr. Hassanin Jassim for supporting me and providing wisdom and guidance no matter what.

I would like to express my heartfelt gratitude to my friends and colleagues at Mile End Dental Practice/London, for their support and encouragement. My special thanks go to Dr. Kristian Chauhan, for his kindness and generosity, and to Deluxme Alvappillat and Shazia Begum for their invaluable help and friendship.

Sincere gratitude to my colleagues from Babylon University/college of dentistry, Dr.Ahmed Ghanim, Dr.Ali Zaki, Dr.Zeyad Nazar, Dr.Ali Mihsein Al-Yassiri, Dr.Haider Ali Hasan, Dr.Suha Hindy, Mr. Najeh Hassan, lecturer Ali Falah Hasan, and his wife Noor, many thanks for your support and help. Thanks to Mr. Hussain Al-Faham for his help.

Finally, I am exceptionally grateful to my family who have always encouraged and believed in me. To my sister Raghad, my uncles and, thank you for all that you have sacrificed for me to achieve my best in education and out. Thank you for always being there.

Above all, I dedicate this work to my beloved children, whose love, patience, and inspiration have been my greatest source of strength. I also wish to honour the memory of my dear father, mother, and sister, who were the most supportive people in my life. Though they are no longer with me, their love, guidance, and faith in me continue to inspire every step I take.

Abstract

Periodontal diseases, including gingivitis and periodontitis, and peri-implant mucositis are plaque-induced inflammations that can progress to irreversible tissue destruction. They result from poor oral hygiene and risk factors modifiable (e.g., tobacco, diabetes) and non-modifiable (e.g., age, genetics) influencing immune and inflammatory responses.

Given the biological complexity and multifactorial nature of these conditions, in vitro models are essential for studying disease mechanisms and testing potential therapies.

To evaluate the current state of such models, a systematic review was conducted, analysing 37 different 3D gingival and peri-implant models reported across 22 studies. However, no single model emerged as the best for studying 3D gingival or peri-implant tissues. Substrate selection is crucial for gingival model construction, requiring biocompatibility, porosity, and mechanical stability. Ten different substrates were reviewed, with most being animal derived. Rat tail collagen type I was the most frequent substrate used, supporting epithelial stratification but prone to shrinkage, high cost, and structural differences from human ECM.

To identify potential target genes in periodontitis, NanoString GeoMx DSP was applied to tissue samples, comparing healthy and diseased gingival tissue. Results revealed similar functionally relevant gene expression in both tissues, providing novel insights for tissue characterization and laying the groundwork for developing a 3D gingival model as an in vitro tool using cell culture techniques.

Experimental investigations evaluated candidate hydrogel biomaterials, focusing on gelatin methacryloyl (GelMA) and sodium alginate (SA) composites. Characterization demonstrated tunable mechanics, biocompatibility, and ECM-mimicking features. Crosslinking methods (UV and CaCl₂) optimized scaffold stability and bioactivity. GelMA-SA composites supported fibroblasts and epithelial

cells, with histological analysis confirming epithelial stratification and demonstrating superior structural integrity and cellular organization in specific formulations. Challenges remained with fibroblast migration, epithelial adhesion, and differentiation, particularly under air-liquid interface conditions, but the optimized composites provided a suitable microenvironment for gingival tissue engineering.

Impact Statement

This research contributes significantly to the field of periodontal tissue engineering by advancing the development of a functional 3D gingival model. The study begins with a systematic review of existing 3D gingival and peri-implant models and evaluating different substrates biomaterials. This research lays the foundation for developing an optimized scaffold that mimics the human gingival extracellular matrix. The findings have profound implications for periodontal research, as a well-characterized 3D gingival model can serve as an invaluable in vitro tool for studying periodontal disease mechanisms, testing novel therapeutics, and exploring regenerative approaches.

The study provides novel insights into gingival tissue characterization through NanoString GeoMx DSP, highlighting spatially resolved gene expression patterns in healthy and diseased tissue. Additionally, it identifies critical limitations in existing 3D gingival models, emphasizing the need for improved biomaterial selection.

Furthermore, the development of a more physiologically relevant gingival model has the potential to reduce reliance on animal models in periodontal research, aligning with ethical considerations in biomedical sciences. Ultimately, this work contributes to advancing personalized and regenerative periodontal therapies, offering promising translational applications in both clinical and research settings.

The main aim of this study is to advance tissue engineering approaches to develop a more effective alternative to currently available 3D gingival models. Specifically, this research focuses on constructing a 3D gingival model with a complex microstructure that closely mimics native human gingival tissue. The development process involves designing a novel composite substrate with tunable mechanical properties and high biocompatibility, suitable for supporting human gingival cell growth and differentiation.

By addressing existing limitations in scaffold materials and optimizing crosslinking strategies, this study establishes GelMA-SA composite hydrogels as a promising candidate for 3D gingival model construction. The findings not only contribute to improving in vitro models for periodontal research but also have broader implications for regenerative therapies and personalized treatment approaches. A well characterized 3D gingival model offers researchers a valuable tool for studying periodontal disease mechanisms, testing therapeutic interventions, and exploring novel regenerative strategies. Moreover, it presents an ethical alternative to animal models, aligning with modern biomedical research principles. Ultimately, this work paves the way for more physiologically relevant models that could enhance both clinical and experimental applications in periodontology.

Publications

- 1-Al-Fatlawi, Zainab; Huang, Mei; Chau, David; D'Aiuto, Francesco; (2023) <u>Three dimensional (3D) gingival models in periodontal research: a systematic review.</u> **Journal of Materials Science: Materials in Medicine**, 34, Article 58. 10.1007/s10856-023-06761-z.
- 2- Alotaibi FF, Al-Fatlawi ZM, Oyhanart SR, Knowles JC, D'Aiuto F, Chau DYS. The eggshell membrane as a barrier membrane for guided bone regeneration. Regen Med. 2025 Aug 9:1-14. doi: 10.1080/17460751.2025.2542056. Epub ahead of print. PMID: 40782041.
- 3- Evaluation of the physical, mechanical and biological properties of novel biomedical hydrogels: implication for gingival-based and oral healthcare applications. Zainab M. Al-Fatlawi, Mei Huang, Mohammad B. Aljaber, Nik S.A.N. Sharifulden, Lady V. Barrios Silva, Jonathan C. Knowles, Linh T.B. Nguyen, Francesco D'Aiuto, D.Y.S Chau.(submitted)

Conference Posters and Presentations

1-Z. Al-Fatlawi, M. Huang, D. Chau, F. D'Aiuto. A systematic review of In vitro three dimensional (3D) gingival model in periodontal research

EuroPerio10 (From June 15-18, 2022 in Copenhagen, Denemark).

2-Z. Al-Fatlawi, M. Huang, F. D'Aiuto, D.Y.S Chau. Evaluation of the physical, mechanical and biological properties of a novel biomedical hydrogel: implication for gingival-based and oral healthcare applications

TERMIS EU - Chapter 2023 Meeting

SYMBOLS	
μm	micrometre
μl	microliter
μΜ	micromolar
mM	micromolar
M	Molar
cm	centimetre
l l	litre
m	meter
mm	millimetre
nm	nanometer
h	hour
min	Minute
S	Second
N	Newton
ppm	Parts per million
D	Day
тм	Trademark
®	Registered trademark
%	Percentage
Mw	Molecular weight
mg	Milligram
ng	Nanogram
g	Gram
μg	Microgram
kg	Kilogram

ABBREVIATIONS	
3D	Three dimensional
ANOVA	Analysis of variance
CO ₂	Carbon dioxide
DMA	Differential mechanical analyses
DMEM	Dulbecco's Minimum Essential Medium
DSC	Differential scanning calorimetry
E	Young's modulus
E' or G'	Storage modulus
E" or G"	Loss modulus
ECM	Extracellular matrix
FBS	Fetal bovine serum
FDA	Food and Drug Administration
FT-IR	Fourier-transform infrared spectroscopy
GelMA	Gelatin methacrylate
PI	Photo initiator
Li	Lithium
SA	Sodium alginate
Professional Mechanical	PMPR
Plaque Removal	
Supportive Periodontal	SPC
Care	

TABLE OF CONTENTS

Chapter 1. Literature review & introduction	34
1.1. Background	34
1.2. Periodontium	34
1.2.1. Gingiva	34
1.2.1.1. Gingival epithelial layer	35
1.2.1.2. Gingival basement membrane	38
1.2.1.3. Gingival connective tissue	38
1.2.1.4. Extracellular matrix (ECM)	39
1.2.2. Periodontal ligament (PDL)	40
1.2.3. Root cementum	40
1.2.4. Alveolar bone	41
1.3. Periodontal diseases	42
1.3.1. Etiologic of periodontal diseases	46
1.3.2. Diagnosis of periodontal diseases	46
1.3.3. Molecular profile of human gingival tissue	47
1.3.3.1. Subunits of RNA molecule	49
1.3.3.2. The central dogma of molecular biology	49
1.3.3.3. Transcription	50
1.3.3.4. Transcript	51
1.3.3.5. Complementary DNA	51
1.3.3.6. Gene expression.	51
1.3.3.7. Transcriptome	52
1.3.3.8. Transcriptomics	52
1.3.3.8.1. DNA microarray technology	53
1.3.3.8.2. RNA sequencing (RNA Seq) technology	54
1.3.4. Treatment of periodontal diseases	59
1.3.4.1. Non-Surgical Therapy (Professional Mechanical Plaque	
Removal - PMPR)	59
1.3.4.2. Surgical periodontal therapy	59
1.3.4.3. Supportive Periodontal Care (SPC)	60
1.3.4.4. Peri-Implant Disease Management	60
1.4. Tissue engineering in periodontal regeneration	61
1.4.1. Two-dimensional (2D) cell cultures	62

1.4.2. Three-dimensional (3D) cell cultures	63
1.4.2.1. Fundamental principles for designing 3D gingival models	64
1.4.2.1.1. Cells	65
1.4.2.1.2. Biomaterials and Scaffolds	66
1.4.2.1.2.1. Hydrogel biomaterials	67
1.4.2.1.2.2. Hydrogel sterilization methods	69
1.5. Mechanical characteristics of human gingival tissue	69
1.6. Rationale for Proposed research	71
1.7. Hypothesis and objectives of the study	72
Chapter 2. Materials & methods	76
2.1. Materials	76
2.2. Methods	78
2.2.1. Synthesis Gelatin methacryloyl and purification (GelMA-UCL)	78
2.2.2. Preparation of hydrogel samples	79
2.2.2.1. GelMA-UCL	80
2.2.2.2. GelMA commercial (GelMA-com)	80
2.2.2.3. ¹ H-NMR (Nuclear Magnetic Resonance) hydrogel samples	81
2.2.2.4. Gelatin	81
2.2.2.5. Sodium alginate (SA)	81
2.2.2.6. GelMA-SA composite	81
2.2.2.7. Rat tail collagen	82
2.2.3. Hydrogel sterilization methods	82
2.2.3.1. Filter method	82
2.2.3.2. Ethanol method	83
2.2.4. Crosslinking procedures for hydrogel samples	83
2.2.4.1. Single crosslinking procedures	83
2.2.4.2. Double crosslinking procedures	84
2.2.5. Preparation of animal gingival and oral mucosal tissues	86
2.2.6. Materials characterization	86
2.2.6.1. ¹ H-NMR spectroscopy	86
2.2.6.2. Scanning electron microscopy (SEM)	87
2.2.6.3. Fourier transform infrared spectrophotometer (FT-IR) spectrum	87
2.2.6.4. Hydrophilic/hydrophobic surface characteristics	87
2.2.6.5. Thermal characteristics	88
2.2.6.6. Rheological characteristics	88

2.2.6.7. Mechanical characteristics	91
2.2.6.8. Degradation test	92
2.2.6.9. Human gingival cells expanding and seeding in samples	92
2.2.6.9.1. Cells expanding	92
2.2.6.9.2. Seeding hydrogel samples with HGF and HGE cells	93
2.2.7. Engineered 3D gingival tissue (3DGT)	93
2.2.8. Metabolic and cytotoxic activities of cells evaluation	95
2.13. Statistical Analysis	98
Chapter 3. Three dimensional (3D) gingival models in periodontal	
research : a systematic review	99
3.1. Introduction	99
3.2. Materials and methods	101
3.3. Results	109
3.3.1. Study selection	109
3.3.2. Quality of studies	109
3.3.3. 3D Gingival model characteristics	113
3.3.4. Macroscopical model appearance	120
3.3.5. Histological analysis	120
3.3.5.1. Epithelium layer	120
3.3.5.2. Connective tissue layer	
3.3.6. Differentiation of gingival model	121
3.3.6.1. Keratinocytes proliferation and differentiation markers	121
3.3.6.2. Basement membrane markers	123
3.3.6.3. ECM components markers	123
3.3.6.4. Vimentin a fibroblast differenciation marker	123
3.3.7. Application of gingival model for periodontal research	123
3.3.8. Types of substrate biomaterials used to construction of gingival model.	124
3.4. Discussion	126
Chapter 4. Targeted spatial expression analysis of periodontitis-associated	
genes in human gingival tissue using NanoString GeoMx profiling	131
4.1. Introduction	
4.2. Materials and Methods	
4.2.1. Tissue samples	

4.2.2. Tissue samples preparation for sequencing	134
4.2.3. Spatial Transcriptomic Profiling and Targeted Gene Analysis	134
4.3. Results	135
4.3.1. Gene expression in inflamed and non-inflamed connective tissue	135
4.3.2. Gene Ontology analysis	141
4.3.3. Gene ontology of the Kyoto Encyclopedia of Genes and Genomes	
(KEGG)pathway	145
4.4. Discussion	148
Chapter 5. The physical and biological properties of hydrogel substrates to	
mimic native human gingival extracellular matrix	156
5.1. Introduction	156
5.2. Materials and methods	159
5.3. Results	160
5.3.1. ¹ H-NMR (Nuclear Magnetic Resonance) spectroscopy	160
5.3.2. Scanning electron microscopy (SEM)	161
5.3.3. Fourier Transform Infrared (FTIR) spectroscopy	163
5.3.4. Contact angel measurements	165
5.3.5. DSC	166
5.3.6. Rheological measurements	167
5.4. Discussion	180
Chapter 6. Evaluation of the Physical, Mechanical, and Biological Proper Novel Biomedical Hydrogels	ties of
	178
6.1. Introduction	178
6.2. Materials and methods	180
6.2.1. Preparation of hydrogel samples	
6.2.1.1. Preparation of sterilized hydrogel samples	180
6.2.1.2. Crosslinking procedures for sterile hydrogel samples	180
6.2.2. Preparation of animal gingival and oral mucosal tissues	
6.2.3. Structural characterisations	
6.2.4. Human gingival cells expanding and seeding in samples	183
6.2.5. Metabolic and cytotoxic activities of cells evaluation	
6.3. Results	184
6.3.1. Macrostructure morphology of hydrogels surfaces	184

6.3.2. Microstructure morphology of samples surfaces	189
6.3.3. Fourier transform infrared spectrophotometer (FT-IR) spectra	197
6.3.4. Hydrophilic/hydrophobic surface properties	199
6.3.5. Thermal Properties	201
6.3.6. Rheological characteristics	203
6.3.7. Mechanical properties	210
6.3.8. Degradation test	211
6.3.9. Biological and cell viability measurements	212
6.4. Discussion	219
Chapter 7. Evaluation of sterilization methods and crosslinking strategies	
on the hydrogels mechanical and biological properties to mimic	
native human gingival extracellular matrix	228
7.1. Introduction	
7.2. Materials and methods	231
7.2.1. Preparation of GelMA hydrogel samples	231
7.2.2. Preparation of sterilized GelMA-SA composite hydrogel samples	231
7.2.2.1. Filter method	231
7.2.2.2. Ethanol method	232
7.2.2.3. Hydrogel crosslinking procedures	232
7.2.4. Structural characterisations	233
7.2.5. Human gingival cells expanding and seeding in samples	233
7.2.6. Engineered 3D gingival tissue (3DGT)	234
7.2.7. Metabolic and cytotoxic activities of cells evaluation	235
7.2.8. Histological investigation	235
7.3. Results	236
7.3.1. Material mechanical characterisation	232
7.3.1.1. Surfaces morphology of samples in photographic images	236
7.3.1.2. Surfaces morphology of samples on SEM images	237
7.3.1.3. FT-IR characteristics	240
7.3.1.4. Hydrophilic/hydrophobic surface properties	241
7.3.1.5. Thermal Properties	242
7.3.1.6. Rheological characteristics	244
7.3.1.7. Mechanical properties	248
7.3.1.8. Degradation test	
7.3.2. Material biological and cell viability characterisation	250

7.3.3. Engineered 3D gingival tissue (3DGT)	258
7.3.4. Histological images of 3DGT models	262
7.4. Discussion	264
Chapter 8. General discussion	275
References	288
Appendix A	314
Appendix B	322
Appendix C	324
Appendix D	326
Appendix E	327
Appendix F	331
Appendix G	339

Index of Tables

Table 2.1. Chemicals/reagents and their suppliers used76
Table 2.2. Hydrogel formulations prepared and tested in this study. Gelatin and GelMA commercial were investigated at both high (10%) and low (2.5%) concentrations. Sodium alginate (SA) was used as an additional hydrogel component at two concentrations (3.5% and 2.5%). GelMA was prepared inhouse at UCL (GelMA-UCL), with photoinitiator (PI, 0.3%) added for crosslinking. Hybrid formulations were developed by combining GelMA with sodium alginate at different concentrations
Table 3.1. Search strategy and terms that based on five electronic databases: MEDLINE (OVID), EMBASE, EBSCOhost, Web of Science Core Collection, and LILACS
Table 3.2. List of journals which have been included in our hand searching for eligible articles108
Table 3.3: Quality assessment and risk of bias (modified from the ARRIVE And CONSORTguidelines)111
Table 3.4: Quality assessment and risk of bias (SYRCLE tool), each item
was scored as "yes", "no", or "unclear"Individual risk of bias each item in the SYRCLE tool was scored as "yes", "no", or "unclear112
Table 3.5. Summary of cellular sources used in construction of gingival or perimplant models113
Table 3.6: Characteristics of selected studies114
Table 4.1. demonstrated up and down-regulated genes expressions for both healthy and diseased gingival tissue samples136
Table 4.2. List of enriched KEGG pathways of the differentially expressed proteins for both healthy and diseased gingival tissue samples146
Table.5.1. Outcome of hydrogels sample investigations327
Table.6.1. DSC thermograms of sheep and porcine gingival, oral alveolar mucosal, and hydrogel samples which were examined under a continuous flowrate of nitrogen gas with the following conditions: equilibrate (-10 °C), isothermal (1 min), and ramp (10 °C/min to 450 °C/min)1201
Table 6.2. Elastic modulus (E'), loss modulus (E"), stiffness, and the corresponding Young's modulus (E) as functions of oscillation frequency ranging from 0.1 to 50 Hz at 5 Hz intervals for each sample. Samples were preloaded with a force of 0.001 N and dynamically tested at low deformation (0.25% strain), taken at the temperature of 37 °C. Samples are animal sheep and porcine, and different hydrogel samples

Index of Figures

Figure.1.1 The anatomy of Periodontium. <i>Adapted from Newman and Carranza's</i> Clinical Periodontology34
Figure1.2 Types of human gingival epithelium (oral gingival, sulcular and junctional) epithelium. Cytokeratin distribution patterns in human gingival epithelium (oral gingival, sulcular and junctional) epithelium. Created with BioRender.com
Figure 1.3 Structure of gingival keratinizing and non-keratinizing stratified epithelial tissues. Created with BioRender.com38
Figure 1.4. Schematic illustration of healthy versus diseased tissues around, A. tooth and, B. implant. Created with BioRender.com
Figure 1.5. Structures of Deoxyribonuclic acid (DNA) vs Ribonucleic acid (RNA). RNA structure compse of Uracil as alternative to Thymine base paires. RNA is shorter helix. https://www.genome.gov/about-genomics/educational-resources/fact-sheets/ribonucleic-acid-fact-sheet
Figure 1.6. Diagram of concept of central dogma for transcription of DNA into RNA and translate to protein. Created in bioRender.com50
Figure 1.7. Tissue engineering triad. Scaffolds, cells, and groth factors are used in isolation or in combination to recapitulate the desired tissue. Created with BioRender.com
Figure 2.1. Schematic drawing illustrating the double crosslinking procedures using CaCl ₂ and UV, with two different techniques: Technique 1 (CaCl ₂ /UV) and Technique 2 (UV/CaCl ₂). Technique 1 was performed by applying CaCl ₂ followed by UV exposure, whereas Technique 2 was performed by applying UV first, followed by CaCl ₂ . Created in BioRender.com85
Figure 2.2. Photos for rheological investigation of animal palatal gingival tissue samples. (A, and B), palatal gingival tissue samples of upper jaws of sheep and porcine, respectively. (C), sample preparation by sharp disectioning. (D, and E), placement of sheep and porcine samples samples, repectively, on lower plate to operate rheometer instrument, (I and J), sheep and porcine samples placement on lower plate, respectively, to operate rheometer instrument (F) lowering the upper plate after placing sample on lower plate.
Figure 2.3. Schematic drawing illustrating the construction of 3D gingival model including crosslinking procedures using CaCl ₂ and UV. Created in BioRender.com94
Figure 3.1. PRISMA flow diagram of the study inclusion process110
Figure 3.2. Flow chart of 3D gingival and peri-implant models125
Figure 3.3. Schematic representation of the experimental protocol togenerate 3D

Figure 4.1. Schematic drawing depicting processes for sample preparation. Created in BioRender.com134
Figure 4.2: Clustering dendrograms identified by Heat map depicts the tissue genes expression. Green represents lower expression, and red represents higher expression. Each branch in the figure represents one gene
Figure 4.3. The identified genes were analyzed according to Gene Ontology (GO) enrichment using WebGestalt (WEB-based GEne SeT AnaLysis Toolkit). (A and B) GO classification from the biological process, of ontology enrichment, for both healthy and diseased samples respectively. The number of proteins enriched in each GO term is shown on the top of each bar. (C and D). Directed Acyclic Graph (DAG) of the enriched GO categories under biological process for both healthy and diseased samples respectively. Each node shows the name of the GO category, the number of gene in the category and the p-value indicating the significance of enrichment. The red colour represents p-values <0.05
Figure 4.4. The identified genes were analyzed according to Gene Ontology (GO) enrichment using WebGestalt (WEB-based GEne SeT AnaLysis Toolkit). (A and C). Directed Acyclic Graph (DAG) of the enriched GO categories under cellular component for both healthy and diseased samples respectively. Each node shows the name of the GO category, the number of gene in the category and the dark colour p-value indicating the significance of enrichment. (B and D) GO classification from the cellular component, of ontology enrichment, for both healthy and diseased samples respectively
Figure 4.5. The identified genes were analyzed according to Gene Ontology (GO) enrichment using WebGestalt (WEB-based GEne SeT AnaLysis Toolkit). (A and C). Directed Acyclic Graph (DAG) of the enriched GO categories under molecular function for both healthy and diseased samples respectively. Each node shows the name of the GO category, the number of gene in the category and the p-value indicating the significance of enrichment. The orange colour represents p-values <0.05. (B and D) GO classification from the molecular function, of ontology enrichment, for both healthy and diseased samples respectively. The number of proteins enriched in each GO term is shown on the top of each bar
Figure 5.1.¹H-NMR spectra of GelMA-com. and prepared GelMA-UCL samples with three batches (GelMA-UCL1, GelMA-UCL2, and GelMA-UCL3). Specific protons of GelMA-com and GelMA-UCL were highlighted as follows: a—e was ascribed to acrylic protons of methacrylamide groups in lysine residues, acrylic protons of methacrylamide groups in hydroxylysine residues, methylene protons of non-modified lysine, methyl protons of methacryloyl groups, and acrylic protons of methacrylate groups, respectively

Figure 5.2. Scanning electron microscopy (SEM) images in 500X,and 5K X for nine hydrogels, GelH, GelL, SAH, SAL, GelMAcH, GelMAcL, and GelMAH vs GelMAL, respectively
Figure 5.3. (A) FT-IR spectra summarising the chemical bonding structure in samples over a range of 4000–500 cm ⁻¹ with a resolution of 4 cm ⁻¹ at 37 °C. (A) Hydrogel samples are: GelH, GelL, SAH, SAL, GelMAcH, GelMAcL, GelMAH, and GelMAL. (B-E) Comparative FTIR spectra showing four grouped plots, each including high and low concentration pairs: GelH vs GelL, SAH vs SAL, GelMAcH vs GelMAcL, and GelMAH vs GelMAL, respectively
Figure 5.4. Water contact angle of the nine hydrogels: GelH, GelL, SAH, SAL, GelMAcH, GelMAcL, GelMAH, and GelMAL. Data representing mean \pm SD (n=3). Sample is significantly different with * p < 0.05
Figure 5.5. DSC thermograms for samples which were examined under a continuous flowrate of nitrogen gas with the following conditions: equilibrate (-10 °C), isothermal (1 min), and ramp (10 °C/min to 450 °C/min). Hydrogel samples are: GelH, GelL, SAH, SAL, GelMAcH, GelMAcL, GelMAH, and GelMAL166
Figure 5.6. Rheological properties of eight hydrogel samples: GelH, GelL, SAH, SAL, GelMAcH, GelMAcL, GelMAH, and GelMAL. Viscosity as a function of shear rate at 37, 20 and 4 °C respectively
Figure 5.7. Rheological properties of eight hydrogels: GelH, GelL, SAH, SAL, GelMAcH, GelMAcL, GelMAH, and GelMAL. Shear stress as a function of shear rate at 37, 20 and 4 °C respectively
Figure 5.8. Rheological properties, with oscillatory amplitude sweeps showing storage (G') and loss moduli (G") at 37, 20 and 4 °C respectively with a constant frequency of oscillation of 1 Hz of eight hydrogels: GelH, GelL, SAH, SAL, GelMAcH, GelMAcL, GelMAH, and GelMAL
Figure 5.9. Rheological properties, with frequency sweep in a linear visco-elastic range (0.1–50 Hz) at the deformation of 0.25 % showing storage (G') and loss moduli (G") at 37, 20 and 4 °C respectively of eight hydrogels: GelH, GelL, SAH, SAL, GelMAcH, GelMAcL, GelMAH, and GelMAL
Figure 6.1. Images (A, B, and C) show the mucogingival junction (MGJ), labial ginigva(L.G), buccal gingiva (B.G), and lingual gingiva (Ling.G), anterior and posterior views of lower sheep jaws. Image (D), display the palatal views of sheep upper jaws

Figure 6.7. SEM images of sheep oral tissue samples, including labial, buccal, and lingual gingival tissue. 'Labial g.' refers to labial gingiva, 'Buccal g.' refers to buccal gingiva, and 'Lingual g.' refers to lingual gingiva. Images are shown at two magnifications: 500X with a scale bar of $20 \mu m$, and 5KX with a scale bar of $2 \mu m$,

different magnifications190
Figure 6.8. SEM images of sheep oral tissue samples, including palatal gingival tissue, buccal alveolar, and lingual alveolar mucosal tissue. 'Buccal alve.' refers to buccal alveolar tissue, and 'Lingual alve.' refers to lingual alveolar tissue. Images are shown at two magnifications: $500X$ with a scale bar of $20 \mu m$, and $5KX$ with a scale bar of $2 \mu m$, highlighting the structural differences between the three tissue types at different magnifications
Figure 6.9. SEM images of porcine oral tissue samples, including labial, buccal, and lingual gingival tissue. 'Labial g.' refers to labial gingiva, 'Buccal g.' refers to buccal gingiva, and 'Lingual g.' refers to lingual gingiva. Images are shown at two magnifications: 500X with a scale bar of 20 μ m, and 5KX with a scale bar of 2 μ m
Figure 6.10. SEM images of porcine oral tissue samples, including palatal gingival tissue, buccal alveolar, and lingual alveolar mucosal tissue. 'Buccal alve.' refers to buccal alveolar tissue, and 'Lingual alve.' refers to lingual alveolar tissue. Images are shown at two magnifications: 500X with a scale bar of 20 µm, and 5KX with a scale bar of 2 µm
Figure 6.11. SEM images of hydrogel samples after crosslinking. 'R collagen (2h)' and 'R collagen' refer to rat collagen crosslinked at 37 °C with 5% CO_2 for 2 hours and overnight, respectively. 'GelMA' refers to GelMA prepared by mixing 10% GelMA with 0.3% (w/v) photoinitiator (PI), crosslinked using UV light for 60 seconds. 'SAH' and 'SAL' refer to hydrogels with concentrations of 3.5% and 2.5%, respectively, crosslinked with 50 mM $CaCl_2$ at room temperature for 5–7 minutes. Images are shown at two magnifications: 500X with a scale bar of 20 μ m, and 5KX with a scale bar of 2 μ m
Figure 6.12. SEM images of hydrogel samples after crosslinking. 'GelMA-SAH/CaCl ₂ ', and 'GelMA-SAL/CaCl ₂ ', refer to hydrogel samples prepared by mixing GelMA (10% concentration with 0.3% w/v photoinitiator (PI)) and SA, with 3.5% and 2.5% concentration, respectively. These samples after crosslinking with 50 mM CaCl ₂ at room temperature for 5–7 minutes. 'GelMA-SAH/UV', and 'GelMA-

Figure 6.13. SEM images of hydrogel samples after crosslinking. 'GelMA-SAH/CaCl₂/UV' and 'GelMA-SAL/CaCl₂/UV' refer to hydrogels prepared by mixing 10% GelMA (with 0.3% w/v photoinitiator) and sodium alginate (SA) at concentrations of 3.5% and 2.5%, respectively. These samples were crosslinked first with 50 mM CaCl₂ at room temperature for 5–7 minutes, followed by UV exposure for 60 seconds. 'GelMA-SAH/UV/CaCl₂' and 'GelMA-SAL/UV/CaCl₂'

Figure 6.14. FT-IR spectra summarising the chemical bonding structure in samples over a range of 4000–500 cm⁻¹ with a resolution of 4 cm⁻¹ at 37 °C. (A), sheep labial, buccal, and lingual gingival tissue samples(Sh.Labial ging., Sh.Buccal ging., Sh.Lingual ging.), sheep buccal, and lingual oral alveolar mucosal tissue samples(Sh.Buccal alveo.m., and Sh.Lingual alveo.m.), and sheep palatal gingival tissue sample (Sh.Palatal ging.). (B) Porcine labial, buccal, and lingual gingival tissue samples(P.Labial ging., P.Buccal ging., and P.Lingual ging.), porcine buccal, and lingual oral alveolar mucosal tissue samples(P.Buccal alveo.m., and P.Lingual alveo.m.), and porcine palatal gingival tissue sample (P.Palatal ging.). (C), hydrogel samples are R collagen(rat collagen with overnight incubation), R collagen(2h incubation), GelMA, SAH, SAL, GelMA-SAH/CaCl₂, GelMA-SAH/UV, and GelMA-SAL/UV. (D), hydrogel samples are R collagen(rat collagen with overnight incubation), GelMA, SAH, SAL, GelMA-SAH/CaCl₂/UV, GelMA-SAL/CaCl₂/UV, GelMA-SAH/UV/CaCl₂, and GelMA-SAL/UV/CaCl₂.

Figure 6.15. WCA measurements for sampls (A), sheep labial, buccal, and lingual gingival tissue samples(Sh.Labial ging., Sh.Buccal ging., Sh.Lingual ging.), sheep buccal, and lingual oral alveolar mucosal tissue samples(Sh.Buccal alveo.m., and Sh.Lingual alveo.m.), and sheep palatal gingival tissue sample (Sh.Palatal ging.). Porcine labial, buccal, and lingual gingival tissue samples(P.Labial ging., P.Buccal ging., and P.Lingual ging.), porcine buccal, and lingual oral alveolar mucosal tissue samples(P.Buccal alveo.m., and P.Lingual alveo.m.), and porcine palatal gingival tissue sample (P.Palatal ging.). (B), hydrogel samples are R collagen, R collagen(2h), GelMA, SAH, SAL, GelMA-SAH/CaCl₂, GelMA-SAL/CaCl₂, GelMA-SAH/UV, and GelMA-SAL/UV. (C), hydrogel samples are R collagen, GelMA, SAH, SAL, GelMA-SAH/CaCl₂/UV, GelMA-SAH/UV/CaCl₂, and GelMA-SAL/UV/CaCl₂. Data representing mean ± SD(n=3). * p < 0.05......200

Figure 6.16. DSC thermograms for samples which were examined under a continuous flowrate of nitrogen gas with the following conditions: equilibrate (-10 °C), isothermal (1 min), and ramp (10 °C/min to 450 °C/min). (A), sheep labial, buccal, and lingual gingival tissue samples(Sh.Labial ging., Sh.Buccal ging., Sh.Lingual ging.), sheep buccal, and lingual oral alveolar mucosal tissue samples(Sh.Buccal alveo.m., and Sh.Lingual alveo.m.), and sheep palatal gingival tissue sample (Sh.Palatal ging.). Porcine labial, buccal, and lingual gingival tissue samples(P.Labial ging., P.Buccal ging., and Lingual ging.), porcine buccal, and lingual oral alveolar mucosal tissue samples(P.Buccal alveo.m., and P.Lingual alveo.m.), and porcine palatal gingival tissue sample (P.Palatal ging.). (B), hydrogel samples are R collagen, R collagen(2h), GelMA, SAH, SAL, GelMA-SAH/CaCl₂, GelMA-SAL/CaCl₂, GelMA-SAH/UV, and GelMA-SAL/UV. (C),

hydrogel	samples	are	R	collagen,	GelMA,	SAH,	SAL,	GelMA-SAH/C	;aCl₂/UV,
GelMA-S	AL/CaCl ₂	/UV,	Ge	IMA-SAH/	UV/CaCl	2, and	GelMA	A-SAL/UV/CaCI	2331

Figure 6.21. Frequency sweep in a linear viscoelastic range at the deformation of 0.25 % measurements for samples at 37, 20, and 4 °C. A, G', and B, G'', respectively of hydrogel samples, which are R collagen, GelMA, SAH, SAL, GelMA-SAH/CaCl₂, GelMA-SAL/UV, GelMA-SAL/UV.......208

Figure 6.23. Elastic modulus E'(A), loss modulus E"(B), and stiffness (C), as a function of frequency oscillations ranging from 0.1 to 50 Hz at 5 Hz intervals for each sample. Samples were pre-loaded with a force of 0.001 N and dynamically tested at low deformation (0.25% strain), taken at the temperature of 37 °C.

Figure 6.25. Elastic modulus E'(A), loss modulus E"(B), stiffness (C), as a function of frequency oscillations ranging from 0.1 to 50 Hz at 5 Hz intervals for each sample. Samples were pre-loaded with a force of 0.001 N and dynamically tested at low deformation (0.25% strain), taken at the temperature of 37 °C. Hydrogel samples are R collagen, R collagen(2h), GelMA, SAH, SAL, GelMA-SAH/CaCl₂, GelMA-SAH/UV, and GelMA-SAL/UV.......335

Figure 6.27. Young modulus E as a function of frequency oscillations ranging from 0.1 to 50 Hz at 5 Hz intervals for each sample. Samples were pre-loaded with a force of 0.001 N and dynamically tested at low deformation (0.25% strain), taken at the temperature of 37 °C. A and B, samples of oral mucosal tissue samples for labial, buccal, and lingual gingival tissue samples (Labial ging., Buccal ging.,Lingual ging.), buccal, and lingual oral alveolar mucosal tissue samples(Buccal alveo.m., and Lingual alveo.m.), and palatal gingival tissue sample (Palatal ging.), of shep and porcine, respectively. Sh referring to sheep, and P referring to porcine. C, and D, crosslinked hydrogel samples. * p < 0.05.

Figure 6.29. Microscopy images of primary human gingival fibroblast cells (HGFs). Scale bars 100 µm (100mm). Magnification 10x213
Figure 6.30. Metabolic activity and cytotoxicity of HGF cells using 3D culturing using different hydrogel samples, SAH, SAL. GelMA-SAH/CaCl2, GelMA-SAL/CaCl2, GelMA-SAH/UV, and GelMA-SAL/UV, on days 1, 3,7 and 14 days. A. metabolic activity of HGF cells. B. LDH release of HGF cells. Data representing mean ± SD(n=3). * p < 0.05
Figure 6.31. Viability and cytotoxicity of HGF cells using 3D culturing using different hydrogel samples, SAH, SAL, GelMA-SAH/CaCl2, GelMA-SAL/CaCl2, GelMA-SAH/UV, and GelMA-SAL/UV, on days 1, 3,7 and 14 days, using flurecent microscope, indicating living cells (green) and dead cells (red). Scale bar: 100 µm
Figure 6.32. A. Metabolic activity, and B. cytotoxicity of HGF cells using 3D culturing using different hydrogel samples, R collagen, GelMA, GelMA-SAH/CaCl ₂ /UV, GelMA-SAH/UV/CaCl ₂ , and GelMA-SAL/UV/CaCl ₂ , on days 1, 3,7 and 14 days. A , metabolic activity of HGF cells. B , LDH release of HGF cells. Data representing mean ± SD(n=3). * p < 0.05
Figure 6.33. Live/dead images of hydrogel samples subjected to sterilization by filtration method. Samples are R collagen, GelMA, GelMA-SAH/CaCl ₂ /UV, GelMA-SAL/CaCl ₂ /UV, GelMA-SAH/UV/CaCl ₂ , and GelMA-SAL/UV/CaCl ₂ , on days, 1, 3, 7, and 14, using flurecent microscope, indicating living cells (green) and dead cells (red). Scale bar: 100 μm
Figure 7.1. Images (A-F) showing GelMA-SAH and GelMA-SAL hydrogel samples in a 6-well plate, prepared and aliquoted with 1 ml per insert, before and after sterilization using ethanol method. This was performed at room temperature (~20°C), (A) and (B) show GelMA-SAH and GelMA-SAL hydrogel samples, respectively, before sterilization. (C&E) and (D&F) show GelMA-SAH and GelMA-SAL hydrogel samples, respectively after sterilized by ethanol method. Images (G-L) showing the same samples before and after sterilized by ethanol method, and before and after different crosslinking methods. (G &H), show GelMA-SAH and GelMA-SAL hydrogel samples, respectively, before sterilization.(I&J) after crosslinking performed using a CaCl ₂ /UV procedure. (K&L) after crosslinking performed using a UV/CaCl ₂ procedure
Figure 7.2. SEM images of different hydrogel samples subjected to sterilization using filtration method. Hydrogel samples at a magnification of 200X with a scale bar of 50 μ m, 500X with a scale bar of 20 μ m, 2KX with a scale bar of 5 μ m, and 5KX with a scale bar of 2 μ m,, showing samples,GelMA-SAH/CaCl ₂ /UV, GelMA-SAL/CaCl ₂ /UV, GelMA-SAH/UV/CaCl ₂ , and GelMA-SAL/UV/CaCl
Figure 7.3. SEM images of different hydrogel samples subjected to sterilization using ethanol method. Hydrogel samples at a magnification of 200X with a scale bar of 50 μ m, 500X with a scale bar of 20 μ m, 2KX with a scale bar of 5 μ m, and 5KX with a scale bar of 2 μ m, showing samples,GelMA-SAH/CaCl ₂ /UV, GelMA

Figure 7.4. FT-IR spectra summarising the chemical bonding structure over a range of 4000–500 cm⁻¹ with a resolution of 4 cm⁻¹ at 37 °C. Samples are: FM.GelMA-SAL/CaCl₂/UV, FM.GelMA-SAH/CaCl₂/UV, FM.GelMA-SAH/UV/CaCl2, FM.GelMA-SAL/UV/CaCl2, E.GelMA-SAH/CaCl2/UV, E.GelMA-SAL/CaCl₂/UV, E.GelMA-SAH/UV/CaCl₂, E.GelMA-SAL/UV/CaCl₂, hydrogel samples. FM and E refer to filtration and ethanol sterilization methods, Figure 7.5. WCA measurements of FM.GelMA-SAH/CaCl₂/UV, FM.GelMA-SAL/CaCl₂/UV, FM.GelMA-SAH/UV/CaCl₂, FM.GelMA-SAL/UV/CaCl₂, E.GelMA-SAH/CaCl₂/UV, E.GelMA-SAL/CaCl₂/UV, E.GelMA-SAH/UV/CaCl₂, E.GelMA-SAL/UV/CaCl₂, hydrogel samples. FM and E refer to filtration and ethanol sterilization methods, respectively. *p< 0.05......242 Figure 7.6. DSC thermograms for samples which were examined under a continuous flowrate of nitrogen gas with the following conditions: equilibrate (-10 °C), isothermal (1 min), and ramp (10 °C/min to 450 °C/min). samples are: FM.GelMA-SAH/CaCl₂/UV, FM.GelMA-SAL/CaCl₂/UV, FM.GelMA-SAH/UV/CaCl2, FM.GelMA-SAL/UV/CaCl2, E.GelMA-SAH/CaCl2/UV, E.GelMA-SAL/CaCl₂/UV, E.GelMA-SAH/UV/CaCl₂, E.GelMA-SAL/UV/CaCl₂, hydrogel samples. FM and E refer to filtration and ethanol sterilization methods, Figure 7.7. Viscosity as a function of shear rate, the rotational tests under destructive shear conditions were performed at shear rates ranging from 0.01 -1500 s⁻¹. Samples are: FM.GelMA-SAH/CaCl₂/UV, FM.GelMA-SAL/CaCl₂/UV, FM.GelMA-SAH/UV/CaCl₂, FM.GelMA-SAL/UV/CaCl₂, E.GelMA-SAH/CaCl₂/UV, E.GelMA-SAL/CaCl₂/UV, E.GelMA-SAH/UV/CaCl₂, E.GelMA-SAL/UV/CaCl₂, hydrogel samples, (A, B, and C) at 37, 20, and 4 °C, respectively. FM and E refer to filtration and ethanol sterilization methods, respectively......244 Figure 7.8. Shear stress as a function of shear rate, the rotational tests under destructive shear conditions were performed at shear rates ranging from 0.01 -1500 s⁻¹. Samples are: FM.GelMA-SAH/CaCl₂/UV, FM.GelMA-SAL/CaCl₂/UV, FM.GelMA-SAH/UV/CaCl₂, FM.GelMA-SAL/UV/CaCl₂, E.GelMA-SAH/CaCl₂/UV, E.GelMA-SAL/CaCl₂/UV, E.GelMA-SAH/UV/CaCl₂, E.GelMA-SAL/UV/CaCl₂, hydrogel samples, (A, B, and C) at 37, 20, and 4 °C, respectively. FM and E refer to filtration and ethanol sterilization methods, respectively......245

Figure 7.16. Live/dead images of hydrogel samples subjected to sterilization by filtration method. Samples are GelMA-SAH/CaCl₂/UV, GelMA-SAL/CaCl₂/UV, GelMA-SAH/UV/CaCl₂, and GelMA-SAL/UV/CaCl₂, on days, 1, 3, 7, and 12, using

flurecent microscope, indicating living cells (green) and dead cells (red). Scale bar: 100 µm253
Figure 7.17. Live/dead images of hydrogel samples subjected to sterilization by ethanol method. Samples are GelMA-SAH/CaCl ₂ /UV, GelMA-SAL/CaCl ₂ /UV, GelMA-SAH/UV/CaCl ₂ , and GelMA-SAL/UV/CaCl ₂ , on days, 1, 3, 7, and 12, using flurecent microscope, indicating living cells (green) and dead cells (red). Scale bar: 100 μm
Figure 7.18. Microscopy images of human gingival epithelium cells (HGE, MOE1 cell line). Scale bar: 100 µm. Magnification: 10×255
Figure 7.19. Metabolic activity and cytotoxicity of HGE cells using 3D culturing using different hydrogel samples, R collagen, GelMA, GelMA-SAH/CaCl ₂ /UV, GelMA-SAH/UV/CaCl ₂ , and GelMA-SAL/UV/CaCl ₂ , on days 1, 3,7 and 14 days. A, metabolic activity of HGE cells. B, LDH release of HGE cells. Data representing mean \pm SD(n=3). Sample is significantly different with * p < 0.05
Figure 7.20. Viability and cytotoxicity of HGE cells using 3D culturing using different hydrogel samples, R collagen, GelMA, GelMA-SAH/CaCl ₂ /UV, GelMA-SAH/UV/CaCl ₂ , and GelMA-SAL/UV/CaCl ₂ , on days 1, 3,7 and 14 days, using flurecent microscope, indicating living cells (green) and dead cells (red). Scale bar: 100um
Figure 7.21. Metabolic activity of engineered 3DGT model constructed in well plates, using different hydrogel samples, R collagen, GelMA, GelMA-SAH/CaCl ₂ /UV, GelMA-SAH/UV/CaCl ₂ , and GelMA-SAL/UV/CaCl ₂ , on days 1, 3,7 and 14 days. Hydrogel samples were submerged in a different ratios of mixture of HGFs medium and HGEs medium for A-E with percentages:100:0, 0:100, 75:25, 25:75, and 50:50, respectively. Data representing mean ± SD(n=3). * p < 0.05
Figure 7.22. Cytotoxicity of engineered 3DGT model constructed in well plates, using different hydrogel samples, R collagen, GelMA, GelMA-SAH/CaCl ₂ /UV, GelMA-SAH/UV/CaCl ₂ , and GelMA-SAL/UV/CaCl ₂ , on days 1, 3,7 and 14 days. Hydrogel samples were submerged in a different ratio of mixture of HGFs medium and HGEs medium for A-E with percentages: 100:0, 0:100, 75:25, 25:75, and 50:50, respectively. Data representing mean \pm SD(n=3). * p < 0.05260
Figure 7.23. Live/dead confocal images of engineered 3DGT model constructed in well plates, using different hydrogel samples, R collagen, GelMA, GelMA-SAH/CaCl2/UV, GelMA-SAH/UV/CaCl2, and GelMA-SAL/UV/CaCl2, on days 1, 3,7 and 14 days. Hydrogel samples were submerged in a different ratios of mixture of HGFs medium and HGEs medium (100:0, 75:25, 50:50, 25:75, or 0:100). Data representing mean ± SD(n=3). using fluorescent microscope, indicating living cells (green) and dead cells (red). Scale bar: 100 μm
Figure 7.24. Image of 3D gingival tissue models cultured in 13 mm Millicell inserts within a 12-well plate. Each insert contains a hydrogel-based construct seeded with cells images at day 14 after culturing and ready for lifting to ALL. The hydrogel

samples are: (A&E) GelMA-SAH/CaCl2/UV,(B,F,C,&G) GelMA-SAH/UV/CaCl2, (D&H) GelMA-SAL/UV/CaCl2, (I&J) R collagen, and (K&L) GelMA hydrogel samples
Figure 7.25. (A, B,C,D, and E) Live/dead confocal images at day 14 of lifting 3DGT model to ALI, using R collagen, GelMA. GelMA-SAH/CaCl2/UV, GelMA-SAH/UV/CaCl2, and GelMA-SAL/UV/CaCl2, respectively. Confocal images captured using flurecent microscope, indicating living cells (green) and dead cell(red). Scale bar: 100 μm. (F, G,and H) H&E stained histological section images showing epithelial layer, and underlying connective tissue. Arrows indicate the distinct tissue layers, (Scale bar: 50 μm) at day 14 of lifting 3DGT model to ALI, using GelMA-SAH/CaCl2/UV, GelMA-SAH/UV/CaCl2, and GelMA-SAL/UV/CaCl2, respectively

CHAPTER 1

1. LITERATURE REVIEW & INTRODUCTION

1.1. Background

The oral mucosa (mucous membrane) is continuous with the skin of the lips and the mucosa of the soft palate and pharynx. The oral mucosa consists of masticatory mucosa, which includes the gingiva, the covering of the hard palate; the specialized mucosa, which covers the dorsum of the tongue; and the third remaining part, called the lining mucosa (1-4).

1.2. Periodontium

Periodontium is the supporting structure of the tooth. Periodontium comprises the gingiva, periodontal ligament, root cementum, and the alveolar bone. The main function of the periodontium is to attach the tooth to the jawbone and to maintain the integrity of the oral cavity (4, 5).

1.2.1. Gingiva

Gingiva is one of four components of the periodontium. The main function of the gingiva is to cover the alveolar process and surround the cervical portion of the teeth. Clinically there are three parts of the gingiva that can be identified, free gingiva, interdental gingiva, and attached gingiva (Fig. 1.1) (6, 7).

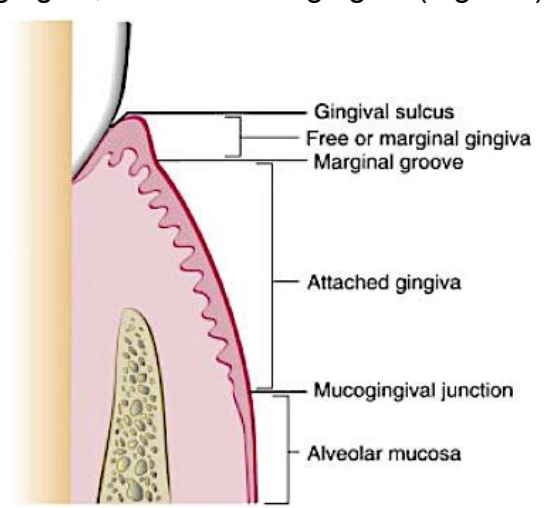


Figure.1.1 The anatomy of Periodontium. *Adapted from Newman and Carranza's Clinical Periodontology.*

Histologically, the gingival tissue consists of an epithelial layer that is separated from underlying lamina propria by a basement membrane (2, 12). These gingival tissues are considered the first sites to be affected by microbial biofilms and as an initiative location of inflammatory processes of periodontal diseases (14).

1.2.1.1. Gingival epithelial layer: -

The gingival epithelial layer plays as a barrier to protect the underlying tissue from the external environment. The epithelial layer of the gingiva consists of keratinized or non-keratinized squamous epithelium. The keratinized epithelium is composed of four layers, stratum basale, stratum spinosum, stratum granulosum, and stratum corneum, while in the non-keratinized epithelium, there were three layers, basal layer, intermediate layer, and superficial layer (8, 9).

A. Gingival epithelial cell layers

Keratinocytes are considered the principal cells of this layer and are connected to each other by a connected component called desmosomes. In addition to the keratinocytes, which comprise about 90% of the total cell population, there are non-keratin producing cells, such as melanocytes, langerhans, markel's, and inflammatory cells (15).

B. Gingival epithelial classification:-

From the morphologic and functional points of view, gingival epithelial layers are classified into three areas, oral epithelium, sulcular epithelium and junctional epithelium.

Oral epithelium, is keratinized epithelium that faces the oral cavity, including the free gingiva and the attached gingiva. It can be divided into basal layer (stratum basale), prickle cell layer (stratum spinosum), granular cell layer, (stratum granulosum), and keratinized cell layer (stratum corneum) (2, 15) (Fig. 1.2 and 1.3) (10).

Sulcular epithelium is a stratified, non-keratinized squamous epithelium, that covers the shallow groove of the gingival sulcus. The location of sulcular epithelium is between the enamel and the top of the free gingiva and faces the tooth without being in contact with the tooth surface. Moreover, the sulcular epithelium is considered a permeable epithelium, and this permeability plays a primary role in the process of periodontal inflammation(15).

Junctional epithelium contacts the enamel surface of the tooth by its connection part which is called hemidesmosome, and by these parts, the underlying gingival connective tissue could remain linked with the tooth surface(11, 12, 15-17).

C. Gingival Epithelial Cell Differentiation

The epithelial layer is considered a physical barrier, in addition, this epithelial layer plays a role in innate host defence by responding to bacteria in an interactive manner; by increased cells proliferation, alteration of cell-signalling events, changes in differentiation and cell death, and ultimately, the alteration of tissue homeostasis.

The differentiation and functions of epithelial cells are represented by the production of specific proteins.

Ki67, a protein expressed in actively dividing cells, is a marker for cell proliferation (18) Similarly, PCNA is a protein that is essential for DNA replication during cell division (19).

Cytokeratin proteins (CK) are intermediate filament proteins composed of different polypeptide subunits, these proteins are considered a major component of the epithelial cytoskeleton. Therefore, these proteins are important because are not only given mechanical stability but are also involved in cell signalling, transport, and differentiation of keratinocytes(20, 21).

Gingival epithelial tissues express different cytokeratins depending upon the cell type. CK6 and CK16 are expressed by highly hyperproliferative keratinocytes(22, 23). CK5 and CK14 are expressed by all stratified squamous epithelia (24).

Suprabasal cells express CK2, while CK1, CK2, CK10, and CK12, are high intensity in orthokeratinized areas and with less intensity in parakeratinized areas. In contrast, parakeratinized areas express CK19, which is usually absent from orthokeratinized normal epithelia (22, 23, 25).

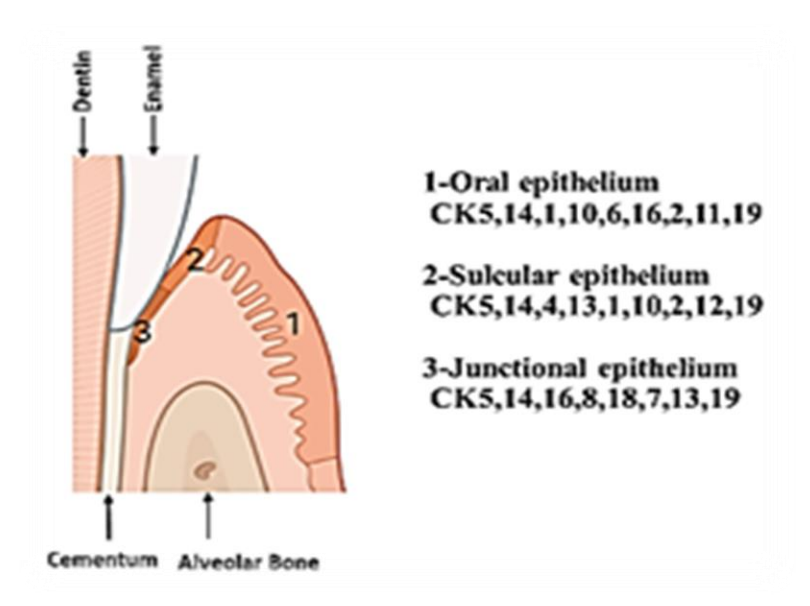


Figure 1.2 Types of human gingival epithelium (oral gingival, sulcular and junctional). Cytokeratin distribution patterns in human gingival epithelium (oral gingival, sulcular and junctional). Created with BioRender.com.

In sulcular epithelium, where stratum granulosum and stratum corneum are lacking, there are expressed of CK1, CK2, CK10, and CK12 cytokeratins, in addition to CK4, CK13, and K19 (11, 26).

While in junctional epithelium, CK5,CK14,CK7,CK8,CK18,CK13,CK16 and CK19 are presented (25) (Fig. 1.2 and 1.3).

Involucrin is a protein that components of the "cornified envelope", its highly soluble protein envelope sheathing the inner face of the keratinocyte membrane (synthesis by stratum spinosum and crosslinked in the stratum granulosum by transglutaminase enzyme that makes insoluble envelope) and provided structural support for these cells, to be resistance to microbial invasion (27).

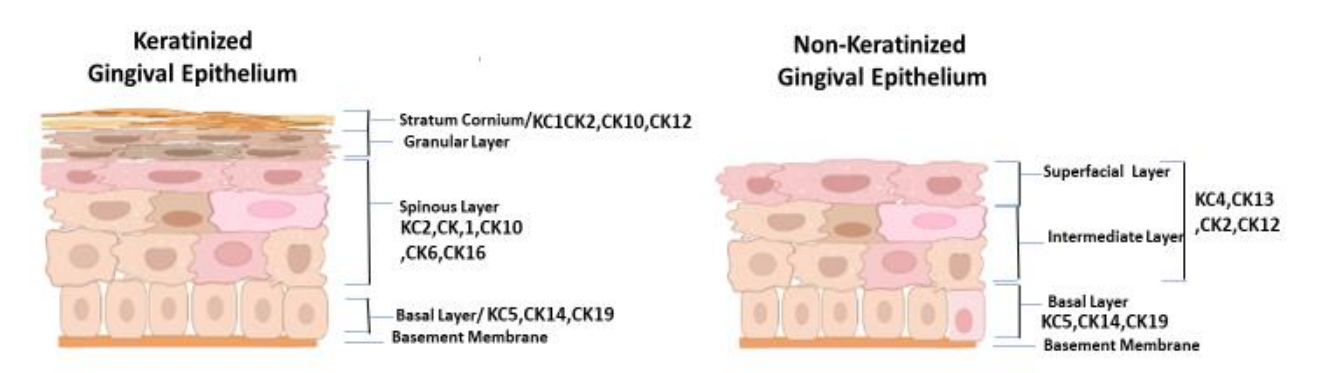


Figure 1.3 Structure of gingival keratinizing and non-keratinizing stratified epithelial tissues. Created with BioRender.com.

E-cadherin is a calcium-dependent homophilic cell adhesion molecule that plays an essential role in cell-cell interaction. And the epithelium acts as a mechanical barrier through E-cadherin(28-30).

Filaggrin is a marker representing late keratinization in orthokeratinized and parakeratinized areas of the human oral epithelium(31, 32).

Transglutaminase (TG) is an enzyme expressed in spinous layers that plays an important role in the late differentiation of the mature keratinocyte (33).

1.2.1.2. Gingival basement membrane

The basement membrane, composed of a complex composition of glycoprotein, separates the epithelial layer from underlying connective tissue and is formed into two zones which are lamina lucida and lamina densa. Lamina lucida zone faces the basal epithelial cells, and the basement membrane is produced from basal cells and connected by hemidesmosomes. The second zone is lamina densa, which contains anchoring fibres project in a fan shaped appearance into the connective tissue(2, 17, 34). Collagen type IV and laminin 5 are two main proteins in the lamina densa. collagen type IV is the major basement membrane collagen while laminin 5 is an important adhesive glycoprotein component of basement membranes (34).

1.2.1.3. Gingival connective tissue

This layer is considered the predominant tissue component of the gingival tissue. The major components of the connective tissue are collagen fibres

(around 60% of connective tissue volume), fibroblasts (around 5% of connective tissue valium, and 65% of all connective tissue cells), mast cells, macrophage cells, inflammatory cells, vessels and nerves (around 35% of connective tissue volume). These connective tissue components are embedded in an amorphous ground substance called extracellular matrix (2, 35).

Fibroblasts are the most common cell in the lamina propria, where they regulate tissue development, organogenesis, homeostasis, and maintenance of the tissue(36-39). It produces various types of fibres found in the connective tissue, such as collagen fibres (type I and III collagens), reticulin fibres, oxytalan fibres, and elastic fibres. The collagen fibres predominate in the gingival connective tissue and constitute the most essential components of the gingiva. Moreover, fibroblasts are involved in the synthesis of the extracellular matrix and remodelling of this matrix to aid in homeostasis. In addition, fibroblasts play an important role in epithelial differentiation, keratin expression, and keratinocyte adhesion(35, 40). Furthermore, the epithelial phenotype and profile of cytokeratin expression are influenced by the nature and origin of the underlying mesenchymal substrate and fibroblasts(41, 42). For gingival connective tissue differentiation, vimentin is the major intermediate filament protein of mesenchymal cells. It shows dynamically altered expression patterns during different developmental stages of connective tissue cells (36).

1.2.1.4. Extracellular matrix (ECM)

ECM is a complex three-dimensional (3D) fibrous meshwork of collagen and elastic fibres embedded in a highly hydrated gel-like and bioactive material of glycosaminoglycans, proteoglycans, and glycoproteins.

Collagens type I and collagen type II are present in the ECM as fibrillar proteins and give structural support to resident cells. All together provide mechanical support with directing cell adhesion, proliferation, differentiation, morphology, and gene expression(13).

1.2.2. Periodontal ligament (PDL)

The PDL is part of the periodontium, as a specialized richly vascularized connective tissue structure composed primarily of collagen fibers. It is situated in the narrow space between the roots of the teeth and the lamina dura, which is the part of the alveolar bone that interfaces directly with the teeth. The width of the PDL varies between approximately 0.2 mm and 0.4 mm, depending on factors such as age, functional load, and physiological conditions (43). One of the primary roles of the PDL is to act as a shock absorber by distributing and dissipating the mechanical forces exerted on the teeth during mastication, biting, and other oral functions (44). This cushioning effect helps protect the alveolar bone and maintain the stability of the dentition. The mobility of the teeth is largely influenced by the condition of the PDL, as its integrity and composition determine the extent to which the teeth can move within their sockets (43).

Beyond its structural role, the PDL is also a highly dynamic and biologically active tissue. It contains a rich network of nerve fibers that contribute to proprioception, allowing the detection of pressure and movement. Additionally, the PDL houses various cell types, including fibroblasts, which are responsible for maintaining and remodeling the ligament fibers, as well as osteoblasts and osteoclasts, which regulate bone formation and resorption. Cementoblasts, another crucial cell type, are involved in the formation of cementum, the calcified tissue covering the tooth root. Epithelial cells, which may originate from the remnants of the Hertwig's epithelial root sheath, are also present and may play a role in periodontal regeneration and repair.

Overall, the periodontal ligament is essential for tooth support, force distribution, and tissue homeostasis, making it a critical component of the periodontium (45, 46).

1.2.3. Root cementum

The root cementum is part of the periodontium. Root cementum is a highly specialized mineralized tissue that covers the root surface of teeth and plays a crucial role in anchoring the PDL to the tooth structure. It serves as a critical

component of the periodontium, facilitating tooth attachment and contributing to the stability of the dentition. The root cementum also plays a vital role in periodontal regeneration and repair following injury or resorption (47, 48).

Structurally, cementum is composed of approximately 65% inorganic material, primarily hydroxyapatite, while the remaining 35% consists of organic components and water. The organic matrix consists predominantly of collagen type I, along with non-collagenous proteins such as osteopontin and bone sialoprotein, which contribute to its mineralization and attachment properties (49). Cementocytes, which are entrapped within the cementum matrix, play a role in its maintenance and remodeling (50).

Cementoblasts, derived from the PDL, are responsible for the continuous deposition of cementum, forming distinct layers that can be classified based on their histological characteristics into acellular and cellular cementum (51). Acellular cementum, which lacks embedded cells, is primarily found in the cervical and middle root regions, while cellular cementum, containing cementocytes, is predominantly located in the apical third and furcation areas.

With aging, cementum continues to undergo appositional growth, leading to an increase in its thickness over time. This thickening is attributed to the continuous deposition of new cementum layers by cementoblasts, which helps to compensate for occlusal wear and maintain tooth stability. Additionally, Sharpey's fibers, which originate from the periodontal ligament, become mineralized and embedded within the cementum, further strengthening the attachment of the tooth to the alveolar bone (52).

1.2.4. Alveolar bone

The alveolar bone constitutes the osseous component of the dentition attachment apparatus, playing a crucial role in supporting and anchoring the teeth. It is a specialized part of the maxilla and mandible that forms the tooth sockets (alveoli), providing structural integrity and stability to the dentition. The development of alveolar bone is intricately linked to tooth eruption and

maintenance, as its presence and remodeling are influenced by functional loading and occlusal forces.

Structurally, the alveolar bone comprises two main components: cortical bone and trabecular bone. The cortical bone forms the dense outer walls of the tooth sockets, offering mechanical strength, while the trabecular (cancellous) bone is located between these cortical layers, contributing to shock absorption and load distribution (47, 49, 53). Additionally, the alveolar bone proper, also referred to as the bundle bone, interfaces directly with the periodontal ligament (PDL), providing attachment sites for Sharpey's fibers, which secure the tooth within its socket.

The alveolar bone is highly dynamic, undergoing continuous remodeling in response to mechanical stimuli and pathological conditions. Inflammatory periodontal diseases, such as periodontitis, can trigger alveolar bone resorption due to the activation of osteoclasts, leading to progressive bone loss and alterations in dentition stability and positioning (54). Such resorption ultimately compromises the structural integrity of the attachment apparatus, increasing the risk of tooth mobility and eventual tooth loss (55).

1.3. Periodontal diseases

Periodontal diseases are a group of inflammatory conditions affecting the supporting structures of the teeth, including the gingiva, periodontal ligament, cementum, and alveolar bone. Gingivitis represents the reversible inflammation of the gingiva, primarily caused by bacterial plaque accumulation. Gingivitis is the mildest form of periodontal disease and can be found in up to 90% of the population If left untreated, gingivitis can progress to periodontitis, which is characterized by irreversible destruction of periodontal tissues, loss of attachment, and eventual tooth loss. The pathogenesis of periodontal diseases is multifactorial, involving microbial dysbiosis, host immune response, and environmental and genetic risk factors (55, 56). (Fig. 1.4A).

Dental implants are widely used to replace missing teeth and restore oral function and aesthetics. They are typically made of biocompatible materials

such as titanium and are surgically placed into the alveolar bone, where they integrate through a process known as osseointegration. Once integration is achieved, the implant supports prosthetic restorations such as crowns, bridges, or dentures. (56-59). The tissues surrounding dental implants collectively referred to as peri-implant tissues include the peri-implant mucosa and the underlying supporting bone. The peri-implant mucosa consists of an epithelial and connective tissue component that forms a seal around the implant, playing a critical role in protecting the underlying bone from microbial invasion and inflammation.

Understanding the normal anatomy and biology of these peri-implant tissues is essential for identifying and managing pathological changes such as peri-implant mucositis and peri-implantitis, which can compromise the longevity and success of dental implants (60-65).

Figure 1.4A illustrates the healthy and diseased conditions around a natural tooth, highlighting the presence of the periodontal ligament and connective tissue attachment. In contrast, Figure 1.4B shows the corresponding structures around a dental implant, where the connective tissue fibres run parallel or circularly around the implant surface rather than inserting directly into it. This anatomical difference makes peri-implant tissues more susceptible to inflammation and bone loss when plaque accumulates, leading to peri-implant mucositis and peri-implantitis.

The peri-implant mucosa shares similarities with the gingiva around natural teeth but differs in its structural organization, particularly in the orientation and density of collagen fibers, vascularization, and immune cell distribution. These differences contribute to a distinct biological environment and influence susceptibility to disease. (56-59). Inflammation of soft tissue surrounding the implant is called peri-implant mucositis. Gingivitis or peri-implant mucositis are terms used to describe the inflammation of the gingiva due to the accumulation of bacteria and debris between the gum line and tooth, also known as dental plaque. It is a reactive condition that is reversible upon the improvement of oral hygiene. Progress of disease beyond gingivitis or peri-implant mucositis into a

chronic, destructive, irreversible inflammatory disease state which is called periodontitis that surrounding the tooth (Fig.1.4A). While its called peri-implantitis if the condition occurred within the tissues that surrounding the implant (Fig.1.4B).

Periodontitis or peri-implantitis lead to loss of attachment of the periodontium, which subsequently progresses to alveolar bone loss, potentially resulting in loss of the affected tooth if left without treatment (57-59). The clinical appearance of the periodontal pocket, which is the deepening of the gingival sulcus and is considered an indicator for periodontal disease. From histological viewing of the periodontal pocket, there is a prominent disappearance of junctional epithelium with the presence of ulcerative sulcular epithelium, which means the connection of gingival connective tissue to the tooth surfaces has become fragile and exposed to oral bacterial invasions and destruction of connective tissues and underlying alveolar bone (16, 60). In addition, recent evidence shows that the effects of periodontal infections may well expand beyond the oral cavity, to be implicated in systemic diseases, such as diabetes mellitus and cardiovascular diseases(61, 62).

The classification of periodontal diseases has evolved over time, with significant updates provided by the European Federation of Periodontology (EFP) and the British Society of Periodontology (BSP) (63). The most recent framework, established in the 2017 World Workshop on the Classification of Periodontal and Peri-Implant Diseases and Conditions, categorizes periodontal diseases into major groups: periodontal health, gingival diseases, periodontitis (staged and graded based on severity and risk factors), and other conditions affecting the periodontium, including systemic influences and developmental disorders.

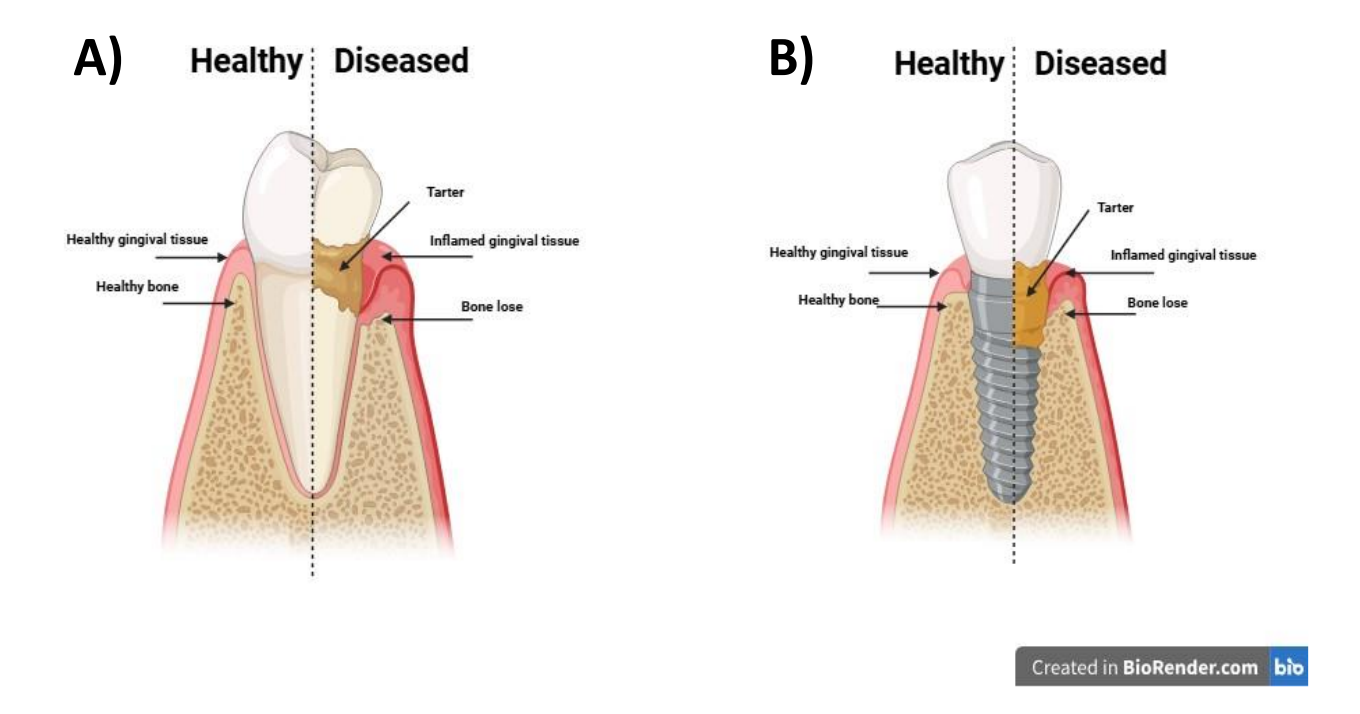


Figure 1.4. Schematic illustration of healthy versus diseased tissues around, A. tooth and, B. implant. Created with BioRender.com.

The EFP and BSP have adopted this system to ensure consistency in diagnosis, treatment planning, and research. This classification system integrates clinical and radiographic findings with risk factors such as smoking and diabetes, allowing for a more individualized approach to patient care (64, 65).

The World Workshop on the Classification of Periodontal and Peri-implant Diseases and Conditions. The workshop was co-sponsored by the American Academy of Periodontology (AAP) and the European Federation of Periodontology (EFP) and included expert participants from all over the world. Planning for the conference, which was held in Chicago on November 9 to 11, 2017, began in early 2015. This classification is necessary for clinicians to properly diagnose and treat patients as well as for scientists to investigate etiology, pathogenesis, natural history, and treatment of the diseases and conditions (66-71). Additional details on periodontal classification are provided in Appendix A (Appendix A).

1.3.1. Etiologic of periodontal diseases

The primary etiological factor in periodontal diseases is bacterial plaque, a complex biofilm that accumulates on the tooth surface adjacent to the gingival margin. The microorganisms within this biofilm release virulence factors such as lipopolysaccharides, enzymes, and toxins, which trigger an inflammatory host response in the surrounding gingival tissues. This local immune response involves the activation of various cell types and the production of proinflammatory mediators, including cytokines, chemokines, matrix metalloproteinases, and prostaglandins, ultimately leading to connective tissue breakdown and alveolar bone loss (72-74).

In addition to plaque accumulation, several patient-specific risk factors influence the severity and progression of periodontal diseases. These can be categorised into modifiable factors such as smoking, poor oral hygiene, diabetes mellitus, and pregnancy, and non-modifiable factors, including age and genetic predisposition (68-70). A number of features of the inflammatory and immune response that seem to play a role in the development of periodontal diseases have a clearly established genetic basis (71).

1.3.2. Diagnosis of periodontal diseases

The diagnosis of periodontal diseases is primarily based on clinical and radiographic assessments that evaluate the condition of the supporting periodontal tissues. Key clinical parameters include probing pocket depth (PPD), clinical attachment level (CAL), and bleeding on probing (BOP), which reflect the extent of periodontal tissue destruction and ongoing inflammation. Radiographic evaluation is essential to assess alveolar bone loss, which helps determine the severity and extent of the disease (75). According to the 2018 classification system jointly developed by the American Academy of Periodontology (AAP) and the European Federation of Periodontology (EFP), periodontitis is diagnosed and categorised based on staging (which reflects disease severity and complexity of management) and grading (which indicates the rate of progression and risk factors influencing the disease course). This

updated system integrates both clinical and radiographic findings to provide a more comprehensive framework for diagnosis and patient stratification (67).

The British Society of Periodontology (BSP) has further adapted this framework for clinical practice, emphasising accurate diagnosis and consistent terminology. The BSP implementation guidelines recommend the use of Professional Mechanical Plaque Removal (PMPR) during initial therapy and Supportive Periodontal Care (SPC) during maintenance, replacing the older term Supportive Periodontal Therapy (SPT) (76).

Despite this standardisation, many clinicians still face challenges in consistently assessing these parameters and accurately assigning the appropriate stage and grade. Inter-examiner variability remains a concern, with studies reporting only fair levels of diagnostic agreement, and accuracy ranging from 31% to 83%.(77).

Given these challenges, there is increasing interest in developing diagnostic models based on cellular, genetic, and molecular markers to improve clinical outcomes. Advances in genetic and genomic technologies have facilitated the development of new diagnostic approaches utilizing genomic analysis. Several studies have explored gene expression in periodontal tissues using RNA sequencing (RNA-seq) or microarray technologies. These studies have identified genetic markers associated with an increased risk of periodontitis, particularly genes involved in immune response, inflammation, and apoptosis (78-82).

1.3.3. Molecular profile of human gingival tissue

Understanding gingival tissue at the molecular level is crucial for elucidating the cellular mechanisms and biochemical pathways that maintain tissue structure, function, and homeostasis. Molecular analyses provide insights into gene expression patterns, signaling networks, and extracellular matrix composition, which collectively define the unique characteristics of gingival tissue. Such knowledge forms the foundation for studying tissue responses to physiological

and pathological stimuli and is essential for guiding the design of accurate and predictive in vitro models (235-237).

At the core of molecular profiling are the nucleic acids DNA and RNA which store and transmit the genetic information that dictates cellular function and tissue behavior. The human genome consists of the complete set of nucleic acid sequences found in humans, encoded within the DNA of 23 distinct chromosomes located in the cell nucleus. This genome is composed of DNA (deoxyribonucleic acid), a long, coiled molecule that carries the instructions necessary for building and maintaining cells. These instructions are encoded in sequences of "base pairs," formed by four specific chemical components, and are organized into approximately 20,000 to 25,000 genes. For these genetic instructions to be executed, DNA must be "read" and transcribed, meaning it is copied into RNA (ribonucleic acid) (Fig. 1.5). The resulting RNA copies of genes are known as transcripts, and the complete set of these gene readouts within a cell is referred to as the transcriptome (83).

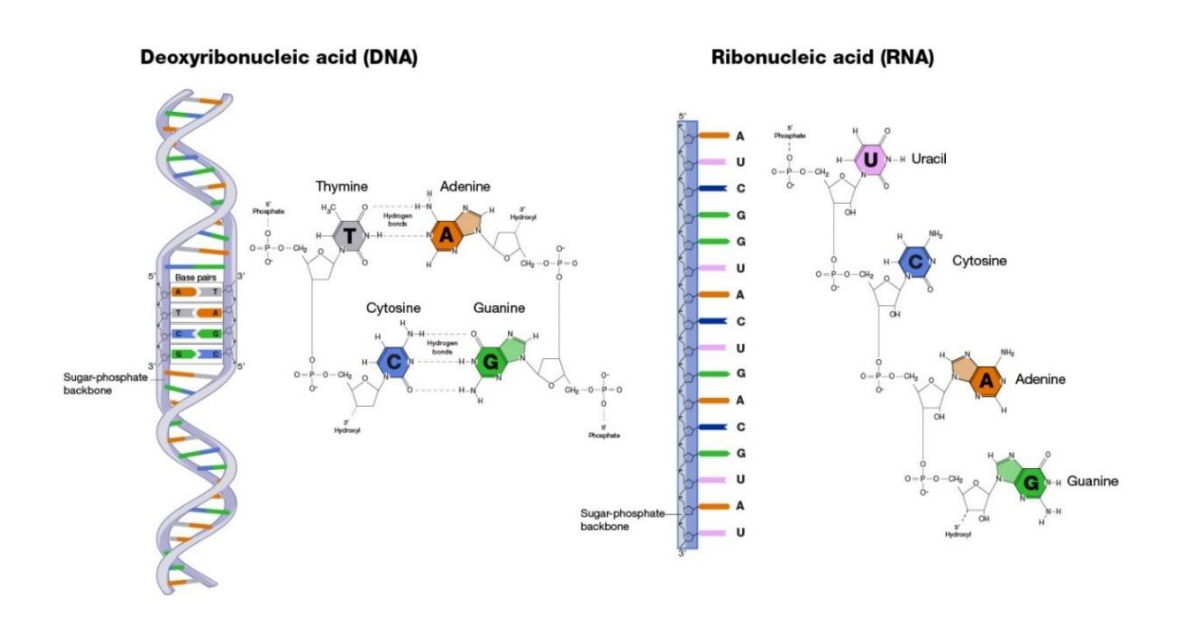


Figure 1.5. Structures of Deoxyribonucleic acid (DNA) vs Ribonucleic acid (RNA). RNA The RNA structure is composed of uracil as an alternative to thymine base pairs. RNA forms a shorter helix. https://www.genome.gov/about-genomics/educational-resources/fact-sheets/ribonucleic-acid-fact-sheet.

RNA is an essential molecule present in nearly all living organisms and viruses. It shares many similarities with DNA, and just as all living organisms contain DNA, they also possess RNA. RNA serves a wide range of crucial biological functions, including storing and transmitting genetic information, providing structural support, catalyzing biochemical reactions, and regulating the activity of both DNA and other RNA molecules. Its diverse roles make it a fundamental component of cellular processes and gene expression.

1.3.3.1. Subunits of RNA molecule

RNA is a fundamental biomolecule composed of nucleotide subunits, each consisting of a ribose sugar, a phosphate group, and one of four nitrogenous bases: adenine (A), guanine (G), uracil (U), and cytosine (C). Unlike DNA, which contains thymine (T) instead of uracil, RNA is primarily single-stranded (Fig.1.4). However, certain RNA viruses exhibit double-stranded forms, demonstrating the structural diversity of RNA. The length and configuration of RNA molecules can vary significantly, ranging from short non-coding RNAs to long messenger RNAs that encode proteins. RNA viruses, in contrast to DNA-based organisms, utilize RNA as their genetic material, making them responsible for a wide range of infectious diseases in humans, including influenza, hepatitis C, and COVID-19 (84-86).

1.3.3.2. The central dogma of molecular biology

The central dogma of molecular biology is a theory outlines the flow of information that is stored in genes as DNA, transcribed into RNA, and finally translated into proteins (Fig.1.6). It was first stated by Crick in 1957, then published in 1958 (87-90).

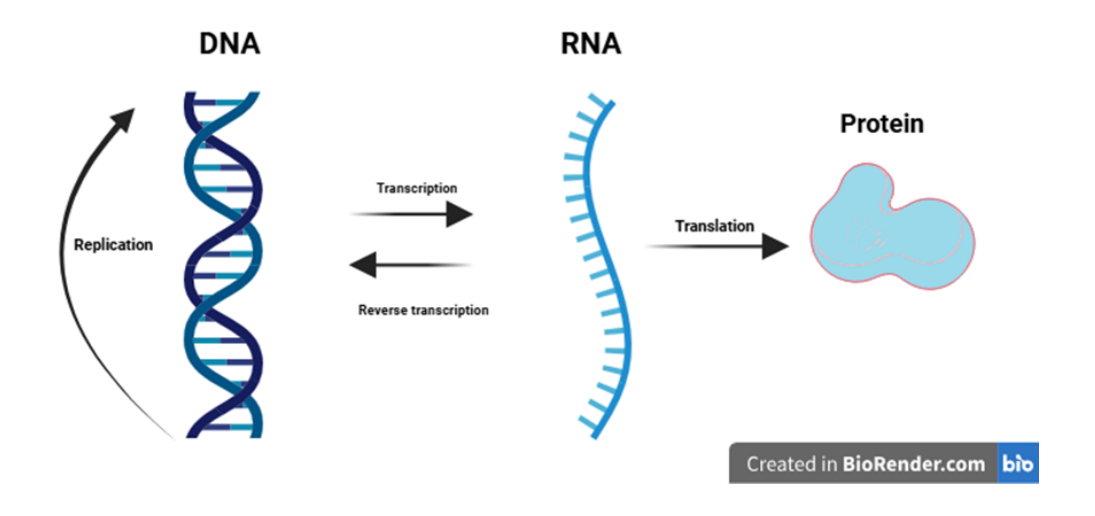


Figure 1.6. Diagram of concept of central dogma for transcription of DNA into RNA and translate to protein. Created in bioRender.com.

1.3.3.3. Transcription

RNA molecules are synthesized through a biological process known as transcription. Transcription process plays a crucial role in gene expression. In this process, a specific segment of DNA serves as a template to guide the formation of an RNA strand. Instead of thymine, which is found in DNA, RNA incorporates uracil (U) as its complementary base. Each of these nucleotides pairs specifically with its counterpart on the DNA strand during transcription.

The transcription process begins when an enzyme called RNA polymerase binds to a specific region of the DNA molecule, known as the promoter. As the enzyme moves along the DNA strand, it unwinds the double helix and reads the nucleotide sequence of one of the DNA strands, called the template strand. Using this sequence as a guide, RNA polymerase adds complementary RNA nucleotides, linking them together to form a growing RNA chain. The resulting RNA strand is a complementary copy of the DNA template, except that uracil (U) replaces thymine (T).

1.3.3.4. Transcript

Transcript in molecular biology term refers to the RNA molecule that is produced during the process of transcription. It is a complementary copy of a specific DNA sequence.

Types of Transcripts:

- Messenger RNA (mRNA) Carries genetic information from DNA to ribosomes for protein synthesis.
- 2. Ribosomal RNA (rRNA) A key component of ribosomes, which help in protein synthesis.
- 3. Transfer RNA (tRNA) Helps transfer amino acids during protein synthesis.
- 4. Non-coding RNA (ncRNA) Includes small RNAs like microRNA (miRNA) and long non-coding RNA (lncRNA) that regulate gene expression.

In summary, a transcript is an RNA copy of a gene that can either be used to produce proteins (mRNA) or have regulatory/structural roles (rRNA, tRNA, ncRNA). These RNA molecules work in coordination to ensure accurate and efficient protein production, a fundamental process essential for cellular function and survival (91-94).

1.3.3.5. Complementary DNA

Complementary DNA (cDNA) is synthetic DNA that has been transcribed from a specific mRNA through a reaction using the enzyme reverse transcriptase. While DNA is composed of both coding and non-coding sequences, cDNA contains only coding sequences. Scientists often synthesize and use cDNA as a tool in gene cloning and other research experiments.

1.3.3.6. Gene expression

Once transcription is complete, the new RNA molecule carries genetic instructions copied from DNA. Different types of RNA have different roles in the

cell. Transcription and RNA production are key parts of gene expression. Gene expression is how DNA's genetic information is used to make functional molecules, like proteins, that help the cell work properly. This process is essential for growth, development, and maintenance in all living things.

Environmental factors can influence gene expression, shaping an organism's traits (phenotype). The specific genes transcribed into RNA determine a cell's identity and control its functions. Together, these RNA molecules make up the transcriptome, which helps us understand development and disease (88, 95).

1.3.3.7. Transcriptome

The transcriptome refers to the complete set of RNA transcripts, for both coding and non-coding RNA that present in an individual cell or a population of cells. Depending on the context, the term may encompass all types of RNA or specifically messenger RNA (mRNA), depending on the focus of a particular study. The word transcriptome is a blend of "transcript" and "genome," highlighting its connection to the transcription process, where RNA molecules are synthesized from DNA.

The annotation of transcriptomes began in the 1980s with the publication of cDNA libraries. The development of high-throughput technologies later revolutionized transcriptome research, enabling more efficient and rapid data collection.

1.3.3.8. Transcriptomics

Transcriptomics is the analysis of the transcriptome, that is present in a sample (a cell, tissue or organ) at a given time. It is a quantitative discipline that involves mapping a collection of sequence reads (reads) to their corresponding transcriptomic units (transcripts) within the genome. The information content of an organism is recorded in the DNA of its genome and expressed through transcription. RNA performs many functions within the cell, and studying the transcriptome provides insights into how genes are working and whether

proteins are being produced as expected. All steps in gene expression, including transcription, RNA processing, translation, and protein turnover, determine a cell's fate and are dedicatedly regulated (96-98).

The expression levels of these transcripts are determined by measuring the density of reads associated with each transcript (99). Initially, transcriptomic analysis utilized expressed sequence tag (EST) libraries and serial analysis of gene expression (SAGE) to investigate gene expression patterns (100).

Today, transcriptomics is primarily driven by two key techniques: DNA microarrays and RNA sequencing (RNA-Seq). Both methods require the isolation of RNA using specialized extraction techniques, followed by the separation of RNA from other cellular components and the enrichment of messenger RNA (mRNA) to ensure high-quality analysis (101, 102).

1.3.3.8.1. DNA microarray technology

The earliest studies of transcriptomes relied on DNA microarray technology, commonly referred to as DNA chips. This method, first introduced in the mid-1990s, enabled researchers to analyze gene expression on a large scale (103). DNA microarrays consist of a solid surface, typically a thin glass slide or silicon wafer, containing thousands to millions of microscopic spots. Each spot is embedded with immobilized single-stranded oligonucleotides, known as probes, which are designed to hybridize with complementary sequences of target RNA or DNA. These probes correspond to specific gene sequences, allowing for the detection and quantification of gene expression levels across an entire genome in a single experiment. One of the major advantages of DNA microarrays is their ability to simultaneously analyze thousands of genes, making them a powerful tool for studying gene expression patterns under different conditions. However, this technology has limitations. DNA microarrays can only detect genes that are already known and represented on the chip, meaning they are unable to identify novel transcripts or previously uncharacterized genes. Additionally,

hybridization-based detection can lead to background noise and crosshybridization, which may affect data accuracy.

By the 2010s, microarray technology was largely replaced by next-generation sequencing (NGS), a high-throughput sequencing approach that offers a more comprehensive and precise analysis of gene expression (89). Unlike microarrays, NGS does not rely on predefined probes but instead sequences RNA molecules directly, enabling the discovery of novel transcripts, alternative splicing events, and variations in gene expression at single-nucleotide resolution. This shift marked a significant advancement in transcriptomics, providing researchers with deeper insights into gene regulation and cellular function.

1.3.3.8.2. RNA sequencing (RNA-Seq) technology

RNA sequencing (RNA-Seq) is a next-generation sequencing (NGS) technology that enables the analysis of RNA transcripts with high sensitivity and accuracy. One of its key advantages is that it requires only a small amount of RNA and does not necessitate prior knowledge of the genome, making it a powerful tool for studying gene expression, transcriptome profiling, and novel transcript discovery. RNA-Seq allows both qualitative and quantitative analysis of RNA transcripts. The qualitative aspect aids in identifying novel transcripts, detecting alternative splicing events, and discovering RNA modifications, while the quantitative aspect measures transcript abundance, providing insights into gene expression levels under various biological conditions (104).

A. Key Steps in RNA Sequencing

The process of sequencing transcriptomes from biological samples consists of three main steps: RNA purification, library preparation, and sequencing.

A.1. RNA Purification and Quality Assessment

RNA purification is the first step and varies depending on whether short or long RNA molecules are being analysed. This step is crucial to eliminate

contaminants such as DNA, proteins, and technical impurities introduced during sample processing. Once purified, RNA quality is assessed using UV spectrometry, which detects an absorbance peak at 260 nm, indicating the presence of nucleic acids.

A more detailed evaluation of RNA integrity is conducted by analyzing the ratio and intensity of 28S ribosomal RNA (rRNA) to 18S rRNA, which is reported as the RNA Integrity Number (RIN) score. A high RIN score (typically above 7) suggests that the RNA is intact and suitable for sequencing, while a lower RIN score indicates RNA degradation, which may affect sequencing accuracy (105).

Since messenger RNA (mRNA) is the primary target for transcriptome analysis but constitutes only about 3% of the total RNA in a cell, enrichment strategies are employed to selectively retain mRNA. This is typically achieved by removing unwanted ribosomal RNA (rRNA), transfer RNA (tRNA), and other non-coding RNAs that make up the majority of total RNA content. Enrichment methods include poly(A) selection, which captures mRNA using oligo-dT beads that bind to polyadenylated tails, or rRNA depletion, which removes ribosomal RNA to enhance the detection of coding and non-coding transcripts (106).

A.2. Library Preparation and cDNA Synthesis

Library preparation is a crucial step in RNA sequencing, as it involves generating short complementary DNA (cDNA) fragments that are compatible with high-throughput sequencing platforms. This process begins with RNA fragmentation, which breaks RNA molecules into short transcript fragments typically ranging from 50 to 300 base pairs in length. Fragmentation can be achieved through several methods:

- Enzymatic digestion using RNA endonucleases
- Chemical fragmentation with tris-magnesium salt buffer or hydrolysis agents
- Mechanical shearing via sonication or nebulization

Following fragmentation, reverse transcription is performed to convert RNA into cDNA. This is achieved using one of three priming strategies:

- Oligo-dT primers, which selectively bind to the poly(A) tails of mRNA, ensuring that only mature mRNAs are converted to cDNA
- Random primers, which enable the capture of a broader range of RNA molecules, including non-polyadenylated transcripts
- Adaptor ligation, where specialized adaptor oligonucleotides are ligated to RNA fragments before reverse transcription, allowing for strand-specific sequencing Once cDNA is synthesized, adapter sequences specific to the sequencing platform are added, allowing for subsequent amplification and sequencing (107).

A.3. Sequencing and Data Analysis

The final step involves high-throughput sequencing using platforms such as Illumina, PacBio, or Oxford Nanopore, which generate millions of short reads. These reads are then processed through bioinformatics pipelines for transcript identification, quantification, and differential gene expression analysis.

RNA-Seq provides a comprehensive view of the transcriptome, enabling researchers to study gene expression dynamics, alternative splicing patterns, and regulatory RNA elements with unprecedented resolution. The data obtained from RNA sequencing can be applied in various fields, including cancer research, developmental biology, neuroscience, and personalized medicine (108).

B. RNA sequencing applications

The advancement of RNA-seq technology and bioinformatics tools has enabled the investigation of gene expression changes between healthy and diseased individuals, providing deeper insights into the underlying mechanisms of various pathologies.

B.1. RNA sequencing applications with molecular mechanisms of epithelial and immune system regulation

The availability of genome sequences provides opportunities for investigators to study the genetic basis for variation in phenotypes. In particular, gene families in which duplications, rate variation and pseudogenization occur frequently are likely involved in functional innovation and adaptation, exploring their roles in human diseases is crucial. For example, proteins called keratins, are the main components of the cytoskeleton of epithelial tissue. The family of keratins has the largest number of gene members (KRT) in humans with 54 distinct functional genes: 31 epithelial keratins (cytokeratins), 15 specific hair keratins, and eight keratins of the inner root sheath(109, 110). In the same stream, keratinocyte differentiation associated protein (KRTDAP) is a gene associated with epithelial differentiation. Moreover, SPRR2B is considered the protective barrier provided by stratified squamous epithelia relies on the cornified cell envelope, and a structure synthesized at late stages of keratinocyte differentiation (111). It is composed of structural proteins, including involucrin, loricrin, and the small proline-rich (SPRR) proteins. Small proline-rich protein (SPRR) gene family is included SPRR2G, SPRR2B, and SPRR2C. SPRR genes are expressed in stratified squamous epithelia, keratinized and non-keratinized mucosal epithelia (112-115). The expression of SPRR genes increases during normal keratinocyte differentiation (114, 116).

On the other hands, human extracellular matrix (ECM) proteins are represented by 28 different collagens that display functional diversity in tissue homeostasis as well as in pathological conditions (117, 118). COL11A1 is collagen type XI alpha 1 chain. This gene encodes one of the two alpha chains of type XI collagen, a minor fibrillar collagen (119). For the metalloproteinase family, matrix metalloproteinases (MMPs), there are 23 existing MMPs of zinc-dependent endopeptidases that belong to the metalloproteinase superfamily (120). MMPs were traditionally regarded to degrade ECM components and grouped according to their substrate specificity in collagenases, gelatinases,

stromelysins, matrilysins, and membrane type MMPs (108). CXCL8 gene, is another example of gene which associated with inflammation or immune reaction. And gene that related to cells apoptosis which is P53 apoptosis effector related to PMP22(PERP) gene (122, 123). For GATA zinc finger family genes, GATA binding protein 4 (GATA4), is a transcription factor and a member of the GATA zinc finger family, plays a crucial role in the development of heart muscle and maxillofacial tissue and tooth development (124-126). Moreover, HLA-DRA gene is one of the HLA class II alpha chain paralogues. HLA-DRA is a Protein Coding gene. HLA system is the main human histocompatibility system, playing an essential role in the presentation of foreign antigens to T lymphocytes (127). It includes three classes of molecules. Class 1, encoded by A, B, C, E, F, G genes, occurs on the surfaces of all nucleated cells and is involved in the recognition of foreign antigens. Class 2, encoded by the DP, DQ, DR genes, is found in antigen-presenting cells. RUNX1T1 is a gene encodes a member of the myeloid translocation gene family. RUNX1 gene plays a role in hematopoiesis and bone formation (128). Nevertheless, previous studies revealed the RUNX1T1 gene is expressed in many normal tissues (128, 129). Protein encoded by this gene is a member of the ADAMTS family of zincdependent proteases. The encoded protein has a signal peptide that is cleaved to release the mature peptide, which is secreted and found in the ECM and play a role in tissue remodelling process (130). TNN gene is also used as a specific marker of glioma- associated blood vessels and stimulates angiogenesis (131). And HOXB9 gene which is a member of Homeobox genes group. Homeobox genes are a group of genes including HOXA5, HOXB7, HOXB8, HOXC8, and HOXB9 (132-135). Homeobox genes are regulate development in multicellular organisms; this includes cell differentiation and morphogenesis. HOX genes encode highly conserved transcription factors and play crucial roles in embryonic development and oncogenesis, as well as tumor suppression (136).

1.3.4. Treatment of periodontal diseases

Current treatments of periodontitis consist of removal of plaque and calculus, which indeed prevents further disease progression, but these treatments do not regenerate the lost tissues. Instead, histological studies have shown epithelial down growth, a mere reparative type of healing. The advanced procedure to treat periodontal diseases is a traditional periodontal repair technique including open flap debridement, with augmentation of bone graft materials and membranes which enhances regeneration and true healing (137, 138).

1.3.4.1 Non-Surgical Therapy (Professional Mechanical Plaque Removal - PMPR)

Non-surgical therapy serves as the cornerstone in managing periodontal diseases, aiming to halt disease progression and maintain oral health. The primary approach involves scaling and root planing, procedures that meticulously remove plaque and calculus from tooth surfaces and root structures, effectively reducing periodontal pockets and inflammation. Studies have demonstrated that such treatments can lead to significant improvements in clinical attachment levels and probing depth reductions, particularly in sites with initial probing depths greater than 6 mm (139). Additionally, non-surgical periodontal therapy has been associated with enhancements in patient-reported outcomes, including reductions in physical disability, psychological discomfort, and functional limitations (140). Moreover, addressing local risk factors, such as anatomical irregularities and restorative overhangs, is crucial for the long-term success of non-surgical interventions (141).

Collectively, these strategies underscore the efficacy of non-surgical approaches in managing periodontal diseases and improving patients' oral health-related quality of life (139).

1.3.4.2. Surgical periodontal therapy

Surgical therapy plays a pivotal role in managing advanced periodontal diseases, particularly when non-surgical interventions prove insufficient. Procedures such as flap surgery (pocket reduction surgery) involve lifting the ginigva to remove tartar and bacteria from deep periodontal pockets, subsequently securing the gingiva to fit snugly around the teeth, thereby reducing pocket depth and mitigating areas where bacteria can thrive. In cases where periodontal disease has led to bone loss, bone grafting procedures may be employed to promote the regeneration of lost bone, using fragments from the patient's own bone, synthetic materials, or donated bone. Soft tissue grafts are also utilized to reinforce thin gums or fill areas where gums have receded, enhancing both aesthetics and function. The selection of a specific surgical approach depends on the individual patient's condition and aims to restore health and function to the periodontium, preserving the teeth for life (141-144).

1.3.4.3. Supportive Periodontal Care (SPC)

Supportive periodontal care (SPC) is essential for maintaining periodontal health following active treatment. Regular SPC, involving professional mechanical plaque removal and patient education, has been shown to reduce disease recurrence and tooth loss. Evidence indicates that patients adhering to consistent SPC schedules experience better long-term outcomes compared to those without maintenance care. Therefore, implementing a comprehensive SPC program is crucial for sustaining periodontal stability and overall oral health (139).

1.3.4.4 Peri-Implant Disease Management

The management of peri-implant diseases is critical for the long-term success of dental implants. Peri-implant mucositis, characterized by inflammation of the soft tissues surrounding the implant without loss of supporting bone, is the precursor to peri-implantitis. Effective management includes professional mechanical plaque removal (PMPR), reinforcement of oral hygiene practices, and regular monitoring. In cases where peri-implantitis is diagnosed, characterized by inflammation and loss of supporting bone, treatment may

involve non-surgical approaches such as debridement and antiseptic application, or surgical interventions like flap surgery with or without bone grafting, depending on the severity of the condition. The choice of treatment should be individualized based on the patient's specific circumstances and the extent of the disease (142, 143).

Development of periodontal therapeutic procedures requires a deep understanding of the healthy and pathological processes of human periodontal tissues. While animal and human clinical studies are widely used to explore these processes, they are often limited by ethical, technical, and physiological differences, as animal models fail to accurately mimic human tissue (32,33). To address these limitations, advanced in-vitro cell culture models are increasingly employed. These models aim to replicate the unique structure and physiological interactions of gingival tissues, facilitating a better understanding of the pathomechanisms of periodontal diseases (143-146). Therefore, advanced in vitro cell cultures are frequently used as alternatives to animal studies to overcome their limitations, and enduring research is trying to reproduce the gingival tissues in terms of their unique structures and physiological interactions to understand the pathomechanisms of periodontal diseases (147, 148). In-vitro studies range from simpler 2D models to more complex 3D organotypic gingival models. While 2D models lack the complexity needed to accurately mimic the in vivo environment, 3D gingival models are designed to better replicate the structural and physiological conditions of human gingival tissue (149). However, developing 3D gingival models requires selecting suitable biomaterials that support cell adhesion, growth, proliferation, and differentiation. Various biomaterials, including natural, synthetic, and semi-synthetic types, have been used for cell culture and scaffold engineering to mimic the human extracellular matrix (ECM) (150).

1.4. Tissue engineering in periodontal regeneration

Tissue engineering (TE) is an interdisciplinary field that has been studied since the 1980s as a method to regenerate pathologically damaged tissues through combined three elements, which are cells, biomaterials as a scaffold, and growth factors (151, 152) (Figure 1.7). TE is viewed as synonymous with periodontal regeneration because the goal is to complete restoring normal physiological functions and health to a diseased site. The regeneration of even a small amount of tissue can be highly beneficial to the patient (153).

Periodontal tissue engineering (PerioTE) has been developed for clinical applications and also for in-vitro studies. Cell culture is one of the major in-vitro tools used in cellular and molecular biology, which provides excellent gingival model systems for studying the normal physiology and biochemistry, the effects of drugs and toxic compounds on the cells, mutagenesis, and carcinogenesis. Moreover, cell culture is considered the most promising area expected to improve the success rates in Perio TE because of in-vitro gingival models that better recapitulate *in vivo* biology and microenvironmental factors (154).

1.4.1. Two-dimensional (2D) cell cultures

Two-dimensional (2D) cell cultures have been used for many years as an acceptable in vitro model to study the responses of gingival cells to different stimulations from external environmental prompts. The cells in 2D cultures are grown as a monolayer in a culture flask or a flat petri dish, and attached to a plastic surface (155-158). Initially Rheinwald and Green (1975) introduced a method of growing monolayer human keratinocytes using a feeder layer of 3T3 mouse fibroblasts and a specific culture medium called Green's medium. This method is frequently used for the culture of keratinocytes and the production of monolayer epithelial sheets, which is achieved by the use of lethally irradiated 3T3 cells at the correct density (159). Later, these monolayer oral keratocytes had been produced without 3T3 cells feeder layer (160, 161). 2D cell culture is a simple and low-cost maintenance tool, in addition, it's commonly used in drug discovery. However, the lack of a heterogeneous cell population in 2D models and normal cell differentiation hindered their potential to form more complex tissue- or organ-like structures which can be found in 3D cell culture (152). These drawbacks lead to failures in understanding cell behaviour in healthy or

diseased states (163-165). To this end, there was a need for 3D cell cultures as an alternative model with a multilayers system, to better mimic the microenvironment of native gingival tissue.

1.4.2. Three-dimensional (3D) cell cultures

3D cell culture is a generalized term that is used to mention the differences between conventional and new cell culture technologies and is defined as a vitro tool of the specific tissue microenvironment. To compare with 2D cell cultures, 3D cell cultures have many advantages. In 3D cell culture, the individual cell has the ability to grow in multilayers pattern, with maintaining their 3D shape and functions, as well as to interact with their surroundings and a heterogeneous population of neighbouring cells, establishing sufficient signalling networks, and providing an accurate way for cell-to-cell and cell-to-extracellular matrix interaction much like the interactions of cells *in vivo* experience (166, 167).

3D functional tissue constructs play a crucial role in regenerative medicine and tissue engineering, as they aim to replicate the structural, biological, and mechanical properties of native tissues. These constructs must be designed with precision to ensure they support cell growth, differentiation, and integration with the surrounding biological environment. Additionally, their mechanical characteristics, such as elasticity, strength, and degradation rates, must be carefully tuned to match the specific requirements of different tissue types. Advancements in biomaterials, bioprinting techniques, and scaffold fabrication have enabled the development of highly specialized 3D tissue constructs that can promote effective tissue regeneration, wound healing, and organ repair (168).

Furthermore, the 3D gingival models are played a significant role in the investigations of physiological and pathological environments of gingival tissues (169, 170). These models are either partial thickness or full thickness cell cultures according to the absence or presence of connective tissue layer within this model.

A. Partial thickness 3D gingival cell cultures

The first engineered 3D gingival model was developed with partial thickness epithelium multilayers without underlying connective tissue, using oral human epithelial cells (161-173). The keratinocytes cultured on permeable cell culture membranes at the air/liquid interface to facilitate the construction of multilayer sheets of epithelium that mimic native epithelial differentiation, such as basement membrane formation, different cytokeratin expression, and keratinization if the origin of the keratinocytes is keratinized mucosa. There are commercial partial-thickness models such as MatTek's EpiGingival, Human Gingival Epithelium HE, and Reconstructed Human Gingival (84-86).

The disadvantage of these model systems is lack of a connective tissue layer represented by fibroblast cells embedded with matrix components. The fibroblast cells are not only critical in promoting growth and differentiation of keratinocytes into stratified squamous epithelia but also ensures mimic of the tissue model to the native human gingival tissue (35,40,41).

B. Full thickness 3D gingival cell cultures

Due to the disadvantages of partial thickness 3D gingival model, Therefore, in the last three decades, research has concentrated on the development and characterization of the gingival model by introducing full thickness of 3D gingival model prepared with multilayer sheets of epithelium grown with underlying dermal scaffolds which represent connective tissue layer by using both epithelial cells and fibroblasts to recapitulate native gingival tissue, and the applications for in vitro studies provided more significant results regarding physiological and pathological conditions (174-181).

1.4.2.1. Fundamental principles for designing 3D gingival models

Proper selection of materials and the environments are considered significant to design a successful 3D gingival model with a high level of physiologic

complexity and mimic native human gingival tissue(172). Designing an engineered 3D gingival model should be included three basic components including cells, scaffold or substrate, and growth factors (Fig 1.7).

1.4.2.1.1. Cells

Numerous cells have been used in 3D gingival model construction, such as human primary cells or immortalized cells. Several studies used primary human gingival keratinocytes and fibroblasts for the construction gingival model (178, 183-188) and one study formed 3D peri-implant model (189) because primary cells are more typical of the morphological and functional features of the tissue they are derived from. However, the primary cells have drawbacks such as difficulty to obtain and maintain for long-term experiments.

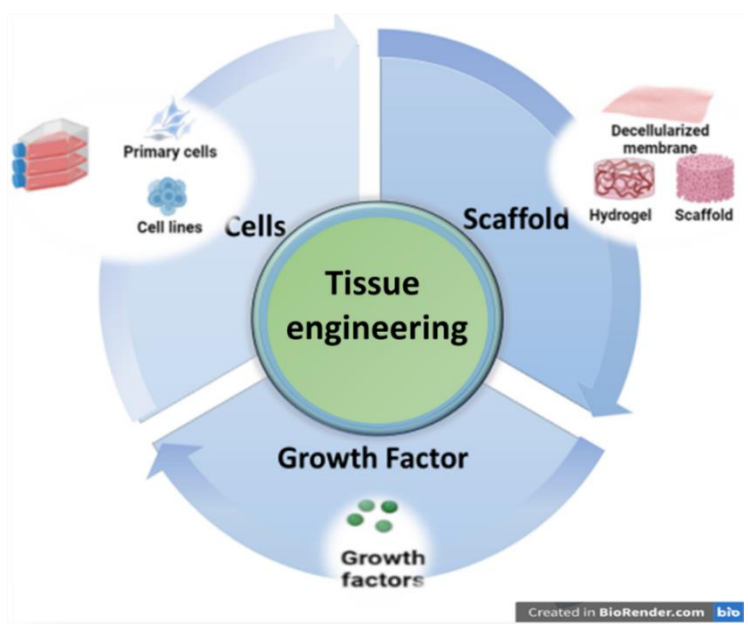


Figure 1.7. Tissue engineering triad. Scaffolds, cells, and growth factors are used in isolation or in combination to recapitulate the desired tissue. Created with BioRender.com.

Moreover, they have low proliferation rates and must be used in early passage stages because they lose their structural, functional, and self-renewal properties as they undergo elderliness processes. Cells from different donors differ in their growth rates and life span in vitro, in addition to behaving differently in case of immune responses (190-192).

Recently, 3D gingival models have been prepared using human gingival cell lines to overcome the limitations belong primary cells (187, 193-198), in addition, using a combination of human primary and cell lines (180, 188, 199-101), because using cell lines has several advantages, for instance, easy to use, inexpensive, unlimited availability, reproducibility, and no need of ethics approval. However, they are not considered ideal sources for modelling human conditions since they do not exhibit normal features, often drifting from the genetic and phenotypic profile of the tissue of origin (191).

1.4.2.1.2. Biomaterials and Scaffolds

Different biomaterials are used to prepare substrates to act as ECM, and the big challenge is to choose the proper one for this mission, to mimic natural human ECM (102). Proper selection of biomaterials to fabricate substrate can aid in designing a 3D gingival model with a high level of structural complexity that mimics native human gingival tissue. In cell culture models, the role of the substrate is to provide embedding cells with the appropriate template to adhere, proliferate, differentiate, maturate embedding cells. A proper scaffold is also necessary to provide cell-cell and cell-scaffold interactions that will enable cells to auto-organize as they would in native tissue.

Biomaterials can be divided into natural and synthetic materials, based on their origin and whether they contain naturally occurring ECM (103). For example, acellular dermis scaffold is used to prepare a 3D gingival model, from this type is acellular cadaver dermis from the human origin (178). While strattice matrix, and Matriderm from porcine and bovine origin respectively (185, 101). The advantages of this type of substrate are good durability, and the ability to retain its structural properties. Whilst the disadvantages are expensive and not easily available. From synthetic substrate used in 3D gingival model, construction was Vicryl, which is a surgical mesh of woven polyglycin (186). The synthetic scaffold has good mechanical properties, and there is no risk of disease transmission. However, this substrate has poor biologic properties. In addition,

several studies have demonstrated different types of hydrogel biomaterials as a substrates to construct 3D gingival model.

1.4.2.1.2.1. Hydrogel biomaterials

Biomaterials, particularly biodegradable polymer hydrogels, are widely utilized in tissue engineering and 3D cell culture due to their structural and functional resemblance to the ECM (138, 139). Hydrogels are hydrophilic, three-dimensional networks composed of water-soluble polymers, providing an environment that closely mimics the complexity of the native ECM (111).

The effectiveness of scaffolds in tissue engineering is largely dependent on the properties of hydrogels, which dictate their physical and biological characteristics. By manipulating biophysical cues, hydrogels can replicate the native ECM where cells reside. Furthermore, their high water content contributes to excellent biocompatibility and superior drug encapsulation capacity (140).

Hydrogels can be categorized into natural and synthetic biomaterials based on their origin and whether they incorporate naturally occurring ECM components. Natural hydrogels, including collagen, hyaluronic acid, fibrin, chitin, gelatin, chitosan, carrageenan, and alginate, are particularly beneficial in tissue engineering. Most natural hydrogels, except for alginate, possess intrinsic binding sites that facilitate interactions between cells and the hydrogel matrix. These properties promote cell adhesion, proliferation, and tissue regeneration (141-143). Given their resemblance to the native cellular microenvironment, hydrogels play a crucial role in tissue engineering applications.

Among the various characteristics of hydrogels, mechanical properties are particularly significant, as they influence cellular behavior during culture. Precise control over hydrogel mechanics is essential for directing cell differentiation, and these properties can be finely tuned to recreate natural microenvironments (144).

Gelatin (Gel) and sodium alginate (SA) are natural polymers that can form hydrogels and have been widely explored in biomaterials research. Gelatin, derived primarily from bovine or porcine sources (145, 146), shares a molecular composition similar to collagen but lacks the same level of organization. It is cost-effective, readily available, highly soluble, and easy to use. Additionally, gelatin from various sources has demonstrated biocompatibility, biodegradability, and minimal antigenicity or toxicity in cells (144).

Alginate, a naturally occurring polysaccharide, is extracted from brown algae and offers several advantages, including low cost, ease of gelation, and excellent biocompatibility. To produce sodium alginate for commercial use, raw alginate undergoes alkaline treatment, typically with sodium hydroxide, followed by further reaction and purification processes (147).

Furthermore, gelatin methacrylate (GelMA) is a semi-synthetic hydrogel derived from gelatin through methacrylamide coupling. It is considered a highly versatile material for numerous bioapplications, particularly in 3D cell culture and tissue engineering (148).Recent studies by various investigators have explored the combination of SA and GL as a potential biomedical hydrogel due to its cell compatibility and ability to form 3D cell cultures (104, 105). In another study , SA has been proved to be offering promising improvements to GelMA-based scaffolds (106). Moreover, in microfluidic bioprinting technique, Liu et al investigated using fiber of alginate which crosslinked by CaCl₂ then UV crosslinking of GelMA hydrogel. Hollow alginate microfibers were used as templates for generating cell-laden GelMA. They considered this strategy might provide broad opportunities in bioprinting 3D constructs with cell favourable microenvironments for applications in tissue engineering and pharmaceutical screening (107).

Recent advances have highlighted the potential of these hydrogels in bioprinting and microfluidic applications. For instance, GelMA-based scaffolds reinforced with alginate fibers allow precise control over architecture and provide mechanically robust yet biologically permissive environments for cells. Such

strategies are particularly promising for developing in vitro gingival models, as they facilitate the recreation of tissue specific microenvironments that closely mimic the native gingiva. By tailoring hydrogel composition, crosslinking methods, and mechanical properties, researchers can design 3D constructs that support functional tissue formation and enable more physiologically relevant studies (230, 233).

1.4.2.1.2.2. Hydrogel sterilization methods

For using hydrogels in various experiments, it is critical to ensure the safety and sterility of these hydrogels biomaterials to prevent infection and ensure the success of the studies (208). Several methods are used to sterilize hydrogel biomaterials, including autoclaving, ethylene oxide gas (EOg) (2) (209, 210), gamma irradiation (211), ethanol treatment (212), and filtration (213). Each method has its advantages and drawbacks. For instance, autoclaving and EOg methods can reduce hydrogel stiffness, while gamma irradiation can increase stiffness (214). Additionally, sterilization methods may affect hydrogel biocompatibility and cellular responses, including cell adhesion, signaling, proliferation, and differentiation (215-218).

1.5. Mechanical characteristics of human gingival tissue

The selection of a suitable hydrogel substrate with properties that mimic native human gingival tissue is required to construct a successful 3D gingival model. Therefore, it's important to understand the structural and functional roles of each counterpart of native human gingival tissue. One of the fundamental parameters in defining material behaviour is elastic modulus, which is the physical description of a material's elasticity. In the human body, the oral mucosa was found to be highly deformable under compression, and the elastic modulus appears to vary over a broad range. Being a heterogeneous material, the mucosal instant stiffness results from both the solid matrix structure (e.g. epithelial layer, fibrous network, blood vessel, etc.) and the fluid components

(e.g. interstitial fluid, blood). Several material models have been developed to interpret such mucosal behaviours (217).

A study investigating the mechanical properties of Thiel-embalmed human oral mucosal tissues across different regions reported variations in elastic modulus. The mean of elastic modulus of human attached gingiva is 37.4 ± 17.4 MPa. This value is considered higher than other regions in the oral cavity, hard palate, and buccal mucosa. In the same vein, the scanning electron microscopy (SEM) images revealed human gingiva tissues with predominantly unidirectional collagen fiber networks and unravelled elastin, which stands behind its elastic properties of it, whereas the buccal mucosa and hard palate displayed multi-directional collagen arrangements, making them more susceptible to tension failure and less elastic (218).

Several studies have characterized 3D gingival and peri-implant models, often constructed using organotypic culture techniques (187, 219-223). Koskinen & Qu found that models using crosslinked rat tail collagen as a substrate were larger than non-crosslinked ones (222). To assess 3D gingival models, histological evaluation remains crucial for assessing these models, employing staining methods such as H&E, PAS, and Masson's trichrome to analyze epithelial thickness, cellular differentiation, and connective tissue structure. While 3D gingival models are widely used in periodontal research, their ability to replicate clinical conditions remains unclear. Recent advancements have led to full-thickness models incorporating human gingival keratinocytes and fibroblasts, yet no standardized fabrication protocol exists. A systematic evaluation of these models is necessary to assess their physiological accuracy, optimize biomaterials, and improve their translational potential for periodontal disease research and regenerative medicine (188, 189, 199, 101, 219, 224-227).

1.6. Rationale for Proposed research

3D gingival model is considered as an advanced vitro tool, used to describe native human gingival structures emerging from the combination of 3D cell biology with tissue engineering principles. The researchers constructed several types of 3D gingival models using different cell origins, and different biomaterials as a substrate to mimic extracellular matrix. However, there are several types of constructed gingival models in terms of potential physiological complexity, and types of substrates to determine the level of mimicking to native gingival tissue. The main limitation in gingival model construction is the lack of specific cell origin and specific scaffold materials to carry these cells.

This knowledge gap underpins the need to:-

- Comprehensively appraise the current available 3D gingival models and the strategies for constructing these models, to evaluate the most proper cell source and suitable scaffold to carry the cells.
- Investigate in vitro commonly used biomaterials for 3D cell culture, evaluating their mechanical properties and biocompatibility to determine how closely they resemble the native human extracellular matrix.
- Engineer a simple and cost-effective hydrogel mimics to natural extracellular matrix to use it in 3D gingival model construction. Engineered hydrogel should be potential to carry human gingival cells.

1.7. Hypothesis and objectives of the study

We hypothesized the possibility to construct a developed 3D gingival model. 3D gingival model is considered as an advanced in-vitro tool, used to describe native human gingival structures emerging from the combination of 3D cell biology with tissue engineering principles. Developed 3D gingival model could recapitulate the microenvironment of human gingival tissue within two different conditions, healthy or diseased.

Heading forward for the next projects in our research areas, we must appraise current available 3D in vitro gingival models in a systematic review. At the same time, we must determine the available substrates that are used successfully in reconstruction of this model.

The primary aim of this study is to identify the molecular, biological differences and functions in native human gingival tissue with two different conditions, healthy and diseased. using NanoString GeoMx profiling technique in the study of gene expression enhances our comprehension of the physiological processes and underlying mechanisms involved in wound healing and soft tissue regeneration of periodontitis compared with healthy human native gingival tissue. The two types of tissue, healthy and diseased gingival tissues might express the same specific genes related to their functions. Results from molecular analysis of both healthy and diseased human gingival tissue samples will provide some novel insight into the characterization and molecular mechanisms of gingival tissues.

According to the fact of that, the success of cell culturing technique based on proper selection of substrate to carry target tissue cells. In our study, we should engineer a simple and cost effective substrate mimics to natural extracellular matrix to construct a developed 3D gingival model. The engineered substrate should have the potential to carry human gingival cells. For this, we must investigate the physical and biological properties of a set of hydrogel

biomaterials, that could help in engineering a novel substrate to construct 3D gingival model.

It is hypothesized that engineering a novel GelMA–sodium alginate (GelMA-SA) composite hydrogel could facilitate the construction of a functional 3D gingival model. Optimization of GelMA-SA composites was performed by characterizing their biochemical, mechanical, and biocompatibility properties in comparison with other hydrogel samples. In this context, GelMA-SA composites provide a supportive platform for human gingival cells. Crosslinking methods were investigated for their role in fine-tuning the mechanical properties of these hydrogels, aiming to match the characteristics of native animal gingival tissue, including sheep and porcine.

Further optimization of the substrate included evaluating sterilization methods and different double crosslinking sequences (CaCl₂/UV and UV/CaCl₂) to enhance the structural and functional properties of GelMA-SA hydrogels.

Briefly, GelMA-SA composites have been researched to optimize their use as a substrate for seeding of both primary human gingival fibroblast, and cell line of human gingival epithelial cells and construct 3D cell culture applications, particularly towards construct 3D gingival model as a developed in vitro tool, has been researched throughout this PhD project and presented in this thesis.

To address this hypothesis, the main objectives of the study are:-

- 1-To appraise current available 3D in vitro gingival models constructed using organoid cell culture system by performing a systematic review. This systematic review is to evaluate the extend of these models to replicate the native human gingival tissue in terms of their structure, differentiation characteristics, and barrier function. Moreover, to determine the types of the available substrates which are frequently used to reconstruct 3D gingival models.
- 2- To explore specific potential genes target of periodontitis gingival tissue and compare with healthy gingival tissue using NanoString GeoMx profiling technique.

- 3- To investigate the physical and biological properties of hydrogels as a physically effective substrate to a construct 3D gingival model.
- 4- To develop and evaluate the biochemical, mechanical, and biocompatibility properties of a number of novel hydrogels that could potentially be used as a substrate for a 3D, human-based, gingival model using different investigation technique. Additionally, the study investigates the effects of single (CaCl₂ or UV) and double (CaCl₂/UV and UV/CaCl₂) crosslinking methods on the structural and functional characteristics of the hydrogels, with the goal of optimising their suitability for seeding human gingival cells and supporting 3D cell culture applications. In addition, the properties of these engineered hydrogels compare to the in vitro biomechanical behaviours of sheep and porcine oral tissues as a representative model system.
- 5- To evaluate and compare the sterilization efficacy and impact of two commonly used sterilization methods, filtration and ethanol on the biochemical, mechanical, and biocompatibility properties of GelMA and SA hydrogels. Additionally, the study investigates the influence of different double crosslinking sequences (CaCl₂/UV and UV/CaCl₂) on the hydrogels' structural and functional characteristics to optimize their use in seeding human gingival cells and construct 3D cell culture applications.

Desired properties ('wish list') of the 3D gingival model:

- Structural fidelity: recapitulate the native gingival epithelial-connective tissue architecture
- Barrier function: intact epithelial layer capable of selective permeability
- Mechanical properties: stiffness and elasticity comparable to native gingival ECM
- Biocompatibility: support adhesion, proliferation, and differentiation of human gingival cells

- > Cost effectiveness and reproducibility: simple, reliable model suitable for routine laboratory use
- > Tunability: ability to modify biochemical and mechanical characteristics for experimental purposes

To accomplish these objectives, the study combines biomaterial development, extensive physical and chemical characterisation, 3D cell culture, cytotoxicity and biocompatibility assessment, and histological evaluation of constructed 3D gingival models.

CHAPTER 2

2. GENERAL MATERIAL & METHODS

2.1. Material

Instruments, equipment, and specific items used in this thesis are mentioned within the methodology section. Meanwhile, commonly used chemicals and reagents are listed in Table 2.1 below.

Table 2.1. Chemicals/reagents and their suppliers used

Chemical/Reagent

Grade/Supplier

Gelatin from bovine skin, Type B,	G9391, Sigma-Aldrich, UK	
powder		
GelMA, 80% (commercial)	(porcine gelatin origin, Sigma, 900496-	
Genuia, 60% (commercial)		
	1G, UK).	
Carbonate bicarbonate buffer	C3041, Sigma-Aldrich, UK	
Methacrylic anhydride (MA)	MAA, 94% Sigma-Aldrich, UK	
HCL	Ab176753, Abcam, UK	
	DOE42 Sigma Aldrigh LIV	
	D9542, Sigma-Aldrich, UK	
NaOH		
Dialysis membrane	12.4 kDa Molecular Weight Cut-off,	
·	Sigma-Aldrich, UK	
	Signia-Alunch, OK	
Deuterium oxide, 99% (D ₂ O)	151882, Sigma-Aldrich, UK	
NMAD tube	Milmod® NMD tubes E mm diam	
NMR tube	Wilmad® NMR tubes 5 mm diam.,	
	precision, Sigma-Aldrich, UK	

Phosphate Buffer Saline	Gibco™ PBS, pH 7.4, Fisher Scientific UK
Photo initiator (PI) of lithium phenyl-	LAP; >95%, Sigma-Aldrich, UK
2,4,6-trimethylbenzoylphosphinate	LAI , 79070, Sigilia-Aldiloli, Olt
Sodium alginate powder	Alginic acid sodium salt from brown
	algae, Algin, Sigma-Aldrich, UK
Calcium chloride	Calcium chloride, Sigma-Aldrich, UK
Collagen type I from rat tail	Roche, UK
Acetic acid	A6283-100MLSigma-Aldrich
10X DMEM, (Dulbecco's Modified	Sigma-Aldrich, UK
Eagle Medium)	
(low glucose 10X, 1000 mg/L	
glucose(1X), without L-glutamine,	
sodium bicarbonate & folic acid, liquid,	
sterile-filtered, suitable for cell culture)	
	ACS reagent, 37%, Sigma-Aldrich, UK
Trypan Blue	
Triton-X	Sigma-Aldrich, UK
DMEM, (Dulbecco's Modified Eagle	Sigma-Aldrich, UK
Medium)	
(high glucose 4500 mg/L , L-	
glutamine, sodium pyruvate, and	
sodium bicarbonate, liquid, sterile-	
filtered, suitable for cell culture)	
Fetal bovine serum (FBS	P4333, Sigma- Aldrich, UK
penicillin-streptomycin	BE17-516F, Lonzo, UK
Serum free media (K-SFM),	Gibco™ Keratinocyte SFM (1X),
(Keratinocyte-SFM is supplied with	Fisher Scientific UK

prequalified human recombinant Epidermal Growth Factor 1-53 (EGF 1- 53))	
Cell freezing media	H1138, Sigma-Aldrich, UK
Ethanol 99% extra pure	Fisher Scientific, 10375842, UK
One Solution Cell Proliferation assay kit	CellTiter®® 96 Aqueous (Promega, Southampton, UK)
lactate dehydrogenase (LDH) release assay kit	CytoTox 96®® Non-radioactive Cytotoxicity Assay kit (Promega, Southampton, UK)
LIVE/DEAD™ imaging kit	(488/570) (Fisher Scientific UK Ltd., Loughborough,UK)
Formalin solution, neutral buffered, 10%	Sigma- Aldrich, UK

2.2. Methods

2.2.1. Synthesis of Gelatin methacryloyl (GelMA) and purification

GelMA-UCL was prepared in three batches (GelMA-UCL1, GelMA-UCL2, and GelMAUCL3), following the protocol described by previous studies (115, 228, 229). In brief, gelatin, (10 g) was dissolved at 10% (w/v) in carbonate-bicarbonate (CB) buffer (0.25 M, 100 mL) at 55 °C, and then the pH of the gelatin solutions was adjusted to 9.4. Methacrylic anhydride (MAA) were separately added to the gelatin solutions under magnetic stirring at 300–400 rpm, in the dark by wrapping the glass conical flask with aluminium foil to prevent light exposure. All subsequent steps were performed under dark conditions to avoid premature photopolymerization. The reaction proceeded for 3 h at 55 °C, and the final pH of the reaction solutions was adjusted to 7.4 using 6 M HCl acid. To

remove salts and unreacted excess free methacrylic acids, solution was filtered and dialyzed against deionized water for five days, and at 40 °C using a cellulose tubing dialysis membrane. The dialysis tubes were placed in a glass conical flask and wrapped with aluminium foil to protect the solution from light exposure. Deionized water was changed 2-3 times per day. Then the dialyses process, purified solution was collected in light-sensitive container and frozen at -80 °C.

The GelMA-UCL solution, kept in the same light-sensitive containers, was transferred to a freeze-drying valve flask, which was then wrapped in aluminum foil to prevent light exposure. The samples were freeze-dried using a Heto Dry Winner freeze dryer connected to an Edwards RV5 pump (UK), operating at a pressure below 50 mbar and a chiller temperature of –100 °C for 48 hours. The resulting foam-like product was then collected and stored at room temperature in light-protected containers for future experiments.

2.2.2. Preparation of hydrogel samples

Type of hydrogel

In this study, a range of hydrogel formulations were prepared to compare their physical and biological properties for gingival tissue engineering (Table 2.2).

Table 2.2. Hydrogel formulations prepared and tested in this study. Gelatin and GelMA commercial were investigated at both high (10%) and low (2.5%) concentrations. Sodium alginate (SA) was used as an additional hydrogel component at two concentrations (3.5% and 2.5%). GelMA was prepared inhouse at UCL (GelMA-UCL), with photoinitiator (PI, 0.3%) added for crosslinking. Hybrid formulations were developed by combining GelMA with sodium alginate at different concentrations.

GelH	Gelatin (high concentration, 10%)
GelL	Gelatin (low concentration, 2.5%)
GelMA-UCL	Gelatin (concentration, 10%), prepared in-house at UCL
	GelL

Composition & Description

GelMA commercial (GelMA-com)	GelMAcH	GelMA commercial (high concentration, 10%) GelMA commercial (low concentration, 2.5%) GelMA-UCL (high concentration, 10%) GelMA-UCL (low concentration, 2.5%) GelMA-UCL (10%) + photoinitiator (0.3%) Sodium alginate (high concentration, 3.5%)		
	GelMAcL	· ·		
GelMA-UCL	GelMAH	GelMA-UCL (high concentration, 10%)		
GENVIA-GGE	GelMAL	GelMA-UCL (low concentration, 2.5%)		
GelMA		GelMA-UCL (10%) + photoinitiator (0.3%)		
SAH				
SAL		Sodium alginate (low concentration, 2.5%)		
GelMA-SA composite	GelMA-SAH	GelMA combined with Sodium alginate (3.5%)		
	GelMA-SAL	GelMA combined with Sodium alginate (2.5%)		

2.2.2.1. GelMA-UCL

GelMA-UCL was prepared in the dark and using light sensitive containers. It was prepared in three formulae. 2.5 wt% (GelMAL) and 10 wt% (GelMAH) solution by weighing the appropriate amount of GelMA-UCLand dissolving in PBS solutions by magnetic stirring in deionized water for up to 1 h at <40 °C. Abbreviation of "L" corresponds to "low" concentration, whereas "H" corresponds to "high" concentration of GelMA-UCL. The third formula was (GelMA). GelMA hydrogel solution was prepared by mixing of prepared GelMAH with 0.3% w/v Photo initiator (PI). Followed by mixing by magnetic stirring for up to 30 minutes at 40 °C.

2.2.2.2. GelMA commercial (GelMA-com)

In addition, GelMA-com was prepared in the dark and using light sensitive containers in two formulae, 2.5 wt% (GelMAcL) and 10 wt% (GelMAcH) solution

by weighing the appropriate amount of Gel and dissolving by magnetic stirring in PBS for up to 1 h at 40 °C.

2.2.2.3. ¹H-NMR (Nuclear Magnetic Resonance) hydrogel samples

GelMA-UCL (GelMA-UCL1, GelMA-UCL2, and GelMA-UCL3), and GelMA-com hydrogel samples were prepared in the dark and using light sensitive containers by dissolving of 20 mg of each sample in 800 µL of D₂O (as a solvent), at 40 °C until fully dissolved. The solutions were then transferred into glass NMR tubes, wrapped with aluminum foil to protect from light exposure, and transported to the NMR laboratory for analysis.(Department of Chemistry, UCL/ https://www.ucl.ac.uk/nmr/)

2.2.2.4. Gelatin

Gelatin from bovine skin, Type B, powder, was prepared in two formulas, 2.5 wt% (GelL) and 10 wt% (GelH) solution by weighing the appropriate amount of Gel and dissolving by magnetic stirring in deionized water for up to 1 h, at 40 °C.

2.2.2.5. Sodium alginate (SA)

Sodium alginate (SA) was prepared in two formulae, 2.5% wt (SAL) and 3.5% wt (SAH). Here, 'L' refers to the low concentration of SA, and 'H' refers to the high concentration. SA solution was prepared by weighing the appropriate amount and dissolving it by magnetic stirring in deionized water for up to 1 hour at 40 °C (230).

2.2.2.6. GelMA-SA composite

GelMA-SA composite hydrogel

solution was prepared in the dark and using light sensitive containers, and in two formulas, GelMA-SAH and GelMA-SAL hydrogel solutions. GelMA-SA composite hydrogel solutions were prepared by mixing equal amounts of prepared GelMA either with prepared SAH to form GelMA-SAH, or with prepared SAL to form GelMA-SAL hydrogel solutions, followed by mixing by magnetic stirring for up to 30 minutes at <40 °C. These formulations are

collectively referred to in this thesis as "composite hydrogels" (GelMA-SAH and GelMA-SAL), reflecting the combination of GelMA with sodium alginate.

2.2.2.7. Rat tail collagen

Collagen type I from rat tail hydrogel solution, was prepared and developed following the modified protocol as described by Dongari-Bagtzoglou and Kashleva (188). The mixture was prepared on ice and neutralized to pH 7.4. Initially, 10 mg of rat tail collagen type I lyophilizate was dissolved by gently pouring 2 ml of sterile 0.2% (v/v) acetic acid into the container without stirring and allowing it to sit for 30 minutes. A sterile stirrer bar was then added, and the solution was stirred for an additional 30 minutes, or until the collagen was fully dissolved. Subsequently, 0.2 ml of 10X DMEM was added, resulting in a yellowish coloration. Neutralization was achieved by gradually adding approximately 8 drops of sterile 1 M NaOH, causing the solution to turn pink. The prepared hydrogel solution was transferred into a container with a tightly sealed lid and stored in the refrigerator until use.

2.2.3. Hydrogel sterilization methods

In this study, two different sterilization methods were used for the hydrogel samples: filtration and ethanol-based sterilization. It is important to note that following sterilization, all sample containers were tightly sealed to maintain sterility. It is important to note that all sterilization procedures were performed inside a laminar flow hood, further more under dark field conditions with GelMA hydrogel solution to protect the light sensitive. Following sterilization, all sample containers were tightly sealed to maintain sterility and were only opened inside the hood when necessary

2.2.3.1. Filter method:

Filtration of hydrogel biomaterials is a commonly used sterilization method (213, 231). In this study, and apart from rat tail collagen hydrogel solution, all hydrogel solutions, were sterilized using 0.22 µm pore-size syringe filters (Fisher Scientific UK Ltd., Loughborough, UK), inside a laminar flow cabinet. The filtered hydrogel solutions were also placed in sterilized tubes but stored at 4 °C until

further use. Sterilization of calcium chloride (CaCl₂), 70% ethanol, acetic acid, and NaOH solutions were also performed by filtration. Each sterilized solution was stored in sterilized tubes at room temperature (~20 °C) until use. Before application, the samples were warmed to 37 °C to ensure complete solubilization for downstream experiments

2.2.3.2. Ethanol method:

70% ethanol is another commonly used sterilization method for hydrogel biomaterials (112, 232). However, the United States Food and Drug Administration (FDA) does not recommend this method for sterilizing Class 3 medical devices. To evaluate the effects of ethanol treatment on hydrogel properties, GelMA-SA composite hydrogel solutions, and inside a laminar flow cabinet were immersed in sterile-filtered 70% ethanol by adding twice the volume of each hydrogel sample. The hydrogels were left in the ethanol solution for 20 minutes within a laminar flow cabinet. The container could be gently shaken to enhance penetration of ethanol. After this, the excess ethanol was removed, with careful discarding it without touching the hydrogels. It might use sterile forceps if was needed to transfer samples. Then, and to help removing any residual ethanol, which harm the cells, the hydrogel samples should be washed with PBS with 1-2 times. After final wash, samples were left for 10 minutes to allow the residual ethanol to evaporate. The sterilized hydrogel solutions were also placed in sterilized tubes and were stored at 4 °C until warm them before use.

2.2.4. Crosslinking procedures for hydrogel samples

Prior to distribution into the well plate inserts for crosslinking, all hydrogel samples, except for the rat tail collagen, were warmed and thoroughly mixed using a magnetic stirrer at 40 °C. to ensure homogeneity. The rat tail collagen was directly distributed into the inserts without warming. Following these steps, the crosslinking procedure was carried out.

2.2.4.1. Single crosslinking procedures

The prepared rat tail collagen hydrogel mixture was crosslinked by incubating at 37 °C with 5% CO₂ for either 2 hours and referred to as R collagen (2h), or overnight, referred to as R collagen, to complete the collagen gelation.

The GelMA solution was cast while warm into the desired well plate and then allowed to rest at 4 °C for 10 minutes to facilitate physical gelation prior to final crosslinking. All steps were performed under dark conditions within a laminar flow cabinet to protect the light sensitive material. The final UV crosslinking was carried out using ultraviolet light inside the UV chamber of the crosslinking device. When transferring the well plates outside the cabinet, they were immediately wrapped in aluminium foil to prevent light exposure (UV) (UV;XYZPrinting UV chamber, Model 3UD10, Taiwan, UV LED (λ 375–405 nm, 16 W)) for 60 s (213).

SA samples were crosslinked using CaCl₂ crosslinking procedure. This method performed by adding an aqueous solution of Ca²⁺, typically prepared using sterile CaCl₂ solution and cross-linked by using sterilized CaCl₂ solution at a concentration of 50 mM (230). SA hydrogels were left in the CaCl₂ solution for 5-7 minutes at room temperature ~20 °C, within a laminar flow cabinet. After this, the excess CaCl₂ solution was removed.

GelMA-SA composite hydrogel solutions were crosslinked using a single crosslinking method with either CaCl₂, or UV to determine properties of these hydrogel solutions. These crosslinking methods, either CaCl₂, or UV are performed as stated above.

2.2.4.2. Double crosslinking procedures

GelMA-SA composite hydrogel solutions were crosslinked using 2 different techniques to ascertain the importance of sequential crosslinking (Fig. 2.1). Double crosslinking procedures are performed by either CaCl₂ crosslinking procedure followed by the UV crosslinking procedure which referred to as (CaCl₂/UV) as shown in figure 2.1 (Technique 1), or with the UV crosslinking procedure and followed by CaCl₂, which referred to as (UV/CaCl₂), as illustrated in Figure 2.1 (Technique 2).

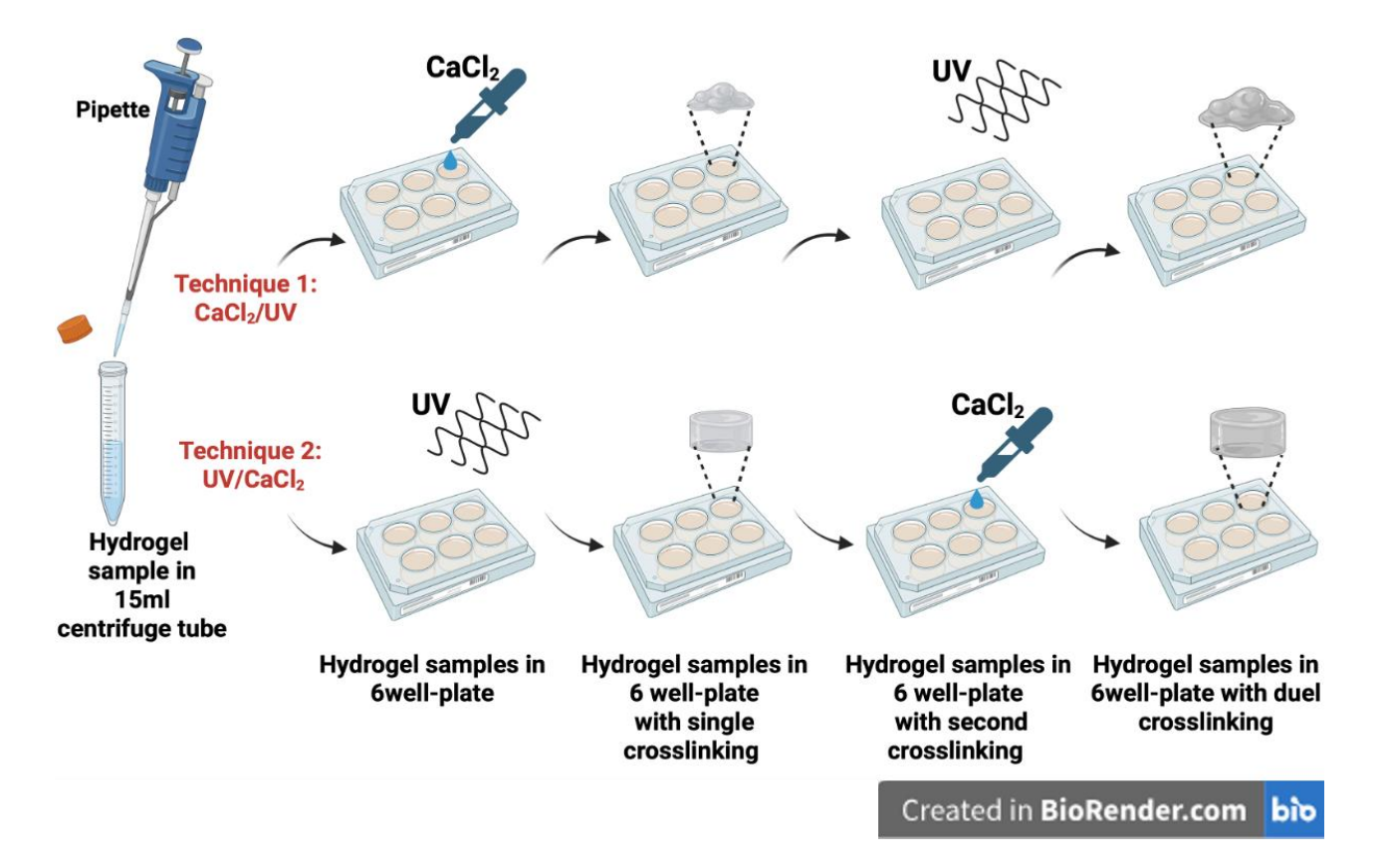


Figure 2.1. Schematic drawing illustrating the double crosslinking procedures for GelMA-SA hydrogels using $CaCl_2$ and UV, with two different techniques: Technique 1 ($CaCl_2/UV$), ionic crosslinking with $CaCl_2$ was carried out first, followed by UV-induced photo-crosslinking. In Technique 2 ($UV/CaCl_2$). was performed by applying UV first, followed by ionic crosslinking with $CaCl_2$. Created in BioRender.com.

Double crosslinking procedures are performed by either CaCl₂ crosslinking procedure followed by the UV crosslinking procedure which referred to as (CaCl₂/UV) as shown in figure 2.1 (Technique 1), or with the UV crosslinking procedure and followed by CaCl₂, which referred to as (UV/CaCl₂), as illustrated in Figure 2.1 (Technique 2).

As mentioned earlier, the UV crosslinking procedure was carried out inside the UV chamber of the device. Throughout the preparation process, all handling of the GelMA hydrogel was performed under dark conditions to prevent premature

photoreaction. Additionally, to ensure sterile and controlled conditions, each sample container lid was securely fastened and only opened inside a laminar flow cabinet.

2.2.5. Preparation of animal gingival and oral mucosal tissues

Animal tissue samples were obtained through prior arrangement with local butchers(London, UK). The shop owners were informed that the samples were required for academic research purposes, and appointments were made in advance to collect the required tissues. Porcine tissues were sourced from a butcher in Homestead Heath, and sheep tissues were obtained from a butcher on Edgware Road.

Oral mucosa samples were harvested from maxillae and mandibles of 6–9 month-old animals. Samples were obtained from the labial attached gingiva of the anterior teeth. Buccal and lingual samples were collected from attached gingiva and alveolar mucosa of the molar sites. Additionally, palatal gingival samples were also collected (Fig 2.1. A, B, C, and D). Epithelial layer from each sample was removed by de-epithelization using surgical blade. A #12 scalpel blade was used to dissect the tissue and measure thickness. Samples were stored in PBS at 4 °C for no more than 3 days before analysis.

2.2.6. Materials characterization

2.2.6.1. ¹H-NMR spectroscopy

One sample from each of the three batches of synthesized GelMA-UCL (GelMA-UCL1, GelMA-UCL2, and GelMA-UCL3) was analyzed using ¹H-NMR spectroscopy (400 plus spectrometer, Bruker Ltd., Coventry, UK) analysis. ¹H-NMR spectra were used to confirm the grafting of methacrylate and methacrylamide groups in three batches of GelMA-UCL products, in comparison to the ¹H-NMR spectra of GelMA-com. sample. ¹H-NMR spectra were also used to identify the presence of the by-product (methacrylic acid). The chemical shifts were represented in parts per million (ppm) downfield. For interpretation of ¹H-NMR results the TopSpin™ software from Bruker was used. Before the

interpretation, phase corrections were applied to all spectra to obtain purely absorptive peaks, and the baselines were corrected. For the evaluation of degree of methacrylation (DoM), was performed using the estimated DoM of GelMA-com, (as reference, DoM = 80%). The DoM was determined using the following equation (228).

DS(%)= [1- (lysine methylene proton of GelMA-UCL / lysine methylene proton of

GelMA-com)] * 100

Equation 1.

2.2.6.2. Scanning electron microscopy (SEM)

The morphology of the surface of all samples were assessed using the SEM (Zeiss EVO HD, Jena,Germany). Before examination the samples were freeze dried (Heto Dry Winner connected with Edwards RV5 pump, UK) at below 50 m-bar pressure ~ 100 °C chiller temperature for 48 h. 500X, and 5KX magnifications were used to visualise the surface morphology of the samples. Equivalent circle diameter of the pores was calculated by using Image J software.

2.2.6.3. Fourier transform infrared spectrophotometer (FT-IR) spectrum

Biochemical properties were analyzed using FT-IR spectrum (ATR-FTIR, System 2000, PerkinElmer, Seer Green, UK) over a range of 4000–500 cm⁻¹ with a resolution of 4 cm⁻¹ at 37 °C. The absorption peaks and frequencies of samples were detected using an attenuated total reflectance (ATR) machine (Golden Gate ATR, Specac Ltd., Orpington, UK).

2.2.6.4. Hydrophilic/hydrophobic surface characteristics

Water contact angle (WCA) measurements were used to evaluate hydrophilic/hydrophobic nature of the hydrogel sample surfaces. WCA was measured using the sessile drop method / optical contact angle profiling. In brief,

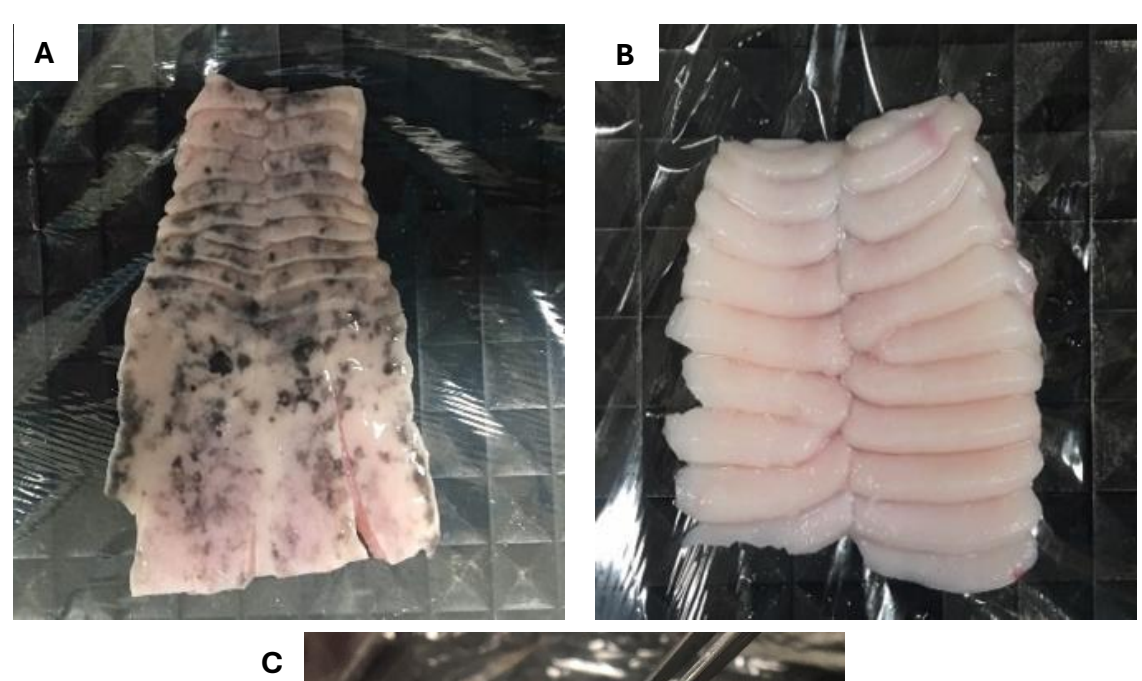
a droplet of distilled water ($\sim 2\mu L$) was deposited on the sample surface, and the contact angle (CA) was measured at room temperature (~ 20 °C) using a CAM 200 optical angle meter (KSV Instruments Ltd., Helsinki, Finland). Three samples were tested for each group (N = 3)..

2.2.6.5. Thermal characteristics

Differential scanning calorimetry (DSC) (DCS25, TA Instruments, New Castle, NSW, USA) was used to evaluate the thermal capacity of hydrogel samples. Weighed samples were placed into Tzero®® Pans and Lids. An empty pan was used as a control reference and the runs were performed in triplicate. Samples were examined under a continuous flowrate of nitrogen gas with the following conditions: equilibrate (-10 °C), isothermal (1 min), and ramp (10 °C/min to 450 °C/min). TRIOS software was used to analyse and report the data. The maximum peak temperature of the endotherm was recorded as the melting point/transition temperature. Experiments were performed using three independent samples for each group (N = 3).

2.2.6.6. Rheological characteristics

A rheometer (HAAKE™ Viscotester™ iQ Rheometers, ThermoFisher Scientific, UK) equipped with cone plate geometry (CP-50/1) (50 mm, gap: 0.1 mm, cone angle: 1°) was used for all the measurements. The samples were equilibrated to temperature for 5 min prior to performing the experiments. Each sample was aliquoted into 6-well plates for investigation.





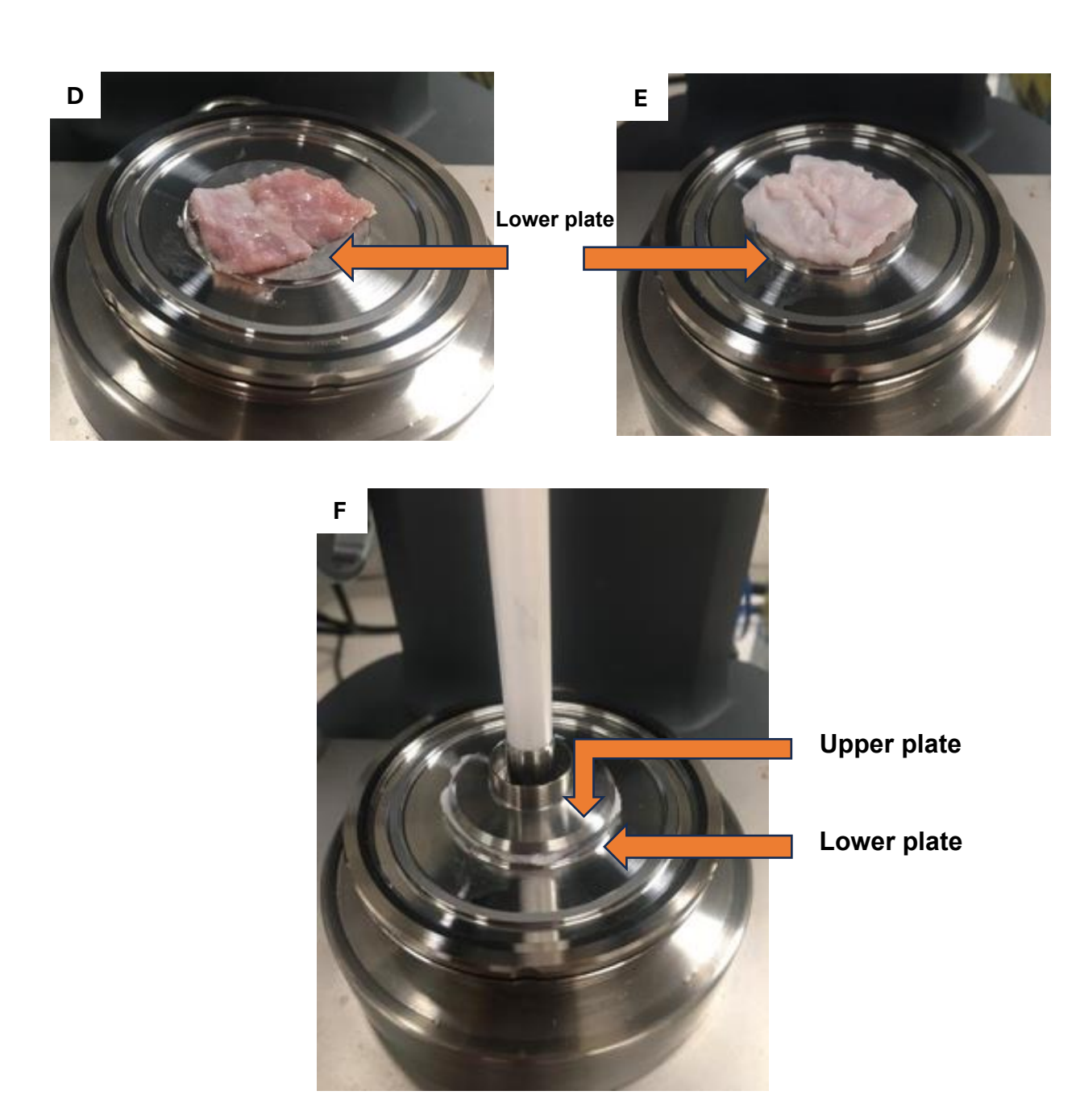


Figure 2.2. Photoss for rheological investigation of animal palatal gingival tissue samples. (A, and B), palatal gingival tissue samples of upper jaws of sheep and porcine, respectively. (C), sample preparation by sharp dissection. (D, and E), placement of sheep and porcine samples, respectively, on lower plate to operate rheometer instrument, (I and J), sheep and porcine samples placement on lower plate, respectively, to operate rheometer instrument (F) lowering the upper plate after placing sample on lower plate.

This was followed by a gentle cut with a diameter of approximately 50 mm and a thickness of about 1 mm, with a flat upper surface, prior to testing. The animal tissue samples included in this investigation were palatal gingival tissue (Fig. 2.1, A and B). Figure 2.1.(A, and B), represented palatal gingival samples from sheep and porcine, respectively. These samples were prepared by sharp dissection (fig.2.1 C). Photographic images in figure 2.1 (D and E), showing placement of sheep and porcine samples on lower plate, respectively. Figure 2.1 (F), showing the sample placing on lower plate after lowering the upper plate.

Rotational tests under destructive shear conditions were performed at shear rates ranging from 0.01 - 1500 s⁻¹ for all samples. Amplitude tests were performed within a range of deformations from $\gamma = 0.01$ to 175 % at a constant frequency of oscillation (f =1 Hz). Frequency tests were conducted at a constant deformation ($\gamma = 0.25$ %) within the linear viscoelastic range with the frequency of oscillation varying from 0.1-50 Hz. at constant temperature of approximately 37,20, and 4 °C. The HAAKERheowin software was used for analysis. Key parameters obtained include the storage modulus (G'), indicating elastic or solid-like behaviour; the loss modulus (G"), representing viscous or liquid-like behaviour (383). These values provide insights into the gel's mechanical stability, stiffness, and suitability for tissue engineering applications. Rheological characterisation (rotational, amplitude sweep, and frequency sweep) was performed on three independent samples for each test (N = 3).

2.2.6.7. Mechanical characteristics

The mechanical properties of the hydrogel samples were characterized using a compression geometry clamp with a diameter of 15 mm, as part of the Dynamic Mechanical Analysis (DMA850, TA Instruments, New Castle, NSW, USA) setup at a controlled temperature. Each sample was aliquoted into 24-well plates for crosslinking, followed by gentle cutting to approximately 7 mm in diameter and 2-4 mm in thickness, with a flat upper surface, prior to testing. The TRIOS software was used to determine the storage modulus, loss modulus, and

stiffness values. A comparison of stiffness, storage modulus (E'), and loss modulus (E") was evaluated. Uniaxial compression testing was conducted at 37 $^{\circ}$ C using cyclic sinusoidal load mode, with frequency oscillations ranging from 0.1 to 50 Hz at 5 Hz intervals for each sample. Samples were pre-loaded with a force of 0.001 N and dynamically tested at low deformation (0.25% strain) compression to ensure repeatable data collection. Three samples were tested for each group (N = 3).

2.2.6.8. Degradation test

The rate of degradation is an important property that defines the stability of hydrogels. In this study, R collagen, GelMA, and GelMA-SA composite hydrogels were investigated to determine their degradation rates. Samples were incubated in PBS at 37 °C, and their weights were recorded on days 1, 3, 7, and 14 (234). Triplicate experiments for time point. Each time point was tested in triplicate. The average mass change was calculated to determine the remaining weight percentage, as shown in Equation 1 below.

Remaining weight (%) = [100 + (weight at time point - initial weight/ initial weight)) * 100.

Equation 2.

2.2.6.9. Human gingival cells expanding and seeding in samples 2.2.6.9.1. Cells expanding

Human primary gingival fibroblasts (HGF) (ATCC – PCS-201-018, see appendix B.1). HGF cells were cultured in T-75 flasks (Corning Life Sciences, UK) with 10 mL and 20 mL of DMEM, respectively, supplemented with 10% FBS, and 1% penicillin-streptomycin, under standard humidified cell culture conditions at 37 °C in 5% CO₂. After reaching confluency, the HGF were expanded, and cells were expanded and used in subsequent experiments between passages 3 and 8.

Immortalized cell lines from human gingival epithelium(HGE), ((MOE1) (Kagoshima University, see Appendix B.2)), were cultured in T-75 flasks

(Corning Life Sciences, UK) with 10 mL and 20 mL of serum free media (K-SFM), respectively (Keratinocyte-SFM is supplied with prequalified human recombinant Epidermal Growth Factor 1-53 (EGF 1-53)), under standard humidified cell culture conditions at 37 °C in 5% CO₂. After reaching confluency, the HGE were expanded, and used in the subsequent experiments between passages 19 and 22.

2.2.6.9.2. Seeding hydrogel samples with HGF and HGE cells

Expanded HGF or HGE cells, suspended at a density of 2×10^4 cells/mL, were mixed with sterilised hydrogel samples at a ratio of $10~\mu L$ of cell suspension per $50~\mu L$ of hydrogel in each well of a 96-well plate, resulting in a final volume of $60~\mu L$ per well. The mixture was pipetted up and down 2–3 times to ensure homogeneity. Subsequently, the samples were crosslinked, and $300~\mu L$ of culture medium was added to each well to maintain hydration and support cell viability. DMEM was used for HGF cells, while K-SFM was used for HGE cells. The plates were then incubated at $37~^{\circ}C$ in a humidified atmosphere with 5% CO_2 .

For R-collagen hydrogel samples, the hydrogels were first distributed into a 96-well plate. The cell suspension, at the same density as above, was mixed with the hydrogel under cold conditions (4 °C) and pipetted gently 2–3 times to ensure even distribution. The samples were then incubated at 37 °C with 5% CO_2 for 15 minutes, after which the appropriate culture medium was added.

2.2.7. Engineered 3D gingival tissue (3DGT)

The method used to develop the 3D gingival tissue (3DGT) model is a modification of previously reported techniques (188), with major changes described below with key changes outlined below. In brief, to prepare the cell-populated hydrogel samples, expanded HGF cells were mixed at a density of 2x10⁴ cells/ml, with sterile hydrogel samples.

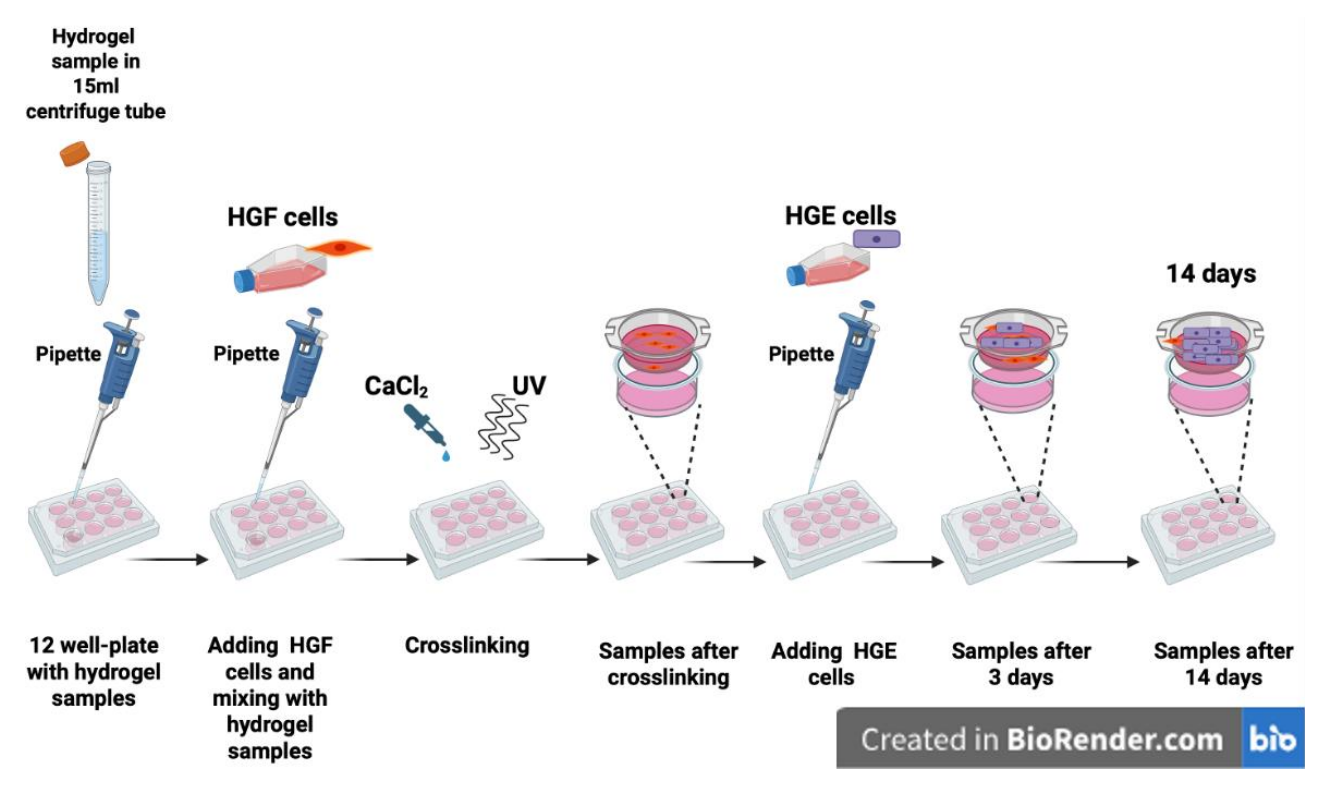


Figure 2.3. Schematic drawing illustrating the construction of 3D gingival model including crosslinking procedures using CaCl₂ and UV. Created in BioRender.com

The mixture was then distributed into 96-well plates and crosslinked. Following crosslinking, the prepared HGF medium was added, and the samples were incubated at 37 °C with 5% CO₂. For the R collagen hydrogel sample, the cell mixture was prepared in a cold environment (4 °C) before distribution into the 96-well plate.

These samples were aliquoting at 37 °C with 5% CO₂ for 15 minutes, after which the prepared HGF medium was added. Incubation continued at 37 °C with 5% CO₂ for 3 days. After 3 days, the medium was removed, and the hydrogel samples were seeded with human gingival epithelial (HGE) cells at a density of 4x10⁴ cells/ml.

To lift the engineered 3DGT to an air-liquid interface (ALI), 3DGT models were constructed inside 13-mm diameter Millicell cell culture inserts (Millipore) placed in 12-well plates (Sigma) (Fig 2.3.). These experiments were performed using three hydrogel sample (N=3).

2.2.8. Metabolic and cytotoxic activities of cells evaluation

The metabolic and cytotoxic activities of the cells were assessed at 1, 3, 7, and 14 days of incubation of samples at 37 °C with 5% CO₂. Each time point was tested in triplicate.

The metabolic activity of the cells was evaluated using the CellTiter® 96 Aqueous One Solution Cell Proliferation assay kit, according to the manufacturer's protocol. The CellTiter 96® Assay is based on the cellular conversion of a tetrazolium salt into a formazan product that is easily detected using a well plate reader. Briefly, to evaluate cell viability, the following groups were included in triplicates:

- (1) Experimental group (hydrogel with cells), hydrogel samples were prepared by adding sterilized hydrogel (50 μ L) into each well of a 96-well plate (see Section 2.2.6.9.2). The expanded cells were subsequently seeded onto the hydrogel. The mixture was pipetted up and down 2–3 times to ensure homogeneity.
- (2) Hydrogel-only controls (hydrogel without cells) to assess any background signal from the scaffold,

Then, the samples of these two groups were crosslinked.

- (3) Medium-only controls (inserts containing only culture medium) to account for medium background, as a negative control.
- (4) Cell only controls (2D monolayer culture), represented cells seeded directly without hydrogel, used as a positive control for viability, to serve as a baseline for untreated cells.

For the proliferation assay, $50~\mu L$ of CellTiter One reagent was added to each well and incubated at $37~^{\circ}C$ with $5\%~CO_2$ for 4~h, whilst wrapped in aluminium foil. Following incubation, the supernatant solution was transferred to a new plate and read at 490~nm using a Tecan Infinite M200 microplate reader (Tecan, Switzerland). The cell viability or absorbance values were calculated as shown in Equations 2 and 3 below.

Absorbance value of hydrogel sample = (Experimental group - medium background) - (Hydrogel-only control - medium background)

Equation 2.

Absorbance value of positive control group(2D monolayer) = (Cell only control group - medium background)

Equation 3.

For cytotoxicity assay, Lactate Dehydrogenase (LDH) detection reagent release release from the cells was quantified. LDH release assay performed using the CytoTox 96®® Non-radioactive Cytotoxicity Assay kit, according to the manufacturer's protocol. In summary, to evaluate cell cytotoxicity, and the following experimental and control groups were included in triplicates:

- (1) Experimental group (hydrogel with cells), hydrogel samples were prepared by adding sterilized hydrogel ($50 \,\mu L$) into each insert of a 96-well plate (see Section 2.2.6.9.2). The expanded cells were subsequently seeded onto the hydrogel. The mixture was pipetted up and down 2–3 times to ensure homogeneity.
- (2) Hydrogel-only controls (hydrogel without cells) to assess any background signal from the scaffold,

Subsequently, the samples of these two groups were crosslinked.

- (3) Medium-only controls (inserts containing only culture medium) to account for medium background.
- (4) Cell only controls, represented 2D monolayer (cells seeded directly without hydrogel), used as a negative control for cytotoxicity, to serve as a baseline for untreated cells. These represent healthy, viable cells and are used to determine the baseline LDH detection reagent release from normal cell turnover.
- (5) Triton X-100-treated cells ($2\,\mu L$ of 10% Triton X-100 added per 100 μL medium) to determine the maximum LDH release, used as a positive control for cytotoxicity. This positive control is required to calculate percent cytotoxicity. All groups were cultured under identical conditions with complete culture

medium. The Triton X-100 group was incubated for 40 minutes prior to sample

collection for LDH assay. All wells were filled with complete culture medium and maintained under identical incubation conditions for subsequent viability or cytotoxicity assays. At each time point of incubation, $50\,\mu\text{L}$ of culture medium was collected from each well and transferred into a new 96-well plate. Then, $50\,\mu\text{L}$ of LDH detection reagent was added to the $50\,\mu\text{L}$ of media suspension in each well, which was then incubated and covered in aluminium foil at ~20 °C for $30\,\mu\text{L}$ of stop solution was added to each well. The absorbance was then immediately read using a Tecan Infinite M200 microplate reader (Tecan, Männedorf, Switzerland). The percent cytotoxicity was calculated as shown in Equations 3 and 4 below.

Experimental LDH release = (Experimental group) - (Hydrogel-only control) or

Experimental LDH release = Cell-only control, used as negative control

Equation 4.

Percent Cytotoxicity = 100 * [(Experimental LDH release – Medium background)/

(Maximum LDH release – Medium background)]

Equation 5.

In addition to above mentioned and to support the quantitative assays, the biocompatibility of the samples was determined with Live/Dead Viability Assay using Live/Dead™ staining. A LIVE/DEAD™ imaging kit was used. Based on the protocol of manufacturer's instructions, Live/DeadTM staining was prepared by adding 20 µL of ethidium homodimer-1 (EthD-1) to 10 mL PBS, combined with 5 µL Calcein AM also added into solution. Hydrogel constructs were prepared by adding sterilized hydrogel (50 µL) into each well of a 96-well plate (see Section 2.2.6.9.2). The expanded cells were subsequently seeded onto the hydrogel samples. The samples were prepared by removing the old medium

and washing with PBS. Prepared stain of live/dead reagent was added to samples in a dark environment. The 96-well plate was incubated for 30 min at 20-25 °C. After incubation, Imaging was performed on confocal laser scanning microscopy (BioRad Radiance2100, Zeiss, UK). Live/Dead Viability Assay was conducted using a dual-staining kit containing calcein-AM and ethidium homodimer-1. In the confocal images, green fluorescence corresponds to viable cells, as calcein AM is converted by intracellular esterases into calcein, which accumulates in live cells with intact membranes. Red fluorescence indicates dead cells, as EthD-1 penetrates only cells with compromised membranes and binds to DNA, emitting red fluorescence. This staining allows for clear visual distinction between live and dead cells within the 3D hydrogel construct. The images were captured using digital capture software. These images were analysed to visualise live and dead cells within the samples using ImageJ Fiji software (https://downloads.micron.ox.ac.uk/fiji_update/mirrors/fiji-latest/fijinojre.zip).

2.13. Statistical Analysis

Quantitative data are expressed as mean \pm standard deviation (SD). For comparisons involving more than two groups, one-way ANOVA was performed, followed by Tukey's post hoc test for pairwise comparisons. In cases where multiple testing was applied, Bonferroni correction was used to adjust for type I error. For comparisons between two groups, unpaired two-tailed Student's t-tests were applied. Prior to analysis, data were assessed for normality (Shapiro–Wilk test) and homogeneity of variance (Levene's test). All analyses and graph generation were conducted using OriginPro 2023 (OriginLab, Northampton, MA, USA). Statistical significance was set at p < 0.05 (*), and highly significant differences at p < 0.01 (**).

CHAPTER 3

3. THREE DIMENSIONAL (3D) GINGIVAL MODELS IN PERIODONTAL RESEARCH: A SYSTEMATIC REVIEW

3.1. Introduction

Several previous studies described the characteristics of 3D gingival and periimplant models. These models were constructed using the organotypic culture technique in a static cell culture condition (187, 219-223). For example, study by Koskinen & Qu, to characterize macroscopical appearance of gingival model (221). The result from their study showed that construction 3D gingival models using crosslinking rat tail collagen as a substrate, were larger in size compared with non-crosslinking substrates.

One of the most crucial methods for assessing and characterizing a constructed 3D gingival model is histological evaluation. Numerous studies have employed various techniques to conduct this assessment, particularly through the use of different staining methods. These include hematoxylin and eosin (H&E) staining, hematoxylin-only staining, Periodic acid-Schiff (PAS) staining, Masson's trichrome staining, and van Gieson staining. Histological analysis has been widely utilized to examine the epithelial layers, focusing on parameters such as epithelial thickness, the number of cell layers, and the degree of cellular differentiation. Additionally, several studies have investigated the characteristics of the connective tissue layer, including its formation and structural organization. The thickness of the connective tissue layer has also been measured, along with an assessment of fibroblast cell embedding within various types of substrates. These evaluations provide valuable insights into the structural integrity and biological functionality of the engineered gingival models. (188, 189, 199, 101, 219, 224-227).

The 3D gingival model has many applications in periodontal research to reflect the clinical situation as much as possible such as assessment of, the biocompatibility of dental materials, potential of host-pathogen interactions, process oral healthcare products, wound healing as well as the study of implant-soft tissue interfaces (184, 189, 194-198, 200, 201).

Numerous studies have proposed different types of 3D gingival models; however, a systematic evaluation of these models is lacking. It remains unclear which models best replicate clinical conditions and could serve as a reliable foundation for future research.

Recent advancements in tissue engineering have led to the development of full-thickness three-dimensional (3D) gingival models that incorporate human gingival-derived keratinocytes to form the epithelial layer and human gingival fibroblasts to construct the underlying connective tissue layer (286). These models aim to replicate the structure and function of native gingival tissue, providing a valuable platform for in vitro studies of oral health, disease mechanisms, and therapeutic interventions. However, despite these advancements, no standardized fabrication protocol or universally accepted biomaterial has been established for constructing these models, leading to variations in their physiological accuracy and reproducibility (287).

A comprehensive critical evaluation of existing models is essential, as their ability to accurately mimic native human gingival tissue has not been systematically reviewed. Key parameters that must be assessed include epithelial and connective tissue layer thickness, the presence of vasculature, biological properties, anatomical organization, cellular distribution, and differentiation processes, particularly in keratinocytes and fibroblasts (288, 289). Additionally, the substrates and scaffolding materials used in these models, such as collagen-based hydrogels, fibrin matrices, and synthetic polymeric scaffolds, must be critically analyzed to determine their effectiveness in replicating the biochemical and mechanical properties of native gingival tissue (290).

A systematic study focused on evaluating current 3D in vitro gingival models is necessary to identify their strengths and limitations and to advance the field toward clinically relevant tissue engineering approaches. Such research will provide insight into the optimization of biomaterials, fabrication methods, and cellular interactions, ultimately improving the translational potential of these models for applications in periodontal disease research, regenerative medicine, and clinical testing of dental biomaterials (291, 292).

3.2. Materials and methods

Systematic review study

Due to the absence of specific tools for defining precise research questions, we adapted the PICOS framework to systematically search for available evidence.

- **(P) Participants**: A 3D gingival cell culture model constructed by seeding gingival fibroblasts into a substrate and co-culturing them with oral epithelial cells.
- (I/E) Intervention/Exposure: Not applicable.
- **(C) Comparison**: Native human gingival tissue.
- (O) Outcomes:
- 1. Resemblance to native human gingival tissue, assessed through histological analysis of its 3D structural layers.
- 2. Differentiation markers for each cell component.
- 3. Functional evaluation of the layers.
- (S) Study Type: In vitro experiments.

A systematic review protocol was developed and registered with the Open Science Framework (OSF) database, hosted by the Center for Open Science (COS) (https://archive.org/details/osf-registrations-6mzw2-v1_-_License:

http://www.gnu.org/licenses/lgpl-3.0.txt). Whenever possible, the systematic review was conducted following PRISMA guidelines (280).

The search strategy was based on five electronic databases: MEDLINE (OVID), EMBASE, Dentistry and Oral Science Source (EBSCOhost), Web of Science Core Collection, and LILACS (Latin American & Caribbean Health Sciences Literature), with searches updated until September 12, 2022 (Tab.3.1). Additionally, a hand-search was conducted (Tab.3.2). Only studies published in English were included. All retrieved articles were exported and de-duplicated using the reference management software EndNote X9.3.3 (Bld 13966).

The inclusion criteria for this review encompass studies on 3D cell culture gingival models that meet the following conditions: they must be constructed with a substrate seeded by human gingival fibroblasts or human periodontal ligament cells along with human gingival/oral epithelial cells, or they must utilize a scaffold-based system. Additionally, studies must include histological analysis and be published in English.

Studies will be excluded if they meet any of the following criteria:

- 3D cell culture gingival models constructed without a substrate-based system.
- Models using a substrate seeded with fibroblasts or epithelial cells from nonhuman sources.
- Models using a substrate seeded with human gingival fibroblasts or human periodontal ligament cells without human gingival/oral epithelial cells.
- Models using a substrate seeded with human gingival/oral epithelial cells without human gingival fibroblasts or human periodontal ligament cells.
- Animal studies.
- Studies lacking clear histological analysis.
- Abstracts without full papers.
- Grey literature and unpublished studies were not considered in this review. Only published articles were included, regardless of whether they had undergone peer review.

Main categories of data were extracted as listed below: Study Characteristics Data: "Study authors, Year of publication and title, Study design, Conclusions", "Participant/ 3D cell culture gingival model with inclusion/exclusion criteria, Human gingival fibroblasts cells, Specific substrate for cells seeding, Human epithelial cells ".

For the study bias protection assessment, and because there are no established criteria for evaluating in vitro studies. Two tools of risk of bias were used in this review. The first one was the modified ARRIVE guidelines ((Supplemental Data 2), Appendix C), to assess the quality of each study (42). A second tool 'Systematic Review Centre for Laboratory Animal Experimentation (SYRCLE)'s risk of bias tool' was also used to analyse data and adapted by ruling out the blind intervention section (294).

Table 3.1. Search strategy and terms that based on five electronic databases: MEDLINE (OVID), EMBASE, EBSCOhost, Web of Science Core Collection, and LILACS.

Search strategy and keywords

Search strategy for Web of Science Core Collection	Search Strategy Medline (Ovid Version)	Search strategy for Ovid Embase 1980 to 2021	Search strategy for Dentistry and Oral Science Source (EBSCOhost)	LILACS
#1.TOPIC: (Cell culture technique*)	1. exp Cell Culture Techniques/	1.exp cell culture technique/	S1.Cell culture technique* OR organotypic cell culture OR tissue engineer*	(cell culture techniques) AND (Gingival cells) AND (implant* OR Fibroblast* OR Keratinocyte s OR periodontal pocket*)
#2.TOPIC: (organotypic NEAR/3(model* or culture*))	2.Tissue Engineering/	2.exp tissue engineering/	S2.gingiva OR oral mucosa OR mouth mucosa OR oral cavity	
#3.TOPIC: (tissue engineer*)	3.(Cell culture technique* or (organotypic adj3 (model* or culture*)) or tissue	3. (Cell culture technique* or (organotypic adj3 (model* or	S3.S1 AND S2	

	engineer*).tw.	culture*)) or tissue	
#4.#3 OR #2 OR #1	4. 1 or 2 or 3	4.1 or 2 or 3	S4.Reconstructed human gingiva OR Organotypic oral mucosa
#5.TOPIC: (gingiva*)	5.exp Gingiva/	5.exp gingiva/	S5.(3D or 3dimensional or "three dimensional" or "3 dimensional") W3 (gingival model*)
#6.TOPIC: ((oral or mouth) NEAR mucosa)	6.Mouth Mucosa/	6.exp mouth mucosa/	S6.S3 OR S4 OR S5
#7.TOPIC: (oral cavity*)	7.(gingiva* or ((oral or mouth) adj mucosa)).tw.	7.(gingiv* or ((oral or mouth) adj mucosa)).tw.	S7.implant* OR Fibroblast* OR Keratinocytes OR periodontal pocket*
#8.#7 OR #6 OR #5	8.oral cavity.tw.	8.oral cavity.tw.	S8.S6 AND S7
#9.#8 OR #4	9.5 or 6 or 7 or 8	9.5 or 6 or 7 or 8	S9.TI ((animal or animals or canine*or dog or dogs or feline or hamster* or lamb or lambs or mice or monkey or monkeys or mouse or murine or pig or pigs or piglet* or porcine or primate* or rabbit* or rats or rat or rodent* or sheep*) NOT (human* or patient*))
#10.TOPIC: (Reconstructed human gingiva)	10.4 and 9	10.4 and 9	S10. S8 NOT S9
#11.TOPIC:(3d NEAR/1 "gingival model*")	11.Reconstructe d human gingiva.tw.	11.Reconstructed human gingiva.tw.	
#12.TOPIC: (3dimentional NEAR/1"gingival model*")	12.((3D or 3dimensional or three dimensional) adj gingival model*).tw.	12.((3D or 3dimensional or three dimensional) adj gingival model*).tw.	
#13.TOPIC: (3 dimentional NEAR/1"gingival model*")	13.Organotypic oral mucosa.tw.	13.Organotypic oral mucosa.tw.	
#14.TOPIC: (three dimentional NEAR/1"gingival model*") #15.TOPIC: (three-dimentional	15.10 or 14	15.10 or 14	
NEAR/1"gingival model*") #16.TOPIC: (Organotypic oral	16.exp	16.exp	
mucosa*) #17.#16 OR #15 OR #14 OR #13 OR #12 OR #11 OR #10 OR #9	Fibroblasts/ 17.exp Keratinocytes/	Fibroblast/ 17.Keratinocyte.t	
#18.TOPIC: (periodont* or implant* or fibroblast* OR keratinocyte*)	18.Fibroblast*.t w.	w. 18.exp tooth implant/	
#19.#17 AND #18	19.Keratinocyte s.tw.	19.periodontal pocket/	
#20.TOPIC: (animal or animals or pisces or fish or fishes or catfish or catfishes or sheatfish or silurus or arius or heteropneustes or clarias or	20.Dental Implants/ or implant*.tw.	20.Fibroblast*.tw.	

gariepinus or fathead minnow fathead minnows pimephales or promelas or cichlidae or trout or trouts or char or chars or salvelinus or salmo or oncorhynchus or guppy or guppies or millionfish or poecilia or goldfish or goldfishes or carassius or auratus or mullet or mullets or mugil or curema or shark or sharks or cod or cods or gadus or morhua or carp or carps or cyprinus or carpio or killifish or eel or eels or anguilla or zander or sander or lucioperca or stizostedion or turbot or turbots or psetta or flatfish or flatfishes or plaice or pleuronectes or platessa or tilapia or tilapias or oreochromis or sarotherodon or common sole or dover sole or solea or zebrafish or zebrafishes or danio or rerio or seabass or dicentrarchus or labrax or morone or lamprey or lampreys or petromyzon or pumpkinseed or pumpkinseeds or lepomis or gibbosus or herring or clupea or harengus or amphibia or amphibian or amphibians or anura or salientia or frog or frogs or rana or toad or toads or bufo or xenopus or laevis or bombina or epidalea or calamita or salamander or salamanders or newt or newts or triturus or reptilia or reptile or reptiles or bearded dragon or pogona or vitticeps or iguana or iguanas or lizard or lizards or anguis fragilis or turtle or turtles or snakes or snake or aves or bird or birds or quail or quails or coturnix or bobwhite or colinus or virginianus or poultry or poultries or fowl or fowls or chicken or chickens or gallus or zebra finch or taeniopygia or guttata or canary or canaries or serinus or canaria or parakeet or parakeets or grasskeet or parrot or parrots or psittacine or psittacines or shelduck or tadorna or goose or geese or branta or leucopsis or woodlark or lullula or flycatcher or ficedula or hypoleuca or dove or doves or geopelia or cuneata or duck or ducks or greylag or graylag or anser or harrier or circus pygargus or red knot or great knot or calidris or canutus or godwit or limosa or lapponica or meleagris or gallopavo or jackdaw or corvus or monedula or ruff or philomachus or pugnax or lapwing or peewit or plover or

vanellus or swan or cygnus or columbianus or bewickii or gull chroicocephalus ridibundus or albifrons or great tit or parus or aythya or fuligula or streptopelia or risoria or spoonbill or platalea or leucorodia or blackbird or turdus or merula or blue tit or cyanistes or pigeon or pigeons or columba or pintail or anas or starling or sturnus or owl or athene noctua or pochard or ferina or cockatiel or nymphicus or hollandicus or skylark or alauda or tern or sterna or teal or crecca or oystercatcher or haematopus or ostralegus or shrew or shrews or sorex or araneus or crocidura or russula or european mole or talpa or chiroptera or bat or bats or eptesicus or serotinus or myotis or dasycneme daubentonii or pipistrelle or pipistrellus or cat or cats or felis or catus or feline or dog or dogs or canis or canine or canines or otter or otters or lutra or badger or badgers or meles or fitchew or fitch or foumart or foulmart or ferrets or ferret or polecat or polecats or mustela or putorius or weasel or weasels or fox or foxes or vulpes or common seal or phoca or vitulina or grey seal or halichoerus or horse or horses or equus or equine or equidae or donkey or donkeys or mule or mules or pig or pigs or swine or swines or hog or hogs or boar or boars or porcine or piglet or piglets or sus or scrofa or llama or llamas or lama or glama or deer or deers or cervus or elaphus or cow or cows or bos taurus or bos indicus or bovine or bull or bulls or cattle or bison or bisons or sheep or sheeps or ovis aries or ovine or lamb or lambs or mouflon or mouflons or goat or goats or capra or caprine or chamois or rupicapra or leporidae or lagomorpha or lagomorph or rabbit or rabbits or oryctolagus or cuniculus or laprine or hares or lepus or rodentia or rodent or rodents or murinae or mouse or mice or mus or musculus or murine or woodmouse or apodemus or rat or rats or rattus or norvegicus or guinea pig or guinea pigs or cavia or porcellus or hamster or hamsters or mesocricetus or cricetulus or cricetus or gerbil or gerbils or jird or jirds or meriones or unquiculatus or

			T	
jerboa or jerboas or jaculus or				
chinchilla or chinchillas or				
beaver or beavers or castor				
fiber or castor canadensis or				
sciuridae or squirrel or				
squirrels or sciurus or				
chipmunk or chipmunks or				
marmot or marmots or marmota or suslik or susliks or				
spermophilus or cynomys or				
cottonrat or cottonrats or sigmodon or vole or voles or				
microtus or myodes or				
glareolus or primate or primates				
or prosimian or prosimians or				
lemur or lemurs or lemuridae or				
loris or bush baby or bush				
babies or bushbaby or				
bushbabies or galago or				
galagos or anthropoidea or				
anthropoids or simian or				
simians or monkey or monkeys				
or marmoset or marmosets or				
callithrix or cebuella or tamarin				
or tamarins or saguinus or				
leontopithecus or squirrel				
monkey or squirrel monkeys or				
saimiri or night monkey or night				
monkeys or owl monkey or owl				
monkeys or douroucoulis or				
actus or spider monkey or				
spider monkeys or ateles or				
baboon or baboons or papio or				
rhesus monkey or macague or				
macaca or mulatta or				
cynomolgus or fascicularis or				
green monkey or green				
monkeys or chlorocebus or				
vervet or vervets or pygerythrus				
or hominoidea or ape or apes or				
hylobatidae or gibbon or				
gibbons or siamang or				
siamangs or nomascus or				
symphalangus or hominidae or				
orangutan or orangutans or				
pongo or chimpanzee or				
chimpanzees or pan				
troglodytes or bonobo or				
bonobos or pan paniscus or				
gorilla or gorillas or				
troglodytes)				
#21.#19 NOT #20	24 noriedental			
#21.#13 NUT #20	21.periodontal pocket*.tw.	21 Koratinoovto*		
	pocket".tw.	21.Keratinocyte*.		
	22.Periodontal	tw.		
		22.lmplant*.tw.		
	Pocket/ 23.16 or 17 or	22 pariodontal		
	18 or 19 or 20	23.periodontal pocket*.tw.		
	or 21 or 22	pocket .tw.		
	24.15 and 23	24.16 or 17 or 18		
	24.10 ailu 23	or 19 or 20 or 21		
		or 22 or 23		
	25 evn animals/	25. 15 and 24		
	25.exp animals/ not humans.sh.	20. 10 and 24		
	26.24 not 25	26.(exp animal/		
	20.24 HUL 20	or nonhuman/)		
		not exp human/		
		THUL WALL HUHINIII		
		27.25 not 26		

Table 3.2. List of journals which have been included in our hand searching for eligible articles.

Keywords

1 Journal of Periodontology Journal of Periodontal Research 2 **Toxicology in Vitro** 3 **Journal of Oral Pathology and Medicine** 4 **Cellular Microbiology** 5 **Journal of Orofacial Orthopedics Tissue Engineering** 6 7 Biorheology 8 **Journal of Applied Toxicology** 9 **Stem Cells and Development Cells Tissues Organs** 10 11 Virulence 12 Lasers in Medical Science 13 Archives of oral Biology 14 Journal of Royal Society Interface 15 **Dental Materials** 16 Journal of Microbiological Methods 17 Acta Biomaterialia 18 Oral and Maxillofacial Surgery

3.3. Results

3.3.1. Study selection

A total of 2,338 articles were identified through database searches, including Midline OVID (n = 743), EMBASE (n = 697), Web of Science (n = 639), EBSCO (n = 250), and LILACS (n = 9). After completing the selection process, 22 articles remained for analysis (Fig. 3.1). Due to the lack of relevant quantitative measures for evaluating gingival models, quantitative analysis and meta-analysis were not feasible. Instead, a qualitative analysis was conducted to summarize the characteristics of 3D gingival models.

3.3.2. Quality of studies

i. Modified ARRIVE guidelines (Supplemental Data 2)

Most of the selected studies were of high quality according to the modified ARRIVE guidelines. However, only seven studies addressed both the scientific implications and limitations of their research (189, 199, 101, 209, 227, 295, 296).

Additionally, five studies failed to provide statements regarding potential conflicts of interest and funding disclosures (183, 187, 225, 297, 298) while one study was published in a non-peer-reviewed journal (221).

ii. SYRCLE bias assessment

The studies demonstrated a balanced distribution of low, unclear, and high risks of selection bias. However, all studies exhibited a high risk of bias in random sequence generation and baseline variable characteristics. Regarding allocation concealment, the majority of selected studies showed an unclear risk of bias, with only two articles classified as having a low risk (187, 196). The randomization process was generally associated with a high risk of bias. Furthermore, when evaluating random outcome assessment, all studies were found to have an unclear risk of bias. On a positive note, all articles maintained a low risk of bias concerning incomplete outcome data, selective outcome reporting, and other potential sources of bias (Tab. 3.3 and 3.4).

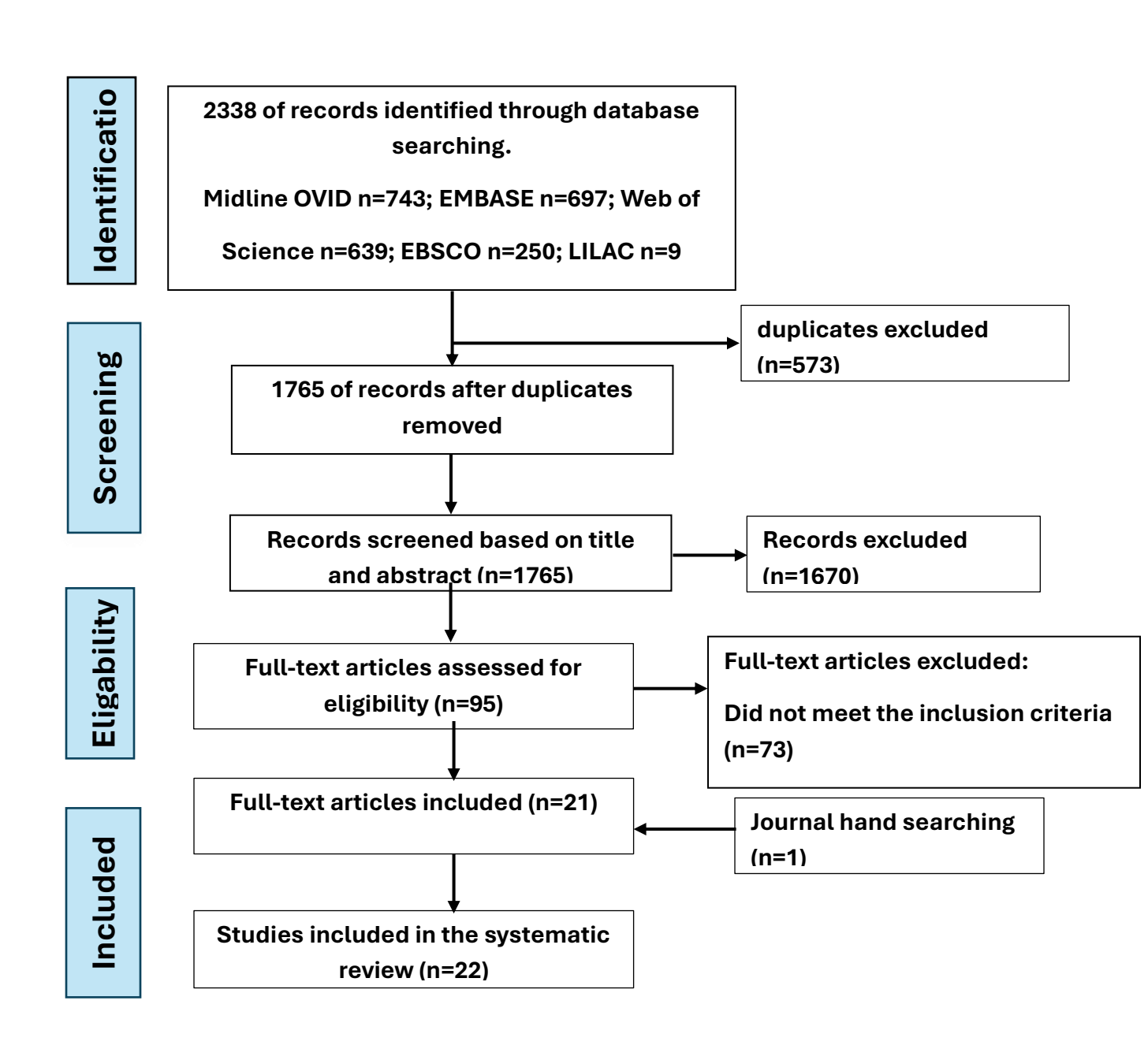


Figure 3.1. PRISMA flow diagram of the study inclusion process

Table 3.3: Quality assessment and risk of bias (modified from the ARRIVE and CONSORT guidelines)

Studies	1	2	3	4	5	6	7	8	9	10	11	12
(188)	1	1	3	2	3	2	2	3	3	1	1	1
(183)	1	1	3	2	3	2	2	3	3	1	0	1
(101)	1	2	3	2	3	2	2	3	3	1	1	1
(189)	1	2	3	2	3	2	2	3	3	2	1	1
(187)	1	1	3	2	3	2	2	3	3	1	0	1
(199)	1	2	3	2	3	2	2	3	3	1	1	1
(299)	1	2	3	2	3	2	2	3	3	1	1	1
(178)	1	1	2	2	3	2	2	3	3	1	1	1
(298)	1	2	3	2	3	2	2	3	3	1	1	1
(225)	1	2	3	2	3	2	2	3	3	1	0	1
(221)	1	1	3	2	3	2	2	3	3	1	1	0
(224)	1	1	3	2	3	3	2	3	3	1	1	1
(297)	1	2	3	1	3	2	2	3	3	1	0	1
(196)	1	2	3	2	3	2	2	3	3	1	1	1
(227)	1	2	3	2	3	3	2	3	3	1	1	1
(296)	1	1	3	2	3	3	2	3	3	1	1	1
(220)	1	2	3	2	3	3	2	3	2	1	1	1
(226)	1	1	3	2	3	3	2	3	2	1	0	1
(219)	1	2	3	2	3	3	2	3	3	1	1	1
(295)	1	2	3	2	3	3	2	3	3	2	1	1
(223)	1	2	3	2	3	3	2	3	3	1	1	1
(222)	1	2	3	2	3	3	2	3	3	1	1	1

Table 3.4: Quality assessment and risk of bias (SYRCLE tool), each item was scored as "yes", "no", or "unclear" Individual risk of bias each item in the SYRCLE tool was scored as "yes", "no", or "unclear"

Studie s	Selection b	ias		Performa	ance bias	Detection bia	Detection bias		Reportin g bias	Other bias
	Random Sequence generatio n	Baseline character - istics	Allocatio n conceal- ment	Rando m housin g	Blindin g	Random outcome assessmen t	Blindin g	Incomplet e outcome data	Selective outcome reporting	Other source s of bias
(188)	no	yes	unclear	yes	unclear	no	no	no	yes	yes
(183)	no	yes	unclear	yes	unclear	no	no	no	yes	yes
(201)	no	yes	unclear	yes	unclear	no	unclear	no	yes	yes
(187)	no	yes	yes	yes	no	no	unclear	no	yes	yes
(189)	no	yes	yes	yes	yes	no	no	no	yes	yes
(199)	no	yes	unclear	yes	unclear	no	unclear	no	yes	yes
(299)	yes	yes	unclear	yes	yes	no	no	no	yes	yes
(178)	no	yes	unclear	yes	unclear	no	no	no	yes	yes
(298)	no	yes	unclear	yes	unclear	no	no	no	yes	yes
(225)	no	yes	unclear	yes	unclear	no	no	no	yes	yes
(221)	no	yes	unclear	yes	unclear	no	no	no	yes	yes
(224)	no	yes	unclear	yes	unclear	no	no	no	yes	yes
(297)	no	yes	unclear	yes	no	no	no	no	yes	yes
(196)	no	yes	yes	yes	unclear	no	unclear	no	yes	yes
(227)	no	yes	unclear	yes	unclear	no	no	no	yes	yes
(296)	yes	yes	unclear	yes	unclear	unclear	no	no	yes	yes
(220)	yes	yes	unclear	yes	unclear	unclear	no	no	yes	yes
(226)	yes	yes	unclear	yes	unclear	unclear	no	no	yes	yes
(219)	no	yes	unclear	yes	unclear	no	no	no	yes	yes
(295)	no	yes	unclear	yes	unclear	no	no	no	yes	yes
(223)	no	yes	unclear	yes	unclear	no	no	no	yes	yes
(222)	no	yes	unclear	yes	unclear	no	no	no	yes	yes

3.3.3. 3D Gingival model characteristics

A total of thirty-seven gingival and peri-implant models were identified across the twenty-two included studies. Among these, thirty-six models were developed using the organotypic culture technique under static cell culture conditions. In contrast, only one study employed a dynamic perfusion bioreactor system, where disc-shaped collagen sponge scaffolds were integrated into a perfusion bioreactor(297). Regarding the cellular source, various types of cells were utilized, including primary cells derived from gingival tissue biopsies, immortalized cell lines, or a combination of both (Tab. 3.5). Out of the twenty-two studies, only six investigated human gingival biopsy samples as a control(187, 219-223).

Table 3.5. Summary of cellular sources used in construction of gingival or periimplant models.

Cells origin	Type of cells	Type & models	no. of	References	
	Keratinocyte	Keratinocyte Fibroblast Gingiva		Peri- implant	
Primary cells	Primary	Primary	13	5	(178, 183, 187- 189, 219, 220, 223, 224, 226, 295)
Immortilized cells	OKG4/bmi1/TERT	Fib-TERT, T0026	3	1	(187, 196, 227, 296)
	KC-HPV	Fib-TERT, T0026	1		(187)
	HGEK-16	GFB-16	2		(297, 299)
	Gie-No3B11	hTERT	1		(298)
	hTERT (TIGKs, CRL-3397, ATCC)	hTERT (hGFBs, CRL-4061, ATCC)	4		(222)
	OKF6/TERT-2	Primary	2	1	(188, 199)
Primary and		Primary	_	1	(201)
Immortilized cells	NOK-si	Primary	1		(225)
	FNB6-TERT	Primary	1		(221)
	H357	Primary	1		(221)

Table 3.6: Characteristics of selected studies.

Authors name (year of publication)	Title	Type of substrate	Type of Cells	Structure/ layers no.	Cell Markers expression	Model functionality
(188)	Development of a novel three- dimensional in vitro model of oral Candida infection	Rat tail collagen type I	Model (1) Primary human gingival keratinocytes and fibroblasts Model (2) Human OKF6/TERT-2 cells with human primary gingival fibroblasts	Model (1) keratinocytes showed a high degree of differentiation. Model (2) 1. (7 -12) cell layers of epithelial cell. 2.The basal layer invaded the submucosal compartment.		Following candida infection:- 1.Degradation of the cornified layer of epithelial cells, extensive cellular necrosis, and loss of cellular junctions in the stratum basale. 2.increased cytokine secretion IL-1a α.
(183)	Histomorphological and biochemical differentiation capacity in organotypic cocultures of primary gingival cells	Rat tail collagen type I	Primary human gingival keratinocytes and fibroblasts	1.keratinocyte cells formed multilayered epithelium. 2.fibroblasts cells incorporated into collagen lattices.	 CK14, CK4 and CK13. some keratinocytes cells are sensitive to vimentin. collagen type IV and laminin. 	
(201)	The biological seal of the implant–soft tissue interface evaluated in a tissue engineered oral mucosal model	Acellular cadaveric dermis (Alloderm)	Human oral keratinocyte cell line (TR146) and human primary gingival fibroblasts	1. 50–100 mm thick, well- formed, stratified squamous epithelium of (4-6) epithelial layers 2.Well cells attached to the Ti surfaces and form a cell network on all the Ti surfaces		1-Normal permeability test for biological seal and cell attachment to Ti disc evaluation 2-Normal Alamar Blue assay test value of residual cells attached to the Ti discs.
(187)	Development of a Full-Thickness Human Gingiva Equivalent Constructed from Immortalized Keratinocytes and Fibroblasts	Rat tail collagen type I	Model (1) Primary human gingival keratinocytes and fibroblasts Model (2) Immortalized human gingiva Keratinocytes cell line, OKG4/bmi1 /TERT, The human gingiva fibroblast cell	1- In both primary and keratinocytes TERT cells, a differentiated stratified epithelium on a fibroblast populated collagen hydrogel was observed and fibroblast-populated collagen was observed without deep rete ridges	Model (1) 1.CK10, and K13 2. Involucrin 3. Ki67 4. Collagen type IV and laminin 5 Model (2)	

			line was TERT immortalized (T0026) Model (3) Immortalized human gingiva Keratinocyte cell line, human papillomavirus type 16 (KC-HPV) and the human gingiva fibroblast cell line was TERT immortalized (T0026)	2. Model constructed with KC-HPV did not form a well-differentiated epithelium with a disorganized multilayer was formed.	 very low expression of involucrin, K10, K13 protein and Ki67 collagen type IV and laminin 5 	
(189)	An In-Vitro Analysis of Peri-Implant Mucosal Seal Following Photofunctionalizatio n of Zirconia Abutment Materials	Acellular cadaveric dermis (Alloderm)	Primary human gingival keratinocytes and fibroblasts. + zirconia implant abutment	1.(4-6) layers of epithelial Cells 2. Model tissue was attached to the implant surface. 3- Long junctional epithelial attachment was observed in smooth titanium than in the rougher surface, whereas the rougher titanium surface had a long dimension of connective tissue attachment		Permeability test for a biological seal of tissues around Ti disc evaluation as normal.
(199)	Commensal and pathogenic biofilms differently modulate peri-implant oral mucosa in an organotypic model	Bovine collagen type I	immortalized human oral keratinocyte cell line (OKF6/TERT-2) and Primary human gingival fibroblast	 (4) different layers of the differentiated epithelium, 2-Tight epithelial barrier Model tissues were attached to the implant surface. 		Following biofilm challenges: - increase in TNF-α and decrease of IL-6, CXCL8, CXCL1 and CCL2 inflammatory cytokine levels.
(299)	Establishment and Characterization of Immortalized Gingival Epithelial and Fibroblastic Cell Lines for the Development of Organotypic Cultures	Rat tail collagen type l	Immortalized human gingival (epithelial keratinocytes (HGEK-16) and fibroblasts (GFB-16)) were induced by E6 and E7 oncoproteins of human papillomavirus	1-Multi layered epithelium with no keratinizing of superficial layer 2- fibroblasts were evenly distributed in the Collagen gel matrix.	1- CK10, CK13, CK16, CK18, and CK19 2- Col I and Col II	

(178)	Phenotypic markers of oral keratinocytes seeded on two distinct 3D oral mucosa models	2-Acellular cadaveric dermis (Alloderm) 3-Porcine acellular dermal matrices (Strattice)	Primary human gingival keratinocytes and fibroblasts	gingival fibroblasts presented homogeneous distribution and lower adhesion and differentiation of oral keratinocytes 2- AlloDerm and Strattice matrices fibroblasts adhered well to the dermal surface.	1-Glucose consumption, proliferation of gingival fibroblasts 2-synthesis of hVEGF 3-gene expression of COLIA1 and hVEGF 4- AlloDerm substrate provided higher values for cell proliferation, and both gene expression, synthesis of hEGF and hKGF by oral keratinocytes	
(299)	BMP4 micro- immunotherapy increases collagen deposition and reduces PGE2 release in human gingival fibroblasts and increases tissue viability of engineered 3D gingiva under inflammatory conditions	Rat tail collagen type I	Immortalized Human Gingival Keratinocytes (iHGK) and Immortalized Human Gingival Fibroblasts- hTERT	1-A good multilayer epithelial 2.fibroblasts embedded in the collagen matrix.	1.Involucrin, CK 19 and 17 2. Vimentin marker for fibroblast.	1- High MTT assay 2-Low measured of (LDH) activity.
(225)	Development and characterization of a 3D oral mucosa model as a tool for host-pathogen interactions	Rat tail collagen type I	NOK-si keratinocytes immortalized human oral keratinocytes cells and Primary human gingival Fibroblast cells	1- 6-8 layers of stratified epithelium tissue cells. 2-Fibroblasts and collagen fibres showed a structural arrangement forming an intricate network	1.CK 13 and 14 . 2. Ki-67. 3.Collagen IV.	Destruction of epithelial layers after bacterial challenges.
(221)	Development and Characterization of In Vitro Human Oral Mucosal Equivalents Derived from	Rat tail collagen type I	Model (1) FNB6-TERT immortalized human oral keratinocytes and Human Primary gingival fibroblasts cells	Model (1) a multi-layered well-defined, stratified epithelium (120 μm) in thickness. The epithelium was stratified, nonkeratinized,	Model (1) a. ki-67. b. CK13. c. E-cadherin. d. CK14.	Increased secreassion of cytokines following bacterial challenge: - CXCL8 and IL-6

	Immortalized Oral Keratinocytes		Model (2) H357, an human oral squamous cell carcinoma (OSCC) cell line derived from the tongue and Human Primary gingival fibroblasts cells	Model (2) produced a multi-layered epithelium.	e.Gene expression for CXCL8 and ICAM-1. Model (2) a. ki-67. b. E-cadherin. c. CK 13 and 14.	
(224)	Limited in-depth invasion of Fusobacterium nucleatum into in vitro reconstructed human gingiva	Rat tail collagen type l	primary gingival keratinocytes and fibroblasts	(12–16) epithelial layers.	CK 13, CK19, and CK 10.	Destruction of epithelial layers after bacterial challenges.
(297)	Establishment of an oral infection model resembling the periodontal pocket in a perfusion bioreactor system	Porcine collagen, type I (3D collagen sponge)	Immortalized human gingival (epithelial keratinocytes (HGEK-16) and fibroblasts (GFB-16)) were induced by E6 and E7 oncoproteins of human papillomavirus	Well defined epithelial cell layers. Fibroblast cells filled most gaps between collagen fibers and formed a dense structure.		Increased secretion of cytokines following bacterial challenge: - IL-1b, IL-2, IL-4, and TFN-a
(196)	Saliva-Derived Commensal and Pathogenic Biofilms in a Human Gingiva Model	Rat tail collagen type I	Immortalized human gingiva cell line (Keratinocytes OKG4/bmi1/ TERT and fibroblast TERT (T0026)	1.Multilayered differentiated epithelium. 2.fibroblast-populated collagen substrate.		1.Destruction of epithelial layers after bacterial challenges. 2. Increased secretion of cytokines following bacterial challenge: - CCL20, IL-6, CXCL8, and CCL2
(227)	Evaluation of a novel oral mucosa in vitro implantation model for analysis of molecular interactions with dental abutment surfaces	Rat tail collagen type I	Immortalized human gingiva keratinocyte (KC-TERT, OKG4/bmi1/TERT And fibroblast cell lines (Fib-TERT, T0026))	 1 -(7-9) layers of well differentiated stratified. 2.fibroblast-populated collagen. 3- epithelial down-growth. parallel to the surface of both abutments. 	 Ki67 A collagen IV/laminin V CK 4 and 19 	The interactions of gingival tissue to implant surface were similar to two types of titanium abutments, anodized and machined,
(296)	Multi-species oral biofilm promotes reconstructed human	Rat tail collagen type I	immortalized human gingiva keratinocyte (KC-	Thick and multiple keratinocyte layers.	1. PCNA protein 2. Ki-67.	1.Increased thickness of epithelial layers

	gingiva epithelial barrier function		TERT,OKG4/bmi1/TERT) and fibroblast (Fib- TERT, T0026) cell lines			after bacterial challenges. 2. Increased secretion of cytokines following bacterial challenge:- IL-6, CXCL8, CXCL1, CCL20.
(220)	Oral mucosa model based on a collagen– elastin matrix	Collagen/elastin matrix (Matriderm, bovine collagen type I with elastin)	Primary human gingival keratinocytes and fibroblasts.	Multilayered formation of gingival keratinocytes Prominent basement membrane	collagen IV.	
(226)	Tissue engineering of human oral mucosa on different scaffolds: in vitro experiments as a basis for clinical applications	1-Dermal Regeneration Template (DRT) 2-Vicryl 3-TissuFoil E (TFE)	Human primary gingival keratinocytes and fibroblast.	1- DRT. Owing to the rough surface, fibroblasts were able to migrate into the scaffold with the seeding of keratinocytes and the epithelium formed 2.7 layers of keratinocytes. 2- On Vicryl, fibroblasts were able to grow as well as keratinocytes, but no stratification of cells was visible in the dermis (fibroblasts) and epidermis (keratinocytes) as occurred on TFE and DRT 3- On TFE demonstrated formation of epithelium with 9.3 layers of keratinocytes which formed a homogeneous stratified cell layer	 Cells on DRT expressed more laminin 1 than cells on TFE Collagen IV in TFE and DRT On Vicryl, no collagen IV staining could be observed. 	
(219)	In vitro reconstruction of human junctional and sulcular epithelium	Rat tail collagen type I	Model (1) Primary human gingival keratinocytes and fibroblasts Model (2) Primary human gingival keratinocytes and primary periodontal fibroblasts	(11–16) epithelial layers	1-Ki-67 2- ODAM 3-FDC-SP 4- CK 8, CK10, CK13, CK16, and CK19. 5-transglutaminase. 6- filaggrin. 7- collagen IV and Laminin-1.	

(295)	Differential influence of Streptococcus mitis on host response to metals in reconstructed human skin and oral mucosa	Rat tail collagen type I	Primary human gingival keratinocytes and fibroblasts	Thick and multiple keratinocyte layers	Кі67.	Increased expression of Toll-like receptors 4 following bacterial challenge.
(223)	3D engineered human gingiva fabricated with electrospun collagen scaffolds provides a platform for <i>in vitro</i> analysis of gingival seal to abutment materials	1-Electrospun bovine collagen type I 2-decellularized dermis 3-Bovine collagen type I type I 4-Released bovine type I collagen	Primary human gingival keratinocytes and fibroblasts	stratified epithelium with a layer of tightly packed basal keratinocytes was present along the junction between the epithelium and connective tissue.	1. CK4, CK5, CK10 2. collagen IV and laminin - 332. 3.collagen type I	There were tissue attachments with the following implant surfaces: - 1. machined titanium. 2. SLA (sandblastedacid etched) titanium. 3. ceramic. 4.PEEK (Polyetheretherketone).
(222)	Engineering a 3D In Vitro Model of Human Gingival Tissue Equivalent with Genipin/Cytochalasin D.	1-Rat tail collagen type I. 2- Rat tail collagen type I that crosslinked with genipin. 3- Rat tail collagen type I that crosslinked with cytochalasin D. 4- Rat tail collagen type I that crosslinked with cytochalasin D,	Immortalized human gingiva keratinocyte hTERT (TIGKs, CRL-3397, ATCC) and Immortalized human gingiva fibriblast hTERT (hGFBs, CRL-4061, ATCC)	multilayered stratified epithelium with clear suprabasal and basal layers in the epithelium, similar to human native gingiva. The epithelium formed on the surface of collagen hydrogel populated with fibroblasts.	1. Ki67 2-CK14, and CK10, Involucrin. 3-vimentin, collagen 1a1, and CD9	1-The sizes of crosslinked models with genipin or genipin/ cytochalasin D were larger than non-crosslinked model and crosslinked model with cytochalasin D. 2-The size of crosslinked model with cytochalasin D was a bit larger than non-crosslinked model.

3.3.4. Macroscopical model appearance

In this review, a study conducted by Koskinen Holm, C., and Qu, C. examined the macroscopic appearance of three gingival models constructed using type I collagen (rat tail), crosslinked with genipin, cytochalasin D, or a combination of both (222). Genipin serves as a chemical crosslinking agent, while cytochalasin D inhibits rapid actin polymerization (300, 301). The findings revealed that the models crosslinked with genipin or the genipin/cytochalasin D combination were larger in size compared to the non-crosslinked model.

3.3.5. Histological analysis

The selected studies conducted histological structural analysis to assess the successful construction of 3D models, utilizing various staining techniques. These included hematoxylin (H), hematoxylin and eosin (H&E), Periodic acid-Schiff (PAS), Masson's trichrome, and van Gieson staining methods.

3.3.5.1. Epithelium layer

The number of epithelial cell layers was reported in nine studies across thirteen models, ranging from 4 to 16 layers (188, 189, 199, 201, 219, 224-227) (Tab.3.6).

Dabija-Wolter et al. provided data on both the number and thickness of epithelial layers. At day 3 of development, the epithelium measured 37.73 μ m in thickness, increasing to 49.79 μ m, 130.93 μ m, and 190.83 μ m at days 5, 7, and 9, respectively (219). Jennings et al. reported a well-stratified epithelium with a thickness of 120 μ m. Chai et al. described a pre-implant gingival model with a thickness ranging from 50 to 100 μ m (201). Meanwhile, Kriegebaum et al. demonstrated gingival model formation, reporting an epithelial thickness of 111.6 μ m when using TFE and 31 μ m with DRT (213).

3.3.5.2. Connective tissue layer

Regarding the formation characteristics of the connective tissue layer, eleven studies utilizing nineteen models confirmed the presence of fibroblasts embedded within well-organized collagen fibrils (178, 183, 187, 220, 222, 223, 225-227, 298, 299). Only one study reported the thickness of the connective tissue layer, revealing that when TFE and DRT were used as substrates for

gingival model construction, the resulting connective tissue layers measured 249.3 µm and 420.9 µm, respectively (226).

3.3.6. Differentiation of gingival model

3.3.6.1. Keratinocytes proliferation and differentiation markers

The expression of keratinocytes proliferation marker Ki67 was investigated in eleven models (196, 221, 222, 224, 225, 227, 295, 296). Shang et al. investigated Ki67 and the expression of PCNA as a markers for cell proliferation to confirm the proliferation potential of keratinocytes in the model (296). Koskinen Holm, C., & Qu, C., detected apoptotic p53 marker in their study. However, this marker was not detected in models which prepared by using collagen type I hydrogel (222).

Cytokeratins (CKs) serve as the primary intermediate filaments within gingival epithelial tissues. Their expression patterns in different regions of the gingival epithelium have been widely used as molecular markers (302, 303).

CK4 is predominantly present in the suprabasal compartment of non-keratinized epithelia, including the buccal mucosa and sulcular gingival epithelium. Tomakidi et al. examined CK4 expression in models developed using primary non-keratinized gingival cells, observing its presence in the suprabasal layer (183). Roffel et al. reported CK4 expression in peri-implant gingival models, specifically in the free gingival and sulcular epithelia, but not in the junctional epithelium (227). Similarly, Sakulpaptong et al. confirmed CK4 expression in peri-implant gingival models derived from human primary gingival cells, along with its presence in native gingival tissues (223).

CK13, a marker for non-stratified epithelium, was analyzed in eight studies (183, 187, 199, 219, 221, 224, 225, 299). Buskermolen et al. demonstrated that CK13 expression in gingival models, constructed using both primary and immortalized gingival keratinocytes, closely resembled native gingiva. However, a gingival model established using KC-HPV exhibited very low CK13 expression (187). In contrast, Jennings et al. reported abnormal CK13 expression in a gingival model using OSCC cells ((221).Tomakidi et al showed the expression of CK14 was only limited to the basal layer (183). Whereas de Carvalho Diasa et al. and Koskinen Holm & Qu, C., reported CK14 expression in both basal and suprabasal layers (222, 225). Jennings et al. observed CK14 expression throughout the entire

epithelium (221), while Bao et al. noted lower levels of CK14 in gingival models compared to native human gingival tissue (299).

CK5 is commonly found in the basal cell compartment in all stratified epithelia. Two studies investigated the expression of CK5 (183, 223) both of which confirmed its confinement to the basal cell layer based on gene expression and immunolocalization studie.. In a study by Sakulpaptong et al. (2022), CK5 was expressed in peri-implant gingival models as well as in human native gingival tissue.

CK10 is known to be largely expressed in cornifying stratified and proliferating epithelia. Six studies analyzed the expression of CK10 in gingival models (183, 187, 199, 222, 224, 299). Buskermolen et al. and Koskinen Holm & Qu, C., observed that CK10 expression patterns in gingival models closely matched those of native human gingiva. However, CK10 levels were significantly lower in models constructed using immortalized KC-HPV cells (187, 222).

Additional cytokeratins, including CK8, CK16, CK17, CK18, and CK19, were investigated in three studies (219, 298, 299).

CK18 and CK19 expression levels were found to be comparable between 3D gingival models and native human gingival tissues (299). Ferra-Cancellas confirmed CK17 and CK19 expression in multilayered keratinocytes within 3D models (298). Dabija-Wolter et al. detected CK16 expression in the suprabasal layer of gingival models, whereas in native gingival tissue, it appeared in both parabasal and suprabasal layers. In the same study, CK19 and CK8 were found in all cell layers of the gingival model, while in native gingival tissues, their expression was limited to specific patterns in the basal layer (219).

Two studies showed the expression pattern of involucrin in the 3D gingival model was similar to native human gingival tissue (187, 222). Other markers such as ODAM, FDC-SP, transglutaminase, and filaggrin were reported as junctional epithelial-specific markers (219).

E-cadherin is a major protein involved in cell-to-cell adhesion. Its expression has been identified in three different models (199, 221, 224), supporting the presence of a robust epithelial barrier.

3.3.6.2. Basement membrane markers

Collagen IV and laminin are important proteins within the basement membrane. Six studies investigated and confirmed the expression of these two proteins in the basement membrane in the models (183, 187, 219, 223, 226, 227).

3.3.6.3. ECM components markers

In this review two studies reported the expression pattern of collagen type I (Col I) and collagen type II (Col II). The levels of expression of these two markers were found not significantly differed from native human gingival tissue (223, 299). However, one study reported expression of both collagen 1, and CD90 by using quantitative Reverse Transcription-PCR (qRT-PCR) technique. qRT-PCR technique is a molecular biology technique that measures the amount of RNA present in a sample by first converting it into cDNA and then amplifying the cDNA using real-time PCR, allowing for accurate quantification of gene expression (222).

3.3.6.4. Vimentin a fibroblast differenciation marker

Buskermolen et al. and Koskinen Holm, C., & Qu, C., showed the expression of vementin marker in gingival model was similar to native gingival tissue. Similarly, Ferrà -Cañellas et al. reported the expression of vimentin in the gingival model, which confirms the development of fibroblast in the gingival model (187, 222, 299).

3.3.7. Application of gingival model for periodontal research

Regarding the use of these gingival models, research has shown their application in various periodontal studies. Additionally, eight peri-implant models were identified across five different studies as shown in Figure 3.2.

In total, nine studies demonstrated the applicability of gingival models in host-microbial interaction studies. Within these nine studies, seven studies reported the response of gingival models to different bacterial challenges (196, 221, 224, 295-299). Four studies (196, 224, 296, 298) demonstrated the alteration of the epithelial layer upon the host-microbial interaction.

The gingival model was also used to investigate candida infection and it showed alteration of the structure by prominent degradation of the cornified layer of epithelial cells (188).

Peri-implant mucosal models were used either for comparing different types of titanium and dental material posts surfaces (201,223,227), or for photofunctionalized effect on the biological seal of different types of abutment materials (189).

Moreover, there was a potential application of 3D gingival models to study wound healing processes of the gingiva either following cold injury (196), micro-immunotherapy medicine (low dose of bone morphogenic protein (LD BMP4))(298), or for the exposed model to sensitizers (295).

3.3.8. Types of substrate biomaterials used to construction of gingival model

In total, 10 different substrate types were identified among all 37 models reported. The most frequent used substrate was type I collagen sourced from rat tail, which was used in twenty-three models (178, 183, 187, 188, 196, 219, 221, 224, 225, 227, 295, 296, 298, 299). The second more frequent substrate was acellular human cadaveric dermis (Alloderm). This substrate was used in three models (178, 189, 201). Decellularized dermis (purose dermis allograft) substrate used in another model (223). The other substrate including porcine collagen type I (297), porcine acellular dermal matrices (Strattice)(178), collagen/elastin matrix substrate (Matriderm) (bovine collagen type I with elastin) (220), dermal regeneration template (DRT) Single Layer substrate, Vicryl substrate, Tissu Foil E (TFE) (226), bovine type I collagen substrate were used to prepare four models (199, 223), (Tab. 3.6) and (Fig. 3.2).

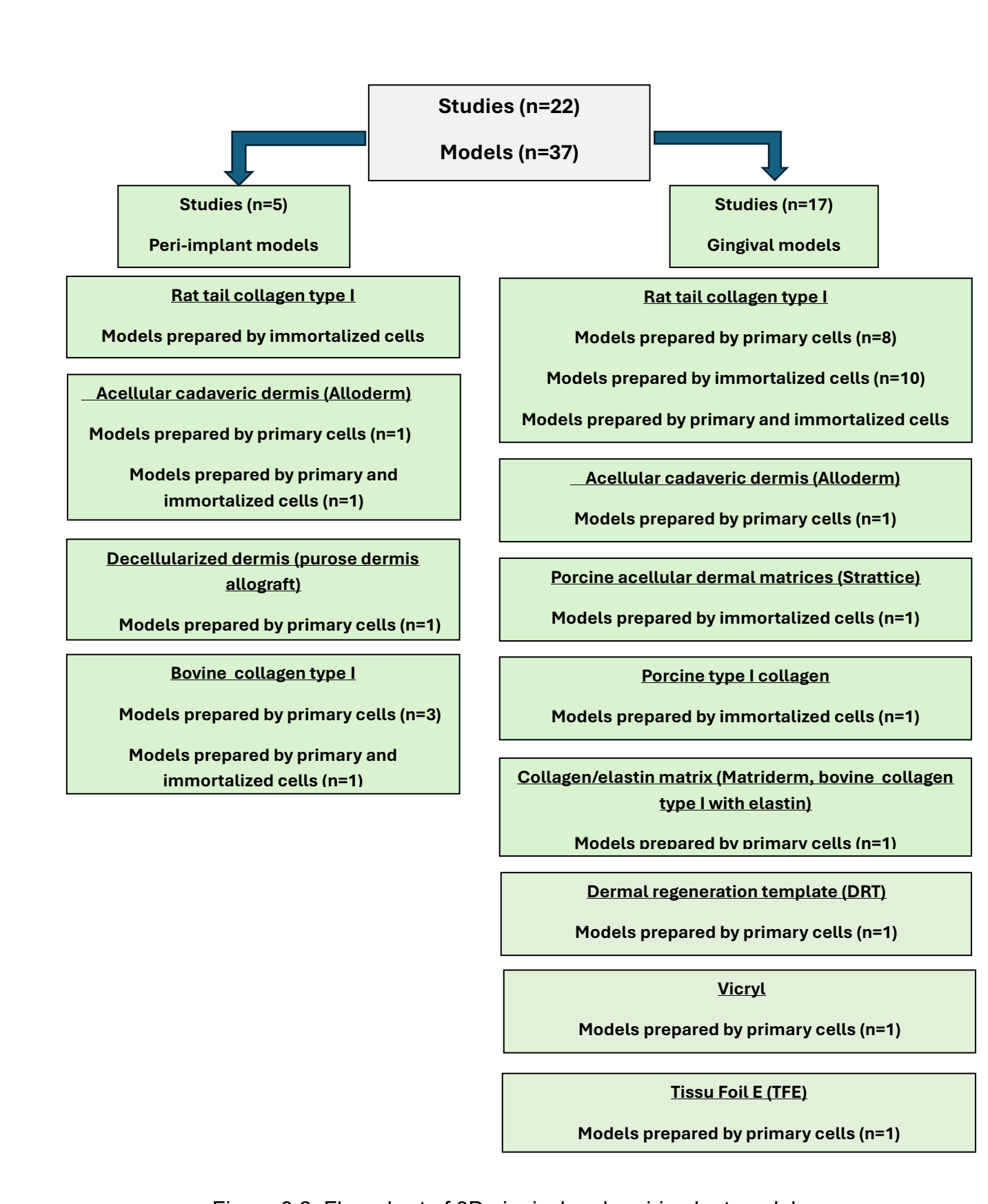


Figure 3.2. Flow chart of 3D gingival and peri-implant models.

3.4. Discussion

This review analyzed 37 different 3D gingival and peri-implant models from 22 studies. Twelve models showed good cell proliferation (Ki67 marker) in basal and suprabasal layers, and most demonstrated epithelial cell differentiation (various CK markers). However, no single model emerged as the best for studying 3D gingival or peri-implant tissues.

Gingival models have been developed using primary cells, immortalized cell lines, or both. Models derived from primary cells formed the most epithelial layers (224). Whereas those using H357 and OSCC cell lines lacked well-differentiated epithelium (187, 221). In contrast, one study reported that established Immortalized cell lines from primary human gingival cell induced by E6 and E7 oncoproteins of human papillomavirus, and resulted in a successful formation of gingival model with multi-layered epithelia (299). These observations confirmed that these two types of immortalized human gingival cells (H357 and OSCC) are not suitable sources for gingival model construction. Additionally, greater clarity is needed when reporting cell-line-based models, as these cells inherit traits from their parent tissues but may not fully replicate normal epithelial behavior (188, 299).

Substrate selection is crucial for gingival model construction, requiring biocompatibility, porosity, and mechanical stability. Ten different substrates were reviewed, with most being animal-derived. Rat tail collagen type I was the most used, supporting epithelial stratification and confirmed to allow the formation of the highest number of epithelial layers (188, 219, 224, 225). However, Rat tail collagen type I substrate is prone to shrinkage, high cost, and structural differences from human ECM. Crosslinking with genipin/cytochalasin D improved shrinkage resistance and cell survival. Other animal-based substrates, including bovine and porcine collagen, showed promise but lacked resemblance to native gingival connective tissue.

A crucial element in the construction of a gingival model is the substrate that provides scaffolding for the cells. The ideal substrate should have a high level of biocompatibility, porosity, biostability, and mechanical properties. In this review ten different substrates demonstrated to be applicable as matrices to mimic native gingival ECM and most of them were of animal origin. Rat tail collagen type I

isolated from rat tail tendon was the most used and confirmed to allow the formation of the highest number of epithelial layers (188, 219, 224, 225). The stratification of epithelial layers indicates the development of a gingival model, at the same time, a high level of stratification of keratinocytes has been demonstrated when there is an underlying homogenous distribution of fibroblasts among substrates. Rat tail collagen is considered the major type of collagen that is used as a substrate to mimic human ECM. Shrinkage is often regarded as a drawback of models prepared using collagen type I, as it can significantly reduce the cell population within the hydrogel. However, studies have shown that crosslinking collagen type I hydrogel with genipin or a combination of genipin and cytochalasin D enhances its resistance to shrinkage, thereby promoting higher cell survival and functionality (222). Additionally, other limitations of this collagen include its high cost and structural differences from human ECM collagen, where type I and III collagens are the predominant components. Moreover, isolated rat tail collagen is inherently fragmented (11). These drawbacks collectively limit the suitability of rat tail collagen hydrogel for constructing gingival models.

Bovine and porcine origin collagen substrates were identified. A bovine collagen type I (199, 223) which demonstrated stratification and differentiation of epithelial layers with underlying connective tissue containing fibroblasts. Porcine substrate was also used as a source of collagen type I to mimic human ECM as 3D collagen sponge scaffolds in a perfusion bioreactor system for easy manipulation (297). However, these two substrates were not counted as a promising type for model construction due to lacking resemblance to native gingival human connective tissue.

In addition to collagen, various dermal substrates have been extensively utilized in tissue engineering and cell culture studies. This review examines four dermal substrates employed in gingival model reconstruction, including acellular cadaveric dermis and decellularized dermis (porous dermis allograft), derived from human (178, 189, 201, 223), porcine (strattice matrix) (178), and bovine (Matriderm) (220) sources. These substrates demonstrated effective keratinocyte proliferation, differentiation, and stratification, along with a high distribution of fibroblasts. However, their application is constrained by limited availability.

Lastly, DRT was utilized as a substrate for gingival model construction, consisting of a porous matrix of crosslinked bovine tendon collagen fibers. Gingival models

with thick tissue layers demonstrated higher cell proliferation when compared to those using equine (TissuFoil E) and synthetic (Vicryl) substrates (226). In one study, electrospun type I crosslinked bovine collagen was employed to recreate a peri-implant gingival model (223), resulting in reduced tissue contraction and promising outcomes. The observed size changes and contraction following model construction are attributed to the slow remodeling activity of the selected substrates in comparison to native gingival tissue. This limitation, along with those previously mentioned, should be considered when selecting an appropriate substrate for developing an advanced gingival model.

It is worth mentioning that all the evidence on the use of different substrates collectively confirmed a high level of heterogeneity and the lack of a clear superior substrate to use for constructing the best 3D gingival model.

This review highlighted high heterogeneity, and lack of standardized fabrication and characterization protocols for the creation of a valid 3D gingival or peri-implant model. We, therefore, propose a new framework for future characterization and construction of a 3D gingival model.

The first step should include histological confirmation that the new model results in well-defined stratified epithelium layers with equal or more than four cell layers, and fibroblasts embedded and distributed homogenously in a well-structured substrate. Secondly well differentiated tissue layers should be confirmed via specific markers expression for each cell or layer regions, as following:

- Ki67 for cell proliferation near basal epithelial layer
- CK14 and CK5 for early differentiation in the basal layer and
 CK4 or CK13 in the suprabasal layer.
- CK16, CK18, CK19 and CK17 in different epithelial layers as late differentiation markers
- Involucrin as terminal differentiation marker for keratinocytes within the upper two third of the epithelium
- CK10 marker to confirm the presence of cornifying stratified epithelia as well as in proliferating epithelia
- Collagen IV and Laminin expression for the basement membrane

- CD90 and Collagen (I and II) in ECM
- Vimentin expression to confirm development of fibroblasts.

Thirdly an ideal 3D gingival model to use for different dental applications will need a well-developed structure including capillary vessels, epithelial and stromal cells as well as immune, neural and bone cells (Fig. 3.3).

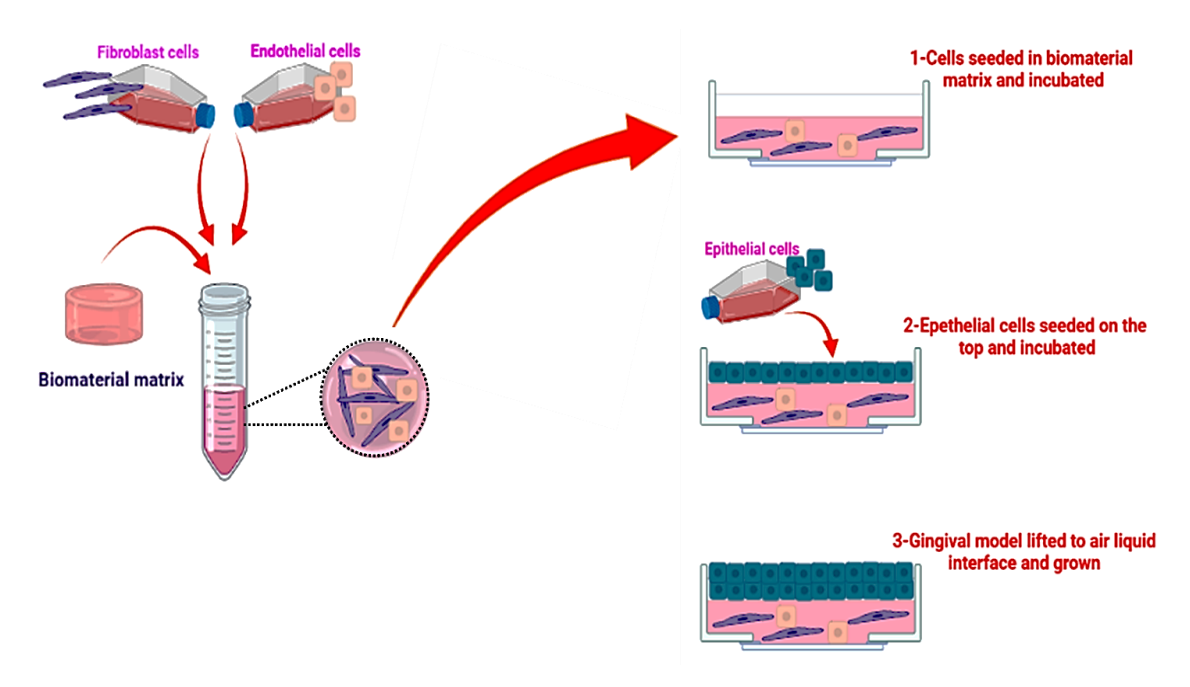


Figure 3.3. Schematic representation of the experimental protocol to generate 3D gingival model

In conclusion, there is currently insufficient evidence to confirm that available 3D gingival models can fully replicate the complexity of native human gingival tissue or serve as reliable platforms for experimental periodontal research. The findings of this review underscore a critical research gap: existing models often lack well-defined cell origins and appropriate substrates, limiting their ability to reproduce the physiological architecture and functional properties of gingival tissues. Addressing these limitations will require the development of standardized protocols, incorporation of tissue-specific cells, and exploration of advanced biomaterials to achieve models that are both physiologically relevant and experimentally robust.

Future research should aim at resolving the current challenges of construction a developed 3D gingival model with complex structure to mimic native human gingival tissue. Construct a developed 3D gingival model should be done by

engineering a new substrate with a high remodeling activity and suitable microenvironment for seeding human gingival cells.

The result from this systematic review showed that rat tail collagen type I is considered a more frequent substrate used for 3D gingival mode construction. However, this substrate has several disadvantages, for example, this substrate is expensive, and isolated rat tail collagen is invariably fragmented in addition to difficult manipulation in the lab (205). Therefore, it's important to prepare an alternative suitable substrate for 3D gingival model construction that recapitulates native human ECM. Moreover, the alternative substrate should be cost-effective and easily scalable from laboratory production. Therefore, and for engineering a novel substrate, additional projects should be contributed for reaching our goals.

CHAPTER 4

4.TARGET SPATIAL EXPRESSION ANALYSIS OF PERIODONTITIS ASSOCIATED GENES IN HUMAN GINGIVAL TISSUE USING NANOSTRING GEOMX PROFILING

4.1. Introduction

Recent studies utilizing different molecular and gene expression analysis have established a significant relationship between periodontitis and specific gene expression profiles. These investigations have provided deeper insights into the molecular mechanisms underlying periodontitis. Transcriptome profiling of gingival tissues was studied by Kim et al. This study analyzed pooled RNA samples from gingival tissues of both healthy individuals and periodontitis patients using RNA sequencing. The findings revealed 400 up-regulated genes in periodontitis tissues, particularly associated with defense and immune responses, receptors, proteases, and signaling molecules. Notably, genes such as CSF3, MAFA, CR2, GLDC, SAA1, LBP, MME, and MMP3 were among the most up-regulated. Conversely, 62 down-regulated genes, mainly related to cytoskeletal and structural proteins, were identified (81).

In a study by Qian et al, single-cell RNA sequencing was employed to investigate the local microenvironment of inflammatory responses in periodontitis. Single-cell transcriptomic profilings of gingival tissues from two patients and two healthy donors were performed. This approach led to the identification of specific cell subsets, including HLA-DR-expressing endothelial cells, CXCL13⁺ fibroblasts, and proinflammatory NLRP3⁺ macrophages, which are highly associated with immune regulation in periodontitis. The study also revealed increased cell-cell communication between macrophages and T/B cells in inflamed periodontal tissues, advancing our understanding of the cellular interactions driving chronic inflammation in periodontitis (235).

Periodontitis and peri-implantitis share similar clinical features; however, they are distinct diseases. Therefore, conducting molecular analyses of gingival tissue samples from peri-implantitis and periodontitis patients is crucial. In recent study, Zhou et al. examined gingival tissue samples from healthy individuals and

compared them with samples from patients with peri-implantitis and periodontitis. These samples were collected for genome-wide sequencing to investigate differential expression of mRNAs, IncRNAs, and miRNAs using high-throughput sequencing and competitive endogenous RNA (ceRNA) analysis. The study concluded that IncRNA-miRNA-mRNA interactions regulate key pathways, including the Hippo signaling pathway, Wnt signaling pathway, Toll-like receptor signaling pathway, NOD signaling pathway, oxidative stress response, and innate immune processes. These regulated pathways and biological processes may contribute to the distinct pathogenesis of peri-implantitis compared to periodontitis (236).

Gene expression of human gingival tissue that affected with periodontitis has been characterized by Lundmark et al. The results from that study revealed distinct clusters of gene expression, which were identified to correspond to epithelium, inflamed areas of connective tissue, and non-inflamed areas of connective tissue. (237).

It is worth mentioning the findings from a recently reported case study by Reddy and Manohar, which investigated the treatment of gingival recession using the coronally advanced flap technique. In that study, gingival tissue samples were collected from treated recession sites that had undergone palatal connective tissue grafting. One year postoperatively, the authors conducted histological analysis and whole-genome sequencing (WGS) on the tissue samples. Clinically, the treated areas appeared non-keratinized. Histological examination confirmed regions of non-keratinization and para-keratinization. However, WGS analysis revealed significant expression of keratinization genes, as well as neural crest and positional marker genes. That study concluded that, despite the clinical appearance of non-keratinization, the underlying genetic expression indicated keratinization activity. This highlights the complex interplay between genomic and phenotypic expression, underscoring fundamental biological Moreover, it is essential to recognize that an organism's phenotype is not solely dictated by genetic expression but is also influenced by intricate interactions between genetic background and environmental factors (238).

Collectively, these studies demonstrate that different sequencing techniques serve as a powerful tool in elucidating the complex gene expression and cellular

interactions involved in periodontitis, thereby enhancing our understanding of its pathogenesis and potential links to systemic diseases.

However, a major limitation of these methods is that RNA is extracted from bulk tissue samples, resulting in gene expression data that reflect an average across all cells present in the tissue. Consequently, assigning gene expression to specific cell types remains a challenge, highlighting the need for more refined methodologies.

To identify potential genes, target of periodontitis tissue and compare with healthy gingival tissue. NanoString GeoMx DSP was applied to analyze tissue samples that had previously undergone RNA sequencing. The data generated enabled a spatially resolved transcriptomic analysis, which was used to interpret the functional gene expression landscape across specific regions of interest. Moreover, this technique is used to evaluate gene expression, gene ontology analysis, and gene ontology of the kyoto encyclopedia of genes and genomes pathways. This study includes different genes that has been proved to be played a vital role in inflammatory process of gingival and periodontal tissue (239, 240). Hopefully, an in depth understanding of the molecular pathogenesis of periodontitis may lead to the development of diagnostic tool and novel therapies. Therefore, combining molecular characterisation with tissue-engineered scaffold development offers a rational strategy to design functional 3D gingival models that closely resemble human periodontal tissues and support translational applications in disease modelling and regenerative therapies.

4.2. Materials and Methods

4.2.1. Tissue samples

Tissues were obtained from 6 patients: three healthy patients and three with periodontitis. Written informed consents were obtained from all the respective parents or legal guardians. Diagnosis of periodontitis was established based on the presence of periodontal pockets ≥5 mm, bleeding on probing, and radiographic evidence of alveolar bone loss. Specific staging or grading of periodontitis (according to the 2017 World Workshop classification) was not applied during sample selection. The patients, age 25–50 years old, were included for this study and all of them are non-smokers. Their identification information has been acquired for this study including, medical history, surgical

history, and dental history. All the information was kept strictly confidential. The patients' individual information was neither utilized for any purpose other than the purpose of the study nor published in this manuscript.

4.2.2. Tissue sample preparation for sequencing

Tissue samples were storage and transported in formalin. These samples were washed three times with phosphate buffer solution (PBS), before putting in 30% sucrose, in PBS, until they settled to the bottom. Embed samples in OCT and keep in -80 °C freezer. Samples were cut into 5um slides, at -20 °C degree, using a freezing microtome (LEICA CM1860 UV CRYOSTAT) and sent for analysis. For spatial transcriptomic analysis using the GeoMx DSP platform, more than one slide per patient was processed, and multiple regions of interest (ROIs) were selected from each slide to represent distinct microenvironments within the gingival tissue.

4.2.3. Spatial Transcriptomic Profiling and Targeted Gene Analysis

The prepared tissue samples were sent to Queen Mary Genomic Centre (https://www.qmul.ac.uk/blizard/genome-centre/). Spatial transcriptomic profiling was performed using the NanoString GeoMx Digital Spatial Profiling (DSP) platform. Analysis was included tissue optimization, sample processing, library quality control, sequencing, and initial data analysis (Fig. 4.1).

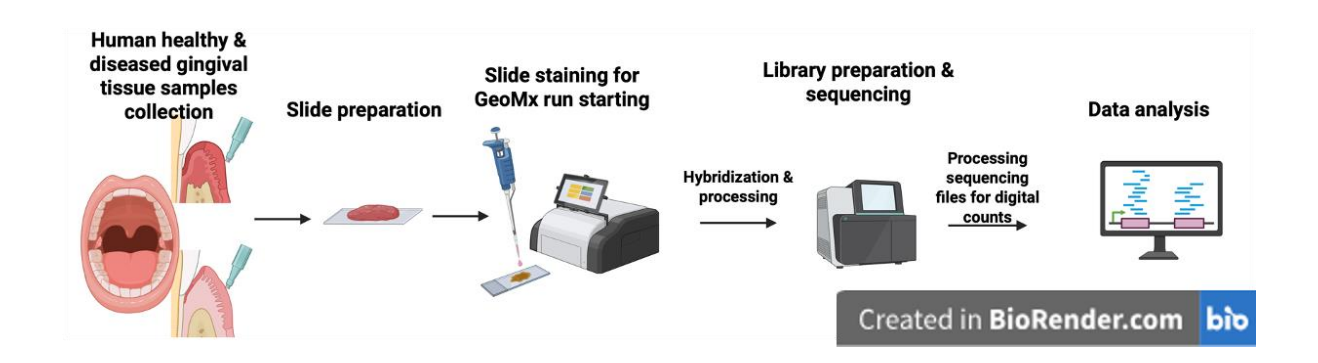


Figure 4.1. Schematic drawing depicting processes for sample preparation. Created in BioRender.com

The bioinformatic analysis was performed using DAVID web-based tool and idep96 web site (http://bioinformatics.sdstate.edu/idep96) (239-241). In addition,

the WEB-based Gene Set AnaLysis Toolkit was performed for the biological interpretation of Differential gene expressions (DEGs) (242, 243). WebGestalt is a system that facilitates the analysis of sets of genes that can be visualized and organized by a user selected method. These genes were classified according to Gene Ontology (GO) terms and Kyoto Encyclopedia of Genes and Genomes (KEGG) pathways. Statistical analysis. Data from image analysis are presented as the means ± SEM. Statistical comparisons were made using a two-way ANOVA. A value of p<0.05 was considered to indicate a statistically significant difference.

4.3. Results

As a result, the final dataset included 25 regions of interest: 12 from healthy tissues and 13 from diseased tissues. This approach allowed for enhanced spatial resolution and a more representative profiling of gene expression patterns across different anatomical or pathological zones within each sample.

Although whole transcriptome data was available through the GeoMx DSP platform, a targeted approach was adopted to enhance the depth and relevance of analysis. Approximately 90 genes were manually selected based on robust evidence from previously published studies indicating their significant involvement in periodontal inflammation, immune response, tissue remodelling, and regeneration processes (239-243).

4.3.1. Gene expression in inflamed and non-inflamed connective tissue

In order to investigate genes differentially expressed between diseased and healthy gingival tissue, gingival tissue samples obtained from patients with periodontitis.

Genes expression from these tissue samples were compared to genes expression from healthy gingival tissue. DGEs for both diseased and healthy groups were displayed by using heatmap (Fig. 4.2). The upregulated as well as the downregulated genes are demonstrated in Table 3.1. Results indicated that the expression of a total of 90 genes was altered by around 1-fold in one sample tissue type relative to the other. From these genes there were 78 down-regulated, and 12 up-regulated genes. In healthy tissue, the expression levels of down-regulated genes were higher compared with diseased tissues, and the

differences were non-significant between these two groups. While in the diseased group, the expression levels of twelve up-regulated genes were almost double values than those in the healthy tissue. The twelve up-regulated genes were (KRT16, KRT14, KRT12, KRT24, KRTDAP, SPRR2B, COL11A1, MMP2, MMP9, CXCL8, PERP, and GATA4) (Table 4.1). Additional details are provided in Appendix D.

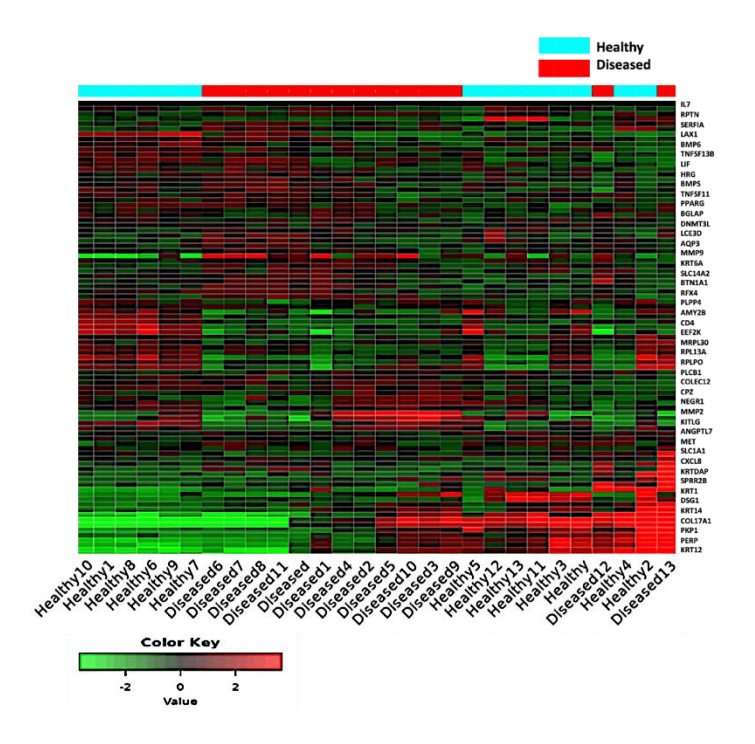


Figure 4.2. Clustering dendrograms identified by Heat map depicts the tissue genes expression. Green represents lower expression, and red represents higher expression. Each branch in the figure represents one gene.

Table 4.1. demonstrated up and down-regulated genes expressions for both healthy and diseased gingival tissue samples.

	ENSEMBL_GENE_ID	Gene Name	Gene symbol	FC(Fold change)	up/down
1	ENSG0000186847	keratin 14	KRT14	1.265727	Up
2	ENSG00000186081	keratin 5	KRT5	0.793068	Down
3	ENSG00000263243	keratin 12	KRT12	1.647641	Up
4	ENSG00000186832	keratin 16	KRT16	1.510421	Up

		p53 apoptosis			
5	ENSG00000112378	effector related to PMP22	PERP	1.246194	Up
6	ENSG00000196805	small proline rich protein 2B	SPRR2B	9.979945	Up
7	ENSG00000285109	GATA binding protein 4	GATA4	1.390595	Up
8	ENSG00000137699	tripartite motif containing 29	TRIM29	0.75974	Down
9	ENSG00000060718	collagen type XI alpha 1 chain	COL11A1	1.957203	Up
10	ENSG00000277263	major histocompatibility complex, class II, DR alpha	HLA-DRA	0.217025	Down
11	ENSG00000081277	plakophilin 1	PKP1	0.726006	Down
12	ENSG00000142541	ribosomal protein L13a	RPL13A	0.289439	Down
13	ENSG00000185069	keratin 76	KRT76	0.428571	Down
14	ENSG00000089157	ribosomal protein lateral stalk subunit P0	RPLP0	0.495678	Down
15	ENSG00000087245	matrix metallopeptidase 2	MMP2	1.254699	Up
16	ENSG0000010095	matrix metallopeptidase 9	ММР9	3.791005	Up
17	ENSG00000065618	collagen type XVII alpha 1 chain	COL17A1	0.735182	Down
18	ENSG00000173801	junction plakoglobin	JUP	0.968685	Down
19	ENSG0000010610	CD4 molecule	CD4	0.25354	Down
20	ENSG00000090382	lysozyme	LYZ	0.317639	Down
21	ENSG00000122188	lymphocyte transmembrane adaptor 1	LAX1	0.245332	Down
22	ENSG00000125780	transglutaminase 3	ТСМЗ	0.629771	Down

23	ENSG00000163751	carboxypeptidase A3	CPA3	0.490221	Down
24	ENSG00000188508	keratinocyte differentiation associated protein	KRTDAP	1.447987	Up
25	ENSG00000167768	keratin 1	KRT1	0.323614	Down
26	ENSG00000134760	desmoglein 1	DSG1	0.825523	Down
27	ENSG00000275903	proteasome 20S subunit beta 3	PSMB3	0.510352	Down
28	ENSG00000186395	keratin 10	KRT10	0.312863	Down
29	ENSG00000169429	C-X-C motif chemokine ligand 8	CXCL8	3.18231	Up
30	ENSG00000104783	potassium calcium-activated channel subfamily N member 4	KCNN4	0.29356	Down
31	ENSG00000167916	keratin 24	KRT24	1.770435	Up
32	ENSG00000049130	KIT ligand	KITLG	0.667404	Down
33	ENSG00000160221	glutamine amidotransferase class 1 domain containing 3	GATD3A	0.469251	Down
34	ENSG00000240038	amylase alpha 2B	AMY2B	0.384152	Down
35	ENSG00000185567	AHNAK nucleoprotein 2	AHNAK2	0.929439	Down
36	ENSG00000172260	neuronal growth regulator 1	NEGR1	0.754368	Down
37	ENSG00000103319	eukaryotic elongation factor 2 kinase	EEF2K	0.446568	Down
38	ENSG00000166825	alanyl aminopeptidase, membrane	ANPEP	0.615302	Down
39	ENSG00000185414	mitochondrial ribosomal protein L30	MRPL30	0.497389	Down

40	ENSG00000017427	insulin like growth factor 1	IGF1	0.606401	Down
41	ENSG00000115009	C-C motif chemokine ligand 20	CCL20	0.924981	Down
42	ENSG00000105810	cyclin dependent kinase 6	CDK6	0.64243	Down
43	ENSG00000026103	Fas cell surface death receptor	FAS	0.48961	Down
44	ENSG00000109625	carboxypeptidase Z	CPZ	0.866555	Down
45	ENSG00000158270	collectin subfamily member 12	COLEC12	0.672862	Down
46	ENSG00000153162	bone morphogenetic protein 6	ВМР6	0.505926	Down
47	ENSG00000132170	peroxisome proliferator activated receptor gamma	PPARG	0.645816	Down
48	ENSG00000102524	TNF superfamily member 13b	TNFSF13B	0.561053	Down
49	ENSG00000128342	LIF interleukin 6 family cytokine	LIF	0.585023	Down
50	ENSG00000079102	RUNX1 partner transcriptional co- repressor 1	RUNX1T1	0.736664	Down
51	ENSG00000173157	ADAM metallopeptidase with thrombospondin type 1 motif 20	ADAMTS20	0.693219	Down
52	ENSG00000104432	interleukin 7	IL7	0.578322	Down
53	ENSG00000124713	glycine N- methyltransferase	GNMT	0.517857	Down
54	ENSG00000203805	phospholipid phosphatase 4	PLPP4	0.607098	Down
55	ENSG00000242252	bone gamma- carboxyglutamate protein	BGLAP	0.635862	Down

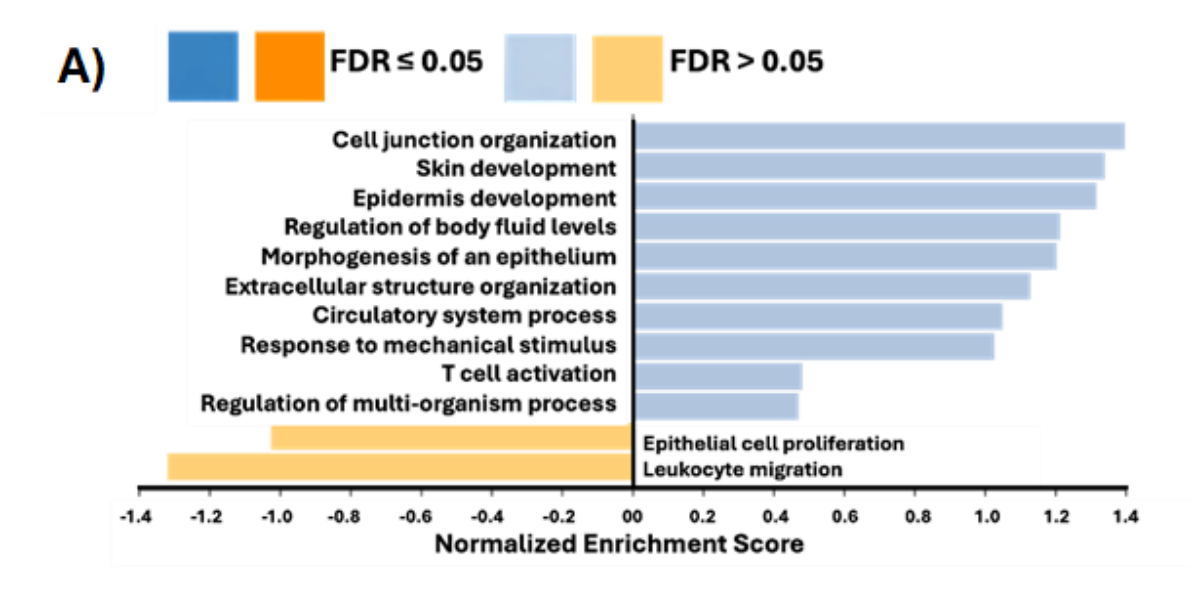
56	ENSG00000126246	IGF like family receptor 1	IGFLR1	0.580016	Down
57	ENSG00000105976	MET proto- oncogene, receptor tyrosine kinase	MET	0.772794	Down
58	ENSG0000013297	claudin 11	CLDN11	0.764595	Down
59	ENSG00000106688	solute carrier family 1 member 1	SLC1A1	0.946572	Down
60	ENSG00000120659	TNF superfamily member 11	TNFSF11	0.609692	Down
61	ENSG00000117009	kynurenine 3- monooxygenase	кмо	0.599613	Down
62	ENSG00000182621	phospholipase C beta 1	PLCB1	0.647243	Down
63	ENSG00000134873	claudin 10	CLDN10	0.68697	Down
64	ENSG00000133063	chitinase 1	CHIT1	0.646793	Down
65	ENSG00000158481	CD1c molecule	CD1C	0.640437	Down
66	ENSG00000029559	integrin binding sialoprotein	IBSP	0.63178	Down
67	ENSG00000118156	zinc finger protein 541	ZNF541	0.630996	Down
68	ENSG00000143768	left-right determination factor 2	LEFTY2	0.714006	Down
69	ENSG00000204866	IGF like family member 2	IGFL2	0.658667	Down
70	ENSG00000113905	histidine rich glycoprotein	HRG	0.688822	Down
71	ENSG00000142182	DNA methyltransferase 3 like	DNMT3L	0.645881	Down
72	ENSG00000101441	cystatin S	CST4	0.660983	Down
73	ENSG00000215853	repetin	RPTN	0.752706	Down
74	ENSG00000112175	bone morphogenetic protein 5	ВМР5	0.702341	Down
75	ENSG00000124557	butyrophilin subfamily 1 member A1	BTN1A1	0.879959	Down

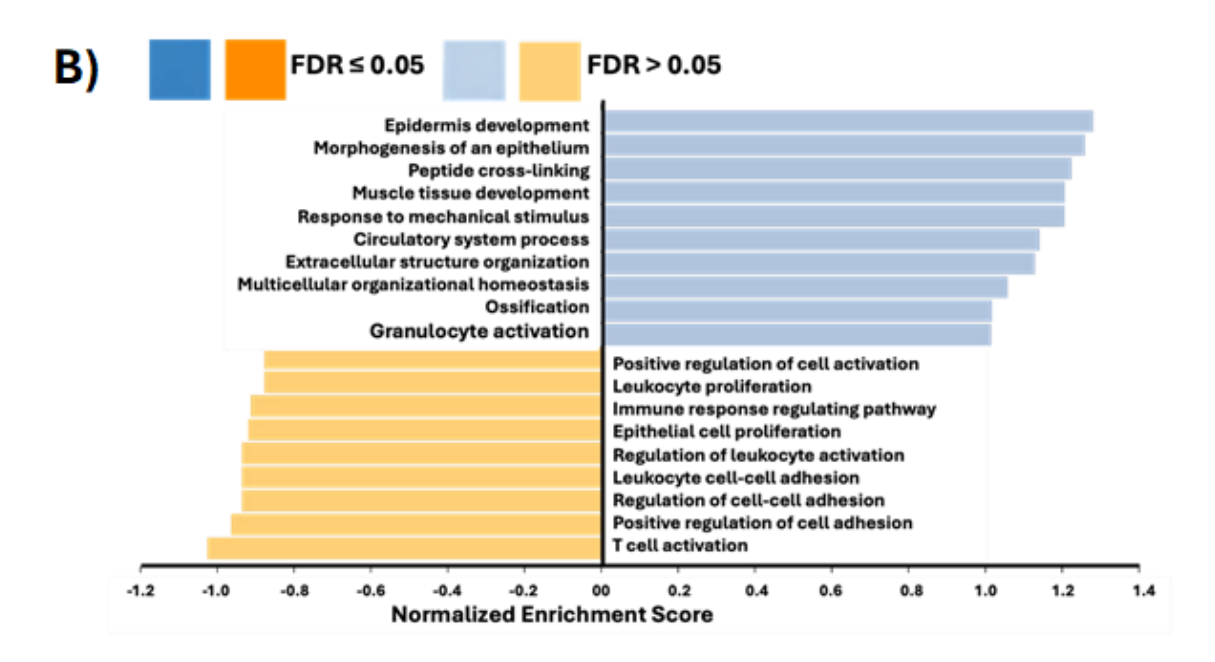
76	ENSG00000171819	angiopoietin like 7	ANGPTL7	0.640698	Down
77	ENSG00000132874	solute carrier family 14 member 2	SLC14A2	0.774131	Down
78	ENSG00000277429	small EDRK-rich factor 1B	SERF1B	0.710364	Down
79	ENSG00000018625	ATPase Na+/K+ transporting subunit alpha 2(ATP1A2)	ATP1A2	0.724563	Down
80	ENSG00000105509	hyaluronan synthase 1	HAS1	0.764759	Down
81	ENSG00000185962	late cornified envelope 3A	LCE3A	0.712111	Down
82	ENSG00000077279	doublecortin	DCX	0.760591	Down
83	ENSG00000165272	aquaporin 3 (Gill blood group)	AQP3	0.741379	Down
84	ENSG00000205420	keratin 6A	KRT6A	0.841564	Down
85	ENSG00000120332	tenascin N	TNN	0.765854	Down
86	ENSG00000140795	myosin light chain kinase 3	MYLK3	0.783669	Down
87	ENSG00000111783	regulatory factor X4	RFX4	0.906952	Down
88	ENSG00000185966	late cornified envelope 3E	LCE3E	0.746683	Down
89	ENSG00000163202	late cornified envelope 3D	LCE3D	0.861111	Down
90	ENSG0000170689	homeobox B9	HOXB9	0.714609	Down

4.3.2. Gene Ontology analysis

To analyse the specific biological functions and features of the selected genes, an analysis toolkit (WebGestalt) was applied for gene ontology (GO) annotation and enrichment analysis. The DEGs for each sample group were classified according to biological process (Bio), molecular function (MoI) or cellular component (CeI) using the WebGestalt software package on the basis of hypergeometric tests. The Resulting Bio, MoI and CeI networks are shown as directed acyclic graphs (DAG), which are color-coded (red for p-values <0.05)

(Fig. 4.3.C&D), and (Fig. 4.4, and 4.5.A&C). In addition to graphs for GO classification from the biological process, of ontology enrichment, for both healthy and diseased tissue samples respectively (Fig. 4.3.A&B), and (Fig. 4.4, and 4.5.B&D). The number of proteins enriched in each GO term is shown on the top of each bar. In the healthy samples, the biological process enrichment was found for genes associated with epithelial cell proliferation, and leucocyte migration. While in diseased samples, the detected biological process enrichment for genes were epidermis development, T cell activation, positive regulation of cell adhesion, morphogenesis of an epithelium, peptide cross-linking, extracellular structure organization, circulatory system process, and response to mechanical stimulus (Fig. 4.3.C&D). Cellular component enrichment was detected in healthy and diseased samples for genes associated with the intermediate filamen cytoskeleton (Fig. 4.4.A&C). Molecular function enrichment was discovered for genes associated non significantly with receptor ligand activity, and cytokine receptor binding in healthy samples, and with receptor ligand activity in diseased samples (Fig. 4.5.A&C).





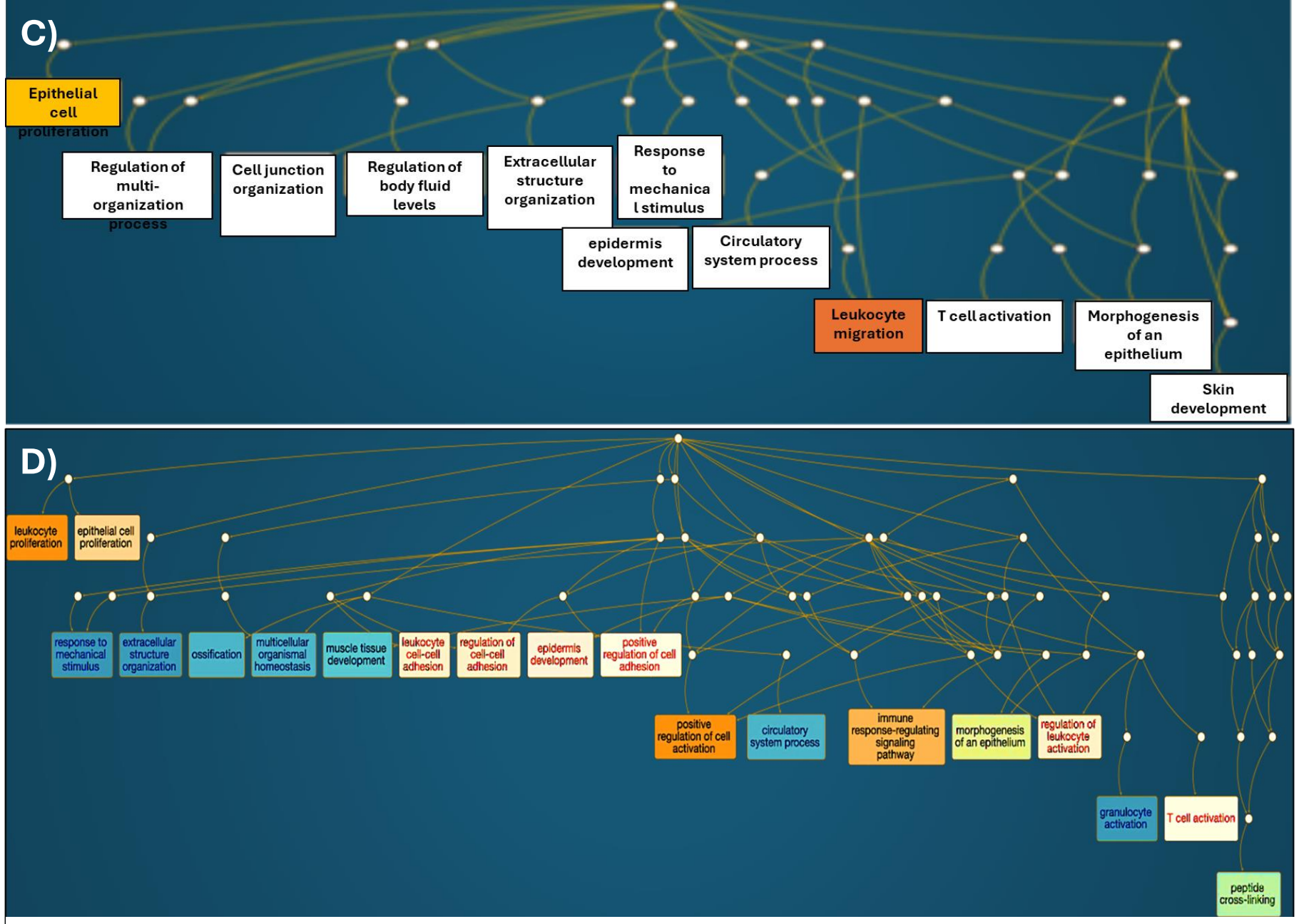


Figure 4.3. The identified genes were analyzed according to Gene Ontology (GO) enrichment using WebGestalt (WEB-based GEne SeT AnaLysis Toolkit). (A and B) GO classification from the biological process, of ontology enrichment, for both healthy and diseased samples respectively. The number of proteins enriched in each GO term is shown on the top of each bar. (C and D). Directed Acyclic Graph (DAG) of the enriched GO categories under biological process for both healthy and diseased samples respectively. Each node shows the name of the GO category, the number of gene in the category and the p-value indicating the significance of enrichment. The red colour represents p-values <0.05.

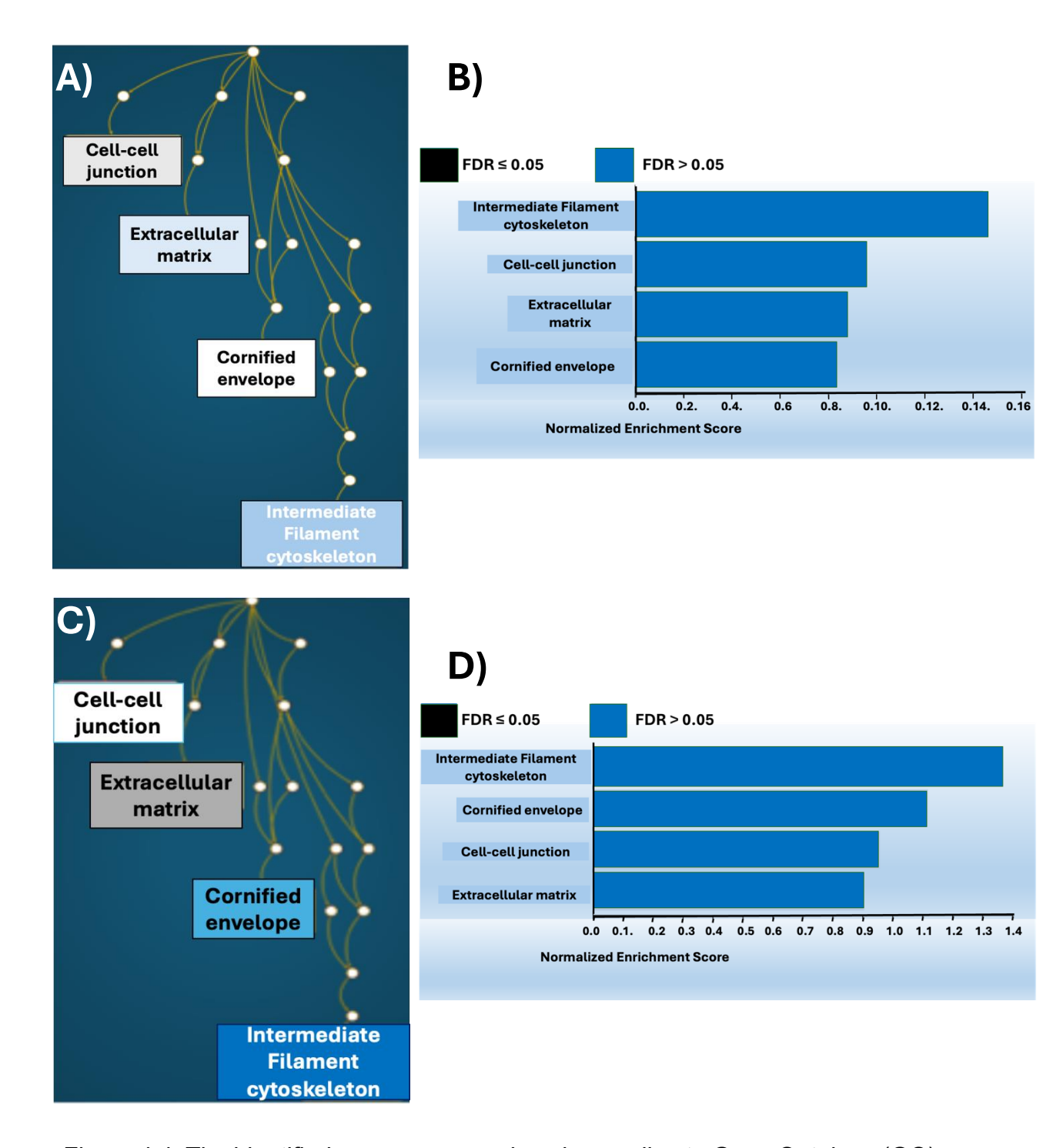


Figure 4.4. The identified genes were analyzed according to Gene Ontology (GO) enrichment using WebGestalt (WEB-based GEne SeT AnaLysis Toolkit). (A and C). Directed Acyclic Graph (DAG) of the enriched GO categories under cellular component for both healthy and diseased samples respectively. Each node shows the name of the GO category, the number of gene in the category and the darl colour p-value indicating the significance of enrichment. (B and D) GO classification from the cellular component, of ontology enrichment, for both healthy and diseased samples respectively.

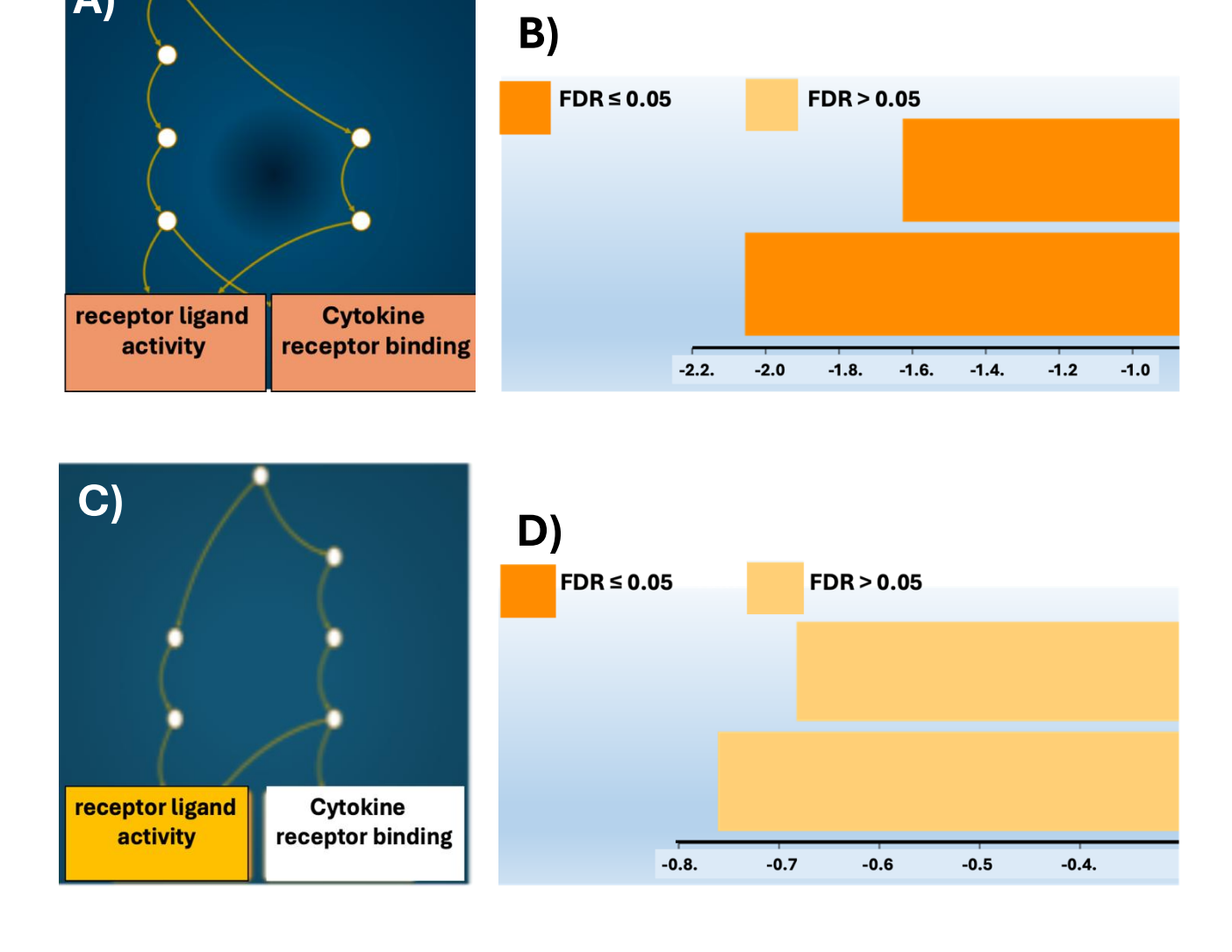


Figure 4.5. The identified genes were analyzed according to Gene Ontology (GO) enrichment using WebGestalt (WEB-based GEne SeT AnaLysis Toolkit). (A and C). Directed Acyclic Graph (DAG) of the enriched GO categories under molecular function for both healthy and diseased samples respectively. Each node shows the name of the GO category, the number of gene in the category and the p-value indicating the significance of enrichment. The orange colour represents p-values <0.05. (B and D) GO classification from the molecular function, of ontology enrichment, for both healthy and diseased samples respectively. The number of proteins enriched in each GO term is shown on the top of each bar.

4.3.3. Gene ontology of the Kyoto Encyclopedia of Genes and Genomes (KEGG) pathway

The included genes were classified using WebGestalt system. This system facilitates the analysis of sets of genes that can be visualized and organized by a user-selected method. The classification of these genes was based on data

on gene function in the gene ontology of the KEGG pathway data- base (Tab.

4.2). The expression of these genes was significantly altered in various

Table 4.2. List of enriched KEGG pathways of the differentially expressed proteins for both healthy and diseased gingival tissue samples.

Description of KEGG pathway	No. of hits	Expressed gene participating in the pathway	Size	Expect	Ratio	P Value	FDR
Protein digestion and absorption	6	ATP1A2, COL11A1, COL17A1, CPA3, KCNN4, SLC1A1	90	0.69889	8.5851	0.000063334	0.0078564
Cytokine- cytokine receptor interaction	10	BMP5, BMP6, CCL20, CD4, CXCL8, FAS, IL7, LIF, TNFSF11, TNFSF13B	294	2.2830	4.3801	0.000074645	0.0078564
Estrogen signaling pathway	8	KRT10, KRT12, KRT14, KRT16, KRT24, MMP2, MMP9, PLCB1	137	1.0822	7.3923	0.000010530	0.0034326
Hematopoietic cell lineage	6	ANPEP, CD1C, CD4, HLA-DRA, IL7, KITLG	97	0.75325	7.9655	0.000096397	0.0078564
Pathways in cancer	13	CDK6, CXCL8, FAS, IGF1, IL7, JUP, KITLG, MET, MMP2, MMP9, PLCB1, PPARG, RUNX1T1	526	4.1550	3.1287	0.00018058	0.011774
Salivary secretion	5	ATP1A2, CST4, KCNN4, LYZ, PLCB1	90	0.69889	7.1542	0.00062946	0.029315

Rheumatoid	5	CCL20, CXCL8,	90	0.69889	7.1542	0.00062946	0.029315
arthritis		HLA-DRA,					
		TNFSF11,					
		TNFSF13B					
p53 signaling	4	CDK6, FAS,	72	0.55911	7.1542	0.0022745	0.092687
pathway		IGF1, PERP					
Transcriptional	7	CXCL8, IGF1,	186	1.4693	4.7643	0.0060575	0.027762
misregulation		JUP, MET,					
in cancer		PPARG,					
		RUNX1T1,MMP9					
Cell adhesion	5	CD4, CLDN10,	144	1.1182	4.4714	0.0050131	0.16343
molecules		CLDN11, HLA-					
(CAMs)		DRA, NEGR1					

functional modules. The shared enriched pathways, including protein digestion and absorption, Cytokine-cytokine receptor interaction, Estrogen signaling pathway, Hematopoietic cell lineage, Pathways in cancer, Salivary secretion, Rheumatoid arthritis, p53 signaling pathway, Transcriptional misregulation in cancer, and cell adhesion molecules (CAMs). These pathways were determined at the significance levels of p<0.05 in WebGestalt. Nine out of twelve upregulated genes, KRT12, KRT14, KRT16, KRT24, MMP2, MMP9, PERP, COL11A1, and CXCL8 were among the enriched pathways. These upregulated genes included within the following pathways, protein digestion and absorption, Cytokine-cytokine receptor interaction, Estrogen signaling pathway, Pathways in cancer, Salivary secretion, Rheumatoid arthritis, and Transcriptional misregulation in cancer. However, thirty-one downregulated expreesed genes (ATP1A2, COL17A1, CPA3, KCNN4, SLC1A1, BMP5, BMP6, CCL20, CD4, FAS, IL7, LIF, TNFSF11, TNFSF13B, KRT10, PLCB1, ANPEP, CD1C, HLA-DRA, KITLG, CDK6, IGF1, JUP, MET, PPARG, RUNX1T1, CST4, LYZ, CLDN10, CLDN11, NEGR1) were included in whole over enriched pathways, as shown in Table 4.2.

4.4. Discussion

This study utilized a targeted spatial transcriptomic approach using the NanoString GeoMx platform, analysing a curated panel of approximately 90 genes selected based on their previously established roles in periodontitis and inflammatory pathways.

This study revealed distinct spatial expression patterns of these genes in human gingival tissue samples. The use of the NanoString GeoMx platform in this context enhances our understanding of the physiological and molecular processes involved in inflammation, wound healing, and soft tissue regeneration. It is worth mentioning again, that we applied this technology to compare gene expression between healthy and periodontitis affected gingival tissues, identifying key molecular differences and functional pathways between the two conditions.

The observation in analysis was the expression of the keratinization genes KRT12, KRT14, KRT16, and KRT24, among all the genes. These genes were in the top most level with highest raw counts in diseased samples. The elevated expression genes in diseased compared with healthy samples, confirmed the important role of these genes in inflammatory process of gingival tissue. Moreover, there was expression of genes of mesenchymal cell markers, CD4, CDK6, and CD1C. PKP1, DSG1, COL17A1, EEF2K, JUP, DCX, RUNX1T1, CPZ, and HLA-DRA genes were also expressed in this analysis. Surprisingly, the expressed genes with up regulated neither down-regulated were significant expressed. Taken together, the results suggested that the two types of tissues have a similar gene expression profile, paralleling the results determined by NanoString GeoMx platform. These molecular findings have direct implications for scaffold design in gingival tissue engineering. The high expression of keratinization-related genes (KRT12, KRT14, KRT16, KRT24) in periodontitisaffected tissue highlights the critical role of epithelial integrity and keratinocyte differentiation in maintaining gingival barrier function. Scaffolds intended for gingival regeneration should therefore support epithelial cell attachment, proliferation, and differentiation, while promoting keratinized tissue formation.

Similarly, the detection of mesenchymal and immune-related markers (such as CD4, CDK6, CD1C, and HLA-DRA) underscores the importance of designing scaffolds that can accommodate stromal-immune interactions, which are central to the inflammatory and wound-healing processes. In this context, scaffold properties such as biocompatibility, porosity, and the incorporation of bioactive cues should be tailored to recreate the cellular microenvironment that enables both epithelial and mesenchymal cell function. By aligning scaffold design with these molecular signatures, it becomes possible to develop more physiologically relevant 3D gingival models that better mimic native tissue structure and function. In human body, the epithelial tissue acts as a protective barrier against damage caused by chemical, physical and biological agents and is essential to the survival of an organism. To perform this function, epithelial keratinocytes undergo a defined program of differentiation that results in the expression of structural proteins that maintain the integrity and function of the tissue. keratinocyte differentiation associated protein (KRTDAP) is a gene which associated with epithelial differentiation and maintenance of stratified epithelia (244). Mutations in most of these genes are now associated with specific tissue fragility disorders which may manifest both in skin and mucosa depending on the expression pattern (245). For example, of keratinization disorders that associated with oral cavity and periodontal tissue, White Sponge Nevus, and Pemphigus (245-248). In this study, there were up-regulate expression of KRT16, KRT14, KRT12, KRT24, and KRTDAP, beside absence of other keratin genes. These results confirmed the influence of these genes on periodontal tissue in both healthy and disease conditions (97, 226). In contrast, the results revealed down-regulation of KRT1, KRT5, KRT76, and KRT6A genes. The expression of whole over these genes confirm their obvious role in periodontal tissue. It's worth to mention the important of mechanical function of stratified epithelial and epidermis type keratins is evident and proven through various human hereditary keratin diseases. Thus, point mutations of distinct keratin genes now widely explain the pathogenesis of several autosomal-dominant familial diseases, many of which are blistering skin diseases. The most wellknown of these inherited skin and mucosa fragility disorders is epidermolysis bullosa simplex, the various variants of which are caused by a spectrum of point mutations of KRT5 or KRT14 (249-251). Moreover, in present study, there was up-regulate expression of SPRR2B gene. It is a keratinocyte protein that first appears in the cell cytosol but ultimately becomes cross-linked to membrane proteins by transglutaminase. All that results in the formation of an insoluble envelope beneath the plasma membrane (111, 252, 253). The expression of this gene which coordinated with keratinocyte differentiation may contribute to a robust innate immune response in health and during initial infections of the oral cavity. Tissue of the periodontium is primarily composed of collagen; however, the gingiva was considered as a specific tissue which receives an attention during initial diagnosis of disease. This because of its function in the attachment of teeth and its role in resisting daily insults. Since collagen types I and III have been proved to be the most abundant collagen in gingiva (254). Results in this study revealed upregulated expression of COL11A1 gene. COL11A1 is collagen type XI alpha 1 chain. In contrast, there was down regulated expression of COL17A1 gene. COL17A1 is collagen type I alpha chain. The expression of this respective genes in this study does not come as a surprise, since the expression of these types of collagens might affected with age and biological sex (119). In addition, its expression related to unhealthy stoma of human tissue (255).

Matrix metalloproteinases (MMPs) are key proteases involved in destructive periodontal diseases (256). There are 23 existing MMPs which are zinc-dependent endopeptidases and belong to the metalloproteinase superfamily (120). MMPs were traditionally regarding to degrade ECM components and grouped according to their substrate specificity in collagenases, gelatinases, stromelysins, matrilysins, and membrane type MMPs (121). Because type I collagen represents the bulk component of periodontal ECM, special attention has been paid to collagenases particularly MMP-8 and MMP-13 and gelatinases—MMP-2, and MMP-9 in periodontitis. In this study, the results of diseased tissue samples showed up-regulate expression of MMP-2 and MMP-

9. In fact, MMP-2 and MMP-9, also known as gelatinases A and B, share similar proteolytic activities and degraded gelatins (denatured collagens), and specific ECM molecules including native type IV, V and XI collagens (257). These findings support the role of MMP-2 and MMP-9 as key regulators of ECM remodelling rather than agents of its outright degradation. Moreover, the diseased tissue samples expressed more genes associated with inflammation or immune reaction than did the healthy tissues. For example, CXCL8 was upregulated in the diseased tissues. Neutrophils in periodontitis are more active and act as an important factor in triggering the disease (258, 259). Neutrophils are affected by secretion of several proinflammatory chemokines, such as interleukin 8 (IL8 which renamed CXCL8). CXCL8 is an important proinflammatory chemokine since its secretion locally induces neutrophil extravasation from peripheral blood to the affected site, and also attracts numerous neutrophils present in the lamina propria and gingival epithelium (260-263). Expression of CXCL8 gene have been associated with periodontitis in different ethnic populations, as also demonstrated by meta-analyses (264, 265). However, the results in this study showed expression of C-X-C motif chemokine ligand 8(CXCL8) gene was up regulated in diseased tissue samples compared with healthy. From these results, we suggest that anti-CXCL8 may be a promising approach to modulate pathogenic immune responses in ginigval tissues.

For genes that related to apoptosis, the results showed the upregulate expression of PERP gene in diseased compared healthy tissue samples. DNA damage induced PERP gene and due to p53 protein accumulation, resulting in the induction of cell cycle arrest or apoptotic target genes (122, 123). Therefore, the expression of this gene might be a predictable for the severity of damaging gingival tissue that affected with periodontal diseases.

In previous studies have shown that GATA4 gene can affect the formation of type I collagen, which is considered a major collagen component of periodontal tissue (266). Therefore, the role of GATA4 in the progression of inflammation has recently received widespread attention. It was reported that the expression

of GATA4 was significantly increased in periodontitis rat models (267). In contrast, the results in present study showed there was upregulate expression of this gene in diseased compared with healthy tissue samples. These findings highlight the importance of GATA4 in maintaining health of periodontal tissue.

Additional to the above mentioned up-regulated genes, the results showed that there were several down-regulated expressed genes as well in present study. From these genes were HLA-DRA, RUNX1T1, ADAMTS20, TNN, and HOXB9. HLA-DRA gene is one of the HLA class II alpha chain paralogues. This class II molecule is a heterodimer consisting of an alpha and a beta chain, both anchored in the membrane. This molecule is expressed on the surface of various antigen presenting cells such as B lymphocytes, dendritic cells, and monocytes/macrophages, and plays a central role in the immune system and response by presenting peptides derived from extracellular proteins, in particular, pathogen-derived peptides to T cells (268, 269). Results revealed there was down-regulate expression of this gene. These results could represent the importance susceptibility or resistance factor to periodontitis. Moreover, previous studies revealed that RUNX1T1 gene is expressed in many normal tissues, especially brain, heart, skeletal muscle, and adipose tissue, with the brain and heart exhibiting the highest expression level (128, 129). Herein, we detected down regulate expression of this gene, indicated its association between RUNX1T1 gene expression and both healthy and diseased gingival tissue. ADAMTS20 gene expression was higher in healthy compared with diseased samples. Tissue cells of periodontium consider playing a role in development of this tissue through the secretion of ADAMTS (270). Human ADAMTS proteins (ADAMTS1, 4, 5, 8, 15, and ADAMTS9 and 20) are controlled production of aggrecanase and proteoglycanase enzymes. These enzymes could be a responsible of cleaving hyaluronan binding chondroitin sulfate proteoglycan of extracellular proteins, including aggrecan, versican, brevican and neurocan (270, 281). Nevertheless, ADAMTS proteins also have effects on angiogenesis (272). The expression of this gene indicated the role of this gene in remodelling process of healthy gingival tissue.

Tenascins are large extracellular glycoproteins participating in tissue modelling processes. Its mainly expressed during embryogenesis. In adults, expression of tenascins becomes more restricted, at least in normal conditions (273-275). Tenascin N gene (TNN) gene was found in the primary culture of osteoblasts which promotes cell migration and mineralization. Its considered to be active in collagen-containing extracellular matrix and extracellular space (276). This gene expressed in human periodontal ligament tissue and might be essential genes for this tissue function (277). It is also used as a specific marker of gliomaassociated blood vessels and stimulates angiogenesis (131). Down-regulated expression of this gene indicated its role in maintaining gingival ECM. This maintenance occurs through the association of angiogenesis function of TNN gene with tissue blood vessels. Another down-regulated gene is HOXB9. This gene is involved in cell proliferation and differentiation. It was reported that increased expression of this gene is associated with some cases of head and neck squamous cell carcinoma (298). And also expressed of this gene in other cancer types, such as in breast, gastric, lung, oesophageal cancers leukemia, prostate cancer and lung cancer (135, 279-281). Whereas it is downregulated in melanoma (282).

In biological process enrichment, both epithelial cell proliferation and leucocyte migration genes that were found to be associated healthy tissue samples. These results indicated a reduced rate of integration of diseased gingival tissue. This implies that the connective tissue underneath in the last tissue samples may not have complete control or effect over the keratinization potential of the epithelium above it (283). In contrast, cellular component enrichment results for genes were associated the intermediate filament cytoskeleton and these were non-significantly for both healthy and diseased tissue samples. These results indicated once more the important roles of keratin genes and epithelial integrity in gingival tissue with both healthy and diseased conditions. In molecular function enrichment analysis, there were genes associated and non-significantly with receptor ligand activity, and cytokine receptor binding in healthy samples, and with receptor ligand activity in diseased samples. These results confirmed

the similarity of molecular functional roles with both healthy and diseased tissue samples. To further analyses the DEGs, functional enrichment analyses were conducted using the WebGestalt tool. Our results revealed that the DEGs were associated with CAMs, transcriptional misregulation in cancer, and p53 signalling pathway which were the three most enriched terms. The most enriched term CAMs which play avital role in connecting gingival epithelial cells to each other and to underlying connective tissue. Human gingival epithelium constitutes a stratified squamous epithelium and forms the initial line of defence against bacteria and their byproducts. In healthy periodontal tissue, epithelia act as a barrier against bacterial exposure and controls it with its antimicrobial peptides. However, in periodontal disease, the epithelium regulates the response against bacteria mainly by interacting with immune cells (284, 285). These results together with gene ontology analysis results in terms of biological process, cellular component, and molecular function enrichment, confirmed gingival epithelia is likely to play a part in maintaining the gingival tissue and underlying structures with both healthy and pathological processes.

In conclusion, the two types of diseased and healthy tissues expressed the same specific genes related to their functions with non-significant differences. Moreover, this study has limitations that should be considered when interpreting the results. First, the analysis was conducted using a targeted panel of approximately 90 genes, which, while selected based on strong evidence of relevance to periodontitis, may not capture the full molecular complexity of the disease. A broader or whole-transcriptome approach could potentially reveal additional differentially expressed genes and pathways. Second, the relatively small sample size (n=6) limits the statistical power and generalizability of the findings. While care was taken to ensure high quality tissue preparation and analysis, inter-individual variability cannot be fully accounted for in this study design. Therefore, future studies with larger cohorts, unbiased transcriptome wide profiling, and single cell resolution could provide more comprehensive insights into the spatial and molecular landscape of periodontal disease.

CHAPTER 5

5. THE PHYSICAL AND BIOLOGICAL PROPERTIES OF HYDROGEL SUBSTRATES TO MIMIC NATIVE HUMAN GINGIVAL EXTRACELLULAR MATRIX

5.1. Introduction

Several biomaterials have been demonstrated for cell culture and cell scaffold engineering to mimic human ECM, for this reason, choosing a suitable biomaterial is critical for cell culturing success to provide (3D) templates to facilitate cell adhesion, growth, proliferation, and differentiation.

Hydrogel biomaterials are considered well suited and attractive biomaterials for 3D cell culture substrate, because of their similarities to natural ECM, by having mechanical properties similar to many soft tissues (305). Furthermore, these hydrogels can be formed from a vast array of natural, synthetic, and semisynthetic materials, offering a broad spectrum of mechanical and chemical properties. These properties can provide a suitable environment for cells. Hydrogel biomaterials are high water content, good biocompatibility, controllable mechanical properties and biodegradability that impact cell proliferation, migration, aggregation, and normal cell activities. Hydrogels, particularly biodegradable polymer hydrogels, are ideal for 3D cell culture due to their hydrophilic nature, biocompatibility, and mechanical properties that resembling natural tissue. They are widely applied in tissue engineering, wound healing, and regenerative medicine (307). Recent studies showed the natural hydrogel biomaterials like collagen, sodium alginate, and gelatin are good candidate for 3D model construction (308-311). These natural hydrogels have good control over quantity of ECM proteins and growth factors (312, 313).

The most frequently used matrix is collagen hydrogel. Collagen is the primary organic constituent of human tissues. It is found in skin, bone, tendon, ligament,

and cornea of animals. Collagen is a natural material with excellent biological compatibility and low antigenicity (314). Therefore, it is considered an attractive scaffold in tissue engineering due to its retention of cells and bioactive molecules. It is the most popular candidate for engineering skin and oral mucosa and has been widely used by clinicians under various commercial brands. Collagen hydrogels are mostly composed of type I collagen, often a source for this hydrogel is rat tail tendon (178, 180, 187, 315). Rat tail collagen type I is also frequently used for the construction of 3D gingival models (195-198, 200). However, bovine skin collagen, porcine collagen type I, and equine collagen I membrane are considered as alternative sources for collagen substrate for 3D gingival model construction (186, 194, 199). In contrast, dermal regeneration template matrix (DRT) is also another source of collagen and is made from cross-linked bovine tendon collagen and a glycosaminoglycan (186). However, there are several drawbacks, including shrinkage, cost, and differences from human ECM collagen (where type I and III collagens are major components), as well as the fact that isolated rat-tail collagen is often fragmented. All these drawbacks prevent considering rat tail collagen hydrogel to be ideal for gingival model construction.

Sodium alginate (SA) isan anionic polysaccharides derived from brown algae (Phaeophyceae). SA is widely utilized in biomedical fields that include drug delivery, cell encapsulation, and 3D bioprinting. It has been widely used for tissue engineering studies due to its potential biomedical applications. SA solution gels fast and has possibility of formulating wide range of hydrogel viscoelasticity by ionic crosslinking with CaCl₂ and generating an ionic interchain bridge to increase its mechanical properties (316, 317). However, this gelation process is unstable and reversible (318, 319).

The viscosity of SA is determined by its concentration. Shear-thinning is another crucial rheological property of alginate solution, where viscosity is lessened by increasing the shear rate. Also, the viscosity decreases as the temperature increases. However, the resultant hydrogel's physical properties improved in

high concentration, the alginate solution becomes greatly viscous, which can cause damage to the cells (391, 392).

Gelatin is less organized structurally but has a molecular composition very similar to collagen (320). Gelatin is normally extracted from highly collagenous raw materials, such as porcine skin, cattle bones and bovine skin and hides. Recent studies present several attempts to obtain gelatin from fish skin and chicken. The advantages of gelatin include being inexpensive, widely available, and easy to use due to its high solubility. Additionally, different gelatin species origin sources are biocompatible, biodegradable, and do not induce antigenicity or toxicity in cells (321, 322). However, application of bovine source of gelatin is considered, as replacement to gelatin from porcine species origin, due to religious or ethical issues (323). In general, biomaterials of natural origin lack strength and mechanical tunability, while synthetic biomaterials often lack essential biological cue. Therefore, recent research emphasizes the need to fabricate novel biomaterials that account for both their biological and physicochemical properties (324).

Van Den Bulcke et al. described combination between gelatin and unsaturated methacrylamide groups. They presented gelatin-methacrylamide (GelMA)(325). In contrast to gelatin, GelMA as a semi-synthetic hydrogel, has better mechanical properties, while still keeping its biological properties. Moreover, GelMA is hydrogel with methacrylamide and methacrylate groups. These groups provide mechanical tunability while retaining gelatin's biological signals (326, 327). GelMA features enzymatic degradability via matrix metalloproteinases (MMPs), biocompatibility, RGD-mediated cell adhesion, and adjustable properties (215, 328). It has been applied in regenerating nerve tissue, soft tissue, muscle, skin, and gingiva, as well as developing vascularization, microvascular channels, and bone formation (205,216,328-334). Despite its advantages, GelMA's weak mechanical strength and rapid degradation limit long-term use. Enhancing GelMA with ECM components improves its mechanical properties and bioactivity (335, 336).

The aims of this project were to investigate the physical and biological properties of various hydrogels as effective substrates for constructing a 3D gingival model. Therefore, the hypothesis of this chapter was that a selected hydrogels, could exhibit properties suitable for this application.

The objectives of this study are to produce and comprehensively characterize the range of candidate hydrogels. Specifically, the study will evaluate the mechanical, chemical, and thermal properties of all selected hydrogel biomaterials as follows:

- a) To determine the morphology of the surface of all samples using the SEM.
- b) To determine the chemical characteristics by FTIR spectroscopy of samples.
- c) To determine the hydrophilic/hydrophobic nature of each hydrogel sample.
- e) To determine the thermal properties of each hydrogel sample.
- f) To determine the rheological characteristics of each hydrogel sample.

5.2. Materials and methods

This project was involveed the in laboratory synthesis and purification of GelMA-UCL using bovine skin gelatin (G9391, Sigma-Aldrich, UK). The materials utilized for GelMA-UCL synthesis and the purification procedures are detailed in Chapter 2, Section 2.2.1.

Hydrogel samples were prepared without crosslinking and at varying concentrations. These hydrogel solution samples were included, GelH, GelL, SAH, SAL, GelMAH, GelMAL, GelMAcH, and GelMAcL. The preparation process is outlined in Chapter 2, Section 2.2.2.

Structural characterization of the GelMA-Udifferent characterization MR and compared with commercial GelMA (GelMA-com) purchased from Sigma-Aldrich (GelMA Sigma), which is derived from porcine skin.Beyond GelMA-UCL and GelMA-com, the other hydrogel samples were examined with different

characterization techniques, including SEM, FTIR, WCA, DSC, and rheological analyses, were also performed.

5.3. Results

5.3.1. ¹H-NMR (Nuclear Magnetic Resonance) spectroscopy

Figure 5.1., illustrates the result of 1H-NMR analyses of three hydrogel samples from synthesised GelMA-UCL (GelMA-UCL1, GelMA-UCL2, and GelMA-UCL3) compared with GelMA-com hydrogel sample. In this graph, the gelatin spectra showed the proton signals are well resolved within the region of chemical shifts ranging from 0.7 to 3.8 ppm. These peaks could be assigned to the methyl resonances of specific amino acids and paired protons of –CH2– and –NH2 groups present in the molecular structure of gelatin (330,331). All hydrogel samples showed a relatively weaker signals observed at 7.2 ppm (Fig.5.1. d), which was assigned to the presence of aromatic ring

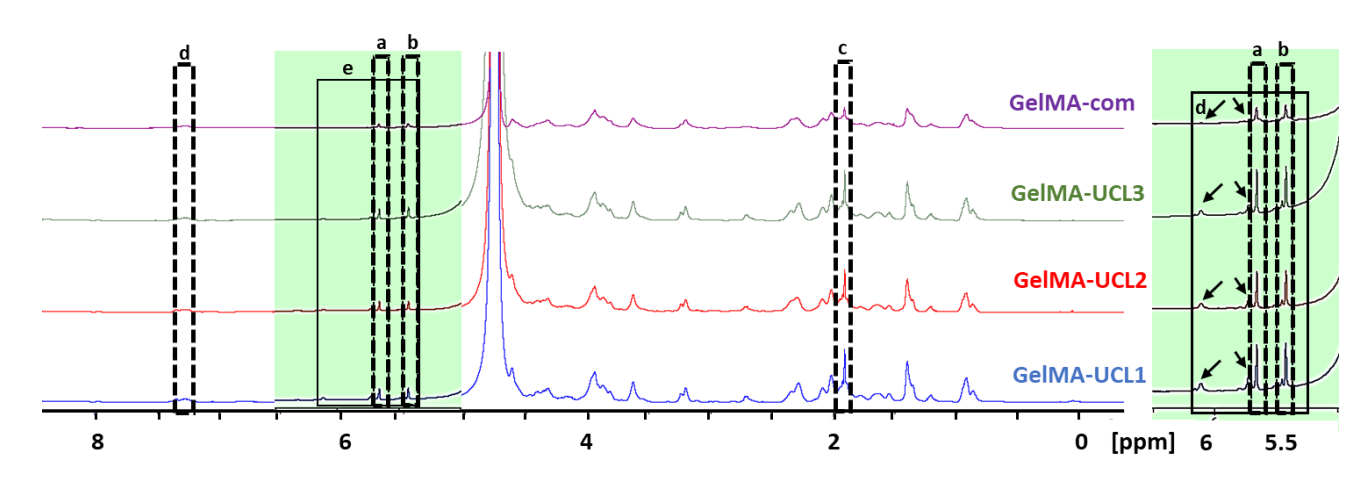


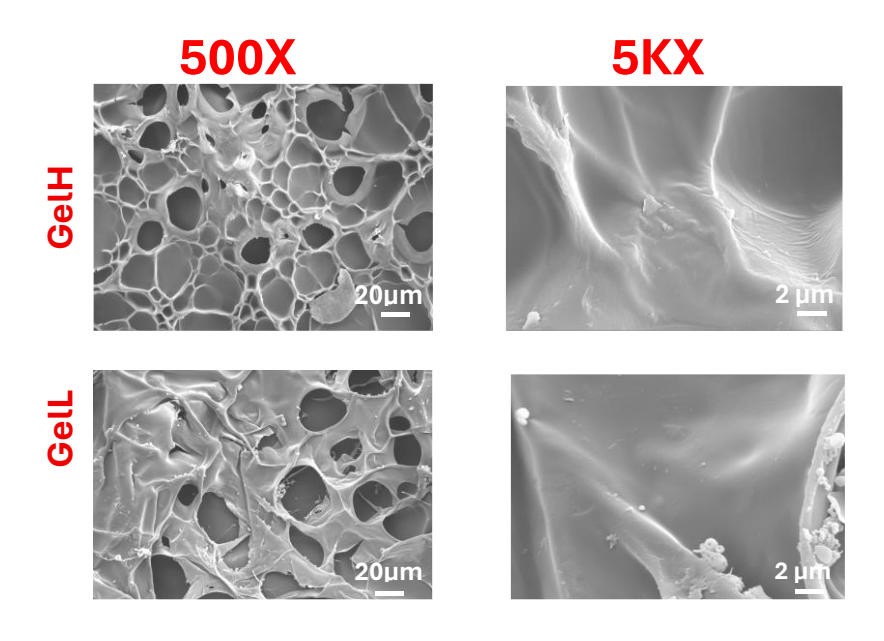
Figure 5.1.¹H-NMR spectra of GelMA-com. and prepared GelMA-UCL samples with three batches (GelMA-UCL1, GelMA-UCL2, and GelMA-UCL3). Specific protons of GelMA-com and GelMA-UCL were highlighted as follows: a—e was ascribed to acrylic protons of methacrylamide groups in lysine residues, acrylic protons of methacrylamide groups in hydroxylysine residues, methylene protons of non-modified lysine, methyl protons of methacryloyl groups, and acrylic protons of methacrylate groups, respectively.

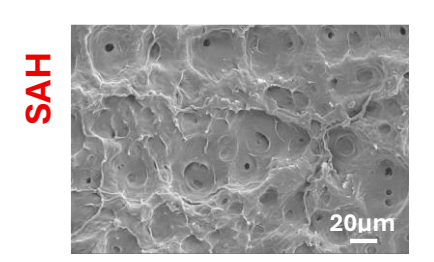
(330). By comparing the spectra of other samples, GelMA-com, has weak peaks observed between (5.4 and 5.6 ppm), corresponding to the two protons of methacrylate double bonds (a) and (b), respectively (Fig.5.1. a&b). In addition, in GelMA-com spectrum, showed a weak intensity peak at 2.15 ppm was present compared with other samples (Fig.5.1.c).

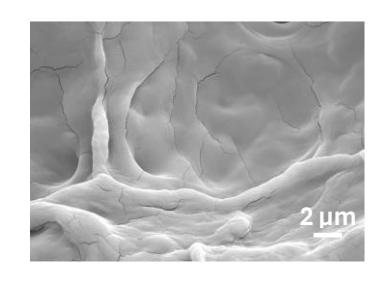
The degrees of methacrylation were calculated to be 65, 69 and 67% for GelMA-UCL1, GelMA-UCL2, and GelMA-UCL3, respectively.

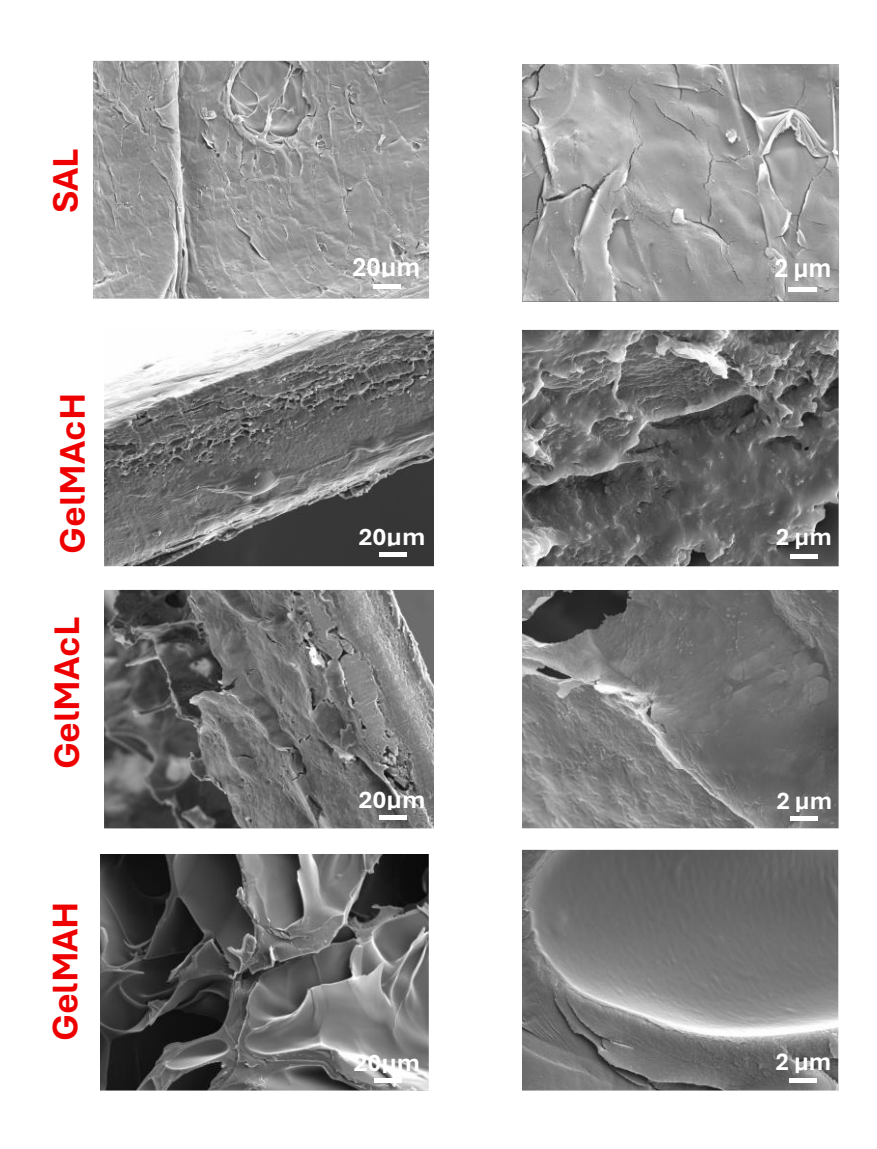
5.3.2. Scanning electron microscopy (SEM)

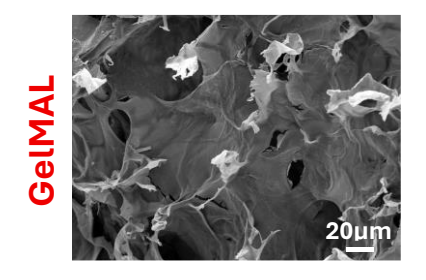
Figures 5.2 presented images with magnifications 500, and 5K X respectively. Different sizes of pores with pocket shapes are separated by thin walls that appeared on the surface of samples. The sizes of pores in all samples decreased with the increasing concentration of hydrogels. Increased porosity has been associated in previous studies with reduced mechanical strength of hydrogels (203, 337). This observation in SEM analysis aligns with the mechanical properties confirmed by subsequent mechanical analyses of the hydrogels.











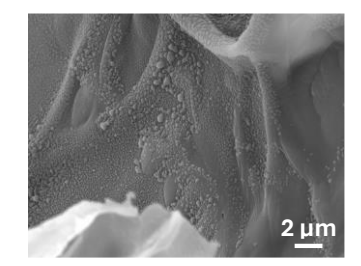


Figure 5.2. Scanning electron microscopy (SEM) images in 500X, and 5K X for nine hydrogels, GelH, GelL, SAH, SAL, GelMAcH, GelMAcL, and GelMAH vs GelMAL, respectively.

5.3.3. Fourier Transform Infrared (FTIR) spectroscopy

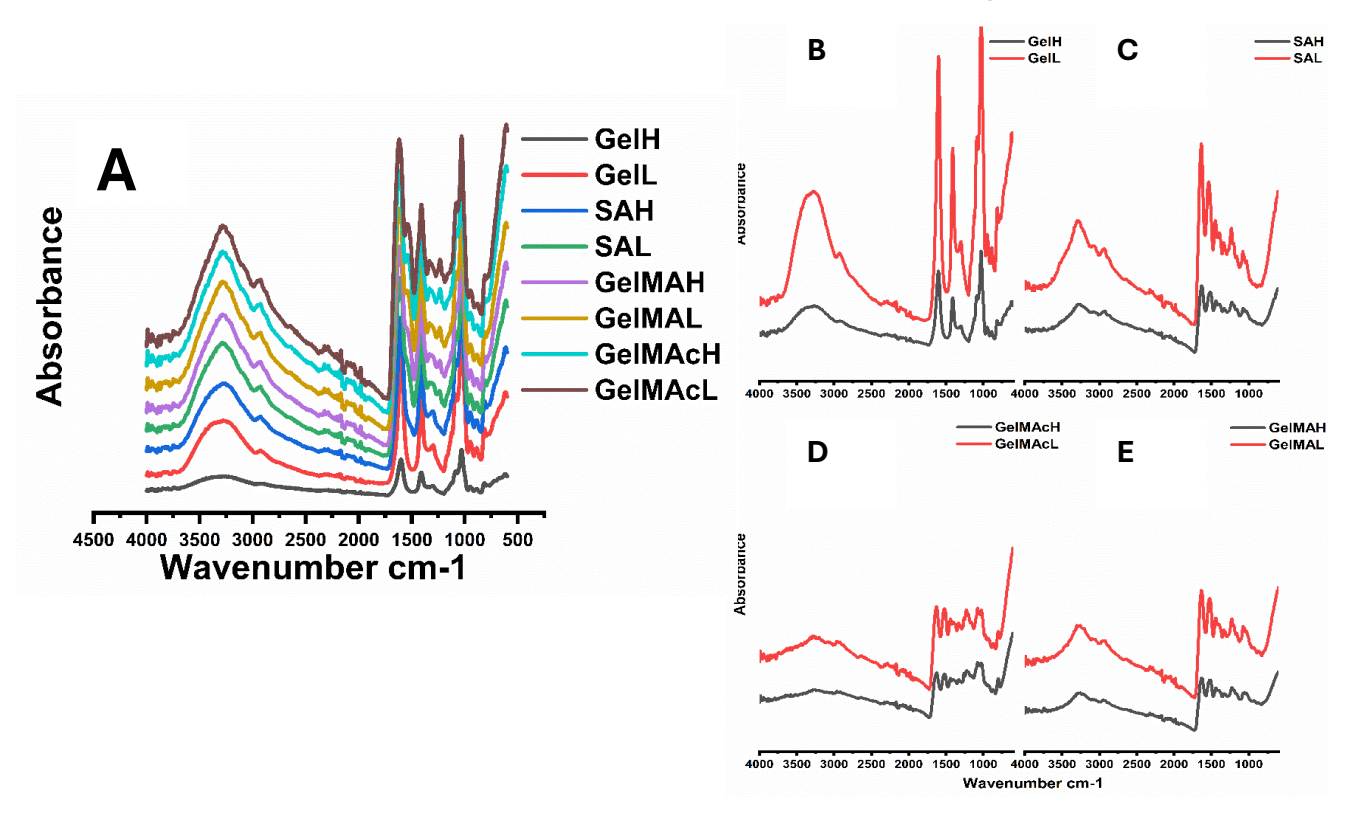


Figure 5.3. (A) FT-IR spectra summarising the chemical bonding structure in samples over a range of 4000–500 cm⁻¹ with a resolution of 4 cm⁻¹ at 37 °C. (A) Hydrogel samples are: GelH, GelL, SAH, SAL, GelMAcH, GelMAcL, GelMAH, and GelMAL. (B-E) Comparative FTIR spectra showing four grouped plots, each including high and low concentration pairs: GelH vs GelL, SAH vs SAL, GelMAcH vs GelMAcL, and GelMAH vs GelMAL, respectively

The FTIR spectroscopy was performed to recognize the molecular changes of the freeze-dried samples by being changed their concentrations, at 37 °C temperature. In general, the major peaks describing amide-bands (I, and II) of all the studied hydrogel samples were nearly similar, and they exhibited the difference in the wavenumber and amplitudes of peaks (Tab. 5.1). For high and low concentrated gelatin samples, the results showed a strong peak for the primary amide (amide I) related C=O stretching groups. The amide II caused by N-H bending in a non-ordered structural state, attributed to the collagen-like triple-helical structures (338) (Fig 5.3). Changes in intensities of these peaks with low concentrated samples are conformationally dependent, indicating an increase of the gelatin molecular order (amide I) and transformation to a higher structure order (because it forms more hydrogen bonding by NH- groups in the amide II region) (339). Similarly, the results showed there was an increase in peak intensities with GelL sample is compared with both GelMAcL and GelMAL indicating the effect of deionized water when used as a solvent on molecular order of gelatin in comparison with PBS solvents that used with other two samples.

These findings suggest that these spectral differences indicated both hydrogel concentration and solvent influence the molecular structure of gelatin. Stronger amide I peaks in higher-concentration samples reflect a higher density of C=O groups and suggest increased molecular interactions, which may contribute to more stable network formation. Variations in the amide II region indicate differences in hydrogen bonding and triple-helical ordering. The higher peak intensity observed in GelL (prepared in deionized water) compared with GelMAcL and GelMAL (prepared in PBS) highlights the effect of solvent on gelatin molecular organization. Together, these findings suggest that structural differences at the molecular level could impact key hydrogel properties relevant for tissue engineering applications (338, 339).

5.3.4. Contact angel measurements

Contact angle measurements on a substrate reflect its hydrophilic/hydrophobic nature, which is a crucial factor that influences cell adhesion and protein absorption on the substrate. Surfaces with contact angles below 90° are considered hydrophilic, while those above 90° are regarded as hydrophobic. This classification is widely accepted in the literatures. Notably, higher contact angle values are often associated with increased hydrophobicity, which can influence biocompatibility depending on the specific biological application and considered the high contact angle values exhibit enhanced biocompatibility (340, 341). The results from this study (Fig. 5.4) showed the contact angle values of high concentrated samples were higher compared with low concentrated samples, whilst the results of all samples indicated their hydrophilic nature.

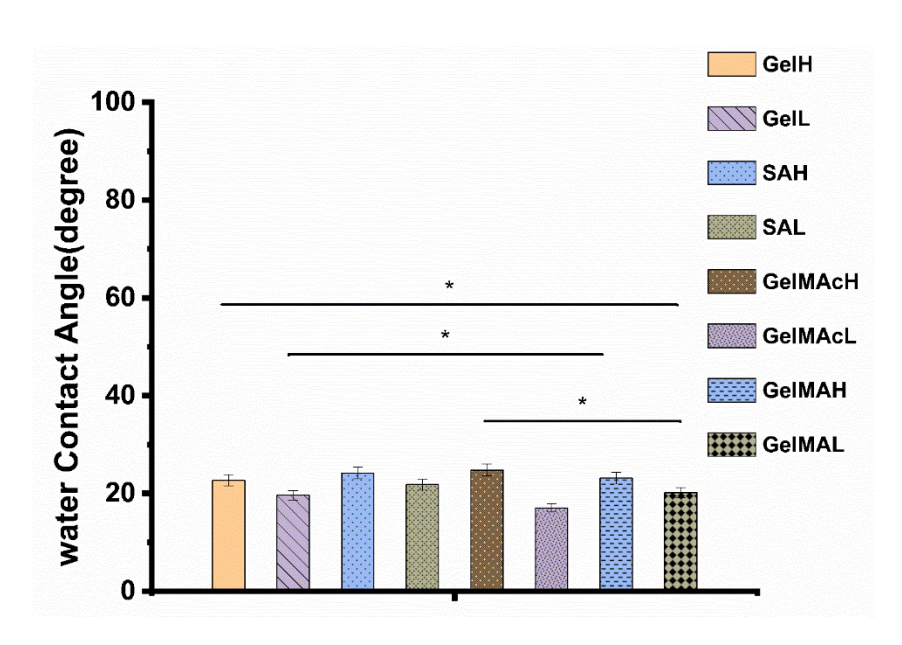


Figure 5.4. Water contact angle of the nine hydrogels: GelH, GelL, SAH, SAL, GelMAcH, GelMAcL, GelMAH, and GelMAL. Data representing mean ± SD(n=3). Sample is significantly different with * p < 0.05.

5.3.5. DSC

The DSC analysis was used to investigate the thermal properties of the gel samples. Melting points of the samples are the maximum point in the first endothermic peak of the DSC thermograms and the melting point value for each hydrogel is presented in Table 5.1(Appendix E).

The results showed that low concentrated samples have high melting temperature values compared with high concentrated samples (Fig. 5.5). In contrast, when the melting point value of GelMAH, was higher in a highly concentrated sample, this result confirmed the effect of adsorbed solvent on gelatin of different sources (GelMAc from porcine gelatin) due to differences in molecular structure (342, 343).

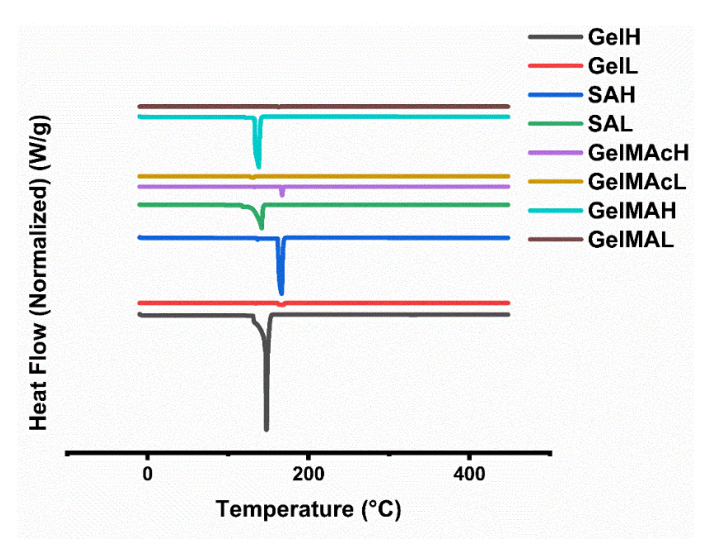


Figure 5.5. DSC thermograms for samples which were examined under a continuous flowrate of nitrogen gas with the following conditions: equilibrate (-10 °C), isothermal (1 min), and ramp (10 °C/min to 450 °C/min). Hydrogel samples are: GelH, GelL, SAH, SAL, GelMAcH, GelMAcL, GelMAH, and GelMAL.

5.3.6. Rheological measurements

The rheological properties of the hydrogels were evaluated using a rotational rheometer equipped with parallel plate geometry. This system applies oscillatory shear deformation to the material and records the corresponding strain response to assess its viscoelastic behaviour. The primary parameters obtained include the storage modulus (G'), which reflects the elastic or solid-like characteristics, and the loss modulus (G"), which corresponds to the viscous or liquid-like behaviour. These measurements provide essential information about the mechanical strength, structural integrity, and overall suitability of the hydrogels for tissue engineering applications (396).

Figure 5.6, and Figure 5.7, presented the effect of different shear rates on viscosity, and share stress, of hydrogel samples with different temperatures respectively. The results showed increased viscosity values with increased hydrogels concentrations indicating that the highly concentrated hydrogels are relatively strong and have more rigid network structures (Tab.5.1, Appendix E).

According to different temperatures, the viscosity values of samples were higher at 20 °C and 4 °C compared with high temperature, i.e. 37 °C, indicating the effects of temperature beside concentration on the stability of hydrogels. Additionally, the viscosity of all the hydrogel samples decreased in low shear rate in range of (0.1-10) s⁻¹ demonstrating shear thinning property of samples and remaining at constant values at high share rates.

The viscoelastic properties were determined by amplitude test and frequency sweep test. As shown in Figures 5.8, and 5.9, for all hydrogel samples at 37, 20 and 4 °C. The G' prevailed over G" in the lower deformation range, while they both increased with low strain value. This result indicated that the samples have a predominantly elastic rather than viscous. character. For the flow point value, which represents G' and G" crossed; in low concentrated samples located at much lower values of the strain compared to high concentrated samples, and this indicated the high concentrated samples

remain in the linear viscoelastic domain longer despite increasing the amplitude. All values of samples increased with decreasing temperature degrees.

To evaluate the strength of a samples network structures, frequency sweeps were performed in the range of 0.1–50 Hz, as shown in Figure 5.9, at 37, 20 and 4 °C. Gelation, with G' increasing and higher than G" for all samples at three different temperatures, and over the entire frequency sweep range, related to its solid-like structure and that indicative of a more stable network of the sample with this given frequency range. Table 5.1. (Appendix E).

The mean values of both G' and G" of all hydrogel samples are increased with increased concentration and decreased temperature. A linear increase of G' values of both GelH and GelMAcH, gave a prominent high level than other samples at 4 °C, indicating a stable network compared to others. Additionally, for long relaxation times (small frequencies), there are constant values of G' with frequency sweep for all samples, indicating the absence of relaxation processes, which may be explained by the stability of the intermolecular junction (396).

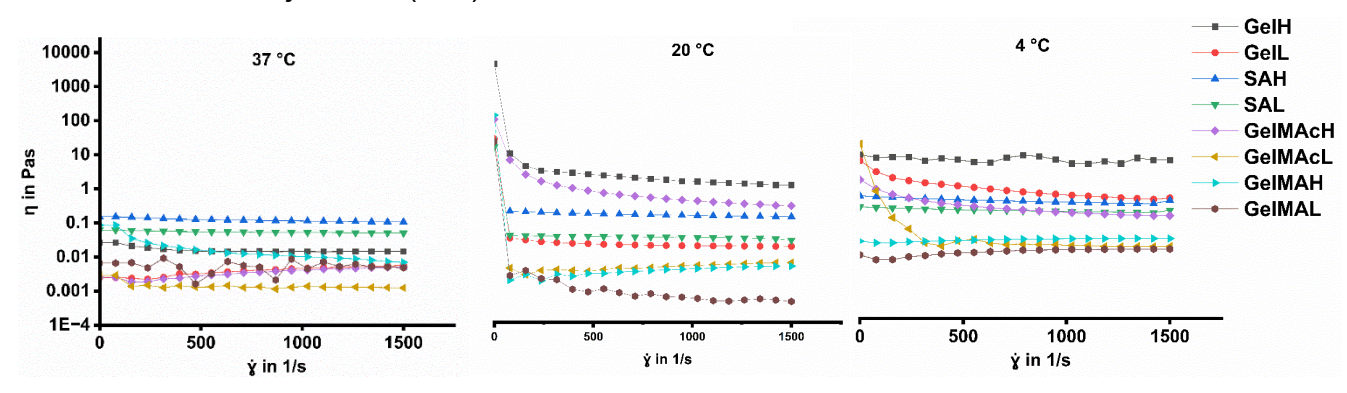


Figure 5.6. Rheological properties of eight hydrogel samples: GelH, GelL, SAH, SAL, GelMAcH, GelMAcL, GelMAH, and GelMAL. Viscosity as a function of shear rate at 37, 20 and 4 °C respectively.

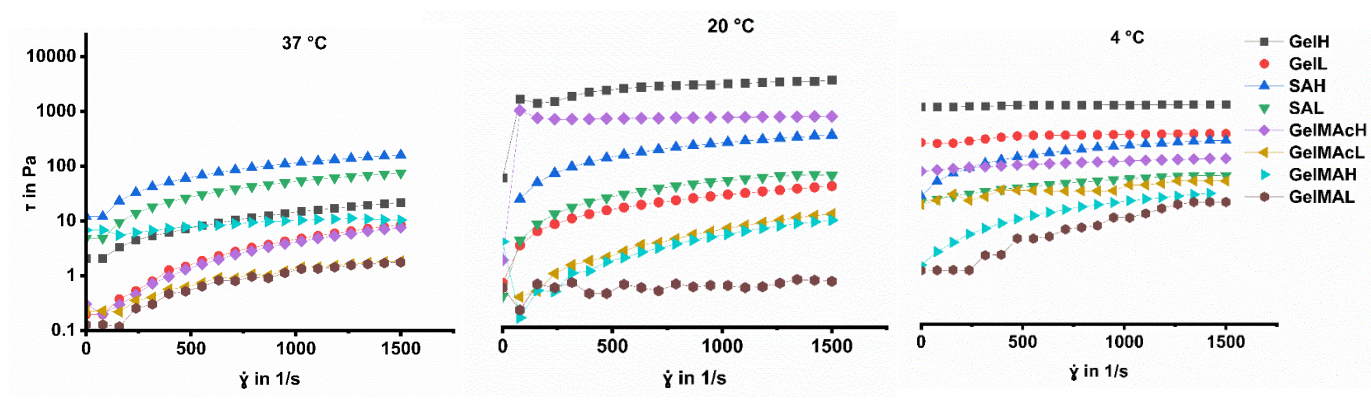


Figure 5.7. Rheological properties of eight hydrogels: GelH, GelL, SAH, SAL, GelMAcH, GelMAcL, GelMAH, and GelMAL. Shear stress as a function of shear rate at 37, 20 and 4 °C respectively.

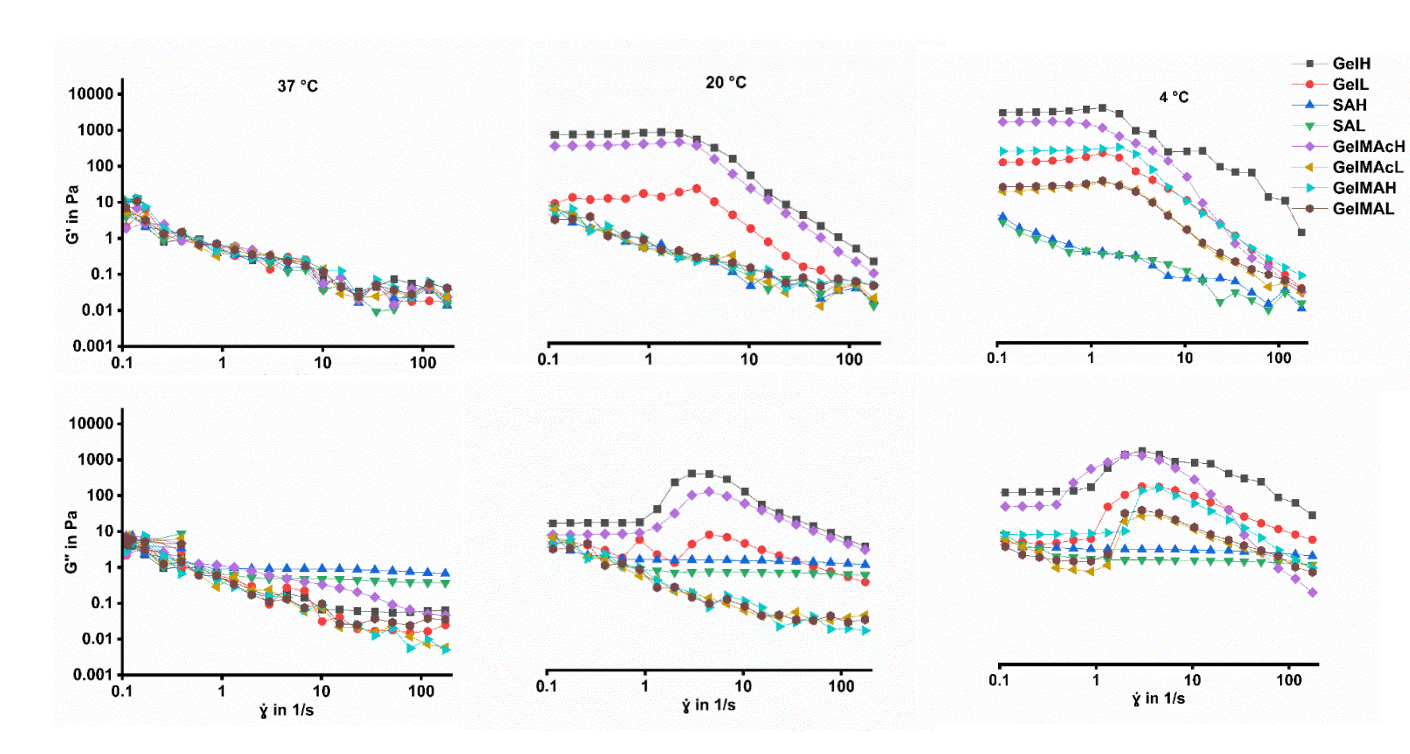


Figure 5.8. Rheological properties, with oscillatory amplitude sweeps showing storage (G') and loss moduli (G") at 37, 20 and 4 °C respectively with a constant frequency of oscillation of 1 Hz of eight hydrogels: GelH, GelL, SAH, SAL, GelMACH, GelMACL, GelMAH, and GelMAL.

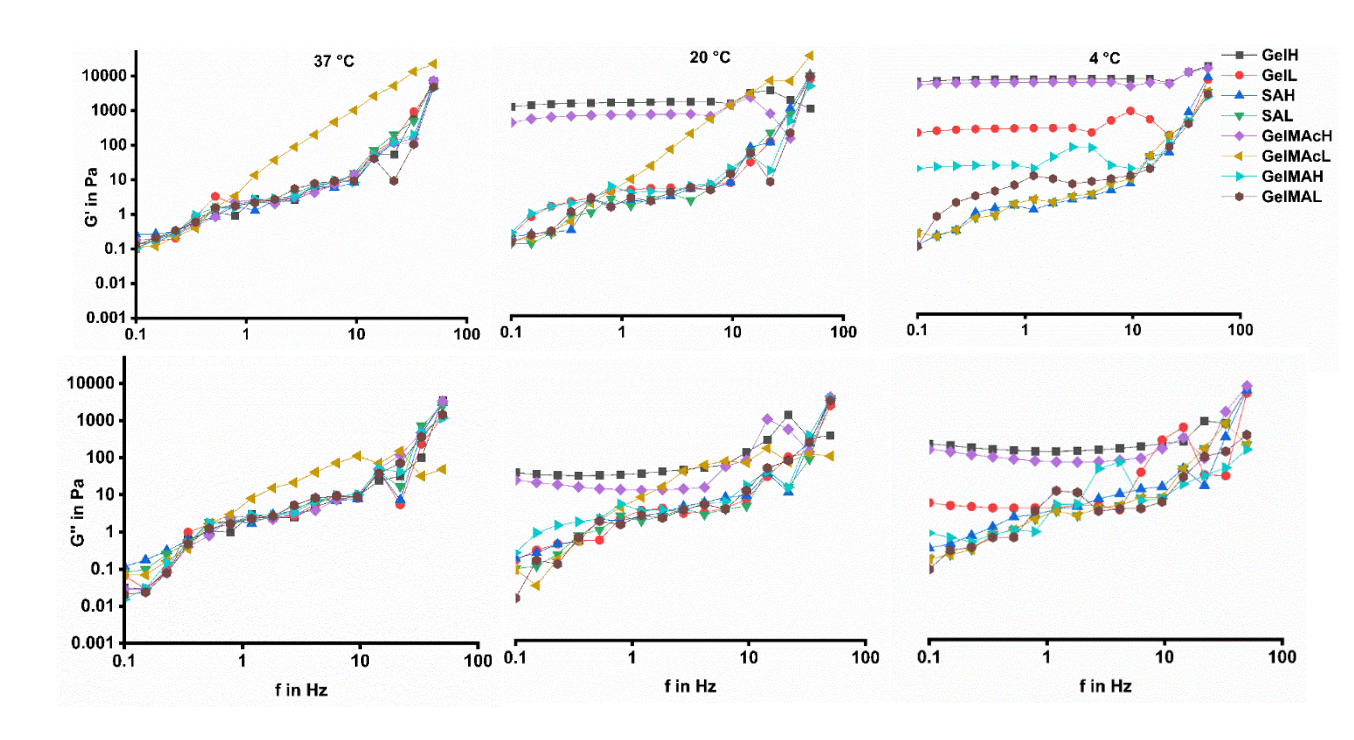


Figure 5.9. Rheological properties, with frequency sweep in a linear visco-elastic range (0.1–50 Hz) at the deformation of 0.25 % showing storage (G') and loss moduli (G") at 37, 20 and 4 °C respectively of eight hydrogels: GelH, GelL, SAH, SAL, GelMAcH, GelMAcL, GelMAH, and GelMAL.

Importantly, the rheological properties of the hydrogels were evaluated using a rotational rheometer with parallel plate geometry. Viscosity and storage modulus (G') increased with hydrogel concentration, indicating the formation of stronger network structures in more concentrated samples (Figs 5.6, and 5.7; Table 5.1, Appendix E). Shear-thinning behaviour was observed across all samples, with viscosity decreasing at low shear rates (0.1–10 s⁻¹) and stabilizing at higher shear rates. Temperature also influenced viscoelasticity: samples exhibited higher viscosity and G' values at 4 °C and 20 °C compared with 37 °C. Frequency sweep analysis (Fig. 5.8), revealed that G' consistently exceeded G" across all samples and temperatures, indicating predominantly elastic behaviour. Higher concentrated samples maintained the linear viscoelastic domain over a wider strain range, while long relaxation times (small frequencies) showed constant G' values, suggesting stability of the hydrogel network (286, 287, 396).

5.4. Discussion

Engineered novel substrates should typically mimic the mechanical properties of their target tissue (154). Therefore, it is important to choose the most suitable biomaterial with mechanical properties that mimic native human gingival tissue to construct a successful 3D gingival model.

The result of ¹H-NMR analyses of three hydrogel samples from synthesised GelMA-UCL compared with GelMA-com hydrogel sample, proved synthesised GelMA-UCL hydrogel samples from bovine skin gelatin can be successfully synthesised. Findings from this analysis, such as presence of weaker signals observed at 7.2 ppm that was assigned to the presence of aromatic ring, weak peaks observed between (5.4 and 5.6 ppm), which correspond to the two protons of methacrylate double bonds. In addition, in GelMA-com spectrum, showed a weak intensity peak at 2.15 ppm was present compared with other samples, which was attributed to the hydrogens of the methacrylate methyl group. The degree of methacrylation of the GelMA samples was determined using ¹H NMR spectroscopy. Moreover, the calculated methacrylation levels were 65%, 69%, and 67% for GelMA-UCL1, GelMA-UCL2, and GelMA-UCL3, respectively. These values indicated a high and consistent degree of functionalization across the different batches, which is expected to support effective photocrosslinking and hydrogel formation for subsequent tissue engineering applications (216, 373). These findings suggest that the gelatin species origin source has a significant influence on the chemical structure of synthesised GelMA-UCL.

In SEM investigation, the results showed the sizes of pores of all samples decreased with increasing concentration of hydrogels. These results were similar to the other studies for tissue engineering applications (278, 279). However, the increased porosity of hydrogel indicated weakened mechanical properties, which affects cell behaviour. Thus, the controlled porosity of hydrogel structures plays a vital role with hydrogels applications in regenerative medicine and tissue engineer properties (278).

FTIR spectroscopy was performed to identify the molecular compositions of samples by determining the intensities of peaks. The results indicated there were increases in peak intensities with low concentrated samples in compared with high concentrated samples, which indicated the weak intermolecular interaction of these low concentrated samples due to the effect of solvent. This trend is consistent with previous studies and can be attributed to reduced intermolecular hydrogen bonding at lower concentrations, where hydrogel chains are more sparsely distributed, allowing solvent molecules to interfere with chain-chain interactions more readily (397). As a result, vibrational modes of the hydrogel backbone are less hindered, leading to increased peak intensities. Moreover, the results also showed the effects of using deionized water as a solvent in gelatin samples by increasing the intensities of peaks compared with samples used PBS as a solvent during their preparation (GelMAH, GelMAL, GelMAcH, and GelMAcL). This result indicated the role of deionized water in breaking the intermolecular connections and weakening the hydrogel's structure (279, 280). This observation reflects the strong hydrogenbonding ability of water, which can disrupt the weak secondary structures within the gelatin network. Deionized water lacks the ionic components of PBS, which normally stabilize gelatin's triple-helix-like structures and facilitate ionic crosslinking (398). Consequently, water competes with gelatin's amide groups for hydrogen bonding, leading to looser, more disordered networks and decreased intermolecular interactions, as evidenced by increased intensity at characteristic FTIR bands such as ~1640 cm⁻¹ (amide I, C=O stretching) and ~1540 cm⁻¹ (amide II, N-H bending) (399). Weakening of intermolecular interactions at low concentrations or in pure water leads to softer gels with lower storage moduli. This may be advantageous for applications requiring highly compliant scaffolds like in soft tissue engineering, but unsuitable where load-bearing strength is needed. Looser networks permit higher water uptake and faster solute diffusion, which could enhance nutrient transport in cell-laden constructs but also risk rapid gel degradation or burst release of incorporated factors. PBS-based hydrogels mimic physiological osmolarity, which is

important for cell health. In contrast, gels prepared with deionized water may initially create osmotic imbalances that could stress encapsulated cells unless carefully equilibrated prior to use (400). Taken together, these FTIR-results underscore the critical role of both hydrogel concentration and solvent environment in tailoring hydrogel network architecture, mechanical behavior, and ultimately and most importantly their suitability for specific tissue-engineering applications.

Additionally, the results from contact angle measurements of included eight hydrogel biomaterials reflected its hydrophilic nature. The contact angle values of high concentrated hydrogels were higher compared with low concentration samples. However, these values are considered low because the tissue engineering substrates need an appropriate balance of the hydrophilic and hydrophobic surface entities. After all, highly hydrophobic surfaces enhance the cell affinity but reduce biocompatibility, while highly hydrophilic surfaces prevent cell-cell interaction (285). Materials that are commercially used in tissue culture applications possess a contact angle in the range of 59–113° (281, 282). Our results were between 17.1°-51.7°, and that depicting their hydrophilic nature.

These findings have important implications for cell-material interactions. While moderate hydrophilicity is known to enhance protein adsorption and cell adhesion, excessive hydrophilicity can hinder initial cell attachment by preventing protein adsorption and disrupting cell—cell interactions (280). Conversely, overly hydrophobic surfaces, although sometimes improving initial cell adhesion, may negatively impact long term cell viability and proliferation due to poor nutrient exchange and unfavourable surface energy for integrin mediated interactions (340). Therefore, the low contact angles observed in this study suggest that the hydrogels provide a surface that may limit efficient cell attachment if used without surface modification or protein pre-coating.

The thermal properties of hydrogel samples were determined by evaluating the melting points by DSC test. The results showed that the melting point values of

low concentrated samples were higher compared with high concentrated samples indicating the effects of solvent in weakening the hydrogel samples by breaking the intermolecular network of their structures. In contrast, the melting point value of GelMAcH (high concentration) was higher than GelMAcL (low concentration). This result had not appeared with GelMA, because melting point value of GelMAH was lower than GelMAL although both of these hydrogels were prepared by using the same solvent, i.e. PBS. However, this result confirmed the effect of gelatin species origin source on the strength of hydrogel structure because the GelMAcH and GelMAcL were from porcine gelatin, while GelMAH, and GelMAL were from bovine origin (283, 284).

This discrepancy highlights the influence of the gelatin species origin on hydrogel thermal behavior. Specifically, GelMAcH and GelMAcL were synthesised from porcine gelatin, while GelMAH and GelMAL were derived from bovine gelatin. Therefore, the differences in melting point trends between these two groups may be attributed to the intrinsic variations in the molecular structure of gelatin from different animal origins, which likely affects the degree of network stability within the hydrogels (283, 284).

In addition to previous characterisations, the rheological properties of the hydrogel biomaterials were assessed using a rheometer to evaluate sample viscosity, viscoelastic behaviour, and the mechanical strength of the hydrogel networks. The results demonstrated that highly concentrated hydrogels exhibited significantly higher viscosity values compared to their lower concentration counterparts. This suggests that high concentration hydrogels possess a more robust and interconnected network, which contributes to their mechanical strength and structural integrity. These findings are consistent with earlier results obtained from SEM, FTIR, contact angle measurements, and DSC analyses. From a tissue engineering perspective, particularly for developing a 3D gingival model, this enhanced viscosity and rigidity in highly concentrated hydrogels imply better scaffold stability, which is critical for maintaining the geometry and support of the construct post fabrication or

implantation. However, higher viscosity may also affect injectability and cell encapsulation efficiency, thus requiring a balance between mechanical strength and workability.

Additionally, it was observed that the viscosity of samples was temperature dependent. At 4 °C, the viscosity values were higher than at 20 °C, and both were higher compared to 37 °C. Moreover, the viscosity values were higher in high concentrated hydrogel samples compared with low concentration. These results confirmed the effects of temperature degrees beside concentration on the stability of hydrogels, and the same results are obtained from the previous study (286). Moreover, these findings highlighted that temperature was not only influenced hydrogel crosslinking kinetics but also affects the physical integrity of the gel. This temperature sensitivity is particularly relevant for in vitro or in vivo applications, where hydrogels must remain stable at physiological temperatures (~37 °C). Notably, at 20 °C and 4 °C, hydrogel samples were exhibited lower viscosity specifically low concentrated, suggesting weaker structural stability compared with 37 °C. These results may compromise using these samples in applications requiring robust scaffolding at lower temperatures (e.g., during storage or handling before implantation).

All hydrogel samples demonstrated a shear-thinning behaviour in the low shear rate range (0.1–10 s⁻¹), with viscosity decreasing under applied stress and then plateauing at higher shear rates. This property is advantageous for bioprinting and injectable scaffold systems in gingival tissue engineering, as it allows hydrogels to flow under pressure but quickly recover their structure once deposited. This behaviour also mimics the mechanical response of native soft tissues under dynamic oral conditions. However, the irreversible mechanical degradation under shear stress, as indicated by reduced viscosity, must be considered when designing hydrogels for load bearing regions or repetitive mechanical loading in the oral cavity (286, 287).

Amplitude and frequency sweep tests further supported the viscoelastic performance of the materials. High concentration samples demonstrated

higher elastic modulus (G') compared with low concentrated, reflected a more stable and elastic network structure. Across all temperatures tested (4 °C, 20 °C, and 37 °C), G' was consistently greater than G", indicated a predominantly solid-like behaviour. This rheological profile is ideal for a 3D gingival tissue model, as it ensures that the scaffold can maintain its shape and mechanical support under physiological conditions while providing a conducive environment for cell growth and extracellular matrix deposition (287).

In summary, the rheological data confirmed the importance of optimising both concentration and temperature conditions when designing hydrogels for 3D gingival tissue models. Hydrogels must possess sufficient mechanical integrity, thermal responsiveness, and viscoelastic behaviour to support tissue architecture, enable surgical handling or printing, and ensure long term stability in the oral environment. Samples FTIR, SEM, DSC, and WCA measurements provided a multidimensional understanding of hydrogel sample properties and their implications for 3D gingival tissue engineering. SEM analysis revealed differences in pore size and distribution depending on hydrogel concentration, which directly influence fluid retention, cell migration, and mechanical stability. These morphological features were closely linked to WCA results, where more porous structures exhibited greater surface roughness and improved lower WCA values (wettability), promoting better cell adhesion and nutrient exchange. WCA values reflected the hydrophilicity of the material, which is influenced by its chemical composition and crosslinking, as confirmed by FTIR. Structural density, indicated by specific functional group interactions, contributes to the formation of a stable polymer network, which in turn affects both porosity and thermal stability, as evidenced by DSC measurements. Rheological data further supported these findings, showing that more concentrated hydrogels possess higher viscosity and elastic modulus, essential for maintaining construct shape and resisting deformation under physiological forces.

Together, these interconnected properties, optimal porosity, hydrophilicity, chemical stability, and mechanical strength confirmed that the hydrogel samples can support cell viability, allow tissue ingrowth, and withstand the mechanical and thermal challenges of the oral environment. This integrated characterisation approach therefore informs the rational selection and optimisation of hydrogel formulations for constructing a functional and durable 3D gingival tissue model. Moreover, the mechanical properties of the hydrogels investigated in this study were lower than those of native human gingival tissue. Mechanical properties of native human gingival tissue with a mean value of elastic modulus are 37.36 ± 17.4 MPa and the unidirectional gingival collagen and elastic fibres are stood behind this high value compared with another oral region (218). In this study, the viscoelastic values of hydrogel samples are low in comparison with the viscoelastic value of native human gingival tissue. This result indicated the mechanical properties of the selected hydrogel samples are not suitable for use as a substrate for the construction of a successful 3D gingival model. Therefore, it is essential to further tune and enhance these properties to better replicate the native tissue environment, thereby supporting the survival, proliferation, and function of human gingival cells. One critical strategy to achieve this is through crosslinking, which can significantly improve the mechanical strength and structural stability of hydrogel scaffolds. There are several well-established methods of crosslinking, including physical processes such as ultra-violet (UV) or thermal treatment (289), or adding of biomolecules such as starch (290), chitosan (291) during cross-linking can be used to improve cell differentiation, migration, or proliferation characteristics, or mechanical properties of the resultant scaffolds (279, 280).

CHAPTER 6

6. EVALUATION OF THE PHYSICAL, MECHANICAL, AND BIOLOGICAL PROPERTIES OF NOVEL BIOMEDICAL HYDROGELS

6.1. Introduction

A 3D gingival model is an advanced in-vitro tool designed to replicate the structure and function of native human gingival tissue. The foundation of constructing an accurate 3D gingival model begins with the selection of a suitable substrate that mimics the native gingival ECM. The ideal substrate should not only replicate the characteristics of the lamina propria but also support the growth and maintenance of both human gingival fibroblasts and epithelial cells (188, 219).

A crucial component in gingival model construction is the scaffolding substrate, which should possess key properties such as high biocompatibility to support cell survival, porosity for adequate nutrient and oxygen exchange, biostability to maintain structural integrity, in addition to mechanical properties resembling the native gingival ECM (224, 225).

The systematic review analysed various animal-derived collagen substrates used in previous studies, including bovine and porcine collagen. While these substrate biomaterials showed promise, they lacked sufficient resemblance to the ECM of native human gingival connective tissue. Among the evaluated substrates, rat tail collagen type I emerged as the most commonly used as a substrate for construction 3D gingival models. This substrate supported epithelial stratification and facilitated the formation of the highest number of

epithelial layers (149). The development of stratified epithelial layers is a crucial indicator of a functional gingival model. Additionally, a homogeneous distribution of fibroblasts within the substrate has been shown to enhance keratinocyte stratification. Despite its widespread use, rat tail collagen type I presents several limitations. For example, shrinkage which is considered as a significant drawback, as it reduces the cell population within the hydrogel. Structural differences from human ECM, and unlike human gingival ECM, which predominantly consists of type I and III collagen, rat tail collagen is inherently fragmented (304). Moreover, rat tail collagen type 1, is high costed and the expense of isolating and preparing rat tail collagen limits its feasibility for widespread use.

Comparing different biomaterials is essential for standardizing and advancing engineered 3D gingival models for both laboratory research and clinical applications. While previous studies have investigated the suitability of rat tail collagen type I and other substrates for engineering human oral mucosa, the potential of GelMA-SA composite hydrogels for this purpose remains unexplored.

Therefore, the aims of this chapter are :-

- 1.Develop and evaluate the mechanical properties of novel hydrogels that could serve as potential substrates for a 3D gingival model and compare the characteristics of these hydrogels with the mechanical behavior of porcine and sheep oral tissues, which serve as representative in-vitro models.
- 2. Evaluate the potential of GelMA-SA composite hydrogels as a novel carrier for human gingival fibroblasts, ensuring that this biomaterial serves as a suitable substrate for mimicking the native human gingival connective tissue environment. This aim is to support the construction of a three-dimensional gingival model using the innovative GelMA-SA composite hydrogel as a foundational scaffold.

6.2. Materials and methods

6.2.1. Preparation of hydrogel samples

The materials utilized for preparation of GelMA, SA, and rat tail collagen hydrogel sample are detailed in Chapters 2, Sections 2.2.2. Moreover, preparation of GelMA hydrogel sample are detailed in Chapters 6, Sections 6.2.1.

6.2.1.1. Preparation of sterilized hydrogel samples

The sterilization methods for samples were detailed in Chapters 2 and 6, Sections 2.2.3, and 6.2.2, respectively. In this study, filter sterilization method was employed for the GelMA, SAH, SAL hydrogel samples.

Sterilization of the samples was conducted within a laminar flow cabinet to maintain a sterile environment throughout the process. Once sterilization was complete, each container was tightly sealed to ensure no contamination occurred. It is important to note that the rat tail collagen hydrogel sample was not sterilized by filter method, as it was prepared inside a laminar flow cabinet.

6.2.1.2. Crosslinking procedures for sterile hydrogel samples

Inside the laminar flow cabinet and before proceeding with the crosslinking process, all hydrogel samples, except for the rat tail collagen, were gently warmed to room temperature at ~20 °C and thoroughly mixed using a magnetic stirrer. This step was performed to ensure homogeneity of the hydrogel. After the respective preparation steps for each hydrogel type, the samples were distributed into the well plate inserts for crosslinking, and the crosslinking procedure was initiated.

In contrast, the rat tail collagen was handled differently; it was kept cold to preserve its structural integrity and was directly distributed into the well plate inserts without warming for starting with crosslinking procedure. Sterile rat tail collagen hydrogel samples were crosslinked by incubating at 37 °C for either 2 hours and referred to as R collagen (2h), or overnight, referred to as R collagen, to complete the collagen gelation.

The crosslinking procedures of hydrogel samples were written in details in Chapter 2, Section 2.2.4. In this study, SAH, and SAL were crosslinked using CaCl₂ crosslinking procedure by adding a sterile CaCl₂ at a concentration of 50 mm with double volume of each sample for 5-7 minutes, then discard the excess (233). This process performed at room temperature which is ~20 °C, and inside laminar flow cabinet. Moreover, GelMA hydrogel sample crosslinked with UV crosslinking process, using UV light for 60 s(ultraviolet light (UV;XYZPrinting UV chamber, Model 3UD10, Taiwan, UV LED (λ 375–405 nm, 16 W)) (213). The UV crosslinking process was conducted inside the UV chamber of the device. To ensure proper conditions, the sample container lid was securely fastened.

For the crosslinking procedures of GelMA-SA composite hydrogel samples, all details were written in Chapters 2 & 6, Sections 2.2.4, & 6.2.2.3, respectively. In this study, GelMA-SA composite hydrogel samples were crosslinked using either single or double crosslinking procedures. The single crosslinking procedure was performed either with CaCl₂, or UV crosslinking procedures.

At room temperature and inside laminar flow cabinet, $CaCl_2$ crosslinking procedure of samples were performed by adding a sterile $CaCl_2$ with double volume of each sample for 10 mins, then discard the excess (233). The other crosslinking method was UV crosslinking procedure using UV light for 60 s (ultraviolet light (UV;XYZPrinting UV chamber, Model 3UD10, Taiwan, UV LED (λ 375–405 nm, 16 W)) (200). The UV cross-linking procedure was conducted inside the UV chamber of the device. To ensure proper conditions, the sample container lid was securely fastened.

For the double crosslinking procedure was performed with two different sequencing, either CaCl₂/UV, or UV/CaCl₂ crosslinking procedures, and the whole procedures are detailed in Chapter 6, Section 6.2.2.3.

The first method is CaCl₂/UV crosslinking procedure, which was performed by doing CaCl₂ crosslinking procedure, followed UV crosslinking procedure. The other method is UV/CaCl₂. This was performed by starting with. UV crosslinking procedure, then followed by the second crosslinking procedure with CaCl₂ crosslinking procedure.

6.2.2. Preparation of animal gingival and oral mucosal tissues

The details of animal samples preparation are found in Chapter 2, Section 2.2.5. In brief, oral mucosa samples from sheep and porcine mandibles were harvested from animals aged 6 to 9 months. Tissue collection was performed with a focus on specific anatomical sites. Samples were obtained from the labial attached gingiva of the anterior teeth. Additionally, buccal and lingual tissue samples were collected from the attached gingiva and alveolar mucosa of the molar regions.

Moreover, to prepare the samples, the epithelial layer was carefully removed from each sample through de-epithelialization using a surgical blade. A #12 scalpel blade was utilized for precise tissue dissection and thickness measurement. After processing, all samples were stored in PBS at 4 °C, ensuring preservation for no more than three days before analysis.

Palatal gingival samples were also obtained for further analysis. Photographic images (Fig. 6.1, and 6.2) demonstrated palatal gingival tissue samples of upper jaws of sheep and porcine, in addition to sample preparation by sharp disectioning, placement of samples on lower plate to operate rheometer instrument, and the view of lowering the upper plate after placing sample on lower plate before operating rheometer instrument.

6.2.3. Structural characterisations

Structural characterisations were performed by investigated macrographic and micrographic analysis for sample surfaces, FTIR, WCA, and DSC. In addition, other characterization methods such as mechanical analysis, rheological,

degradation, and biocompatibility analyses, were also performed. More details of performing these investigations were found in Chapter 2, Section 2.2.6.

These investigations will help optimize GelMA- SA composite hydrogels application in seeding human gingival cells and constructing 3D cell culture models for periodontal research. Detailed methodologies for these investigations are provided in Chapter 2, Section 2.2.6.

These investigations were essential for comparing the GelMA-SA composite hydrogel with animal oral mucosa samples and other hydrogel samples. By analyzing structural and functional similarities.

6.2.4. Human gingival cells expanding and seeding in samples

In this study, HGF cells were expanded and used in experiments, and more details regarding cell expansion and seeding in hydrogel samples were found in Chapter 2, Section 2.2.6.9. In brief, the expanded HGF cells were suspended at a density of 2x10⁴ cells/ml, respectively, and thoroughly mixed with sterilized hydrogel samples to generate cell-populated hydrogels.

6.2.5. Metabolic and cytotoxic activities of cells evaluation

The metabolic activity values of the HGF cells were evaluated using the CellTiter®® 96 Aqueous One Solution Cell Proliferation assay kit, according to the manufacturer's protocol. For cytotoxicity assay, lactate dehydrogenase (LDH) release from the cells was quantified. LDH release assay performed using the CytoTox 96 Non-radioactive Cytotoxicity Assay kit. More details were found in Chapter 2, Section 2.2.8. In summary, following 1, 3, 7, and 14-days of incubation, the supernatant solution was transferred to a new plate and read at 490 nm using a Tecan Infinite M200 microplate reader (Tecan, Switzerland).

Moreover, the biocompatibility of the samples was determined using Live/DeadTM staining. A LIVE/DEAD™ imaging kit was used. Based on the protocol of manufacturer's instructions, The prepared stain of live/dead reagent was added to samples in a dark environment.. After incubation, Imaging was

performed on confocal laser scanning microscopy (BioRad Radiance2100, Zeiss, UK). The images were captured using digital capture software. These images were analysed to visualise live and dead cells within the samples using ImageJ Fiji software (https://downloads.micron.ox.ac.uk/fiji_update/mirrors/fiji-latest/fiji-nojre.zip).

6.3. Results

Material Characterization

6.3.1. Macrostructure morphology of hydrogels surfaces.

The macrostructure morphology of the samples is demonstrated in Figures 6.1, and 6.2., show images of sheep and porcine jaws, respectively. These images were taken from different views, including labial, buccal, and lingual aspects of the lower jaw, and the palatal aspect of the upper jaw. Similarly, Figures 6.3-6 presented the macrostructure morphology of hydrogel samples in well plates.



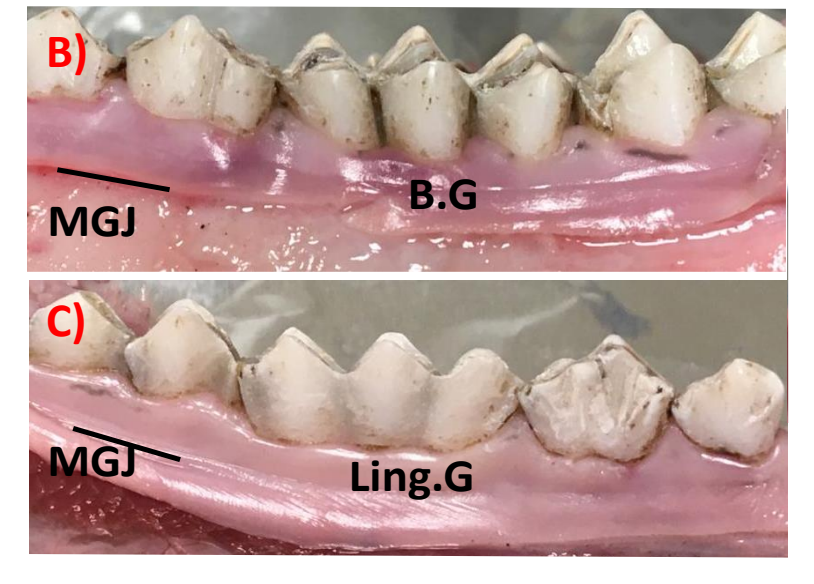




Figure 6.1. Images (A, B, and C) show the mucogingival junction (MGJ), labial ginigva(L.G), buccal gingiva (B.G), and lingual gingiva (Ling.G), anterior and posterior views of lower sheep jaws. Image (D), display the palatal views of sheep upper jaw.

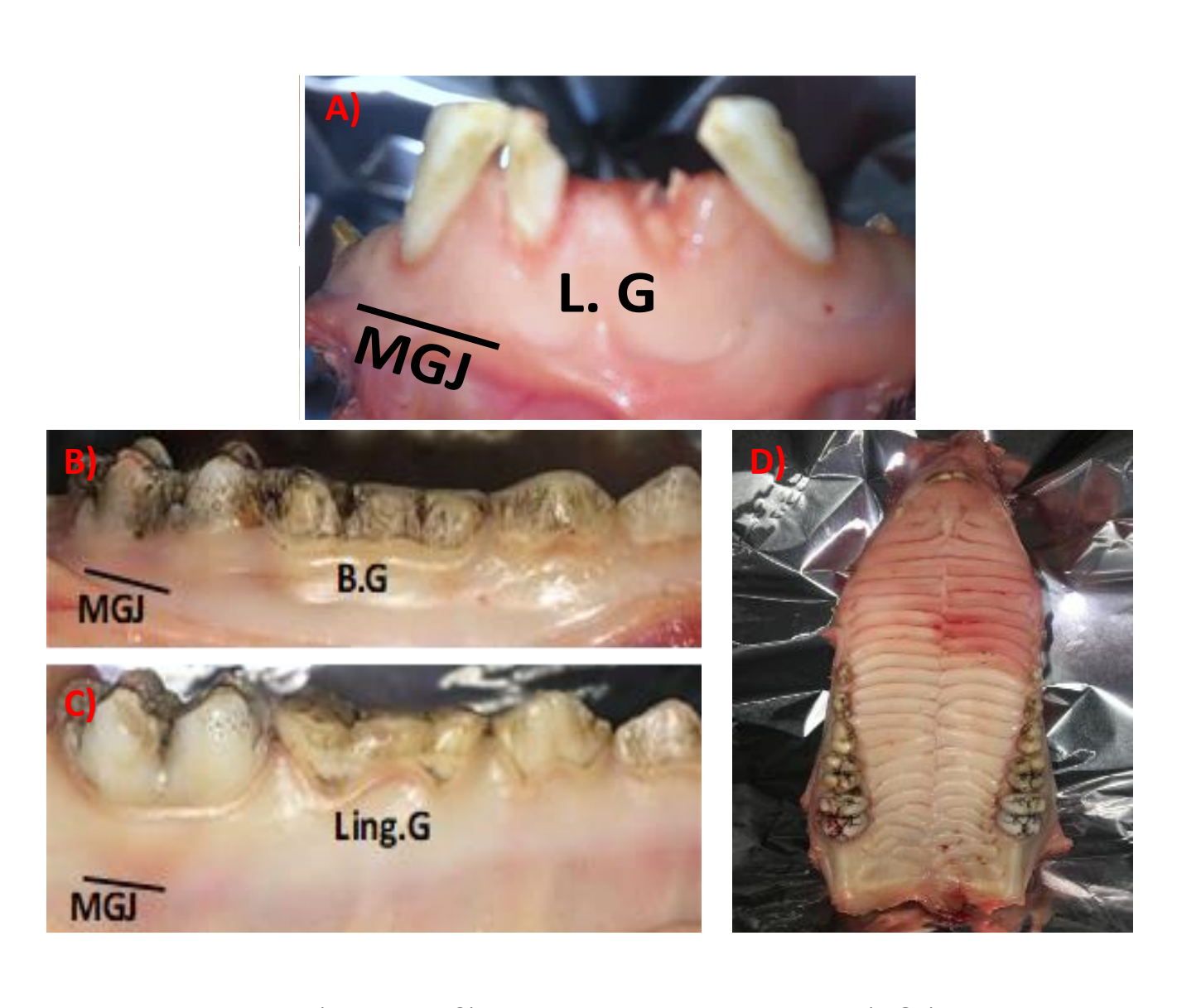


Figure 6.2. Images (A, B, and C) show the mucogingival junction(MGJ), labial ginigva(L.G), buccal gingiva (B.G), and lingual gingiva (Ling.G), anterior and posterior views of lower porcine jaws. Image (D), display the palatal views of porcine upper jaws

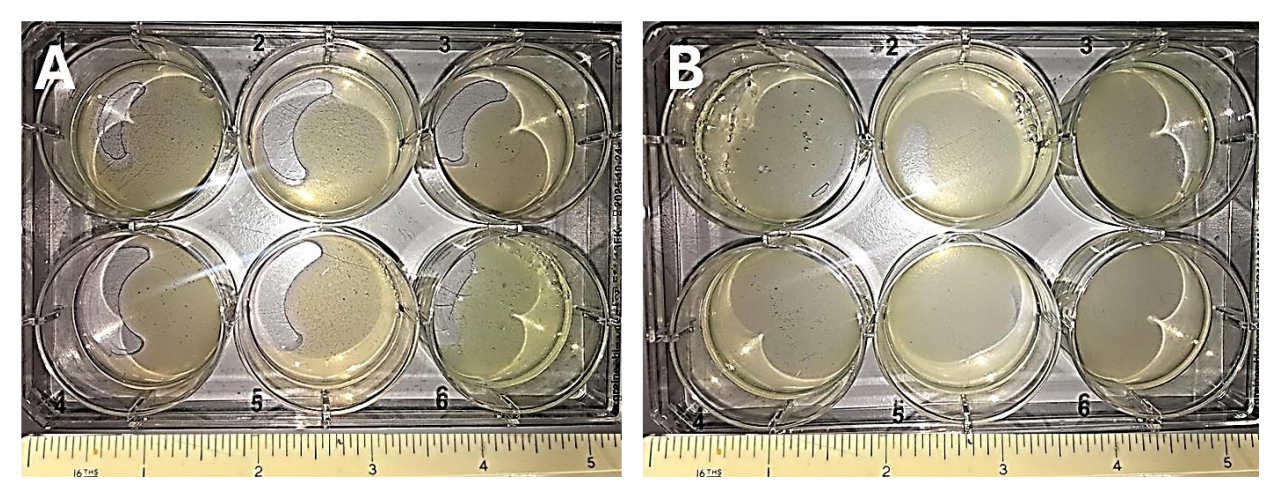


Figure 6.3. Images showing the rat collagen hydrogel samples in 6-well plates. Rat collagen hydrogel samples were prepared and aliquoted with 1ml per insert, then incubated for 2 hours (A) and overnight (B) in an incubator set at 37 °C with 5% CO₂.



Figure 6.4. Images showing hydrogel samples in a 6-well plate before and after the crosslinking procedure. Samples were prepared and aliquoted with 1 ml per insert. (A) and (B) show GelMA hydrogel samples before and after crosslinking using UV light exposure for 60 s at room temperature. GelMA was prepared by mixing GelMA (10% concentration) with 0.3% w/v photoinitiator. (C) and (E) show SAH and SAL hydrogel samples at concentrations of 3.5% and 2.5%, respectively, before crosslinking. (D) and (F) show SAH/CaCl₂ and SAL/CaCl₂ samples, respectively, which are SAH and SAL samples after crosslinking with 50 mM CaCl₂ at room temperature for 5–7 minutes. (PI).

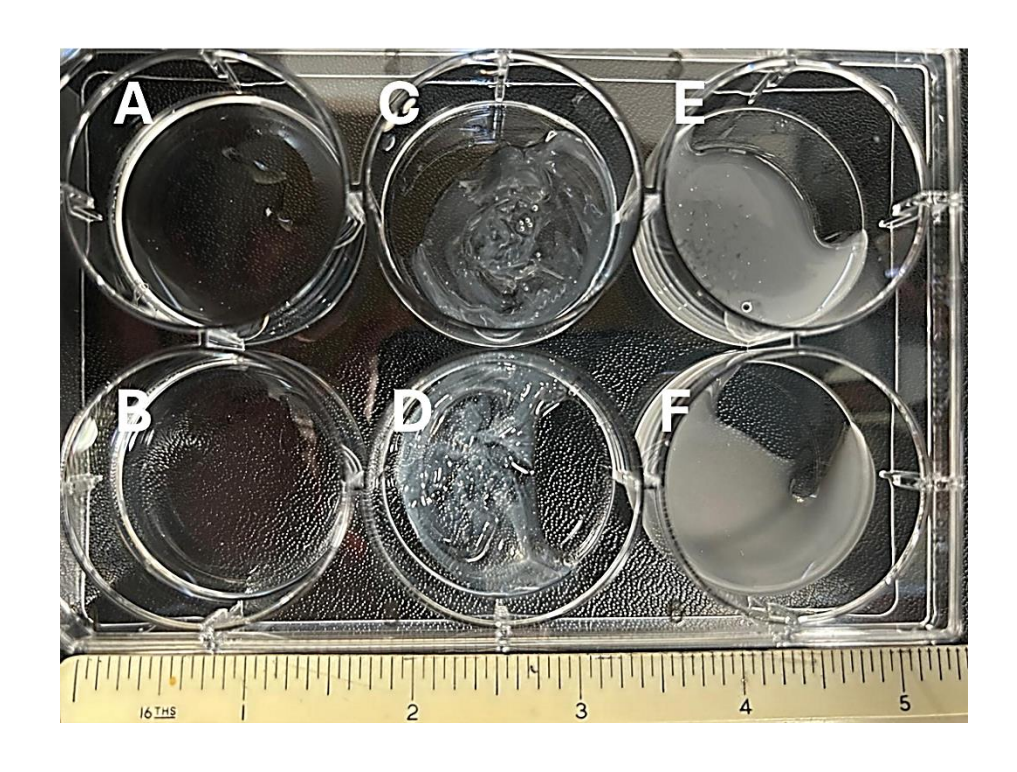


Figure 6.5. Images showing GelMA-SAH and GelMA-SAL hydrogel samples in a 6-well plate, prepared and aliquoted with 1 ml per insert, before and after the single crosslinking procedure. This was performed at room temperature (~20°C),. Samples were prepared by mixing GelMA (10% concentration) with 0.3% w/v photoinitiator (PI), and either SAH or SAL, resulting in final concentrations of 3.5% and 2.5%, respectively. (A) and (B) show GelMA-SAH and GelMA-SAL hydrogel samples, respectively, before crosslinking. (C) and (D) show same hydrogel samples, after crosslinking using a CaCl₂ procedure. where CaCl₂ solution was added for 5–7 minutes. (E) and (F) show the samples after crosslinking using the UV procedure, using UV light exposure for 60 s.

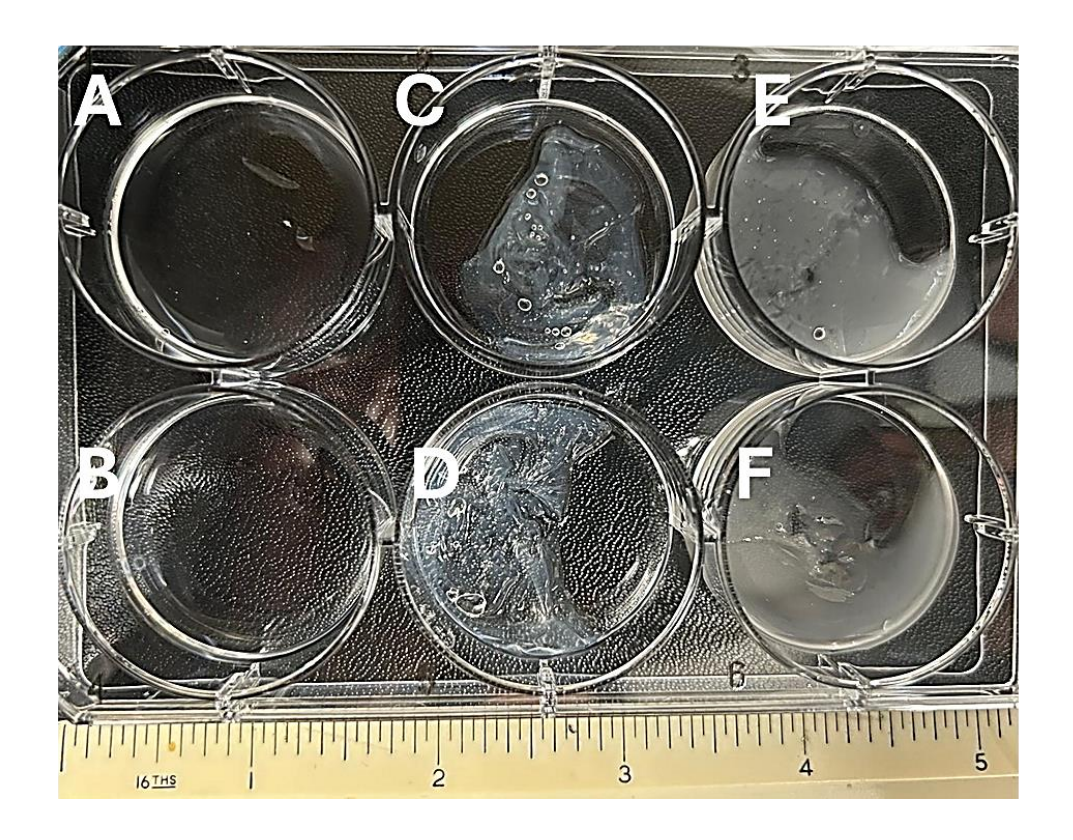


Figure 6.6. Images showing GelMA-SAH and GelMA-SAL hydrogel samples in a 6-well plate, prepared and aliquoted with 1 ml per insert, before and after the double crosslinking procedure. This was performed at room temperature (~20°C),. Samples were prepared by mixing GelMA (10% concentration) with 0.3% w/v photoinitiator (PI), and either SAH or SAL, resulting in final concentrations of 3.5% and 2.5%, respectively. (A) and (B) show GelMA-SAH and GelMA-SAL hydrogel samples, respectively, before crosslinking. (C) and (D) show same hydrogel samples, after crosslinking using CaCl₂/UV procedure. where CaCl₂ solution was added for 5–7 minutes, followed by removal of excess solution and UV light exposure for 60 s. (E) and (F) show the same samples after crosslinking using the UV/CaCl₂ procedure, where UV light exposure was applied first, followed by the addition of CaCl₂ solution.

6.3.2. Microstructure morphology of samples surfaces

SEM images displayed the microstructure morphology of both gingival and oral mucosal tissue from animal samples, in addition to hydrogel samples. In this study all SEM images were shown at 500X, and 5KX magnifications. SEM images of sheep and porcine oral tissue samples are labial, buccal, and lingual gingival tissue samples were shown in Figures 6.7, and 6.9, respectively. In Figures 6.8, and 6.10, presented the SEM images of the palatal gingival tissue sample, and buccal and lingual oral mucosal tissue samples for sheep and porcine respectively.

Figures 6.11 to 6.13 presented SEM images of crosslinked hydrogel samples. Images showed rat tail collagen samples after overnight incubation (R collagen), 2 hours incubation (R collagen(2h)), GelMA, SAH, and SAL, respectively (Fig.6.11). Figures 6.11 illustrated images of GelMA-SA composite samples with high and low concentrations, after single crosslinking procedure, CaCl₂, and UV, respectively. The samples were GelMA-SAH/CaCl₂, and GelMA-SAL/CaCl₂, GelMA-SAH/UV, and GelMA-SAL/UV, respectively.

Lastly, Figure 6.13 depicted the same GelMA-SA composite samples images after double crosslinking procedure, CaCl₂/UV, and UV/CaCl₂, respectively. The samples were GelMA-SAH/CaCl₂/UV, GelMA-SAL/CaCl₂/UV, GelMA-SAH/UV/CaCl₂, and GelMA-SAL/CaCl₂/UV, respectively. The SEM images revealed a predominant unidirectional collagen fibres network in the palatal and alveolar mucosa of animal samples. In hydrogel samples, the images also displayed randomly oriented, interconnected fibrillary microstructures in the rat collagen hydrogel, compared to other hydrogel samples. However, these fibre networks were not recognizable in the rat collagen sample incubated for 2 hours. Pore sizes were larger in low-concentration hydrogel samples compared to high-concentration ones. recognizable also in the rat collagen sample incubated for 2 hours compared with R collagen hydrogel sample which is incubated overnight for gelation. Pore sizes of all hydrogel samples were larger in low-concentration hydrogel samples compared to high concentration ones.

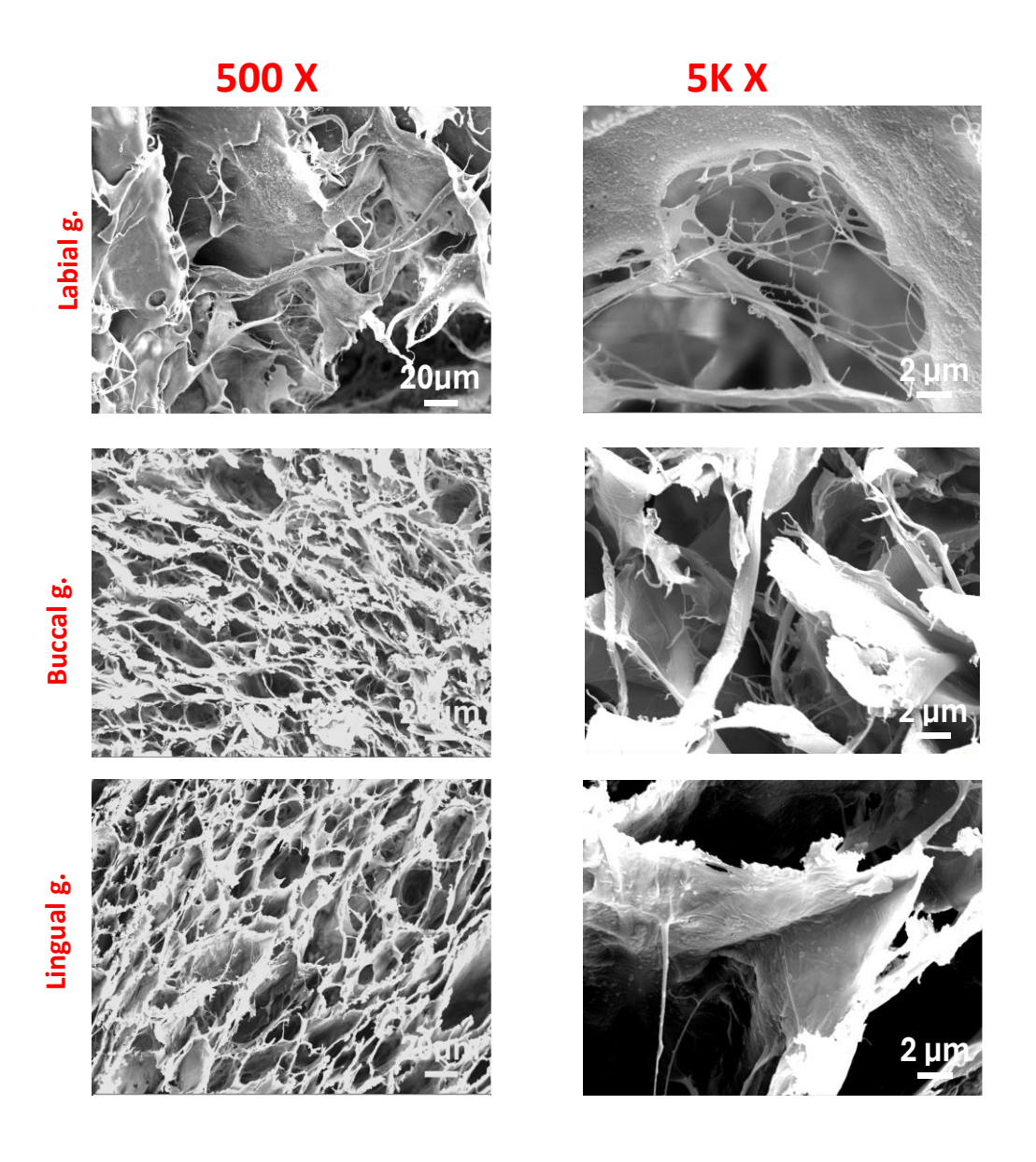


Figure 6.7. SEM images of sheep oral tissue samples, including labial, buccal, and lingual gingival tissue. 'Labial g.' refers to labial gingiva, 'Buccal g.' refers to buccal gingiva, and 'Lingual g.' refers to lingual gingiva. Images are shown at two magnifications: 500X with a scale bar of 20 μ m, and 5KX with a scale bar of 2 μ m, highlighting the structural differences between the three types of gingival tissue at different magnifications.

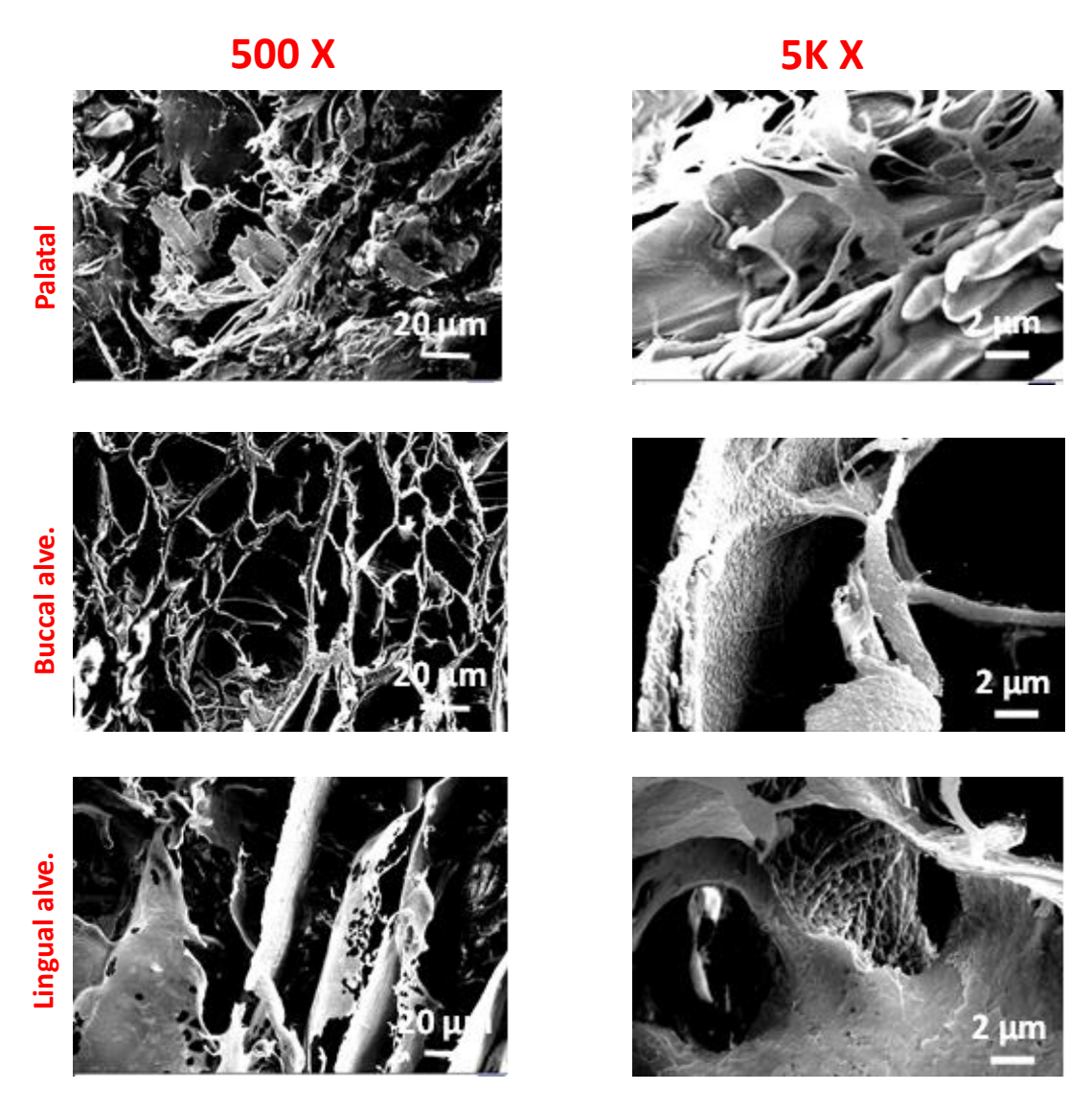


Figure 6.8. SEM images of sheep oral tissue samples, including palatal gingival tissue, buccal alveolar, and lingual alveolar mucosal tissue. 'Buccal alve.' refers to buccal alveolar tissue, and 'Lingual alve.' refers to lingual alveolar tissue. Images are shown at two magnifications: 500X with a scale bar of 20 μ m, and 5KX with a scale bar of 2 μ m, highlighting the structural differences between the three tissue types at different magnifications.

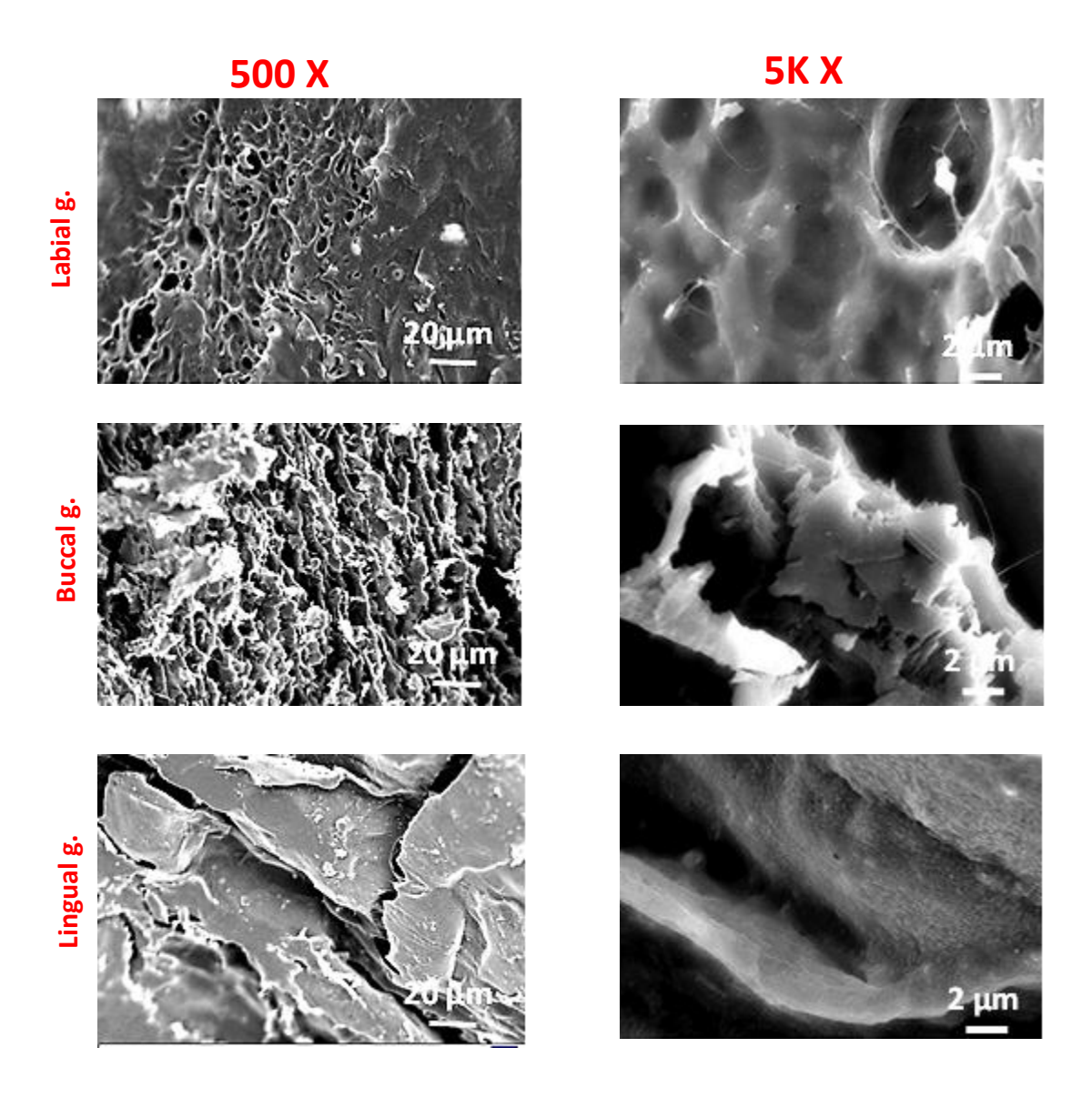


Figure 6.9. SEM images of porcine oral tissue samples, including labial, buccal, and lingual gingival tissue. 'Labial g.' refers to labial gingiva, 'Buccal g.' refers to buccal gingiva, and 'Lingual g.' refers to lingual gingiva. Images are shown at two magnifications: 500X with a scale bar of 20 μ m, and 5KX with a scale bar of 2 μ m.

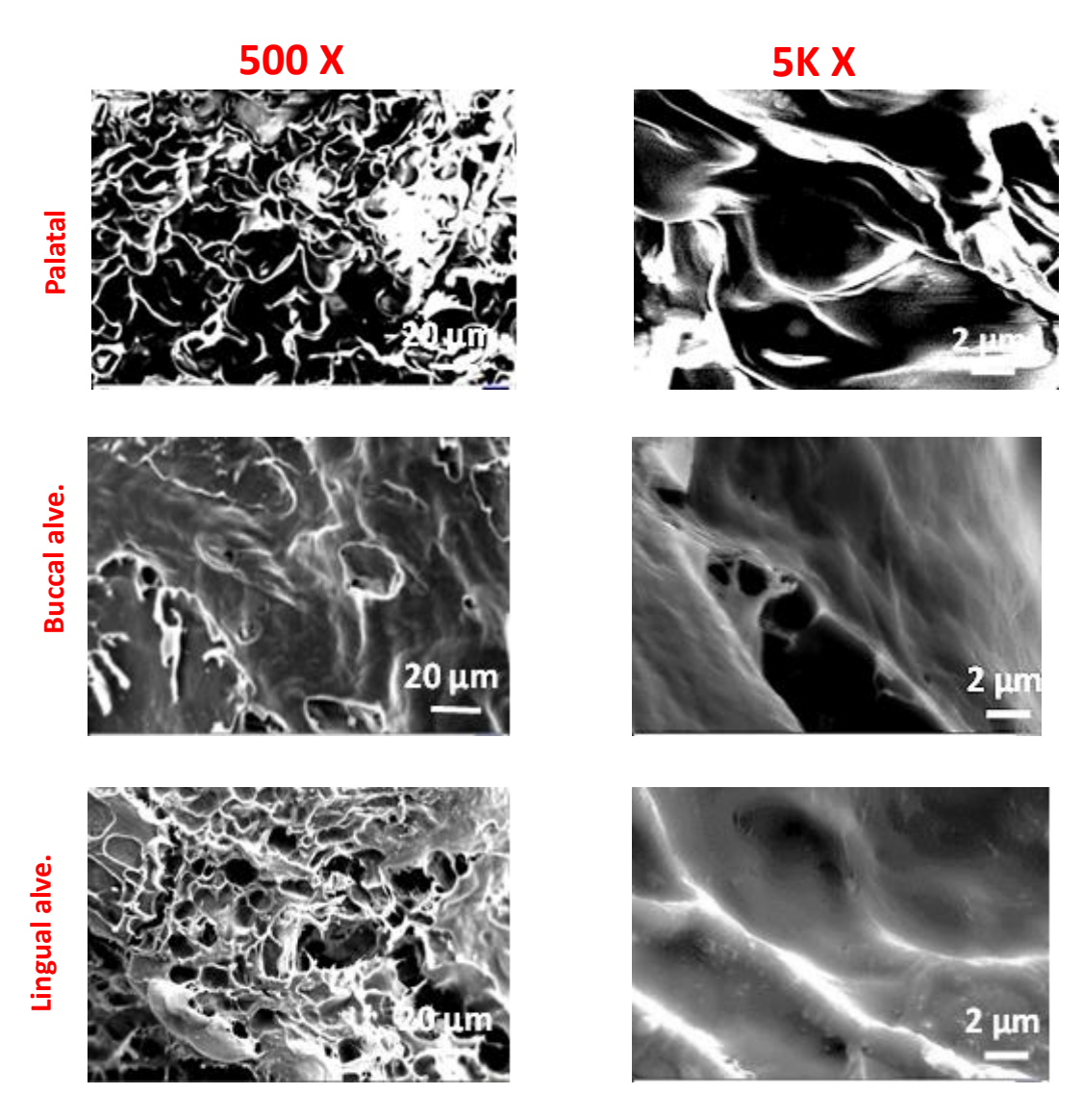


Figure 6.10. SEM images of porcine oral tissue samples, including palatal gingival tissue, buccal alveolar, and lingual alveolar mucosal tissue. 'Buccal alve.' refers to buccal alveolar tissue, and 'Lingual alve.' refers to lingual alveolar tissue. Images are shown at two magnifications: 500X with a scale bar of 20 μ m, and 5KX with a scale bar of 2 μ m.

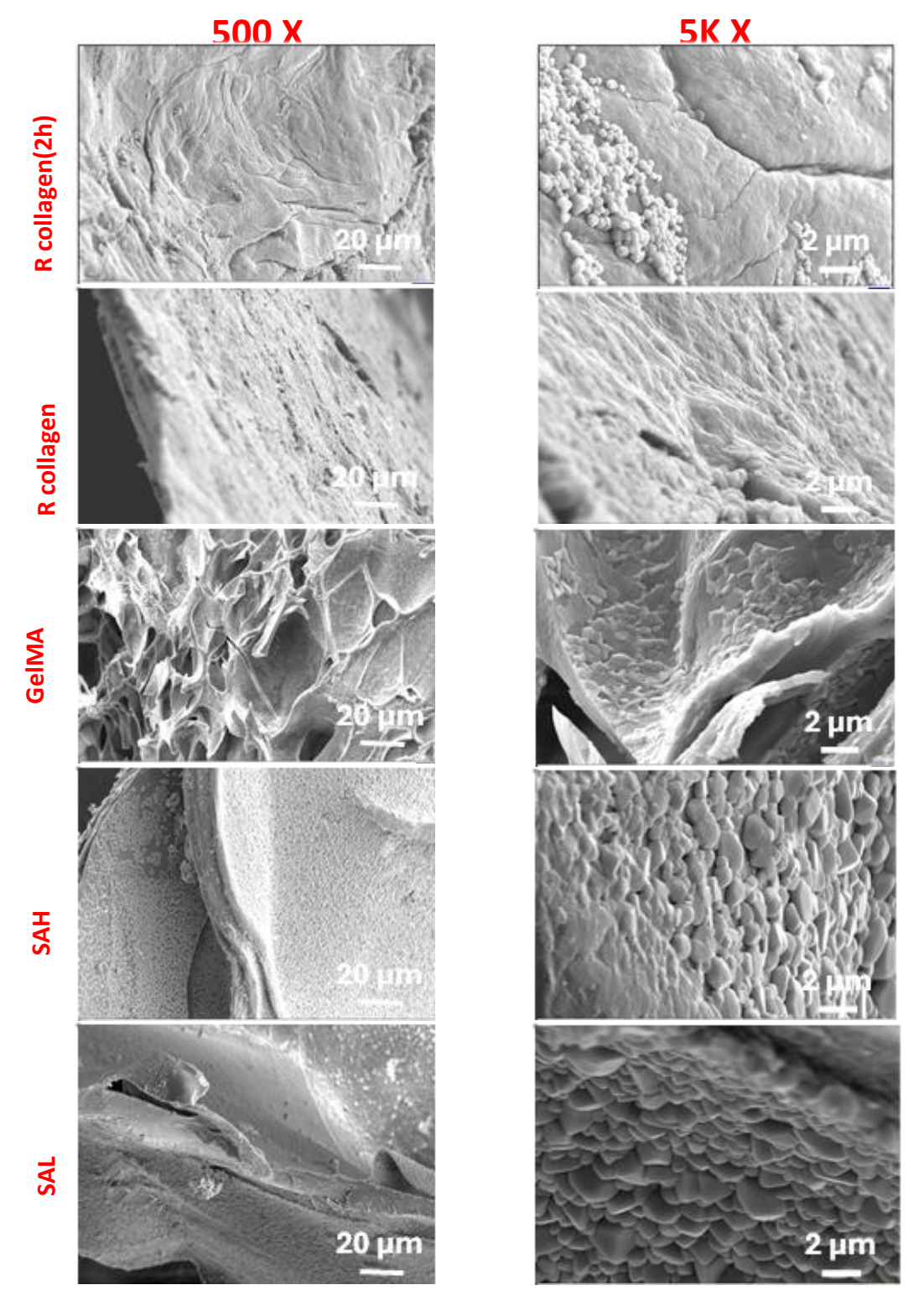


Figure 6.11. SEM images of hydrogel samples after crosslinking. 'R collagen (2h)' and 'R collagen' refer to rat collagen crosslinked at 37 °C with 5% CO_2 for 2 hours and overnight, respectively. 'GelMA' refers to GelMA prepared by mixing 10% GelMA with 0.3% (w/v) photoinitiator (PI), crosslinked using UV light for 60 seconds. 'SAH' and 'SAL' refer to hydrogels with concentrations of 3.5% and 2.5%, respectively, crosslinked with 50 mM $CaCl_2$ at room temperature for 5–7 minutes. Images are shown at two magnifications: 500X with a scale bar of 20 μ m, and 5KX with a scale bar of 2 μ m.

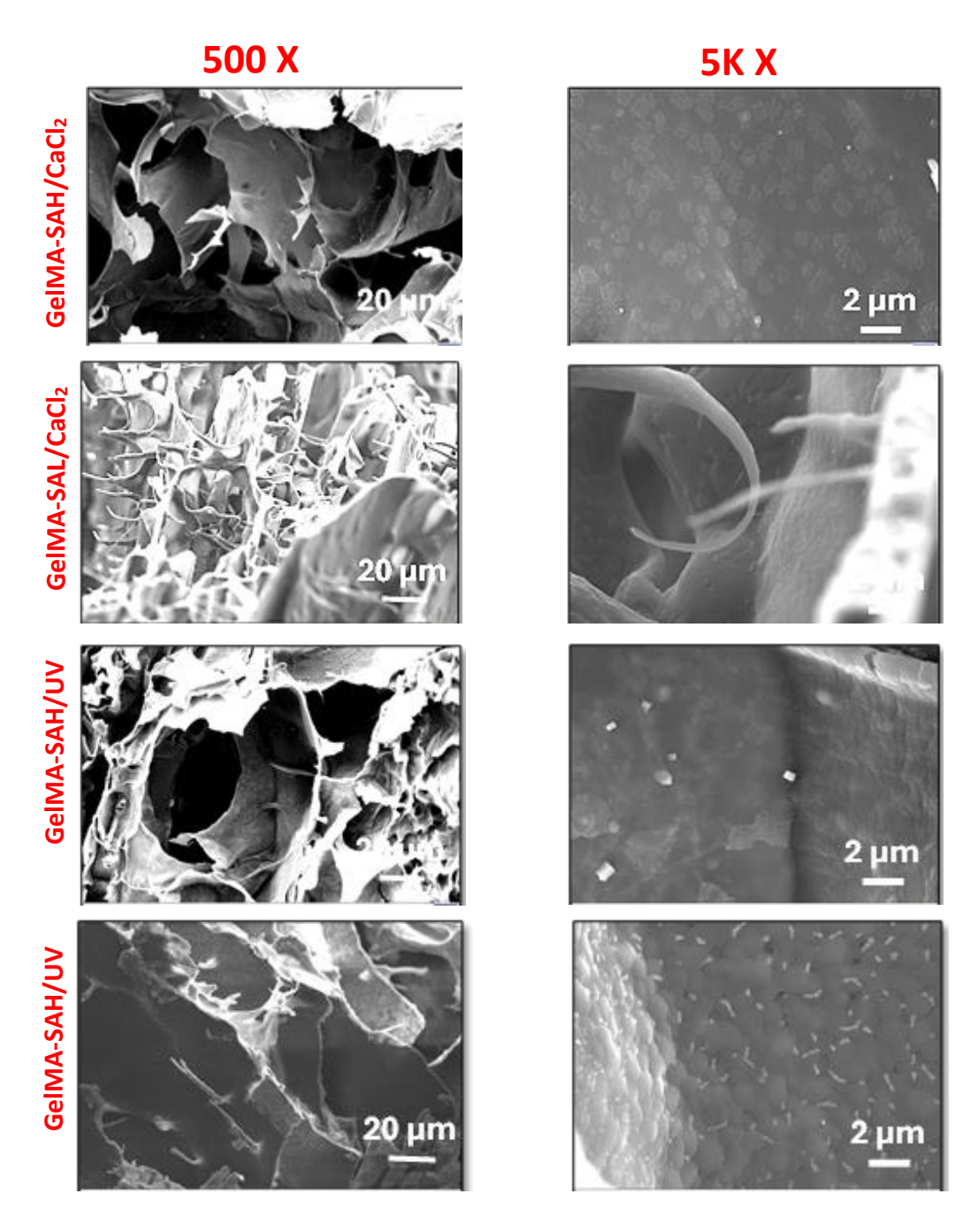


Figure 6.12. SEM images of hydrogel samples after crosslinking. 'GelMA-SAH/CaCl₂', and 'GelMA-SAL/CaCl₂', refer to hydrogel samples prepared by mixing GelMA (10% concentration with 0.3% w/v photoinitiator (PI)) and SA, with 3.5% and 2.5% concentration, respectively. These samples after crosslinking with 50 mM CaCl₂ at room temperature for 5–7 minutes. 'GelMA-SAH/UV', and 'GelMA-SAL/UV', refer to crosslinking mixture of GelMA and SA by using UV light for 60 s. Images are shown at two magnifications: 500X with a scale bar of 20 μ m, and 5KX with a scale bar of 2 μ m.

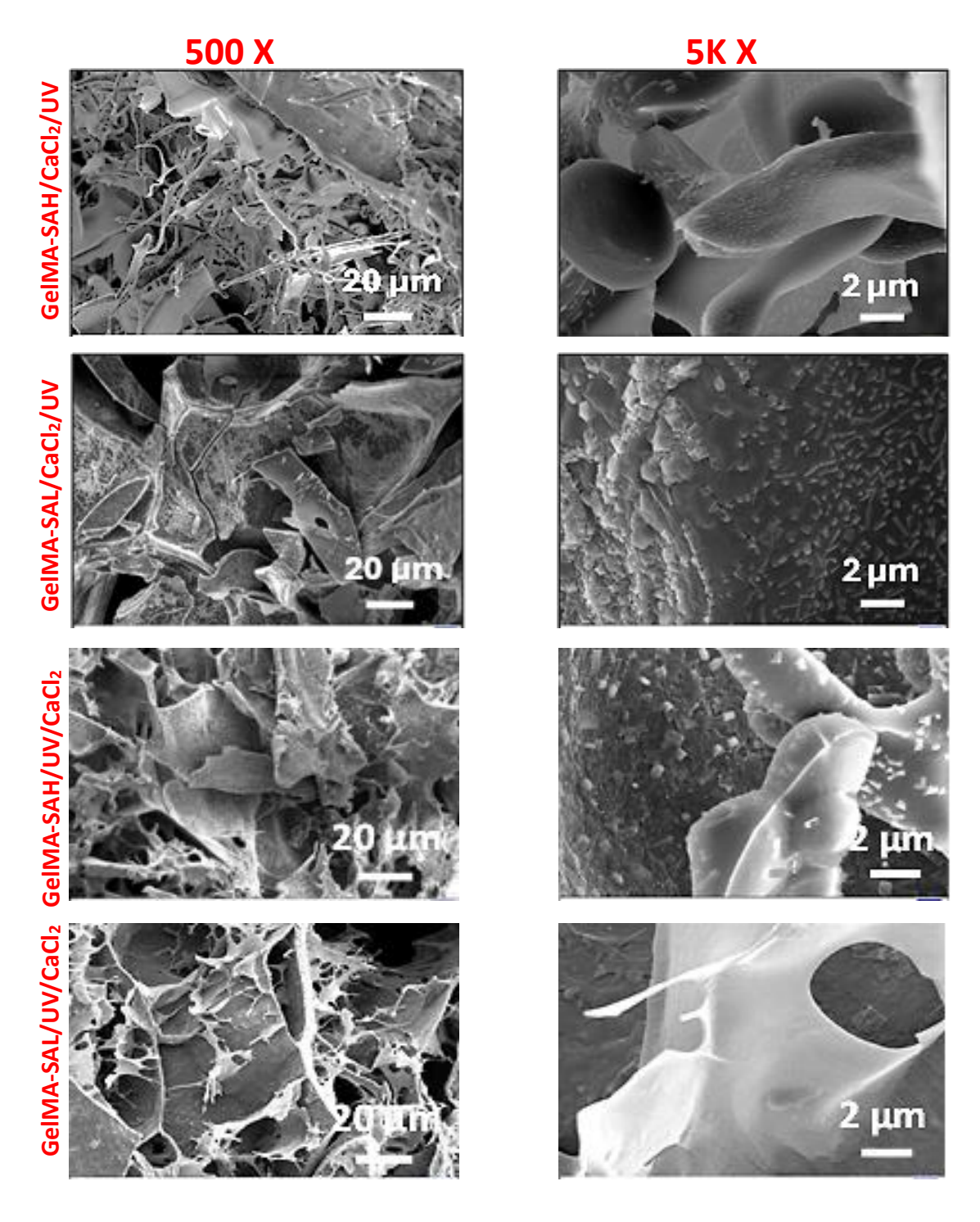


Figure 6.13. SEM images of hydrogel samples after crosslinking. 'GelMA-SAH/CaCl $_2$ /UV' and 'GelMA-SAL/CaCl $_2$ /UV' refer to hydrogels prepared by mixing 10% GelMA (with 0.3% w/v photoinitiator) and sodium alginate (SA) at concentrations of 3.5% and 2.5%, respectively. These samples were crosslinked first with 50 mM CaCl $_2$ at room temperature for 5–7 minutes, followed by UV exposure for 60 seconds. 'GelMA-SAH/UV/CaCl $_2$ ' and 'GelMA-SAL/UV/CaCl $_2$ ' refer to mixtures of GelMA and SA crosslinked first by UV light for 60 seconds at room temperature, then submerged in 50 mM CaCl $_2$ solution for 5–7 minutes.Images are shown at two magnifications: 500× with a scale bar of 20 μ m, and 5000× with a scale bar of 2 μ m.

6.3.3. Fourier transform infrared spectrophotometer (FT-IR) spectra

Biochemical properties were analysed using a Fourier transform infrared spectrophotometer (FT-IR) for animal tissues and hydrogel samples (Fig. 6.14). The Amide I and II bands represent major protein bands in the infrared spectrum and can be associated with C=O stretching, N-H bending, and C-N stretching vibrations (48). In animal tissue samples the spectral differences were noted in terms of broadening of amide II and amide I. Amide I bands from sheep gingival tissue samples, represented by attached gingiva, were visualized as peaks at 1649.23±2.4 cm⁻¹, which is characteristic of high protein content compared to porcine gingival tissue (Fig. 6.14A and B). The average FTIR spectra in the fingerprint range (720–1770 cm⁻¹), specifically the amide II and amide I C=O stretching vibrations of peptide groups in proteins, were observed in all animal tissues, and also in hydrogel samples (Fig. 6.14C and D). FTIR data also, demonstrated an increase in peak intensities in hydrogel samples compared to rat tail collagen samples for both R collagen and R collagen(2h). However, FTIR data demonstrated an increase in peak intensity in R collagen, compared with R collagen(2h) hydrogel samples (Fig.6.14C). Additionally, the peak intensities were higher in highly concentrated hydrogel samples compared to low-concentration ones

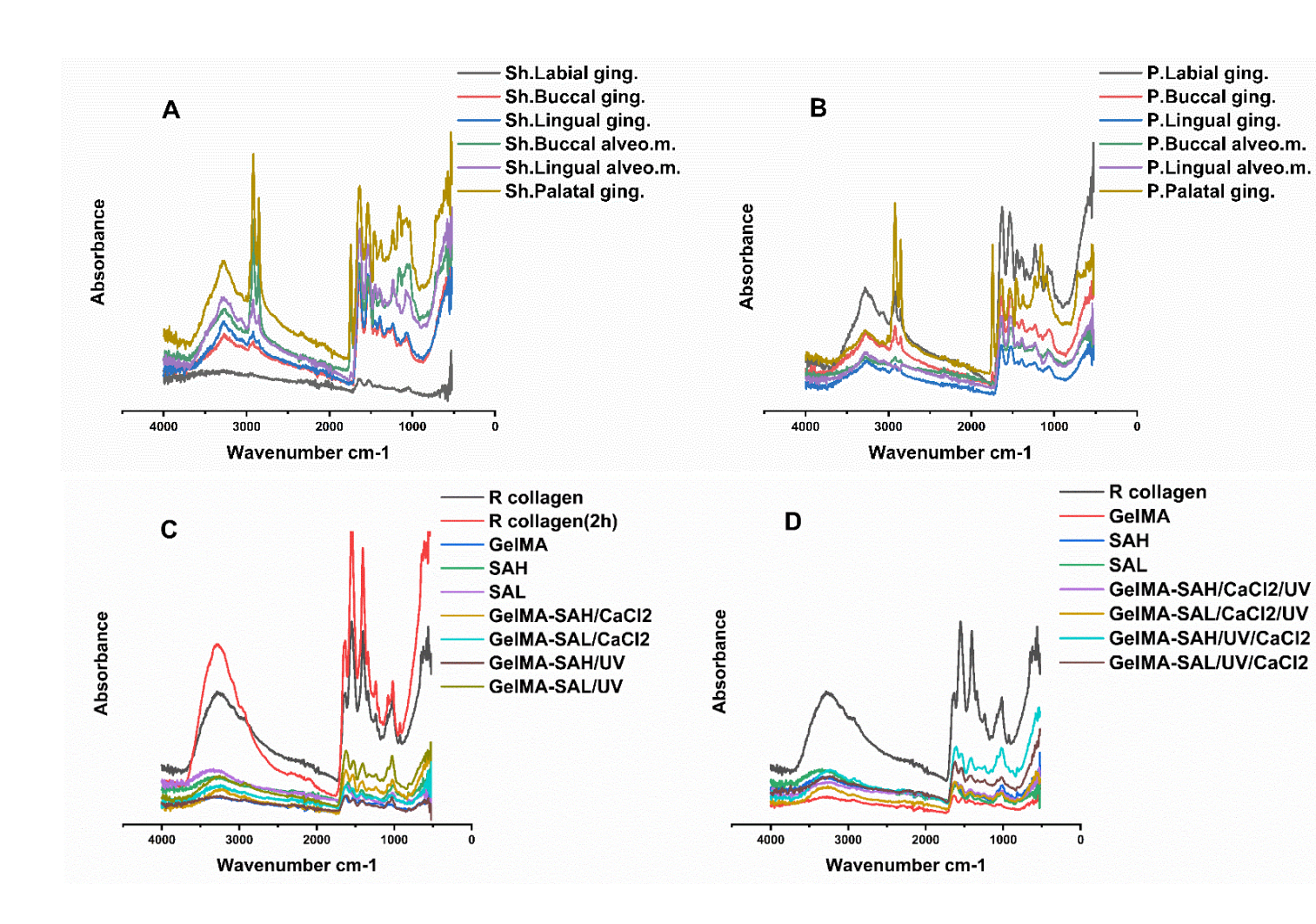
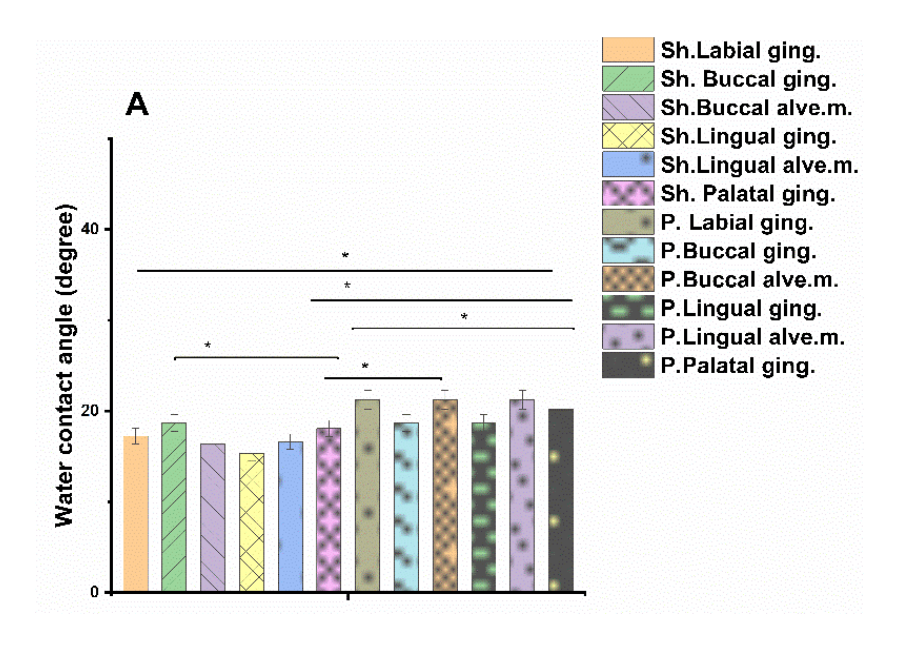


Figure 6.14. FT-IR spectra summarising the chemical bonding structure in samples over a range of 4000–500 cm⁻¹ with a resolution of 4 cm⁻¹ at 37 °C. (A), sheep labial, buccal, and lingual gingival tissue samples (Sh.Labial ging., Sh.Buccal ging., Sh.Lingual ging.), sheep buccal, and lingual oral alveolar mucosal tissue samples(Sh.Buccal alveo.m., and Sh.Lingual alveo.m.), and sheep palatal gingival tissue sample (Sh.Palatal ging.). (B) Porcine labial, buccal, and lingual gingival tissue samples (P.Labial ging., P.Buccal ging., and P.Lingual ging.), porcine buccal, and lingual oral alveolar mucosal tissue samples(P.Buccal alveo.m., and P.Lingual alveo.m.), and porcine palatal gingival tissue sample (P.Palatal ging.). (C), hydrogel samples are R collagen(rat collagen with overnight incubation), R collagen(2h incubation), GelMA, SAH, SAL, GelMA-SAH/CaCl₂, GelMA-SAL/CaCl₂, GelMA-SAH/UV, and GelMA-SAL/UV. (D), hydrogel samples are R collagen(rat collagen with overnight incubation), GelMA, SAL. GelMA-SAH/CaCl₂/UV, GelMA-SAL/CaCl₂/UV, SAH. GelMA-SAH/UV/CaCl₂, and GelMA-SAL/UV/CaCl₂.

6.3.4. Hydrophilic/hydrophobic surface properties

The mean values of water contact angle degree for sheep and porcine oral mucosal tissue samples are showen in Figure 6.15A. In addition to all 13 hydrogel samples after single and double crosslinking procedures are shown in Figure 6.15B and C. The results displayed a hydrophobic nature of GelMA, and GelMA-SA composite hydrogels when crosslinked by UV or UV/CaC methods. While the other samples were with hydrophilic nature. The mean values (mean ± SD, N = 3) were (87.5±0.2, 76.836, 66.34, 62.6±0.5, 54.4±0.32) for GelMA, GelMA-SAH/UV, GelMA-SAL/UV, GelMA-SAH/UV/CaCl2, and GelMA-SAL/UVCaCl2 hydrogel samples, respectively. These results indicated the effects of UV crosslinking method alone or followed by ionic crosslinking by CaCl2 on surface nature of GelMA and GelMA-SA composite hydrogel samples. The results from animal samples, sheep and porcine, were with hydrophilic nature.



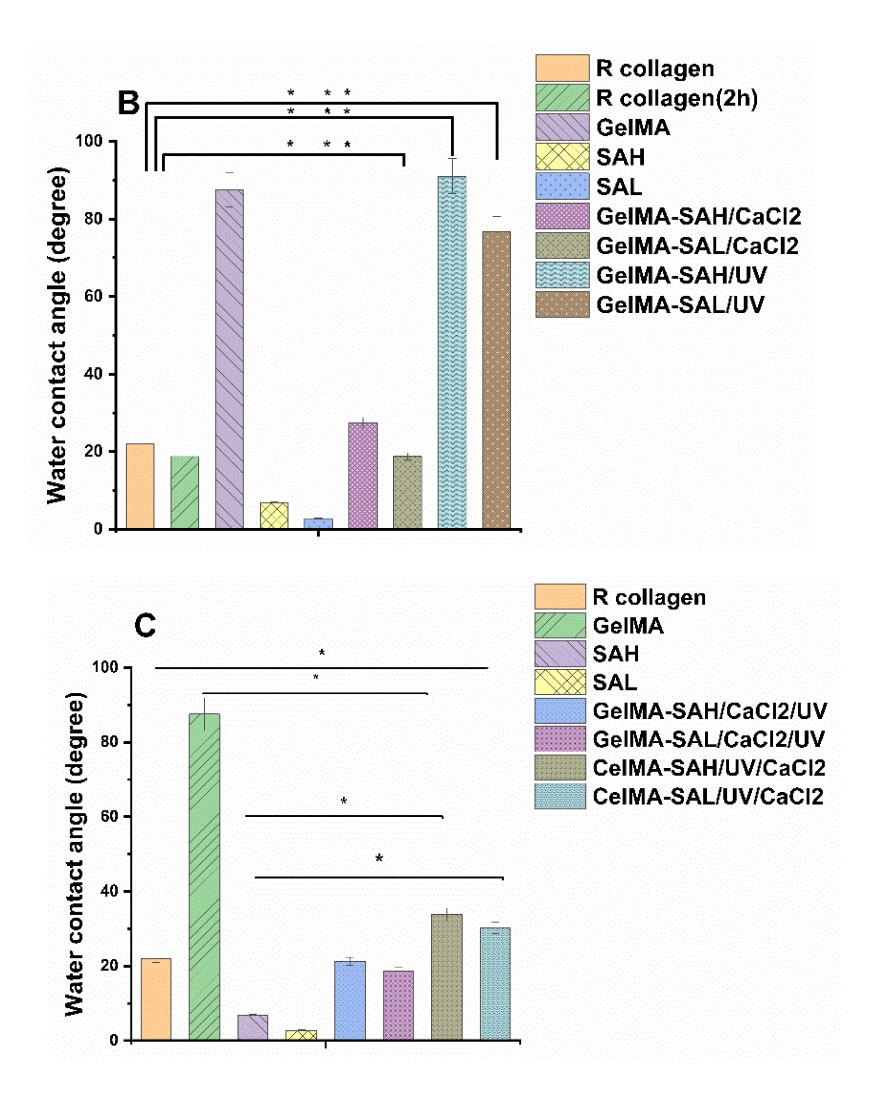


Figure 6.15. WCA measurements for sampls (A), sheep labial, buccal, and lingual gingival tissue samples(Sh.Labial ging., Sh.Buccal ging., Sh.Lingual ging.), sheep buccal, and lingual oral alveolar mucosal tissue samples(Sh.Buccal alveo.m., and Sh.Lingual alveo.m.), and sheep palatal gingival tissue sample (Sh.Palatal ging.). Porcine labial, buccal, and lingual gingival tissue samples(P.Labial ging., P.Buccal ging., and P.Lingual ging.), porcine buccal, and lingual oral alveolar mucosal tissue samples(P.Buccal alveo.m., and P.Lingual alveo.m.), and porcine palatal gingival tissue sample (P.Palatal ging.). (B), hydrogel samples are R collagen, R collagen(2h), GelMA, SAH, SAL, GelMA-SAH/CaCl₂, GelMA-SAH/CaCl₂, GelMA-SAH/UV, and GelMA-SAL/UV. (C), hydrogel samples are R collagen, GelMA, SAH, SAL, GelMA-SAL/CaCl₂/UV, GelMA-SAH/UV/CaCl₂, and GelMA-SAL/UV/CaCl₂. Data representing mean ± SD(n=3). * p < 0.05.

6.3.5. Thermal Properties

Melting points of the samples as a maximum point in the first endothermic peak of the DSC thermograms and the melting point mean values (mean \pm SD, N = 3) for samples were evaluated (Tab.6.1).

In animal oral mucosal tissue samples, the results showed that the melting point values of gingival and palatal tissues were higher in compared with alveolar mucosal tissue samples. Similarly, these values from porcine tissue samples were higher compared with sheep tissue samples except with the buccal attached gingival sample, which was higher in sheep compared with porcine tissue sample. The results showed also, all hydrogel samples have high melting temperature values compared with rat tail collagen samples. In addition, the melting point values were higher in high concentrated hydrogel samples compared with low concentrated, however, there were no significant differences between high and low concentration hydrogel samples. For GelMA-SA composites, the melting point values were higher when crosslinked with single method in compared with double methods. However, these values were higher when crosslinked by CaCl₂/UV compared with UV/CaCl₂. Full figure (Fig. 6.16) is presented in Appendix F.

Table.6.1. DSC thermograms of sheep and porcine gingival, oral alveolar mucosal, and hydrogel samples which were examined under a continuous flowrate of nitrogen gas with the following conditions: equilibrate (-10 $^{\circ}$ C), isothermal (1 min), and a ramp at 10 $^{\circ}$ C/min up to a final temperature of 450 $^{\circ}$ C.. Values represent the mean \pm standard deviation (SD) of three independent measurements (N=3).

Samples	Peak Temp (°C)
Sh.Labial ging.	112.83±0.6
Sh.Buccal ging.	161.28±0.75
Sh.Lingual ging.	155.64±0.1
Sh.Buccal alveo.m.	72.36±0.4
Sh.Lingual alveo.m	70.99±1.1
Sh.Palatal ging.	103.62±0.2
P.Labial ging.	123.70±0.21
P.Buccal ging.	157.27±0.4
P.Lingual ging.	131.01±0.6
P.Buccal alveo.m.	127.17±0.9
P.Lingual alveo.m	105.5±2.2
P.Palatal ging.	125.97±0.3
R collagen	55.42±1.4
R collagen (2h)	54.34±4.14
GelMA	116.4±14.2
SAH	130.86±3.38
SAL	107.51±2.1
GelMA-SAH/CaCl₂	146.77±1.91
GelMA-SAL/CaCl ₂	143.76±2.33
GelMA-SAH/UV	155.57±8.6
GelMA-SAL/UV	140.54±19.6
GelMA-SAH/CaCl ₂ /UV	154.2±7.58

GelMA-SAL/CaCl₂/UV	142.35±1.7
GelMA-SAH/UVCaCl ₂	115.57±0.28
GelMA-SAL/UVCaCl ₂	126.75±2.26

Note:- Samples are sheep labial, buccal, and lingual gingival tissue samples(Sh.Labial ging., Sh.Buccal ging., Sh.Lingual ging.), sheep buccal, and lingual oral alveolar mucosal tissue samples(Sh.Buccal alveo.m., and Sh.Lingual alveo.m.), and sheep palatal gingival tissue sample (Sh.Palatal ging.). Porcine labial, buccal, and lingual gingival tissue samples (P.Labial ging., P.Buccal ging., and Lingual ging.), porcine buccal, and lingual oral alveolar mucosal tissue samples(P.Buccal alveo.m., and P.Lingual alveo.m.), and porcine palatal gingival tissue sample (P.Palatal ging.). Hydrogel samples are R collagen, R collagen(2h), GelMA, SAH, SAL, GelMA-SAH/CaCl₂, GelMA-SAH/UV, GelMA-SAL/UV. GelMA-SAH/CaCl₂/UV, GelMA-SAH/UV/CaCl₂, and GelMA-SAL/UV/CaCl₂.

6.3.6. Rheological characteristics

The rheological properties of included hydrogel samples, in addition to palatal tissue from animal samples were investigated at 37, 20, and 4 °C as shown in Figures 6.17–6.22. All measurements were performed in triplicate (mean ± SD, N = 3). The viscosities of these samples were examined with different shear rates. Figures 7.17 and 6.18, presented the effect of different shear rates on viscosity, and share stress, of animals and hydrogel samples with different temperatures, 37, 20, and 4°C, respectively. As seen from the rheograms, the viscosity decreased with increasing the shear rate, indicating their shear thinning behaviour. The viscosity values of all hydrogel samples were higher compared to both rat collagen samples. In addition, the viscosity values of the hydrogel samples increased with decreasing temperature. However, this trend was not observed in the rat tail collagen samples and was more pronounced in the R collagen (2 h) sample (Fig.6.17A and B). In addition, the viscosity values of hydrogel samples increased as the alginate concentration was increased. Moreover, the double crosslinking (CaCl₂/UV or UV/CaCl₂) of GelMA-SA

composite hydrogel samples caused further increases in viscosity values compared to the single crosslinking. GelMA-SAH/CaCl₂/UV, GelMA-SAL/CaCl₂/UV, and GelMA-SAH/UV/CaCl₂ viscosity values were higher in compared with GelMA-SAL/UV/CaCl₂. However, the viscosity values of both animal tissues were higher in compared with GelMA-SA composites (Fig. 6.17B).

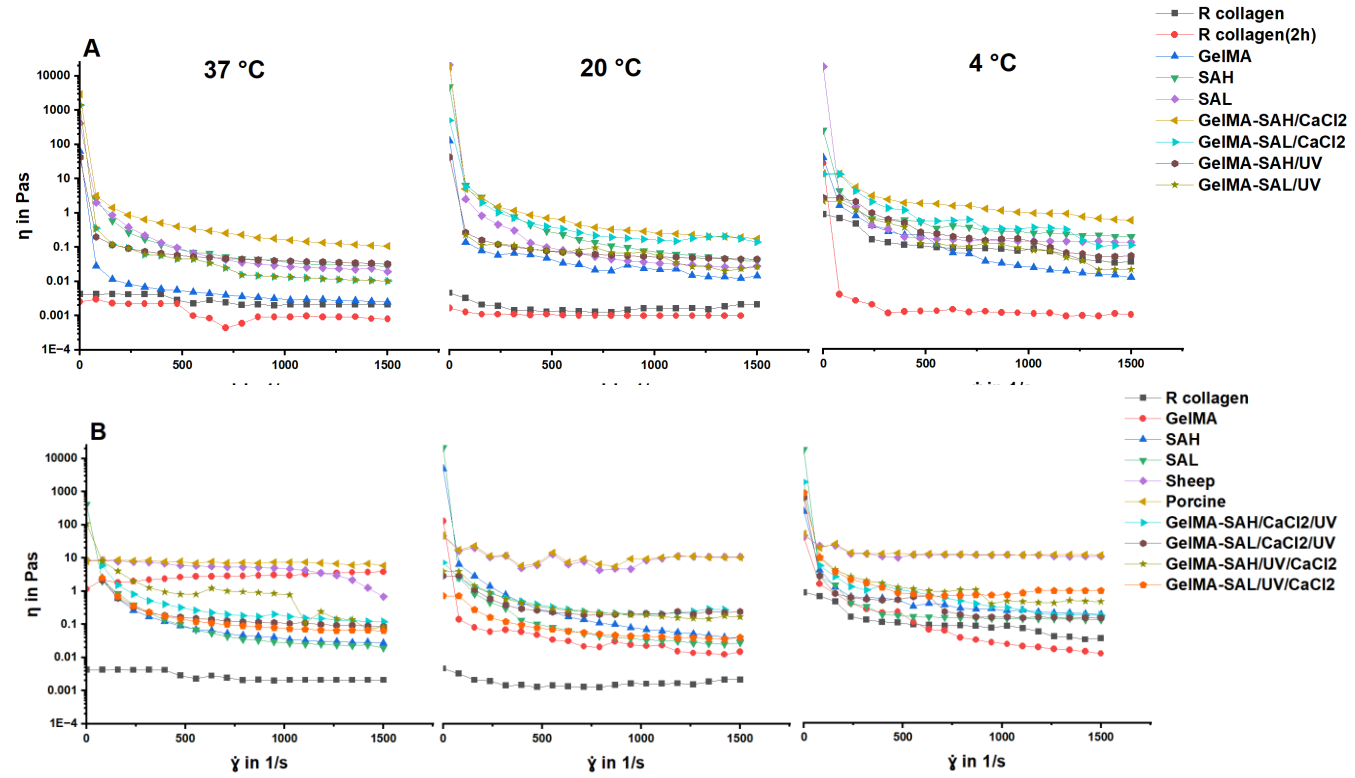


Figure 6.17. Shear dependent viscosity measurements for samples at 37, 20, and 4 °C. Hydrogel and animal samples are, (A) R collagen, R collagen(2h), GelMA, SAH, SAL, GelMA-SAH/CaCl₂, GelMA-SAL/CaCl₂, GelMA-SAH/UV, and GelMA-SAL/UV. (B), R collagen, GelMA, SAH, SAL, animal palatal tissue samples sheep and porcine, respectively, GelMA-SAH/CaCl₂/UV, GelMA-SAL/UV/CaCl₂, and GelMA-SAL/UV/CaCl₂

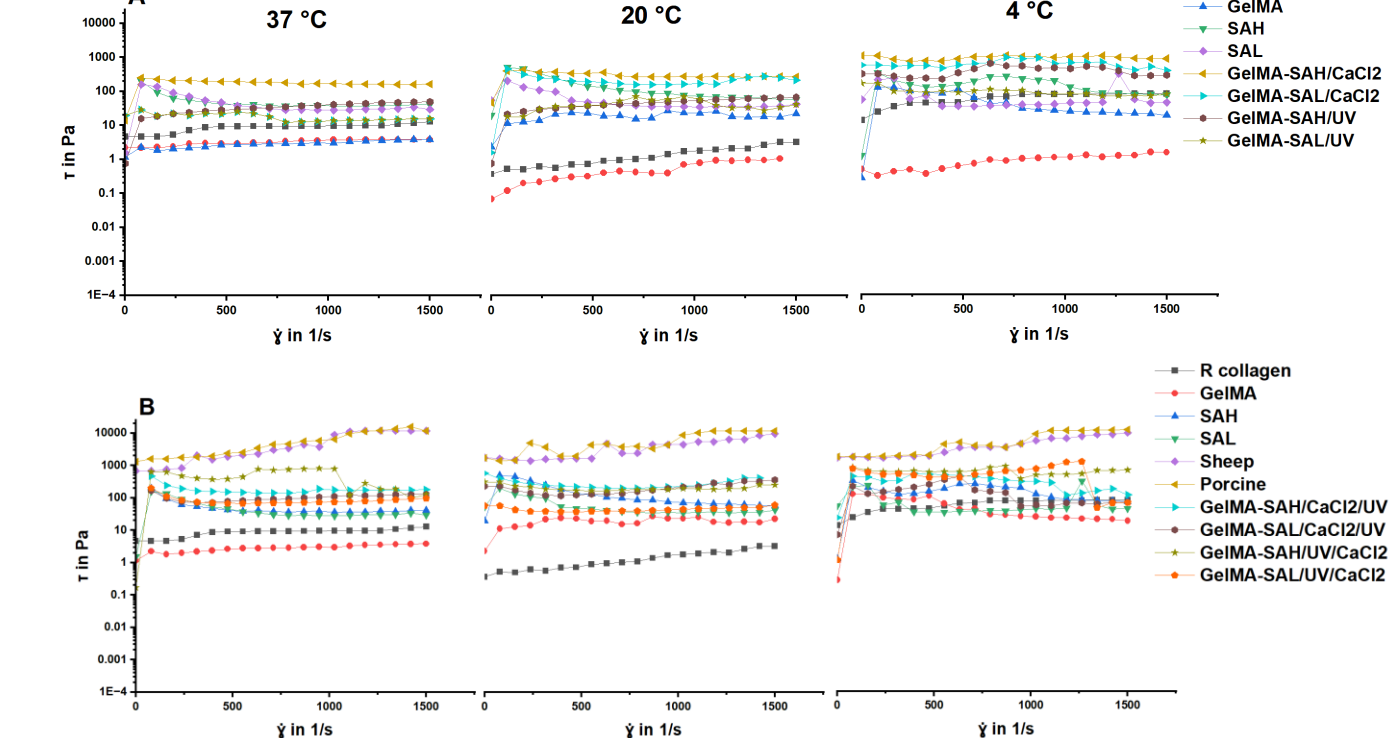


Figure 6.18. Shear stress as a function of shear rate for samples at 37, 20, and 4 °C. Hydrogel and animal samples are, (A) R collagen, R collagen(2h), GelMA, SAH, SAL, GelMA-SAH/CaCl₂, GelMA-SAL/CaCl₂, GelMA-SAH/UV, and GelMA-SAL/UV. (B), R collagen, GelMA, SAH, SAL, animal palatal tissue samples sheep and porcine, respectively, GelMA-SAH/CaCl₂/UV, GelMA-SAL/CaCl₂/UV, GelMA-SAH/UV/CaCl₂, and GelMA-SAL/UV/CaCl₂.

In Oscillatory Rheology as shown in Figures 6.19 and 6.20, the samples are subjected to an increasing oscillating strain (strain sweep) at a constant frequency, or vice versa (a decreasing frequency of oscillation at the constant strain in the linear viscoelastic range; frequency sweep). G' (the storage modulus) is a measure of the energy stored in the material and recovered from it per cycle, indicating its solid or elastic characters, while G" (the loss modulus) defines their liquid-like or viscous behaviours. A combination of both parameters, which exhibit a special response regarding linear viscoelasticity, provides important information on viscoelastic behaviour. All samples exhibited gel-like behaviour at operating temperatures of 37 °C, 20 °C, and 4 °C, as indicated by higher storage moduli (G') than loss moduli (G") during oscillation

R collagen R collagen(2h)

GelMA

4°C

(Figs 6.19 and 6.20) and frequency tests (Figs 6.21 and 6.22) (352). The viscoelastic values increased as the temperature decreased. As expected, the alginate concentration and the application of double crosslinking had positive effects on the mechanical properties of the GelMA-SA composite hydrogels. The double crosslinking method further enhanced the viscoelasticity of the hydrogels compared to the single crosslinking method. Moreover, the viscoelastic properties of the GelMA-SA composites were comparable to those of the animal tissue samples that also underwent double crosslinking.

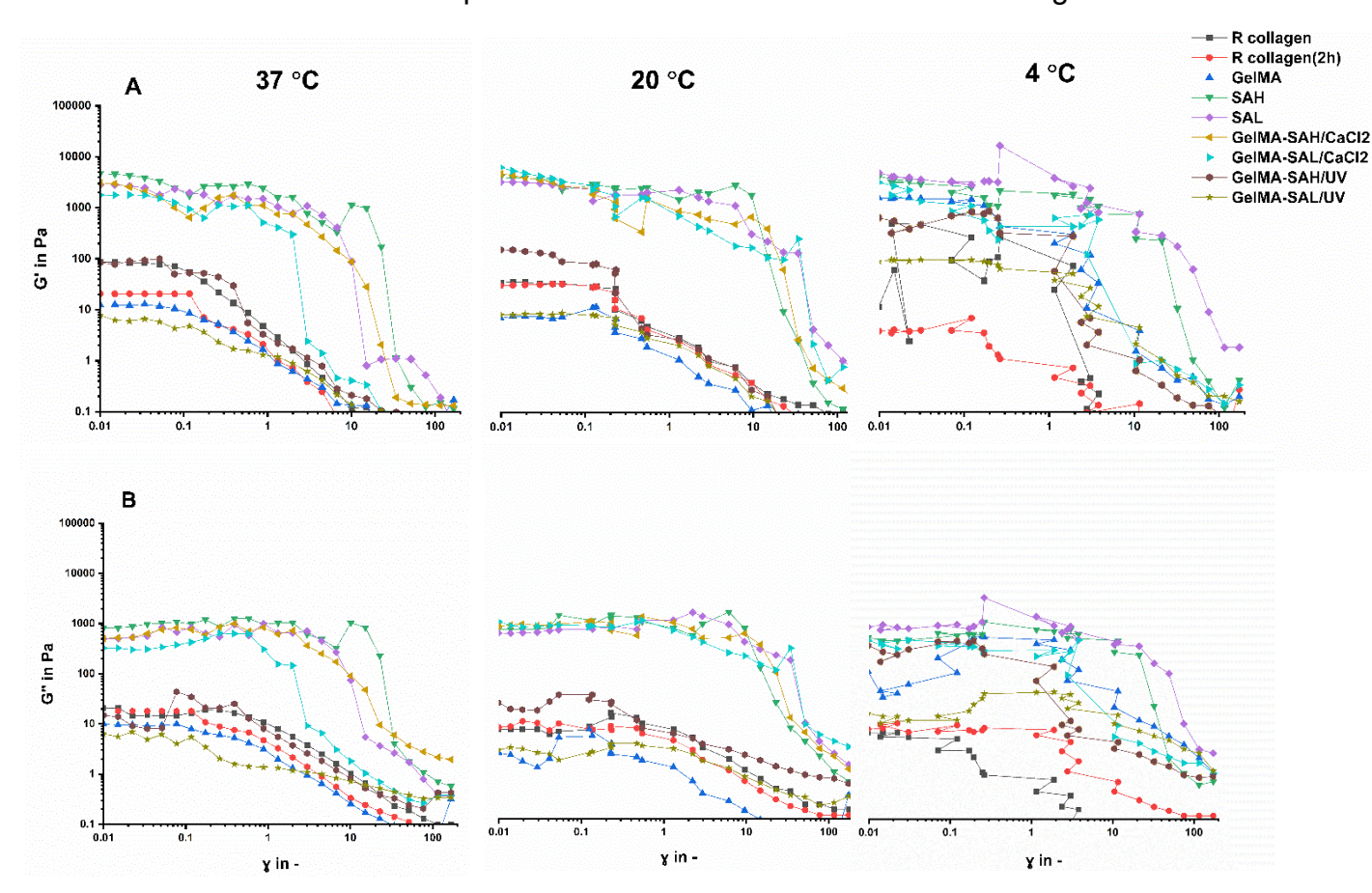
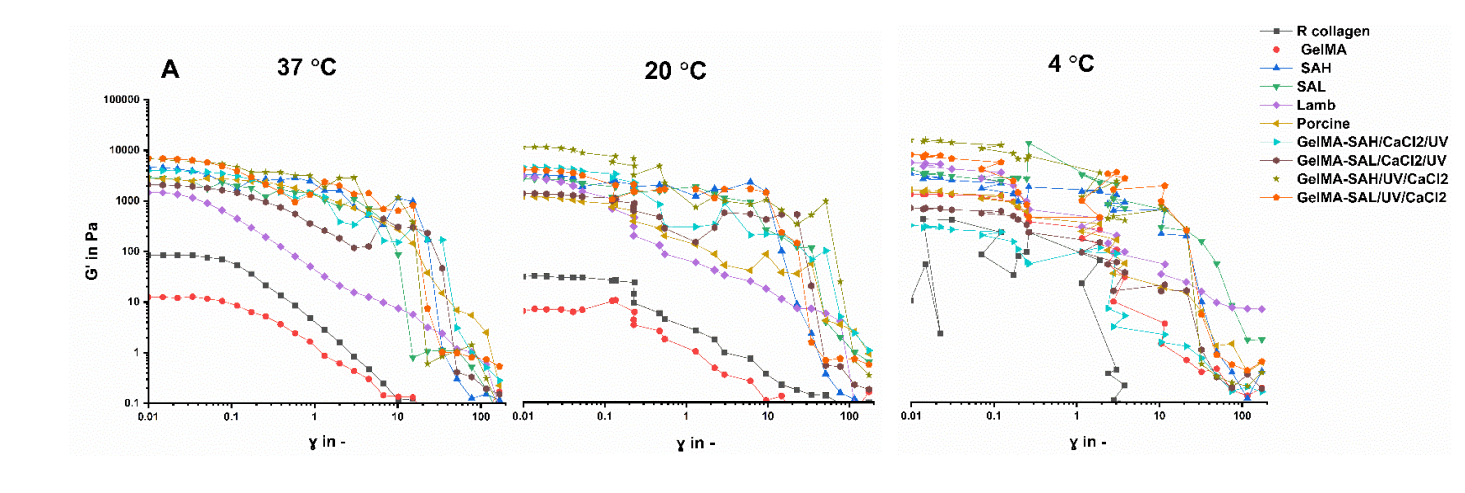


Figure 6.19. Oscillatory amplitude sweeps at a constant frequency of oscillation of 0.01 Hz measurements for samples at 37, 20, and 4 °C. A, G', and B, G", respectively of hydrogel samples, which are R collagen, R collagen(2h), GelMA, SAH, SAL, GelMA-SAH/CaCl₂, GelMA-SAL/CaCl₂, GelMA-SAH/UV, and GelMA-SAL/UV.



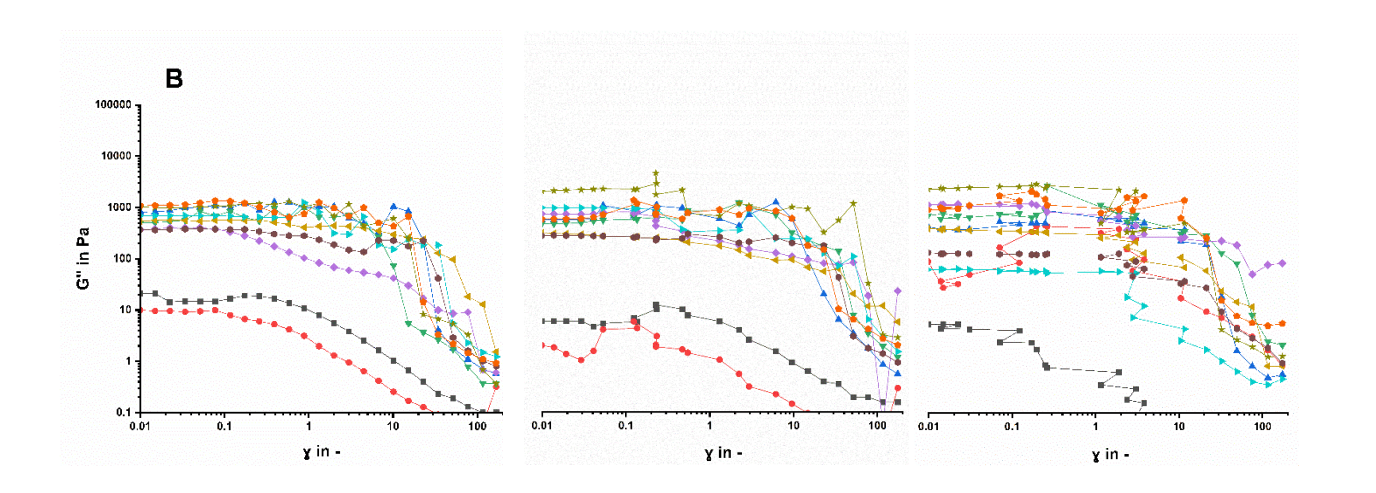
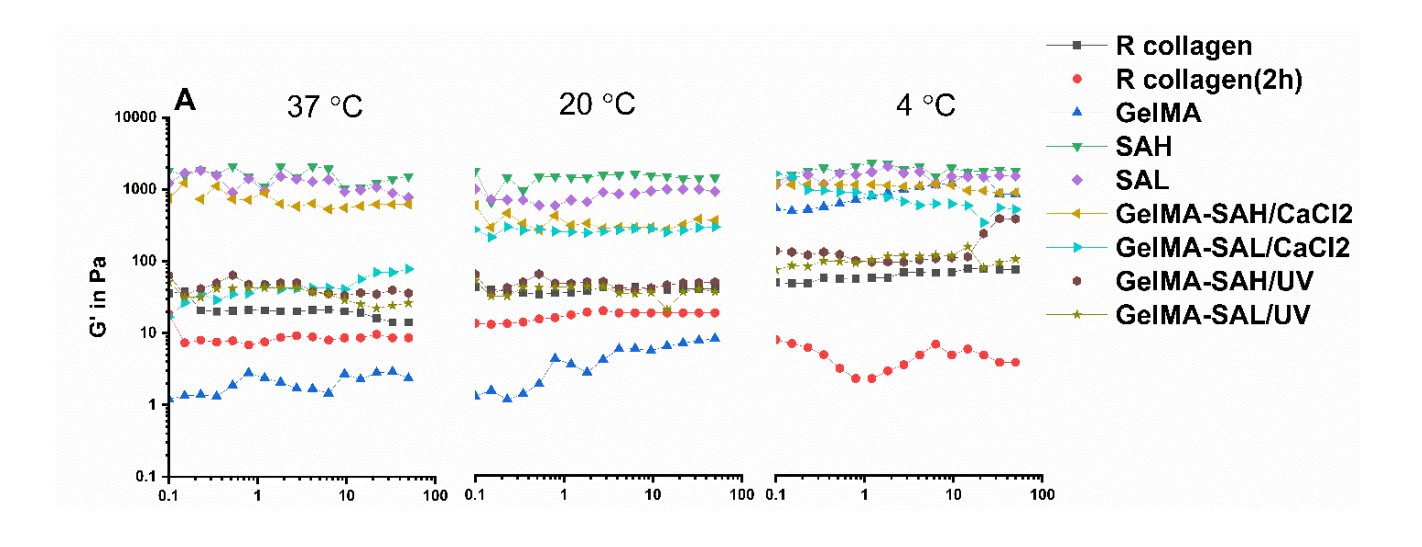


Figure 6.20. Oscillatory amplitude sweeps at a constant frequency of oscillation of 0.01 Hz measurements for samples at 37, 20, and 4 °C. A, G', and B, G", respectively of hydrogel samples, which are R collagen, GelMA, SAH, SAL, and animal palatal tissue samples for sheep and porcine, respectively, and hydrogel samples are GelMA-SAH/CaCl₂/UV, GelMA-SAL/CaCl₂/UV, GelMA-SAH/UV/CaCl₂, and GelMA-SAL/UV/CaCl₂.



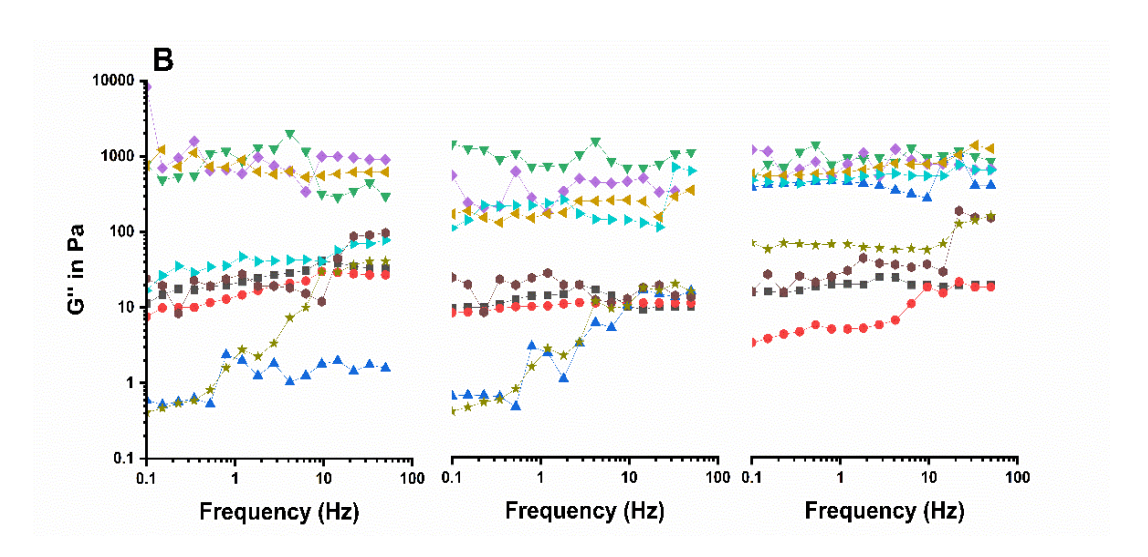
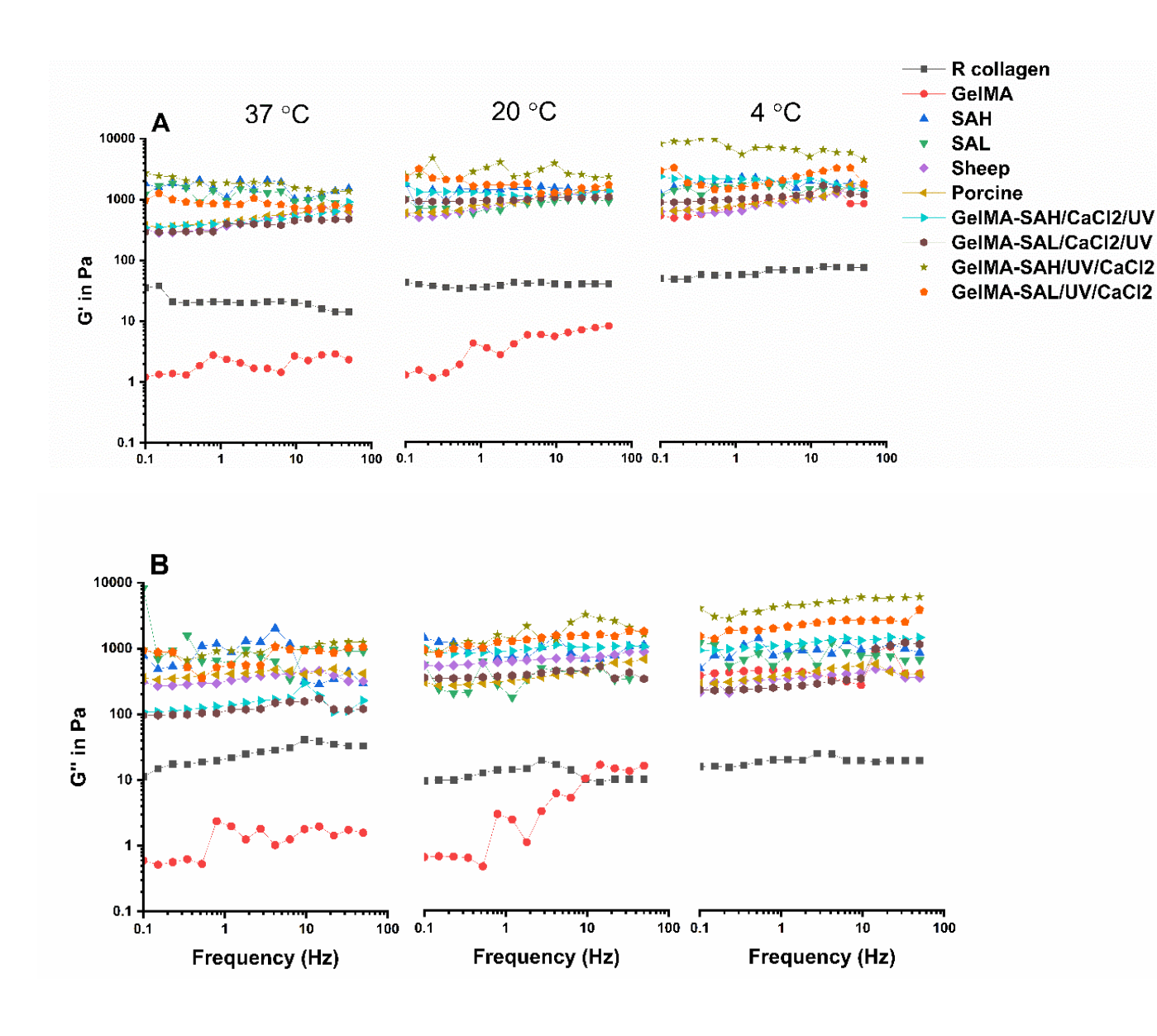


Figure 6.21. Frequency sweep in a linear viscoelastic range at the deformation of 0.25 % measurements for samples at 37, 20, and 4 °C. A, G', and B, G", respectively of hydrogel samples, which are R collagen, GelMA, SAH, SAL, GelMA-SAH/CaCl₂, GelMA-SAL/CaCl₂, GelMA-SAL/UV, GelMA-SAL/UV.



.Figure 6.22. Frequency sweep in a linear viscoelastic range at the deformation of 0.25 % measurements for samples at 37, 20, and 4 °C. A, G', and B, G", respectively of hydrogel samples, which are R collagen, GelMA, SAH, SAL, and animal palatal tissue samples for sheep and porcine, respectively, and hydrogel samples are GelMA-SAH/CaCl₂/UV, GelMA-SAL/CaCl₂/UV, GelMA-SAH/UV/CaCl₂, and GelMA-SAL/UV/CaCl₂.

6.3.7. Mechanical properties

The viscoelastic properties were determined by evaluating storage modulus (E') and loss modulus (E''), in addition to stiffness values via DMA-uniaxial compression at a range of frequencies between 0.1 and 50 Hz under 37 °C (Appendix F, Figs. 6.23-.26). In addition, the Young's modulus was calculated to further characterise the mechanical behaviour (Fig 6.27). All measurements were performed in triplicate and were reported as mean \pm SD (N = 3).

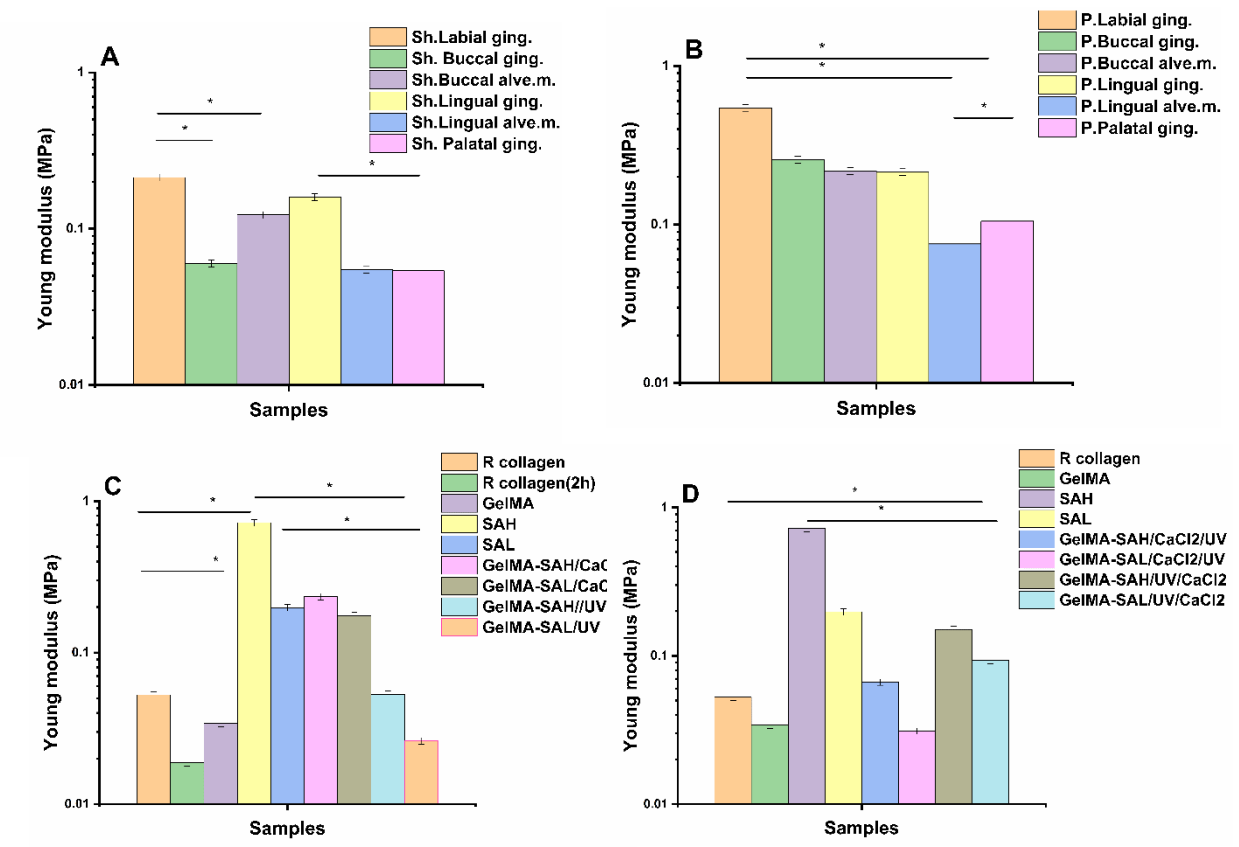


Figure 6.27. Young modulus E as a function of frequency oscillations ranging from 0.1 to 50 Hz at 5 Hz intervals for each sample. Samples were pre-loaded with a force of 0.001 N and dynamically tested at low deformation (0.25% strain), taken at the temperature of 37 °C. A and B, samples of oral mucosal tissue samples for labial, buccal, and lingual gingival tissue samples (Labial ging., Buccal ging.,Lingual ging.), buccal, and lingual oral alveolar mucosal tissue samples(Buccal alveo.m., and Lingual alveo.m.), and palatal gingival tissue sample (Palatal ging.), of shep and porcine, respectively. Sh referring to sheep, and P referring to porcine. C, and D, crosslinked hydrogel samples. * p < 0.05.

The results showed the values of E' was higher than the E", which indicates a predominantly elastic behaviour rather than viscous behaviour of investigated sample's structure (352). The mean values of elastic modulus of gingival (Labial, Buccal, and Lingual), alveolar mucosal (Labial and Buccal), and palatal tissues samples from sheep were (0.12±0.0363, 0.06±0.02, 0.053±0.012, 0.046 ± 0.013 , 0.022 ± 0.006 , 0.019 ± 0.003), and porcine were $(0.23\pm0.11$, 0.11±0.05, 0.078±0.021, 0.010±0.002, 0.069±0.018, 0.040±0.011), respectively (Appendix F, Tab 6.2). In addition, the stiffness means values of double crosslinking hydrogel samples, as shown in Figure 6.26 were close to same values of animal samples, which are palatal gingival and lingual mucosal tissues of sheep (Fig 6.23), and porcine palatal gingival tissue (Fig. 6.24). From the results, the Young's modulus values of labial gingival tissue in animal samples were significantly higher compared with other oral tissue samples. For the hydrogel samples, the SAH showed significantly higher values compared with the other samples. Moreover, GelMA-SA composite hydrogels crosslinked with the double UV/CaCl₂ method exhibited higher Young's modulus values compared with those crosslinked using the CaCl₂/UV sequence. However, in GelMA-SA composite hydrogels, UV-only crosslinking resulted in lower Young's modulus values compared with CaCl₂-only crosslinking. Further data can be found in Appendix F Table 6.2.

6.3.8. Degradation test

Degradation test results of GelMA-SA composites with R collagen and GelMA hydrogel samples are shown in Figure 6.28. The degradation was assessed by measuring the percentage of remaining weight of the hydrogel samples over time. All measurements were performed in triplicate (mean ± SD, N = 3). The results showed that both GelMA-SAH/CaCl₂/UV and GelMA-SAL/CaCl₂/UV

exhibited a faster degradation rate compared to the other hydrogel samples, which was clearly evident from the data.

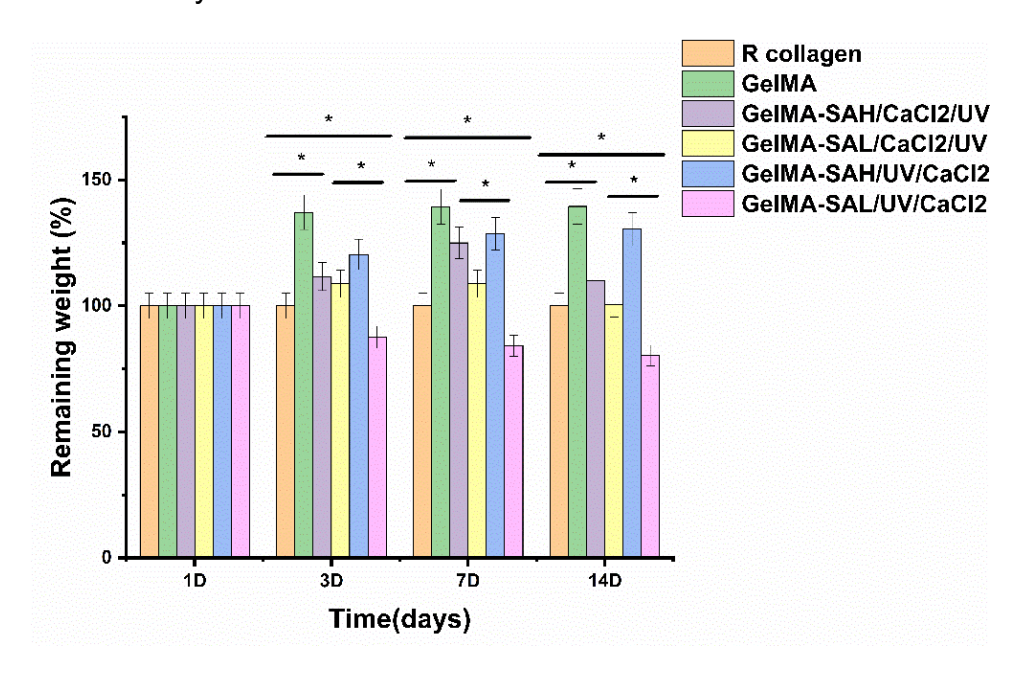


Figure 6.28. Remaining weight of hydrogel samples using 3D culturing. The samples are, R collagen, GelMA, GelMA-SAH/CaCl₂/UV, GelMA-SAL/CaCl₂/UV, GelMA-SAH/UV/CaCl₂, and GelMA-SAL/UV/CaCl₂, on days 1, 3,7 and 14 days. remaining weight (%) of hydrogel samples incubations in PBS at 37 °C (n = 3). * p < 0.05.

6.3.9. Biological and cell viability measurements

As shown in Figure 6.29, primary human gingival fibroblast cells (HGFs) exhibit typical spindle-shaped morphology when cultured in vitro. The cells were illustrating the cellular organization prior to incorporation into the 3D gingival model.

Figure 6.30 A and B showed the metabolic activity, cytotoxicity data of seeding HGF cells into 3D culturing using different hydrogel samples as a substrates. The tested hydrogel samples included SAH and SAL, along with GelMA-SA composites crosslinked using either CaCl₂ or UV.These samples were GelMA-SAH/CaCl₂, GelMA-SAL/CaCl₂, GelMA-SAH/UV, and GelMA-SAL/UV.

Metabolic activity and cytotoxicity were assessed on days 1, 3, 7, and 14. All measurements were performed in triplicate (mean \pm SD, N = 3). The results in Figure 6.30 A, demonstrated increased metabolic activity in all hydrogel samples after three days of culture, with SAH and SAL showing significantly higher values compared to other samples. By day 7, GelMA-SAH/CaCl₂ and GelMA-SAL/CaCl₂ exhibited significantly higher metabolic hydrogel samples compared to the control group (HGF cells cultured in 2D conditions with standard culture media).



Figure 6.29. Microscopy images of primary human gingival fibroblast cells (HGFs). Scale bars 100 μm (100mm). Magnification 10x.

Notably, among the GelMA-SA composite samples, those crosslinked using UV displayed the lowest metabolic activity throughout the experiment.

Figure 6.30 B, presented the cytotoxicity results, measured through LDH release. On day 1, SAH and SAL exhibited the lowest LDH release among all hydrogel samples, but these values increased over time. However, from day 1 onward, LDH release exceeded 30% for all hydrogel samples and continued to rise until day 14.

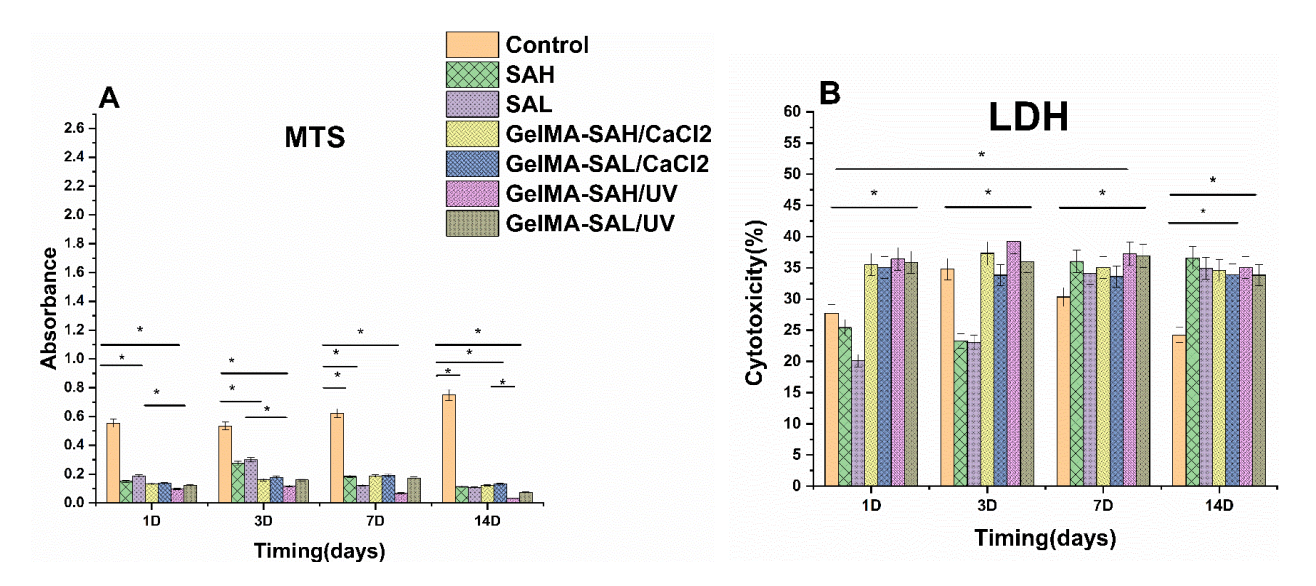


Figure 6.30 B, presented the cytotoxicity results, measured through LDH release. On day 1, SAH and SAL exhibited the lowest LDH release among all hydrogel samples, but these values increased over time. However, from day 1 onward, LDH release exceeded 30% for all hydrogel samples and continued to rise until day 14.

To further confirm metabolic activity and cytotoxicity, confocal imaging was performed using the live/dead staining method (Fig. 6.31). Fluorescence microscopy images were captured on days 1, 3, 7, and 14 to evaluate cell viability within the hydrogel samples. As shown in Figure 6.31, cell viability progressively increased over time, with GelMA-SAH/CaCl₂ and GelMA-SAL/CaCl₂ demonstrating the highest viability on day 7, compared to the other hydrogel formulations. However, cell viability decreased by day 14 across all hydrogel samples.

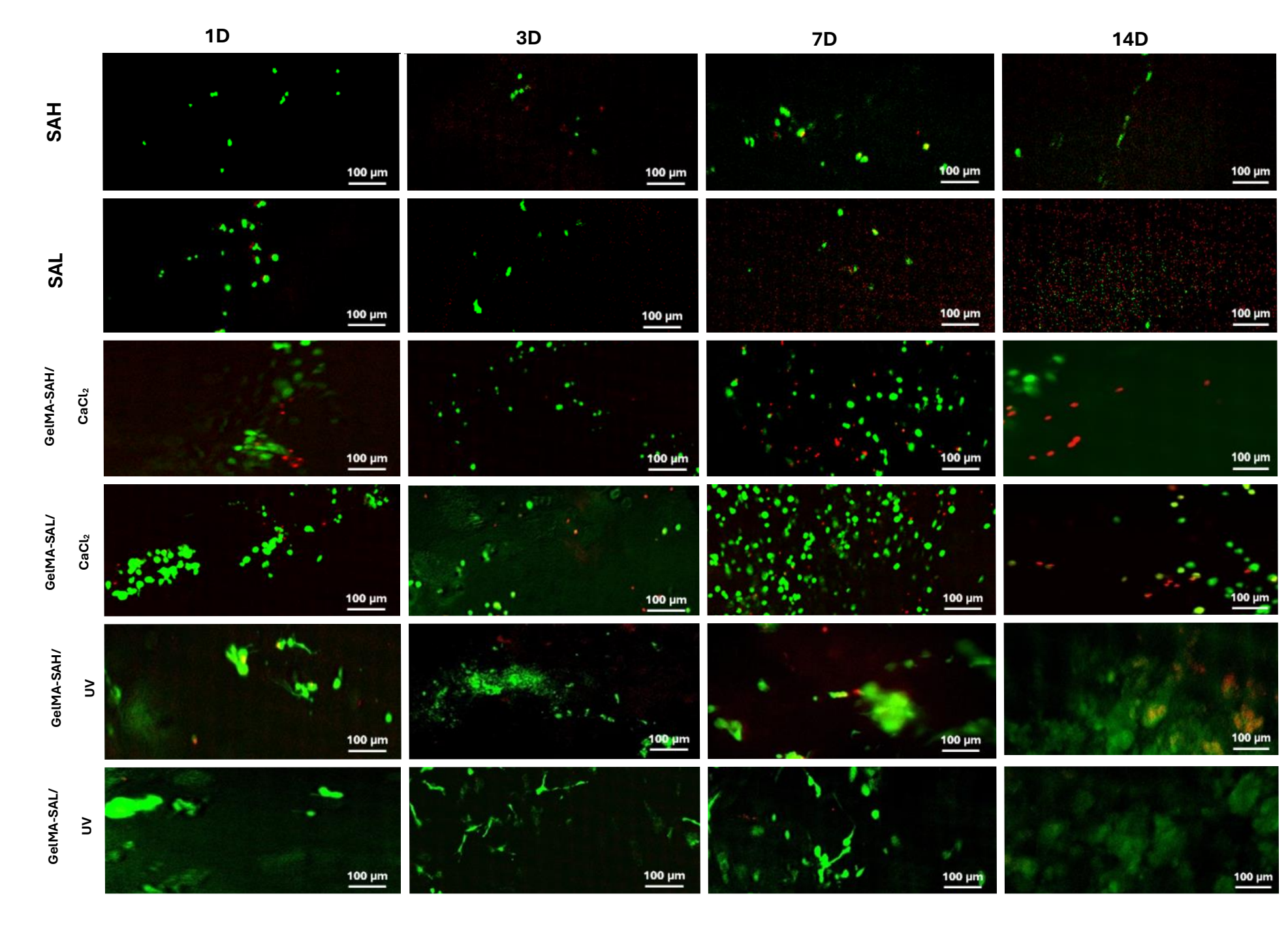


Figure 6.31. Viability and cytotoxicity of HGF cells using 3D culturing using different hydrogel samples, SAH, SAL, GelMA-SAH/CaCl₂, GelMA-SAL/CaCl₂, GelMA-SAH/UV, and GelMA-SAL/UV, on days 1, 3,7 and 14 days, using flurecent microscope, indicating living cells (green) and dead cells (red). Scale bar: 100 μm.

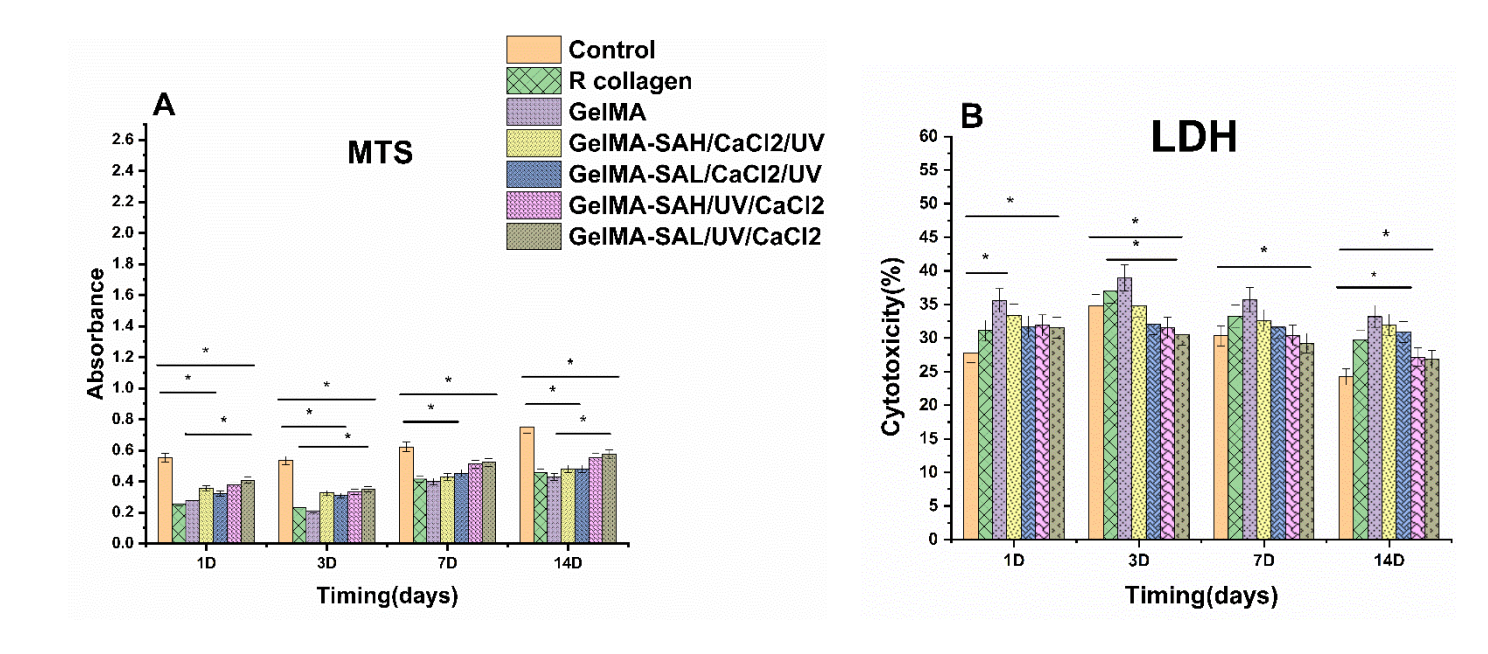


Figure 6.32. A. Metabolic activity, and B. cytotoxicity of HGF cells using 3D culturing using different hydrogel samples, R collagen, GelMA, GelMA-SAH/CaCl₂/UV, GelMA-SAH/UV/CaCl₂, and GelMA-SAL/UV/CaCl₂, on days 1, 3,7 and 14 days. A, metabolic activity of HGF cells. B, LDH release of HGF cells. Data representing mean \pm SD(n=3). * p < 0.05.

Figure 6.32 showed the metabolic activity, cytotoxicity data of seeding HGF cells into 3D culturing using different hydrogel samples as a substrates. These methods performed on days 1, 3, 7 and 14 days. Hydrogel samples were GelMA-SAH/UV/CaCl₂, GelMA-SAL/UV/CaCl₂, GelMA-SAH/CaCl₂/UV, and GelMA-SAL/CaCl₂/UV, R collagen and GelMA. The results demonstrated higher metabolic activity of cells after 3 days of culture in the hydrogel samples. For metabolic activity values, R collagen was highly significantly higher than other GelMA-SA composite samples on day 3. In addition, in comparing with all hydrogel samples, the GelMA-SAH/UV/CaCl₂, GelMA-SAL/UV/CaCl₂ hydrogel samples were higher on day 14. GelMA-SAL/CaCl₂/UV samples was significantly high in compared with control group which represented the 2D culturing of HGF cells using culture media (Fig. 6.32.A).

In cytotoxicity data, results showed there was low LDH release observed on days 1 and 7 with higher than 30% for R collagen and GelMA, while other

hydrogel samples were with around 30%. These values were increased with the day 14 for all samples (Fig. 6.32 B).

Metabolic activity and cytotoxicity values confirmed by confocal imaging for live/dead staining method (Fig.6.33). Confocal images in Figure 6.33, for live/dead staining present the HGF cells viability encapsulated within above mentioned hydrogel samples. By using the fluorescence microscope for image capturing on days 1, 3, 7,and 14. As shown from these images, cell viability increased over the culture in GelMA-SAH/CaCl₂/UV, and GelMA-SAL/CaCl₂/UV on the first and third days compared with GelMA-SAH/UV/CaCl₂, GelMA-SAL/UV/CaCl₂. However, these values were higher in the last two hydrogel samples and GelMA-SAH/CaCl₂/UV compared to other hydrogel samples.

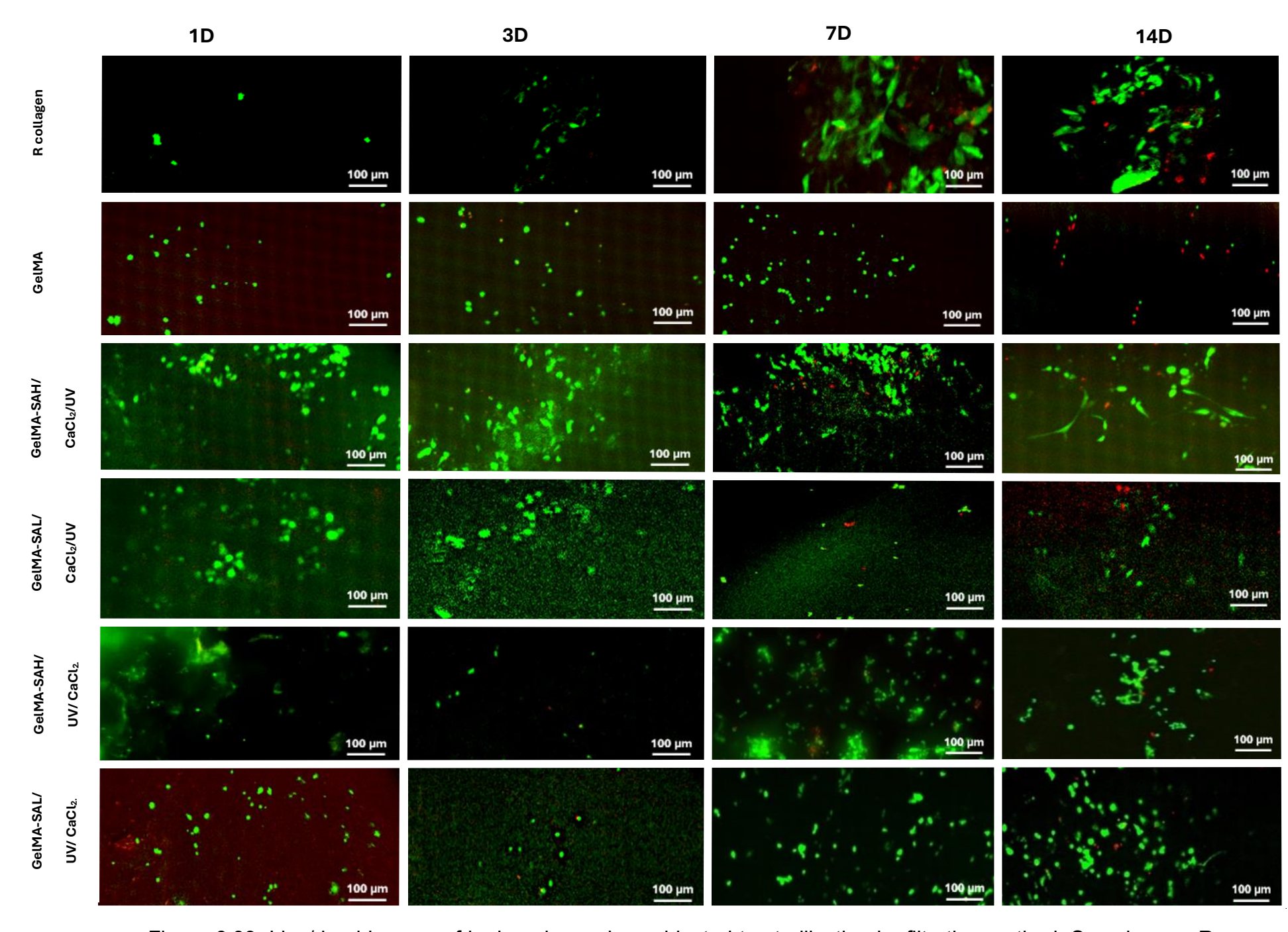


Figure 6.33. Live/dead images of hydrogel samples subjected to sterilization by filtration method. Samples are R collagen, GelMA, GelMA-SAH/CaCl $_2$ /UV, GelMA-SAL/CaCl $_2$ /UV, GelMA-SAH/UV/CaCl $_2$, and GelMA-SAL/UV/CaCl $_2$, on days, 1, 3, 7, and 14, using flurecent microscope, indicating living cells (green) and dead cells (red). Scale bar: 100 μ m.

6.4. Discussion

Herein, we hypothesize that the mechanical and biological properties of GelMA-SA composite hydrogels could be tuned using a double crosslinking method. Due to ethical and practical challenges in obtaining human gingival tissue, we compared our novel composite with animal gingival samples. Among the available options, porcine and sheep gingival tissues were selected, as they are considered the most representative models of human gingival tissue in terms of structure and composition (218). Our findings suggest these composites can regulate human gingival fibroblast behavior within a 3D gingival model.

The surface morphology and porosity of the samples were investigated using SEM. A prominent network of collagen fibers was observed in the animal samples, as well as in the rat tail hydrogel sample after overnight incubation. However, this network was not discernible in the rat collagen hydrogel sample incubated for only 2 hours. These results suggest that the incubation time for R collagen samples is crucial to achieving complete gelation. The choice of the 2-hour incubation period was based on a previously published study by Tabatabaei et al. (2020), who used 2 hour incubation for rat tail collagen in their oral mucosa tissue engineering model (359). Their protocol demonstrated successful fibroblast encapsulation and hydrogel formation within this time frame, making it a relevant comparison point for evaluating the gelation behaviour of our samples. These findings suggest that incubation time is a critical factor influencing the structural integrity and gelation of rat collagen hydrogels.

Pore size is a critical factor in tissue engineering scaffolds, influencing cell behavior and infiltration into the scaffold (353). Additionally, pore size mediates vascularization, highlighting its importance in scaffold design (337). In this study, the pore size of GelMA-SA composite hydrogel samples was larger in low-concentration samples compared to high-concentration ones, indicating the lower mechanical properties of the low-concentration samples.

Human gingival connective tissue typically consists of circular pores ranging from 30 to 80 μm (354). In this study, the pore size values in sheep gingival tissue fell within this range. as shown in the SEM analysis (Figures 6.6 and 6.7). Similarly, only the buccal and lingual attached gingiva, along with the buccal alveolar mucosa of porcine samples, exhibited pore sizes within this range. For the hydrogel samples, the pore size values in GelMA, GelMA-SAH/CaCl₂, GelMA-SAL/CaCl₂, GelMA-SAH/CaCl₂/UV, GelMA-SAL/CaCl₂/UV, GelMA-SAH/UV/CaCl₂, and GelMA-SAL/UV/CaCl₂, ranged from 32.1 to 36.6 μm, were also within this range, indicating their structural similarity to the morphology of human gingival tissue.

FT-IR spectroscopy was employed to analyze the biochemical properties of the samples. One of the major advantages of FT-IR imaging is its ability to provide a biochemical fingerprint, offering detailed information about the composition, structure, and chemical modifications of key biomolecules in the samples. The Amide I and II bands are prominent features of the protein infrared spectrum, associated with C=O stretching, N-H bending, and C-N stretching vibrations (355). The average FT-IR spectra within the fingerprint range (720–1770 cm⁻¹) revealed amide I and amide II vibrations from peptide groups in proteins across all hydrogel and animal tissue samples. The FT-IR data indicated increased peak intensities in hydrogel samples compared to rat tail collagen, suggesting strong intermolecular interactions between sodium alginate (SA) and GelMA chains. Furthermore, higher peak intensities were observed in hydrogels with higher concentrations compared to those with lower concentrations.

For animal tissue samples, spectral differences were evident, particularly in the broadening of amide I and amide II bands. The amide I band in sheep gingival tissue, specifically attached gingiva, exhibited a peak at 1649.23 ± 2.4 cm⁻¹, indicating high protein content compared to porcine tissue. This discrepancy may be attributed to the limited proliferation and extracellular matrix synthesis by porcine fibroblasts under standard conditions (356). Notably, the observed amide I spectra and biochemical characteristics of sheep gingival tissue aligned

with those previously reported for healthy human oral tissue. Naurecka et al. documented a peak maximum for the C=O stretching band at 1650 cm⁻¹ (357). For amide II, Fukuyama et al. identified the peak maximum around 1550 cm⁻¹ in normal human oral connective tissue (358). In terms of amide II intensity, the mean values for rat tail collagen (incubated overnight or for 2 hours) and hydrogel samples (GelMA-SAH/CaCl₂/UV and GelMA-SAH/UV/CaCl₂) closely resembled those reported by Fukuyama et al. for human gingival tissue (359). These results indicated that these hydrogel samples are more likely to have more bioactivity due to higher protein/peptide functionality compared with other hydrogel samples. making it potentially more favorable for applications such as cell adhesion or biofunctionalization.

Water contact angle measurement is considered a critical physicochemical property for biomaterial surfaces. This property significantly influences protein adsorption and cell behavior. When a hydrogel sample is exposed to body fluids or culture media, protein adsorption plays a crucial role in initial cell attachment (360). Our results revealed the hydrophobic nature of GelMA and GelMA-SA hydrogels when crosslinked using UV or UV/CaCl₂ methods, whereas other samples exhibited hydrophilic characteristics. The mean water contact angles for GelMA, GelMA-SAH/UV, GelMA-SAL/UV, GelMA-SAH/UV/CaCl₂, and GelMA-SAL/UV/CaCl₂ hydrogel samples were comparable to the values reported for human gingival tissue in a study by Van der Mei, White, and Busscher (2004). Their study demonstrated the hydrophobic nature of gingival surfaces in 10 volunteers, with intra-oral water contact angles ranging from 72° to 79° (361). Measurements were conducted at various times, including before and after toothbrushing, and before and after meals. In this study, however, animal gingival samples from sheep and porcine exhibited hydrophilic properties, with water contact angle values of 27.1 ± 1.5° and 29.7 ± 2.1°, respectively. This hydrophilic nature was attributed to the removal of the epithelial layer, leaving only connective tissue for analysis. The hydrophilic property of the oral epithelial layer plays a protective role, which can vary throughout the day due to dietary components and oral hygiene practices. This

protective function is vital in preventing bacterial adhesion and invasion into the underlying connective tissue, helping to mitigate the risk of oral diseases. Our findings highlight the effects of UV crosslinking alone or in combination with ionic crosslinking via CaCl₂ on the surface characteristics of GelMA and GelMA-SA composite hydrogels. These results further emphasize the significance of tailoring biomaterial surface properties to enhance their functional compatibility with biological tissues.(362).

In addition, Differential Scanning Calorimetry (DSC) is considered an appropriate method for assessing protein thermal stability and conformational changes in materials (363). From the thermal analysis, the melting point is identified as the maximum point of the first endothermic peak in the DSC thermograms. The melting points for each hydrogel sample were evaluated, revealing higher values compared to 2-hour and overnight rat tail collagen samples. The melting points of the latter samples were approximately 55 °C, consistent with values reported by González-Masís et al (346). These findings suggest that the intermolecular bonds in rat tail collagen are weaker compared to those in the hydrogel samples. Higher-concentration hydrogels demonstrated higher melting points compared to their lower-concentration counterparts, reflecting stronger intermolecular bonds in the former. Additionally, hydrogels crosslinked by a single method exhibited higher melting points than those subjected to double crosslinking. This difference may result from the double crosslinking's effect on reducing water retention, which alters the hydrogel's hydration behavior and lowers its melting point. Additionally, changes in hydration impact thermal behavior, as water can act as a heat sink or influence the composite's viscoelastic properties (364, 365).

Among the double crosslinking methods, samples crosslinked using the CaCl₂/UV sequence demonstrated greater thermal stability compared to those crosslinked with the UV/CaCl₂ sequence. This indicates that GelMA-SA composite hydrogels crosslinked using the CaCl₂/UV method possess enhanced thermal stability, making them well-suited for applications requiring

structural integrity under conditions of heat or mechanical stress. These findings underscore the significant impact of crosslinking sequence on the thermal properties of GelMA-SA composites.

In animal gingival tissue samples, the melting point values were higher than those of hydrogel samples. In addition, in animal gingival tissue samples, the melting points of gingival and palatal tissues were notably higher than those of alveolar mucosal tissues. These differences in thermal properties across oral mucosal regions can be attributed to variations in connective tissue composition, specifically higher levels of carbohydrates, collagens, and glycosaminoglycans (366). The elevated melting points observed in gingival connective tissues confirm a greater abundance of these molecules compared to alveolar mucosa. Furthermore, porcine samples generally exhibited higher melting points than sheep tissue samples, with the exception of buccal attached gingival tissue, where sheep samples showed a higher melting point. These results suggest that the protein molecules in porcine oral connective tissues exhibit greater thermal stability compared to those in sheep oral tissues.

In this study, rheological properties had been evaluated as an additional investigation to prove the effects of concentration of alginate on mechanical properties of GelMA-SA composite. These values of hydrogel samples increased as the alginate concentration was increased. However, the single crosslinking (CaCl₂ or UV) of GelMA-SA composite samples did not cause further increases in gel viscosity compared to the crosslinked GelMA, SAH and SAL samples indicating the role of these crosslinking methods on GelMA-SA composite samples network structure. Furthermore, the double crosslinking (CaCl₂/UV or UV/CaCl₂) of GelMA-SA composite samples led to further increases in viscosity compared to the single crosslinking method. These findings underscore the role of double crosslinking in forming a stronger and more rigid hydrogel network structure. The single crosslinking method may allow for greater water retention within the internal hydrogel network, whereas

the double crosslinking process likely compacts the hydrogel network, reducing water retention and enhancing mechanical properties (364, 365).

The viscosity values of GelMA-SAH/CaCl₂/UV, GelMA-SAL/CaCl₂/UV, and GelMA-SAH/UV/CaCl₂ were higher compared to those of GelMA-SAL/UV/CaCl₂. Additionally, the viscosity values of both animal tissue samples were higher compared to the GelMA-SA composites. This can be attributed to the fact that the examined animal tissue samples were exclusively obtained from the palatal region. It is important to note that this test requires a sample with a diameter of 50 mm. Due to this requirement, it was not feasible to include gingival tissue from different regions as part of the study samples.

The rheological data for the hydrogels underscore the significance of fabricating GelMA-SA composites with double crosslinking, which may provide a suitable substrate for constructing a 3D gingival model. On the other hand, the mechanical properties, represented by the mean elastic modulus values of animal gingival (labial, buccal, and lingual), alveolar mucosal (labial and buccal), and palatal tissues in sheep and porcine models, were found to align closely with previously reported results from early studies on the viscoelastic properties of oral mucosa. Experimental data revealed a wide range of possible elastic moduli, spanning from 0.06 to 8.89 MPa (367-369). In contrast, a study by Kydd and Mandley in 1967 reported elastic moduli values for human gingival tissue ranging from 0.91 to 11.12 MPa (370). Additionally, two more values (10 MPa (371) and 5 MPa (372)) were first documented in non-English publications. For the hydrogel samples, the mean elastic modulus values increased with higher concentrations of sodium alginate (SA) in the GelMA-SA composite formulations. Specifically, the elastic modulus values were 0.03 ± 0.01 MPa for GelMA-SAH/CaCl₂/UV, 0.01 ± 0.004 MPa for GelMA-SAL/CaCl₂/UV, 0.06 ± 0.01 MPa for GelMA-SAH/UV/CaCl₂, and 0.03 ± 0.01 MPa for GelMA-SAL/UV/CaCl₂ samples. These results were comparable to the elastic modulus values observed in buccal and lingual gingiva, alveolar mucosa, and palatal tissues of sheep. Similarly, the values also closely

matched those of alveolar mucosa and palatal tissues in porcine models. The observed variations in Young's modulus among the oral tissue samples reflect differences in their structural and functional roles. The significantly higher values recorded for labial gingival tissue, particularly in animal samples, indicate a stiffer, more rigid structure compared with other oral tissues. This increased stiffness is likely associated with the higher collagen content, organised fibre alignment, and reduced water content characteristic of keratinised gingiva, which provide greater resistance to deformation under mechanical loading (366). Notably, the mean values of elastic modulus of the GelMA-SAH/UV/CaCl₂ hydrogel sample approximated the values reported for both human and animal gingival and mucosal tissues. This finding highlights the significant influence of SA concentration and the sequencing of crosslinking (UV/CaCl₂) on improving the viscoelastic properties of the fabricated GelMA-SA composites. Similarly, among the hydrogel formulations, the SAH exhibited higher Young's modulus values, suggesting a denser network structure and stronger crosslinking efficiency. In the case of GelMA–SA composite hydrogels, the double UV/CaCl₂ crosslinking method enhanced stiffness compared with the CaCl₂/UV sequence, possibly due to more uniform ionic and covalent crosslink formation. Conversely, the lower modulus observed in UV-only crosslinked samples compared with CaCl₂ only crosslinking highlights the greater contribution of ionic interactions to the mechanical strength of these composites. Overall, these findings demonstrate that both the intrinsic composition of oral tissues and the crosslinking strategy in hydrogels play critical roles in determining mechanical properties relevant to their functional performance in tissue engineering applications.

The biodegradability of the hydrogel samples was evaluated to confirm the results. GelMA is a well known biodegradable hydrogel (360). The findings revealed that the degradation rates of both GelMA-SAH/CaCl₂/UV and GelMA-SAL/CaCl₂/UV hydrogel samples were significantly higher after day 7 compared to GelMA-SAH/UV/CaCl₂ and GelMA-SAL/UV/CaCl₂. This observation indicated a reduction in the mechanical properties of the former

samples beyond day 7. In contrast, GelMA-SAH/UV/CaCl₂ and GelMA-SAL/UV/CaCl₂ hydrogel samples maintained their integrity until the end of the experiment, i.e., day 14.

The biodegradability results further underscored the impact of crosslinking sequence on the stability of the fabricated composite hydrogels. Specifically, the UV/CaCl₂ crosslinking method enhanced the stability of the GeIMA-SA composite hydrogel and enabled its fabrication into predesigned shapes. This is crucial in tissue engineering, where achieving a balance between biomaterial degradation and tissue regeneration is a key challenge.

Importantly, the degradability of the biomaterial can be tailored to match the remodeling rate of the target tissue. These results demonstrated that the GelMA-SA composite exhibits tunable degradation properties, making it suitable for applications tailored to specific tissues and their required degradation periods.

The results of this study highlight the influence of different hydrogel compositions and crosslinking methods on the metabolic activity and cytotoxicity of HGF cells in 3D cultures. Metabolic activity assessments showed that HGF cells exhibited increased activity over the first few days of culture, particularly in SAH and SAL hydrogels, indicating that these formulations provided a more favourable microenvironment for cell growth. The higher metabolic activity observed in GelMA-SAH/CaCl₂ and GelMA-SAL/CaCl₂ on day 7 suggests that CaCl₂ crosslinking may enhance cell viability and proliferation compared to UV crosslinking (374) . However, by day 14, metabolic activity declined in all hydrogel samples, which may be attributed to either nutrient depletion, accumulation of waste products, or changes in hydrogel properties affecting cellular behavior .

Cytotoxicity results revealed an increasing trend in LDH release over time, with all hydrogel samples showing levels above 30% starting from day 1. While SAH and SAL initially exhibited lower cytotoxicity, their values increased with prolonged culture duration. This suggests that despite their biocompatibility in

the early phase, hydrogel degradation, crosslinking stability, or accumulated cellular stress might contribute to increased cytotoxicity over time. Notably, GelMA-SA composites crosslinked with UV demonstrated the lowest metabolic activity and relatively higher cytotoxicity, indicating that the UV crosslinking method may adversely affect cell viability, possibly due to residual photoinitiator toxicity or inadequate crosslinking efficiency (216).

Confocal imaging provided further confirmation of these findings, as live/dead staining images showed enhanced cell viability in GelMA-SAH/CaCl₂ and GelMA-SAL/CaCl₂ by day 7, supporting the conclusion that CaCl₂ crosslinking offers a more cell-friendly environment than UV crosslinking. However, despite initial improvements in cell viability, the reduction observed on day 14 suggests that long-term cell survival may require modifications to the hydrogel composition, crosslinking strategy, or culture conditions (375).

The findings suggest that GelMA-SA hydrogels crosslinked with CaCl₂ provide better cell viability and metabolic activity compared to UV-crosslinked samples. However, despite the initial success, a decline in cell viability and metabolic activity by day 14 indicates the need for improved structural stability and long-term biocompatibility.

Further work was needed to investigate whether GelMA-SA double crosslinked hydrogels provide a more stable microenvironment, allowing for prolonged cell viability, improved nutrient diffusion, and controlled degradation rates, making them more suitable for tissue engineering applications.

CHAPTER 7

7. EVALUATION OF STERILIZATION METHODS AND CROSSLINKING STRATEGIES ON THE HYDROGELS MECHANICAL AND BIOLOGICAL PROPERTIES TO MIMIC NATIVE HUMAN GINGIVAL EXTRACELLULAR MATRIX

7.1. Introduction

Ensuring the sterility of hydrogel biomaterials is a fundamental requirement for their application in various experimental and biomedical studies. Contamination by microorganisms can compromise experimental outcomes, increase the risk of infection, and negatively impact the biocompatibility of hydrogels. Therefore, selecting an appropriate sterilization method is essential to maintain the integrity, safety, and effectiveness of hydrogel-based materials used in tissue engineering, drug delivery, and other biomedical applications (208).

Several sterilization techniques are commonly employed to achieve sterility in hydrogel biomaterials, including autoclaving, ethylene oxide gas (EOg) treatment (209, 210), gamma irradiation (211), ethanol treatment (212), and filtration (213). Each method presents unique advantages and limitations that influence the physicochemical properties of the hydrogel, including mechanical strength, structural integrity, biocompatibility, and cellular interactions.

Autoclaving: This method involves exposure to high pressure saturated steam at elevated temperatures (typically 121 °C for 15–30 minutes). Although highly effective in eliminating microbial contaminants, autoclaving can lead to hydrogel degradation or changes in mechanical properties, such as reduced stiffness and altered crosslinking density. These effects may compromise the functionality of certain hydrogel formulations, particularly those sensitive to thermal and moisture-related degradation (214).

Ethylene Oxide Gas (EOg) Sterilization: This technique utilizes a low-temperature gaseous sterilant that effectively eliminates bacteria, fungi, and viruses without causing significant thermal damage. However, EOg sterilization has been

associated with residual toxicity concerns, as residual gas and its byproducts may remain within the hydrogel matrix, potentially affecting biocompatibility and cellular responses (209, 210). Additionally, EOg exposure can alter hydrogel swelling properties and mechanical characteristics, potentially reducing stiffness.

Gamma Irradiation: A commonly used method for hydrogel sterilization, gamma irradiation involves exposing materials to high-energy ionizing radiation (typically from cobalt-60 or cesium-137 sources). This process effectively destroys microbial contaminants while inducing free radical formation, which may modify the hydrogel's structural integrity. Unlike autoclaving and EOg treatment, gamma irradiation can increase hydrogel stiffness due to radiation-induced crosslinking, which may alter its viscoelastic properties and biological interactions (214). Ethanol Treatment: This chemical sterilization method involves immersing hydrogels in ethanol solutions (typically 70%–100%) to inactivate microbial contaminants. Ethanol treatment is a relatively simple and cost-effective sterilization method; however, it may cause dehydration, shrinkage, or excessive swelling in certain hydrogel formulations, leading to structural instability and variations in porosity that affect cell adhesion and migration (112).

Filtration: This technique relies on the passage of hydrogel precursors or solutions through sterile membrane filters (typically 0.22 µm pore size) to remove microbial contaminants. Filtration is particularly suitable for liquid or pre-polymerized hydrogel formulations but is not effective for sterilizing pre-formed solid hydrogels. While this method does not induce thermal or chemical modifications, it may be less effective against viruses or endotoxins (213).

Each sterilization method can influence hydrogel performance, including its mechanical properties, degradation rate, and ability to support cellular functions such as adhesion, proliferation, and differentiation. The choice of sterilization technique should be carefully evaluated based on the specific hydrogel formulation, intended application, and required biological and physicochemical properties (215, 216).

Building on the findings from the previous chapter, where the individual hydrogels neither GelMA-SA composite hydrogel samples were evaluated after single crosslinkling technique, and found to have mechanical and biocompatible properties were suboptimal for supporting a 3D gingival tissue model. Therefore, the GelMA-

SA composite hydrogel samples with double crosslinking technique were selected for this study. These hydrogel samples were chosen based on their relatively favorable characteristics such as biocompatible properties, mechanical strength, handling properties, and potential for chemical modification despite their initial mechanical limitations. It was hypothesized that blending these two hydrogel samples, GelMA and SA, with double crosslinking technique could yield a composite hydrogel with synergistic properties, potentially overcoming the individual shortcomings.

In this chapter, two crosslinking strategies have been performed. These strategies were included double crosslinking applied in different sequences, to enhance the structural integrity of the mixed hydrogel samples. Additionally, the impact of two commonly used sterilization techniques (filtration and ethanol), on samples properties was assessed to identify a suitable approach for future clinical or in vitro applications. This approach reflected a systematic attempt to optimize the hydrogel system for 3D gingival tissue engineering applications.

Therefore, the aims of this chapter are :-

- 1.Investigate the effects of two different sterilization methods (filtration and ethanol) on the properties of GelMA-SA composite hydrogels. Following sterilization, each hydrogel type is crosslinked using two different sequences: CaCl₂/UV and UV/CaCl₂.
- 2.Evaluate and compare the sterilization efficacy and its impact on the biochemical, mechanical, and biocompatibility properties of the GelMA-SA composite hydrogels.
- 3.Explore how the double crosslinking sequences influence the structural and functional characteristics of the GelMA-SA composite hydrogels.
- 4. Assess the potential of GelMA-SA composite hydrogels as a novel carrier for oral epithelial cell seeding.
- 5.Construct 3D gingival model using novel GelMA-SA composite hydrogel biomaterial as a substrate. In addition to construct 3D gingival models using rat tail collagen, and GelMA as a substrates.
- 6. Characterising the biocompatibility of 3D gingival models constructed using GelMA-SA composite compared with constructed models using rat tail collagen or GelMA hydrogel biomaterials.

These insights will help optimize their application in seeding human gingival cells and constructing 3D cell culture models for periodontal research.

7.2. Materials and methods

7.2.1. Preparation of GelMA hydrogel samples

The materials utilized for preparation of GelMA hydrogel sample are detailed in Chapter 2, Section 2.2.2. In brief GelMAH which is with high concentration (10%), were prepared, by dissolving of GelMA-UCL lyophilized in deionized BPS and mixing by magnetic stirring for up to 30 minutes at ~ 40 °C. Then followed by adding 0.3% w/v Photo initiator (PI) of lithium phenyl-2,4,6-trimethylbenzoylphosphinate (LAP; >95%, Sigma-Aldrich, UK). Then the solution was continued for mixing by magnetic stirring for up to 30 minutes at ~ 40 °C.

7.2.2. Preparation of sterilized GelMA-SA composite hydrogel samples

The sterilization methods for samples were detailed in Chapter 2, Section 2.2.3. In this study, two different sterilization methods were employed for the hydrogel samples: filter and ethanol sterilization methods. It is worth mentioning that the sterilization of samples should be performed using light-sensitive containers and inside the laminar flow cabinet. Additionally, after sterilization, the lid of each container was tightly sealed and only opened inside the cabinet to prevent contamination.

6.2.2.1. Filter method

GelMA, SAH, and SAL hydrogel solutions, were sterilized using 0.22 μ m pore-size syringe filters (Fisher Scientific UK Ltd., Loughborough, UK) inside a laminar flow cabinet. Each filtered hydrogel solutions were placed in sterilized tubes but stored at 4 °C until further use.

This method was also used to sterilized Calcium chloride (CaCl₂), and 70% ethanol solutions. CaCl₂ solution is used for crosslinking SA, and GelMA-SA composite hydrogel samples. While 70% ethanol solution is used for sterilization of the hydrogel samples. Inside a laminar flow cabinet, these two solutions, CaCl₂, and 70% ethanol were sterilized using syringe filters. Each filtered solutions were also placed in

sterilized tubes and stored at room temperature until used, however, CaCl₂ solution should be warmed at ~37 °C before used.

GelMA-SAH and GelMA-SAL hydrogels were prepared by mixing equal amounts of prepared GelMA and prepared SAH, or SAL, hydrogel solutions to form GelMA-SAH, and GelMA-SAL hydrogel solutions, respectively. This is followed by mixing by magnetic stirring for up to 30 minutes at 40 °C.

The prepared sterilized GelMA-SAH and GelMA-SAL hydrogel solutions were placed in sterilized tubes and stored at 4 °C until further use. These samples should be warmed at ~ 37 °C. before used.

7.2.2.2. Ethanol method

samples.

Sterilized 70% ethanol is used to sterilized GelMA-SA composite hydrogel. In contrast to filter sterilization method, ethanol method is performed after mixing GelMA with SAH, and GelMA with SAL hydrogel solutions. This is performed inside a laminar flow cabinet. GelMA-SA composite hydrogels were prepared by mixing equal amounts of prepared GelMA and prepared SAH, or SAL, hydrogel solutions to form GelMA-SAH, and GelMA-SAL hydrogel solutions, respectively. This is followed by mixing by magnetic stirring for up to 30 minutes at 40 °C. At room temperature within a laminar flow cabinet GelMA-SAH and GelMA-SAL hydrogel solutions were immersed in sterilized 70% ethanol by adding twice the volume of the hydrogel sample. After 20 minutes, the excess ethanol was removed, and the hydrogels were left for 10 minutes to allow the residual ethanol to evaporate. The prepared sterilized GelMA-SAH and GelMA-SAL hydrogel solutions were placed in sterilized tubes and stored at 4 °C until further use. These samples should be warmed before used. In this study, GelMA-SA composite hydrogel solutions sterilized using the filtration

7.2.2.3. Hydrogel crosslinking procedures

Prior to distribution into the well plate inserts for crosslinking, the sample was first warmed and thoroughly mixed using a magnetic stirrer to ensure homogeneity. Following this step, the samples were distributed into the inserts, and the

method were referred to as FM. GelMA-SA hydrogel samples. Conversely, those

sterilized using the ethanol method were referred to as E.GelMA-SA hydrogel

crosslinking procedure was then carried out. Crosslinking of sterile GelMA-SA composite hydrogel samples was written in details in Chapter 2, Section 2.2.4.

In this study was double technique with two different sequencing, either CaCl2/UV, or UV/CaCl2. CaCl2/UV procedure is performed by start crosslinking using CaCl2 crosslinking procedures for the samples, and that followed by UV crosslinking procedure. This procedure was performed by adding a sterile CaCl2 with double volume of each sample for 5-7 mins, then discard the excess (233). CaCl2 crosslinking procedures of samples were performed at room temperature and inside laminar flow cabinet. The second UV crosslinking procedure is followed that. UV crosslinking procedure performed using ultraviolet light (UV), for 60 s (UV;XYZPrinting UV chamber, Model 3UD10, Taiwan, UV LED (λ 375–405 nm, 16 W)) (213). This process was conducted inside the UV chamber of the device. To ensure proper conditions, the sample container lid was securely fastened.

The other method is UV/CaCl₂. This performed was performed by starting with UV crosslinking procedure. This step was performed inside the UV chamber of UV device and ensure the lid of each sample container was securely closed. Then followed by the second crosslinking procedure which is CaCl₂ crosslinking procedure.

In this study, GelMA-SA composite hydrogel solutions crosslinked using the CaCl₂ followed by UV method were referred to as GelMA-SA/CaCl₂/UV hydrogel samples. Conversely, those crosslinked using the UV followed by CaCl₂ method were referred to as GelMA-SA/UV/CaCl₂ hydrogel samples.

7.2.4. Structural characterisations

Structural characterisations were performed by investigated macrographic and micrographic analysis for sample surfaces, FTIR, WCA, and DSC. In addition, other characterization methods such as mechanical analysis, rheological, degradation, and biocompatibility analyses, were also performed as described in Section 2.2.6.

7.2.5. Human gingival cells expanding and seeding in samples

In this study, HGF and HGE cells were expanded and used in experiments, and more details regarding cell expansion and seeding in hydrogel samples were found in Chapter 2, Section 2.2.6.9. In brief, the expanded HGF or HGE cells were suspended at a density of 2x10⁴, and 4x10⁴ cells/ml, respectively, and thoroughly mixed with sterilized hydrogel samples to generate cell populated hydrogels.

7.2.6. Engineered 3D gingival tissue (3DGT)

The engineering of 3D gingival model details in Chapter 2, Section 2.2.7. The method used to develop the 3D gingival tissue (3DGT) model is a modification of previously reported techniques (188), with modification. To prepare the cell-populated hydrogel samples, expanded HGF cells were mixed at a density of 2x10⁴ cells/ml, with sterile hydrogel samples. The mixture was then distributed into 96-well plates and crosslinked. Following crosslinking, the prepared HGF medium was added, and the samples were incubated at 37°C with 5% CO₂. For the R collagen hydrogel sample, the cell mixture was prepared in a cold environment (4 °C) before distribution into the 96-well plate. These samples were incubated at 37°C with 5% CO₂ for 15 minutes, after which the prepared HGF medium was added. Incubation continued at 37°C with 5% CO₂ for 3 days. After 3 days, the medium was removed, and the hydrogel samples were seeded with human gingival epithelial (HGE) cells at a density of 4x10⁴ cells/ml. The HGE cells were allowed to attach for 14 days in a mixture of HGF medium and HGE medium at different ratios: 100:0, 75:25, 50:50, 25:75, and 0:100.

To lift the engineered 3DGT to an air-liquid interface (ALI), 3DGT models were constructed inside 13-mm diameter Millicell cell culture inserts (Millipore) placed in 12-well plates (Sigma). After seeding with HGFs as described previously, 0.5 ml of hydrogel was added to each insert and crosslinked. Following crosslinking, 1 ml of fibroblast growth medium was added inside each insert, and another 1 ml was added outside the insert. The samples were incubated at 37 °C in a humidified atmosphere with 5% CO₂ for 3 days.

After 3 days, the medium was removed, and the hydrogel samples were seeded with HGE cells, which were allowed to attach for 3 days in a mixture of HGF and HGE media. The samples remained submerged and were incubated at 37 °C in a humidified atmosphere with 5% CO2. After 4 days, the 3DGT models were lifted to an ALI using transwell inserts in a 6-well plate and cultured in differentiation medium.

3DGT model medium was consisting of DMEM low glucose/Ham's F12 (3/1), supplemented with 5 μ g/mL insulin; 0.4 μ g/mL hydrocortisone; 2 × 10-11M 3,3′, 5-triiodo-L-thyronine (T3); 1.8 × 10-4M adenine; 5 μ g/mL transferrin;10-10M cholera toxin; 2mM L-glutamine; 5%(v/v) FBS; 100 μ g/mL penicillin and 100 μ g/mL streptomycin. Cultures were maintained in air-liquid interface for 14 days with the medium changed every 2 days.

7.2.7. Metabolic and cytotoxic activities of cells evaluation

The metabolic activity values of the HGF or HGE cells were evaluated using the CellTiter®® 96 Aqueous One Solution Cell Proliferation assay kit, according to the manufacturer's protocol. For cytotoxicity assay, lactate dehydrogenase (LDH) release from the cells was quantified. LDH release assay performed using the CytoTox 96®® Non-radioactive Cytotoxicity Assay kit. More details were found in Chapter 2, Section 2.2.8. In summary, following 1, 3, 7, and 14-days of incubation, the supernatant solution was transferred to a new plate and read at 490 nm using a Tecan Infinite M200 microplate reader (Tecan, Switzerland).

Moreover, the biocompatibility of the samples was determined using Live/DeadTM staining. A LIVE/DEAD™ imaging kit was used. Based on the protocol of manufacturer's instructions, The prepared stain of live/dead reagent was added to samples in a dark environment.. After incubation, Imaging was performed on confocal laser scanning microscopy (BioRad Radiance2100, Zeiss, UK). The images were captured using digital capture software. These images were analysed to visualise live and dead cells within the samples using ImageJ Fiji software (https://downloads.micron.ox.ac.uk/fiji update/mirrors/fiji-latest/fiji-nojre.zip).

However, for the 3DGT model, the evaluation of cytotoxicity and biocompatibility of the samples were performed using, LDH, and the Live/DeadTM staining, respectively.

7.2.8. Histological investigation

For histological examination, samples were fixed in 10% v/v buffered formalin, then washed with PBS and stored in it until further processing.

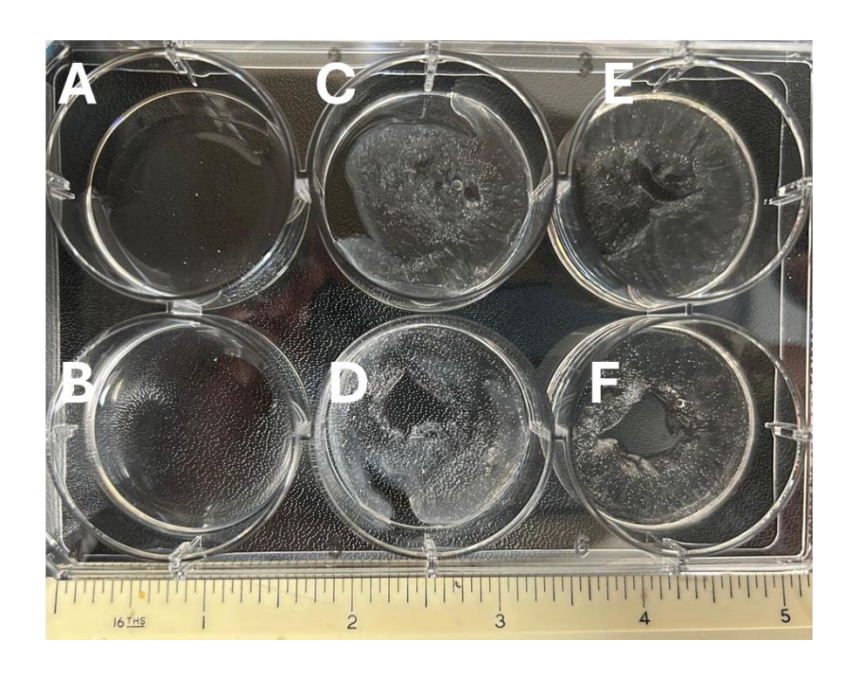
Tissue processing was performed using the Leica ASP300 automated tissue processor, followed by embedding in paraffin wax. Sections of 5µm thickness were cut from the paraffin blocks using the Leica RM2235 microtome. The samples were stained with hematoxylin and eosin (H&E) using the Leica ST5020 Autostainer. Images were captured with a camera connected to a computer and organized using (NDP.view2 image viewing software). Each sample was examined by analyzing images from three to five different fields.

7.3. Results

7.3.1. Material mechanical characterisation

7.3.1.1. Surfaces morphology of samples in photographic images

Figure 7.1, showed photographic images for hydrogel samples with high and low concentrations were subjected ethanol sterilization method (7.1). The sterilization methods were followed by different double crosslinking sequences. The first double crosslinking technique was CaCl₂/UV (Fig. 7.1I & J). The second double crosslinking technique was UV/CaCl₂ (Fig. 7.1K & L).



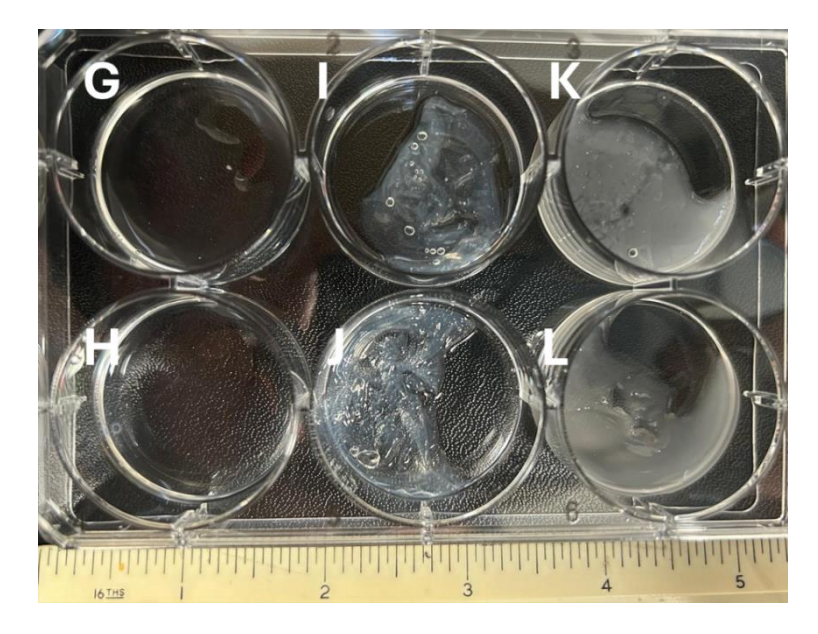


Figure 7.1. Images (A-F) showing GelMA-SAH and GelMA-SAL hydrogel samples in a 6-well plate, prepared and aliquoted with 1 ml per insert, before and after sterilization using ethanol method. This was performed at room temperature (~20°C), (A) and (B) show GelMA-SAH and GelMA-SAL hydrogel samples, respectively, before sterilization. (C&E) and (D&F) show GelMA-SAH and GelMA-SAL hydrogel samples, respectively after sterilized by ethanol method. Images (G-L) showing the same samples before and after sterilized by ethanol method, and before and after different crosslinking methods. (G &H), show GelMA-SAH and GelMA-SAL hydrogel samples, respectively, before sterilization.(I&J) after crosslinking performed using a CaCl₂/UV procedure. (K&L) after crosslinking performed using a UV/CaCl₂ procedure.

The ethanol sterilization method appeared to cause noticeable changes in the hydrogel samples, in compared with filtration sterilization method. Specifically, the ethanol-treated samples exhibited shrinkage, irregular surface morphology, and increased opacity. These alterations could potentially be attributed to the cooling effect of ethanol during the sterilization process, which might have induced structural changes in the hydrogel network. Further investigation is needed to confirm the exact cause of these modifications and their impact on the hydrogel's properties.

7.3.1.2. Surfaces morphology of samples on SEM images

SEM images revealed that pore sizes were larger in low-concentration hydrogel samples compared to high-concentration ones. Regarding sterilization methods, samples treated with the ethanol sterilization (Fig.7.2.) method exhibited smaller pore sizes compared to those sterilized using the filtration method (Fig.7.3). The pore sizes of the hydrogel samples fell within 30–80 µm rang. This range is comparable to reported pore dimensions of human gingival connective tissue, where

interfibrous spaces typically fall between $20-100 \mu m$, suggesting that the fabricated hydrogels possess pore structures within a physiologically relevant scale for supporting cellular infiltration and nutrient diffusion (354).

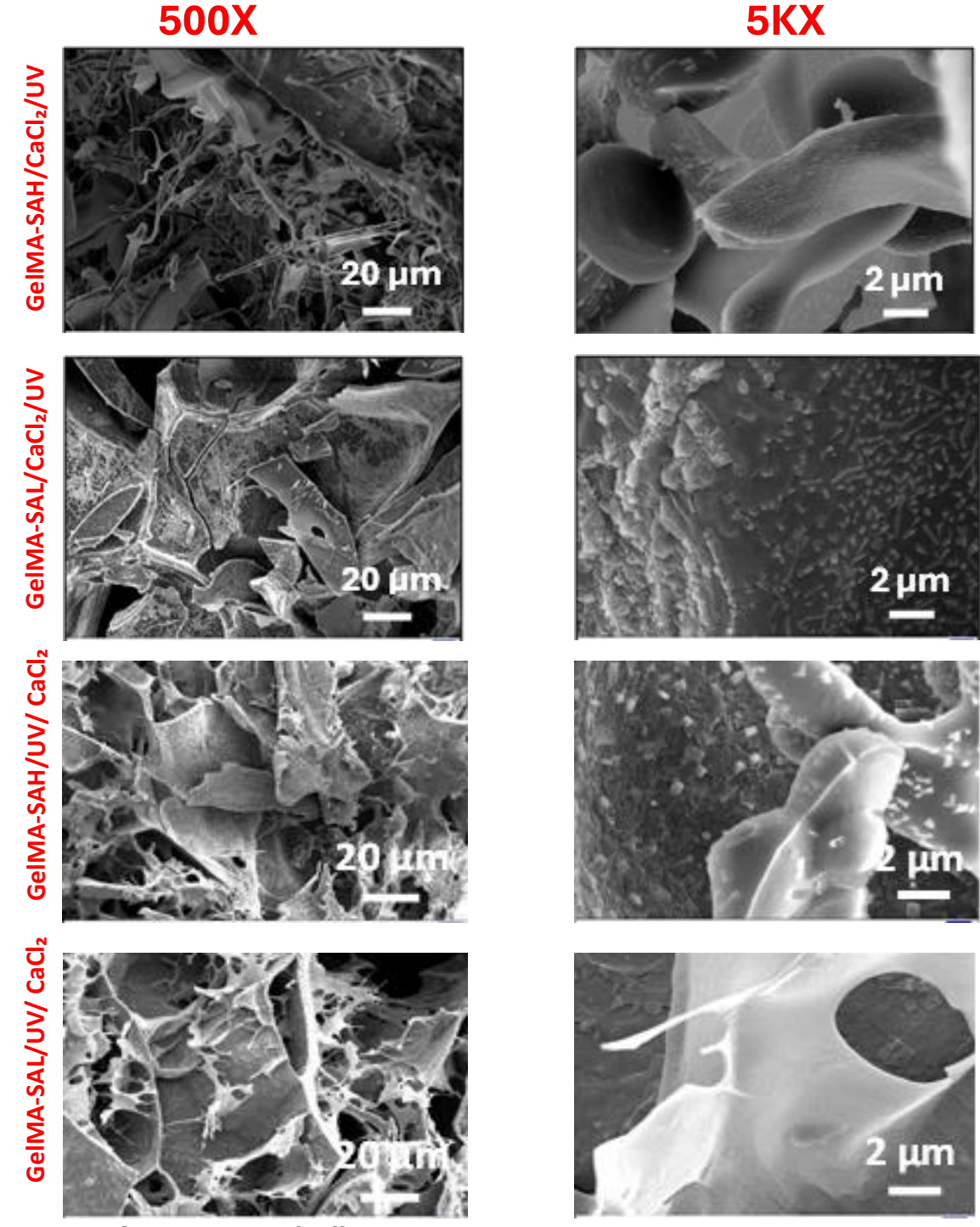


Figure 7.2. SEM images of different hydrogel samples subjected to sterilization using filtration method. Hydrogel samples at a magnification of 200X with a scale bar of 50 μ m, 500X with a scale bar of 20 μ m, 2KX with a scale bar of 5 μ m, and 5KX with a scale bar of 2 μ m,, showing samples,GelMA-SAH/CaCl₂/UV, GelMA-SAL/CaCl₂/UV, GelMA-SAH/UV/CaCl₂, and GelMA-SAL/UV/CaCl₂.

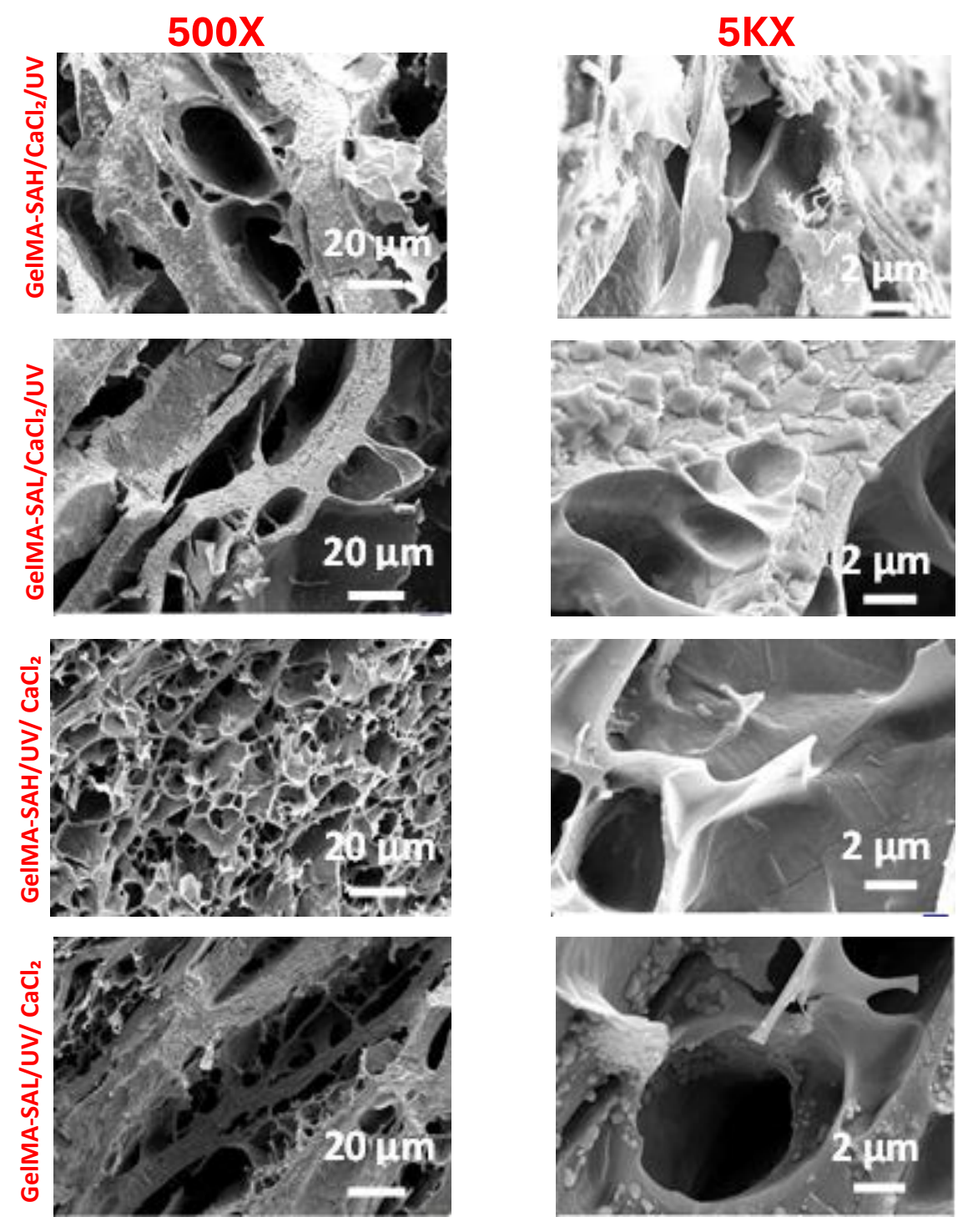


Figure 7.3. SEM images of different hydrogel samples subjected to sterilization using ethanol method. Hydrogel samples at a magnification of 200X with a scale bar of 50 μ m, 500X with a scale bar of 20 μ m, 2KX with a scale bar of 5 μ m, and 5KX with a scale bar of 2 μ m, showing samples,GelMA-SAH/CaCl₂/UV, GelMA-SAL/CaCl₂/UV, GelMA-SAH/UV/CaCl₂, and GelMA-SAL/UV/CaCl₂.

7.3.1.3. FT-IR characteristics

Figure. 7.4 demonstrated biochemical properties were analysed using FT-IR. One of the primary advantages of FTIR imaging is its ability to provide a biochemical fingerprint, offering detailed information on the content, structure, and chemical modifications of key biomolecules in the sample (355). The Amide I and II bands are major components of the protein infrared spectrum, corresponding to C=O stretching, N-H bending, and C-N stretching vibrations. The average FTIR spectra in the fingerprint range (720–1770 cm⁻¹) revealed amide I (C=O stretching) and amide II vibrations from all hydrogel samples. High-concentration hydrogels exhibited increased peak intensities compared to low-concentration ones. Furthermore, hydrogels sterilized using the filtration method demonstrated higher peak intensities compared to those sterilized with ethanol.

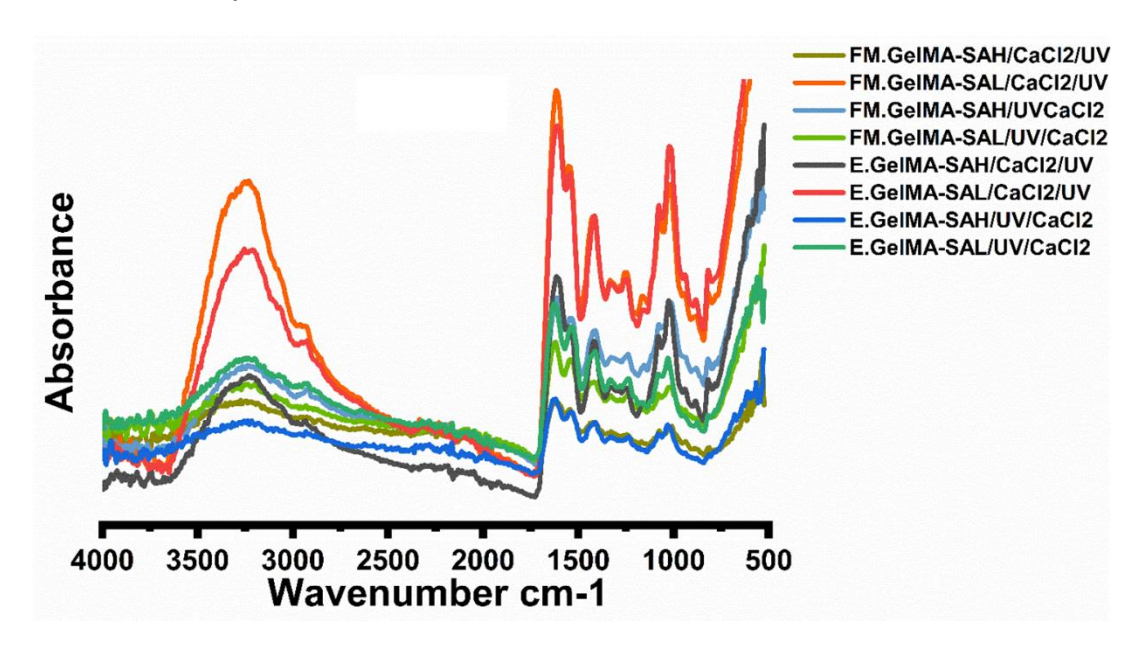


Figure 7.4. FT-IR spectra summarising the chemical bonding structure over a range of 4000–500 cm⁻¹ with a resolution of 4 cm⁻¹ at 37 °C. Samples are: FM.GelMA-SAH/CaCl₂/UV, FM.GelMA-SAH/UV/CaCl₂, FM.GelMA-SAL/CaCl₂/UV, FM.GelMA-SAL/UV/CaCl₂, E.GelMA-SAH/CaCl₂/UV, E.GelMA-SAL/CaCl₂/UV, E.GelMA-SAH/UV/CaCl₂, E.GelMA-SAL/UV/CaCl₂, hydrogel samples. FM and E refer to filtration and ethanol sterilization methods, respectively.

Amide II intensity mean values for hydrogel samples sterilized via filtration were as follows: FM.GelMA-SAH/CaCl₂/UV (1558.1 \pm 0.24), FM.GelMA-SAL/CaCl₂/UV (1555.73 \pm 3.09), FM.GelMA-SAH/UV/CaCl₂ (1550.01 \pm 0.58), and FM.GelMA-SAL/UV/CaCl₂ (1547.33 \pm 1.36). For ethanol-sterilized hydrogel samples, values were: E.GelMA-SAH/CaCl₂/UV (1552.35 \pm 1.91), E.GelMA-SAL/CaCl₂/UV (1549.4 \pm 5.66), E.GelMA-SAH/UV/CaCl₂ (1545.37 \pm 0.32), and E.GelMA-SAL/UV/CaCl₂ (1540.37 \pm 0.32).

Moreover, when compared the results to reported FT-IR spectra of native human oral tissue, the hydrogel samples exhibited amide I and II bands in a similar wavenumber range (approximately 1650 cm⁻¹ for C=O stretching and 1550 cm⁻¹ for N-H bending/C-N stretching) (357, 358), reflecting the proteinaceous nature of the matrices

7.3.1.4. Hydrophilic/hydrophobic surface properties

Water contact angle measurement is a critical physicochemical property for evaluating the surface characteristics of biomaterials. When a material is exposed to body fluids or culture media, protein adsorption significantly influences initial cell attachment (333). The mean contact angle values for all hydrogel samples are presented in Figure 7.5. The results indicated that GelMA-SAH and GelMA-SAL hydrogels, when crosslinked using UV/CaCl₂ methods with both ethanol and filtration sterilization, exhibited a hydrophobic nature. In contrast, the other hydrogel samples demonstrated a hydrophilic nature. These findings highlight the influence of UV crosslinking followed by ionic crosslinking with CaCl₂ on the surface properties of GelMA-SA composite hydrogels.

Comparable results were observed in a study by Van der Mei, White, and Busscher (2004), which reported the hydrophobic nature of gingival surfaces among 10 volunteers. Intra-oral water contact angles were measured under various conditions, including in the morning before brushing, immediately after brushing, and before and after lunch. The study found that gingival surfaces were hydrophobic, with water contact angles ranging from 72° to 79° (334).

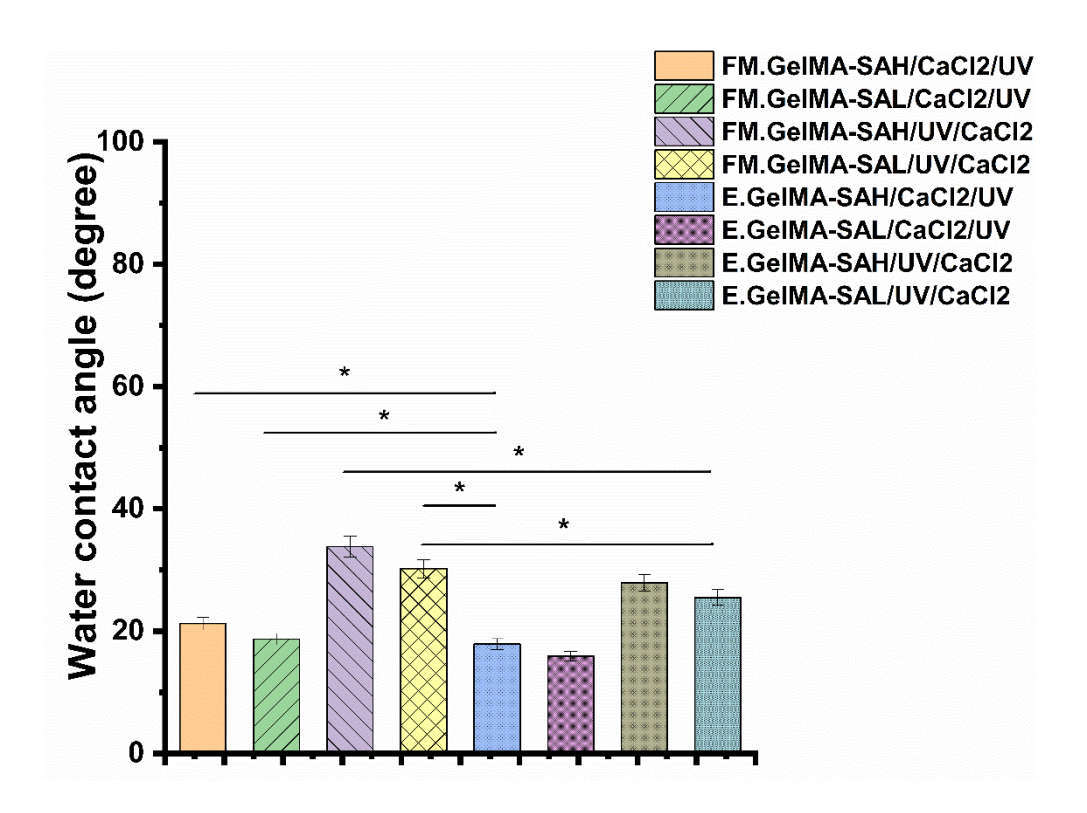


Figure 7.5. WCA measurements of FM.GelMA-SAH/CaCl $_2$ /UV, FM.GelMA-SAL/CaCl $_2$ /UV, FM.GelMA-SAH/UV/CaCl $_2$, FM.GelMA-SAL/UV/CaCl $_2$, E.GelMA-SAH/CaCl $_2$ /UV, E.GelMA-SAL/CaCl $_2$ /UV, E.GelMA-SAH/UV/CaCl $_2$, E.GelMA-SAL/UV/CaCl $_2$, hydrogel samples. FM and E refer to filtration and ethanol sterilization methods, respectively. *p< 0.05.

7.3.1.5. Thermal Properties

For DSC analysis, Figure 7.6 showed the melting point values of investigated hydrogel samples. The melting points of the samples, identified as the maximum point of the first endothermic peak in the DSC thermograms, were evaluated. The melting point values were higher in high-concentration hydrogel samples compared to low-concentration ones. Additionally, the results showed that hydrogels sterilized using the ethanol method exhibited higher melting temperatures than those sterilized with

the filtration method. In the same stream, hydrogel samples crosslinked with CaCl₂/UV showed higher melting point values compared to those crosslinked with UV/CaCl₂.

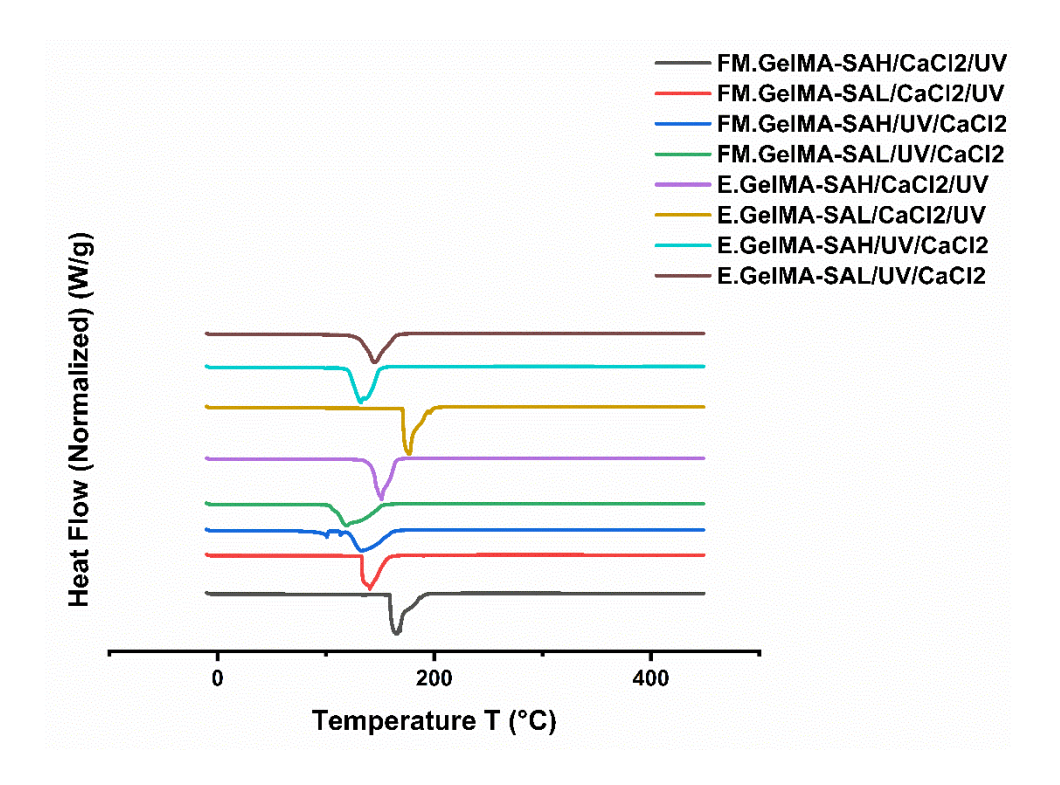


Figure 7.6. DSC thermograms for samples which were examined under a continuous flowrate of nitrogen gas with the following conditions: equilibrate (-10 °C), isothermal (1 min), and ramp (10 °C/min to 450 °C/min). samples are: FM.GelMA-SAH/CaCl₂/UV, FM.GelMA-SAH/UV/CaCl₂, FM.GelMA-SAL/UV/CaCl₂, E.GelMA-SAH/CaCl₂/UV, E.GelMA-SAL/CaCl₂/UV, E.GelMA-SAL/UV/CaCl₂, E.GelMA-SAL/UV/CaCl₂, hydrogel samples. FM and E refer to filtration and ethanol sterilization methods, respectively.

For context, the thermal denaturation temperature of native human gingival tissue has been reported to be approximately 69.8 °C, as determined by DSC analysis of oral mucosa biopsies (395). While the hydrogel melting points are much higher than tissue denaturation.

7.3.1.6. Rheological characteristics

The rheological properties of the hydrogel samples were investigated at a temperature of 37, 20, and 4 °C (Fig.7.7, and 7.8). Viscosities were analysed under varying shear rates, as shown in the rheograms in Figure 7.7. The results revealed that viscosity decreased with increasing shear rate. High-concentration hydrogel samples exhibited higher viscosity values compared to low-concentration samples.

In oscillatory rheology (Fig.7.9), the hydrogels were subjected to either an increasing oscillatory strain (strain sweep) at a constant frequency or a decreasing frequency of oscillation at a constant strain within the linear viscoelastic range (frequency sweep) (Fig. 7.9),. The storage modulus (G'), which measures the energy stored and recovered during deformation, indicates the solid or elastic properties of the hydrogels.

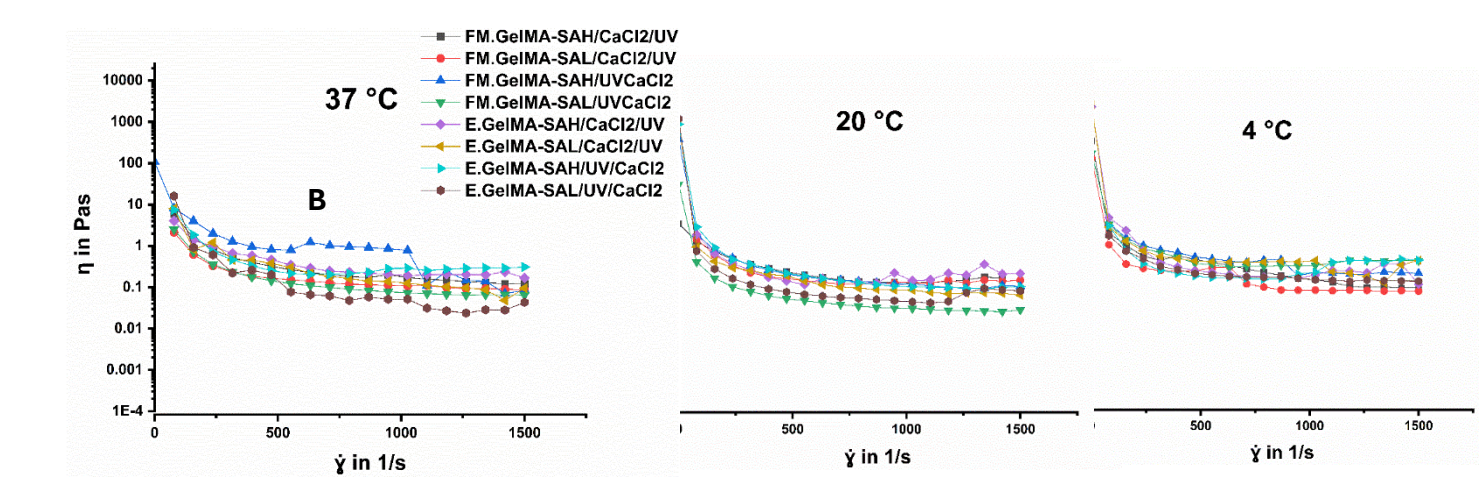


Figure 7.7. Viscosity as a function of shear rate, the rotational tests under destructive shear conditions were performed at shear rates ranging from 0.01 - 1500 s⁻¹. Samples are: FM.GelMA-SAH/CaCl₂/UV, FM.GelMA-SAL/CaCl₂/UV, FM.GelMA-SAH/UV/CaCl₂, E.GelMA-SAH/CaCl₂/UV, E.GelMA-SAL/CaCl₂/UV, E.GelMA-SAL/UV/CaCl₂, E.GelMA-SAL/UV/CaCl₂, hydrogel samples, (A, B, and C) at 37, 20, and 4 °C, respectively. FM and E refer to filtration and ethanol sterilization methods, respectively.

The loss modulus (G"), which measures energy dissipation, reflects liquid-like or viscous behavior. Together, these parameters provide critical insights into the viscoelastic behavior of the hydrogels. All hydrogel samples demonstrated gel-like behavior at three different temperature degrees, 37, 20, and 4 °C, as evidenced by higher G' values compared to G" in both oscillatory and frequency tests (Fig. 7.9 and 7.10). G' values increased as the temperature decreased.

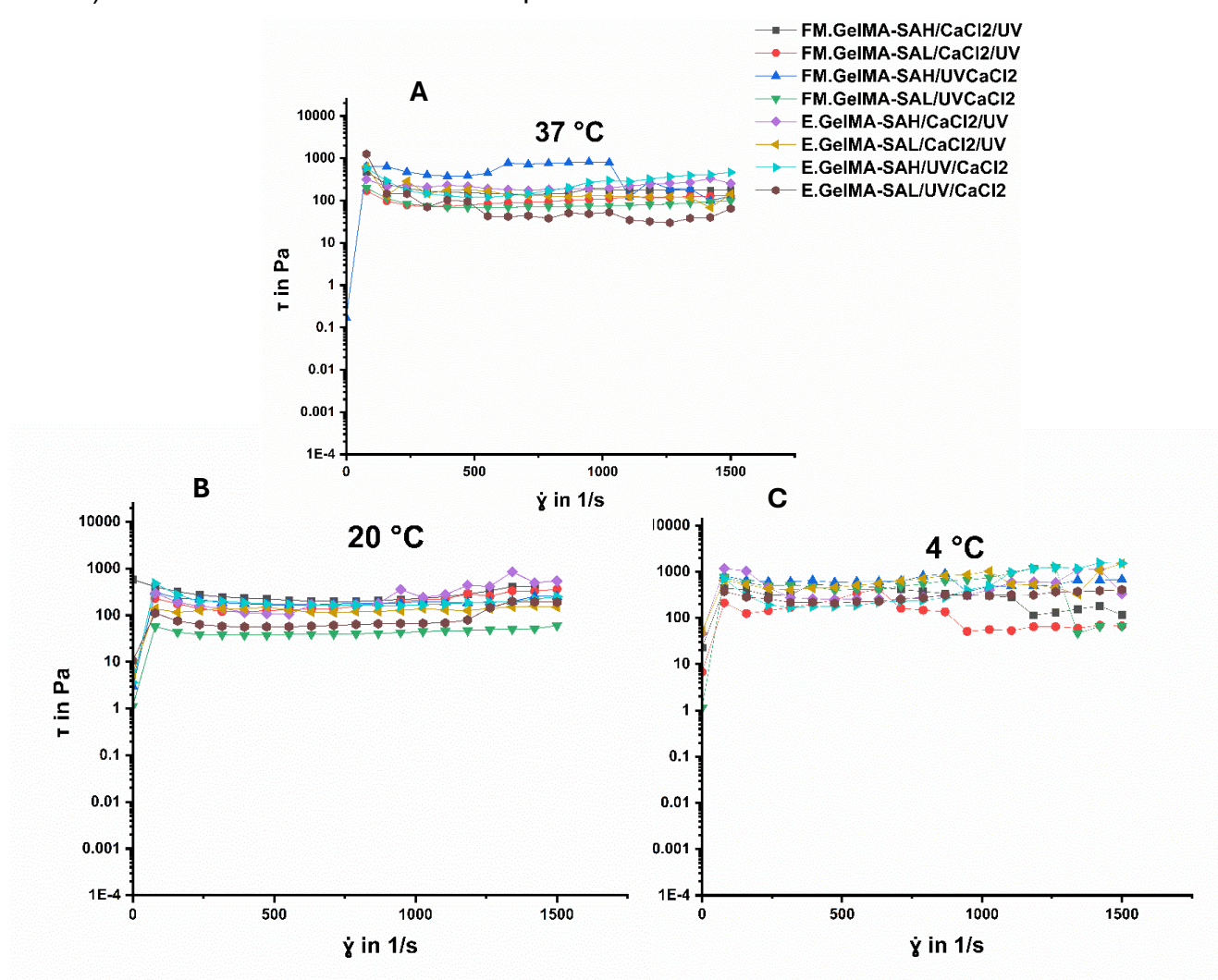


Figure 7.8. . Shear stress as a function of shear rate, the rotational tests under destructive shear conditions were performed at shear rates ranging from 0.01 - 1500 s⁻¹. Samples are: FM.GelMA-SAH/CaCl₂/UV, FM.GelMA-SAL/CaCl₂/UV, FM.GelMA-SAH/UV/CaCl₂, E.GelMA-SAH/CaCl₂/UV, E.GelMA-SAL/UV/CaCl₂, E.GelMA-SAH/UV/CaCl₂, hydrogel samples, (A, B, and C) at 37, 20, and 4 °C, respectively. FM and E refer to filtration and ethanol sterilization methods, respectively.

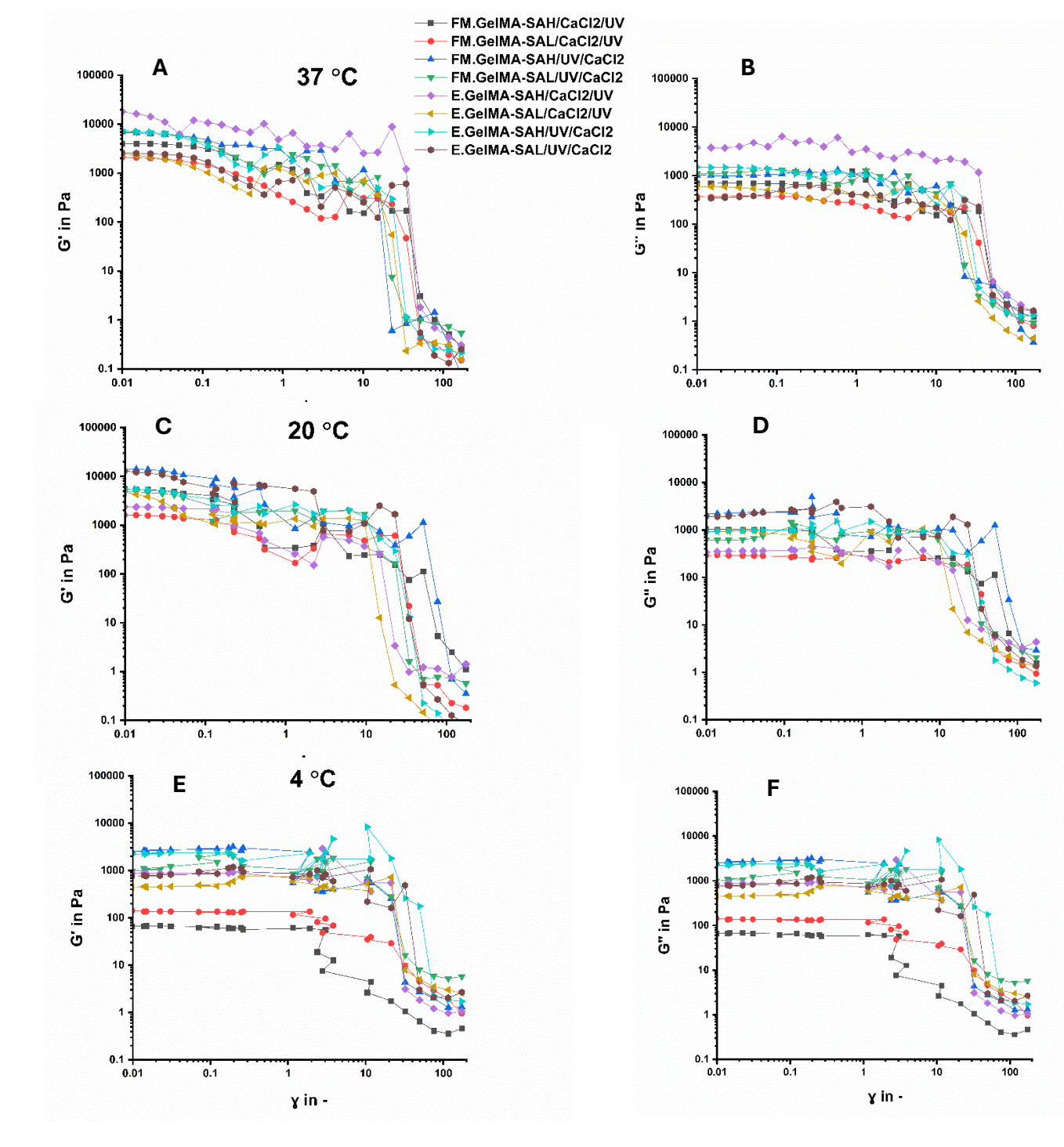


Figure 7.9. Shear dependent viscosity hydrogel samples, FM.GelMA-SAH/CaCl $_2$ /UV, FM.GelMA-SAL/CaCl $_2$ /UV, FM.GelMA-SAH/UV/CaCl $_2$, FM.GelMA-SAL/UV/CaCl $_2$, E.GelMA-SAH/CaCl $_2$ /UV, E.GelMA-SAL/UV/CaCl $_2$, E.GelMA-SAL/UV/CaCl $_2$, at 37, 20, and 4 $_{\circ}$ C. oscillatory amplitude sweeps at a constant frequency of oscillation of 0.01 Hz. (A,C, and E), represent the storage modulus (G') of samples, (B, D, and F) represent the loss modulus (G'), at 37, 20, and 4 $_{\circ}$ C, respectively. FM and E refer to filtration and ethanol sterilization methods, respectively.

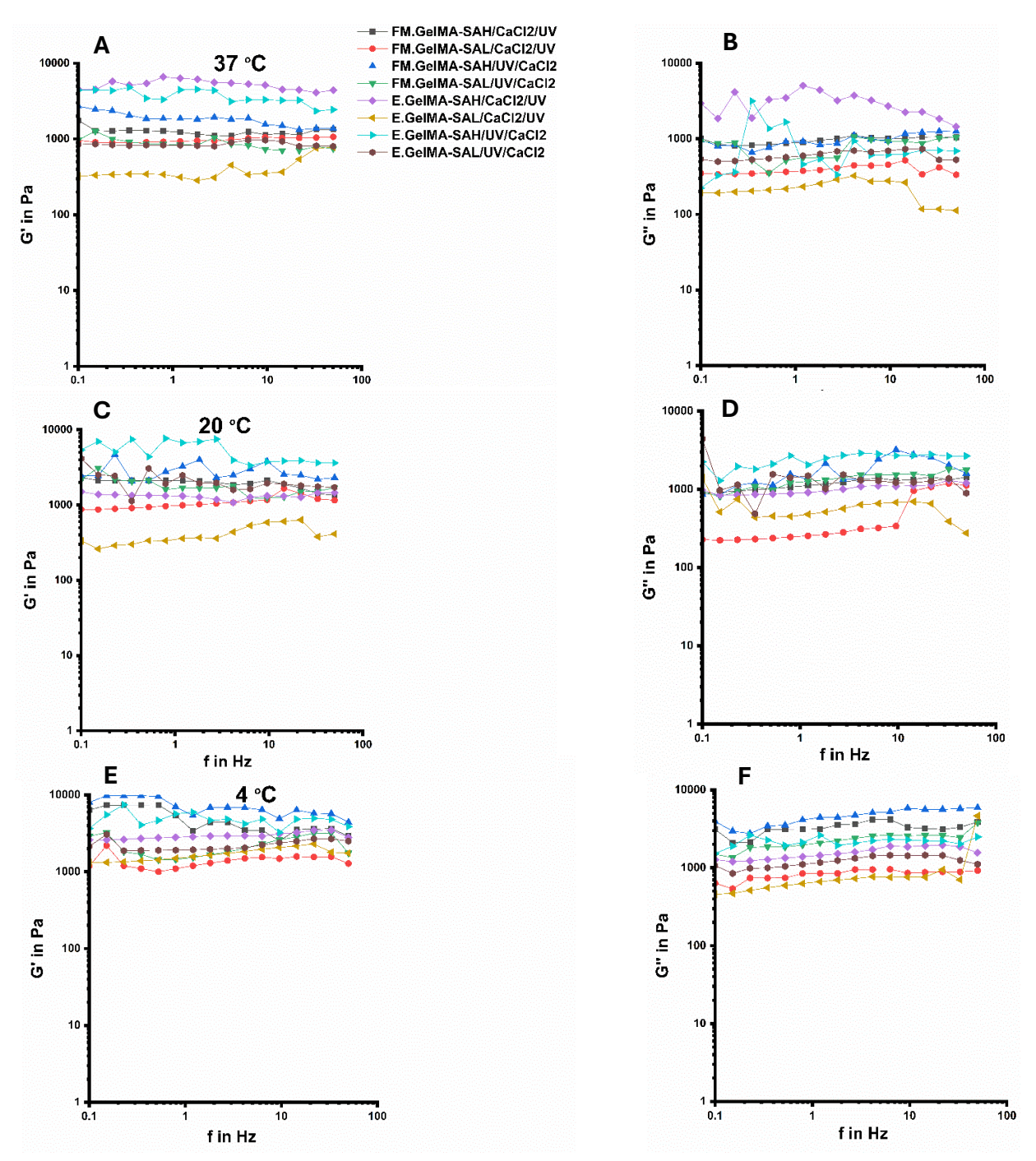


Figure 7.10. Frequency sweep in a linear viscoelastic range at the deformation of 0.25 % measurements for FM.GelMA-SAH/CaCl₂/UV, FM.GelMA-SAL/CaCl₂/UV, FM.GelMA-SAH/UV/CaCl₂, FM.GelMA-SAL/UV/CaCl₂, E.GelMA-SAH/CaCl₂/UV, E.GelMA-SAH/UV/CaCl₂, E.GelMA-SAL/UV/CaCl₂, hydrogel samples (n=8). (A,C, and E), represent the storage modulus (G') of samples, (B, D, and F) represent the loss modulus (G'), at 37, 20, and 4 °C, respectively. FM and E refer to filtration and ethanol sterilization methods, respectively

7.3.1.7. Mechanical properties.

The viscoelastic properties of the hydrogel samples were assessed by measuring the storage modulus (E') and loss modulus (E"), as well as stiffness values, using DMA-uniaxial compression across a frequency range of 0.1 to 50 Hz at 37 °C (Fig.7.11). Young's modulus values were calculated to further characterise the mechanical behaviour. The results demonstrated that E' values were consistently higher than E" for all hydrogel samples. Additionally, the elastic modulus values of hydrogels sterilized using ethanol were significantly higher compared to those sterilized by the filtration method.

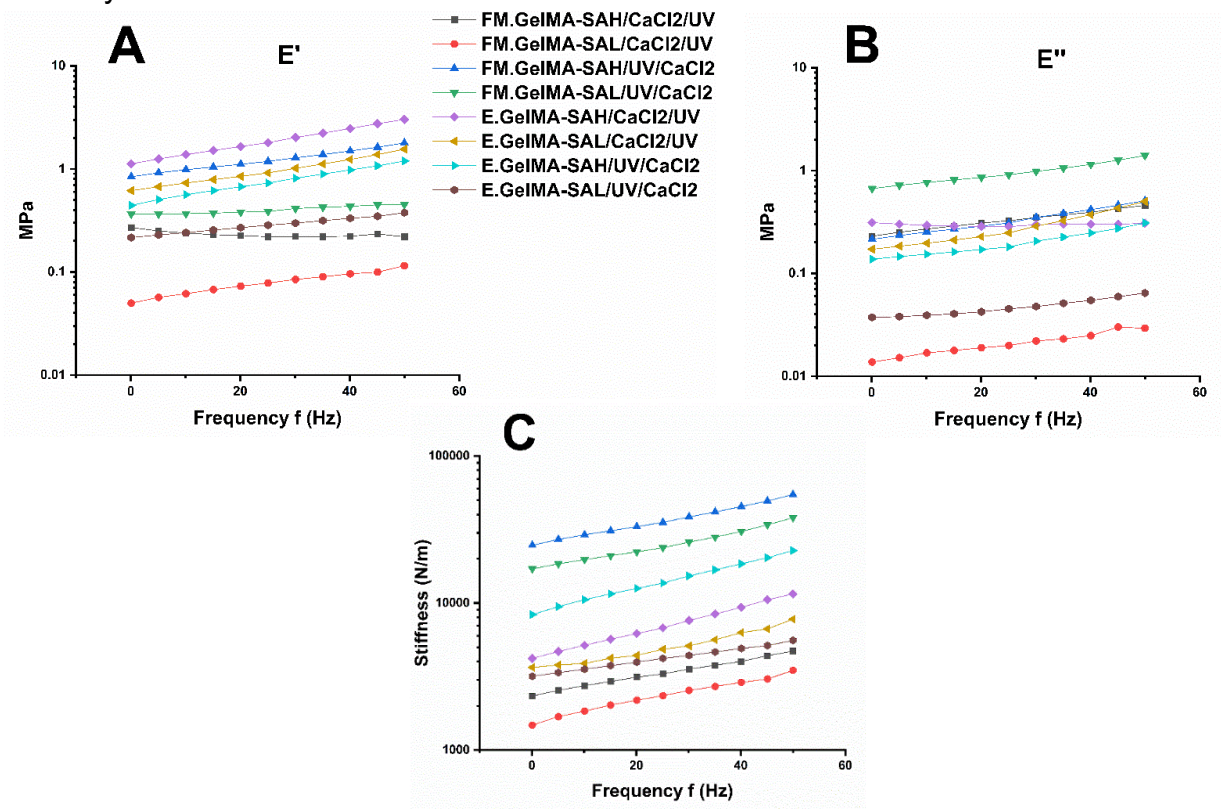


Figure 7.11. Elastic modulus E'(A), loss modulus E"(B), and stiffness (C), as a function of frequency oscillations ranging from 0.1 to 50 Hz at 5 Hz intervals for each sample. Samples were pre-loaded with a force of 0.001 N and dynamically tested at low deformation (0.25% strain), taken at the temperature of 37 °C. Samples are FM.GelMA-SAH/CaCl₂/UV, FM.GelMA-SAH/UV/CaCl₂, FM.GelMA-SAH/UV/CaCl₂, E.GelMA-SAH/CaCl₂/UV, E.GelMA-SAL/CaCl₂/UV, E.GelMA-SAL/CaCl₂/UV, E.GelMA-SAH/UV/CaCl₂, E.GelMA-SAL/UV/CaCl₂, hydrogel samples (n=8). FM and E refer to filtration and ethanol sterilization methods, respectively.

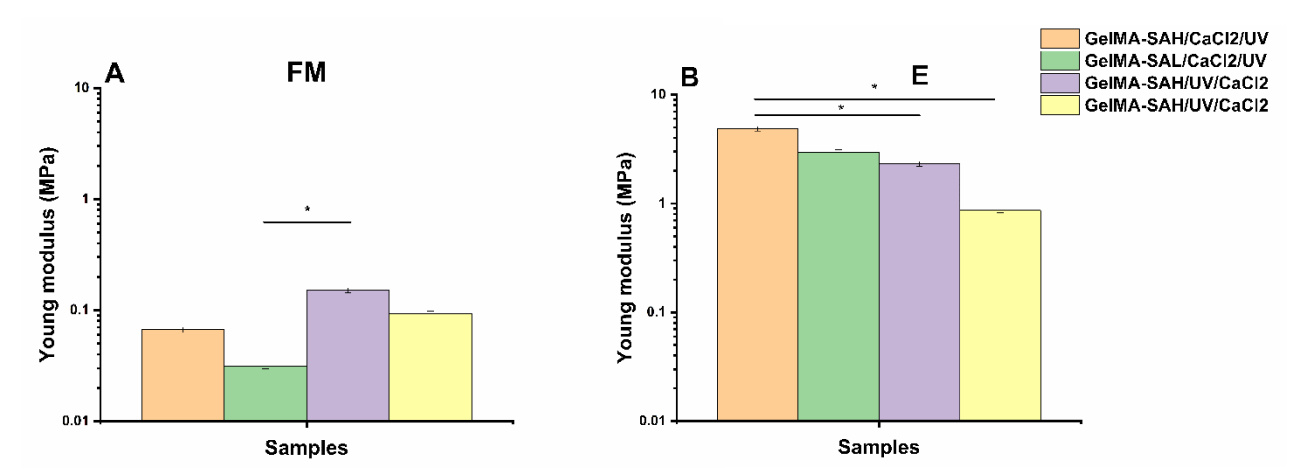


Figure 7.12. Young modulus E as a function of frequency oscillations ranging from 0.1 to 50 Hz at 5 Hz intervals for each sample. Samples were pre-loaded with a force of 0.001 N and dynamically tested at low deformation (0.25% strain), taken at the temperature of 37 °C. Samples are GelMA-SAH/CaCl₂/UV,GelMA-SAL/CaCl₂/UV,GelMA-SAH/UV/CaCl₂,GelMA-SAL/UV/CaCl₂, hydrogel samples (n=8). FM and E refer to filtration and ethanol sterilization methods, respectively. *p< 0.05.

The Young's modulus values were higher in samples sterilised with ethanol compared with those sterilised by filtration. Within the filtration group, GelMA–SA composites crosslinked using the $UV/CaCl_2$ method exhibited higher modulus values than those crosslinked using the $CaCl_2/UV$ sequence. In contrast, within the ethanol-sterilised group, the $CaCl_2/UV$ crosslinking sequence resulted in higher modulus values compared with $UV/CaCl_2$ (Fig.7.11). When compared with reported values for the elastic modulus of native human gingiva (37.36 \pm 17.4 MPa) (218), the hydrogel values were generally lower.

7.3.1.8. Degradation test

Figure 7.13 demonstrated remaining weight of hydrogel samples after 14 days of incubations in PBS at 37 °C. In this study, the degradation rate of hydrogel samples was evaluated by recording their weight at specific time points: days 1, 3, 7, and 14. The results indicated that the remaining weight values of the hydrogel samples,

E.GelMA-SAH/UV/CaCl₂, E.GelMA-SAL/UV/CaCl₂, and FM.GelMA-SAL/CaCl₂/UV, gradually decreased over time, reaching their lowest values on day 14.

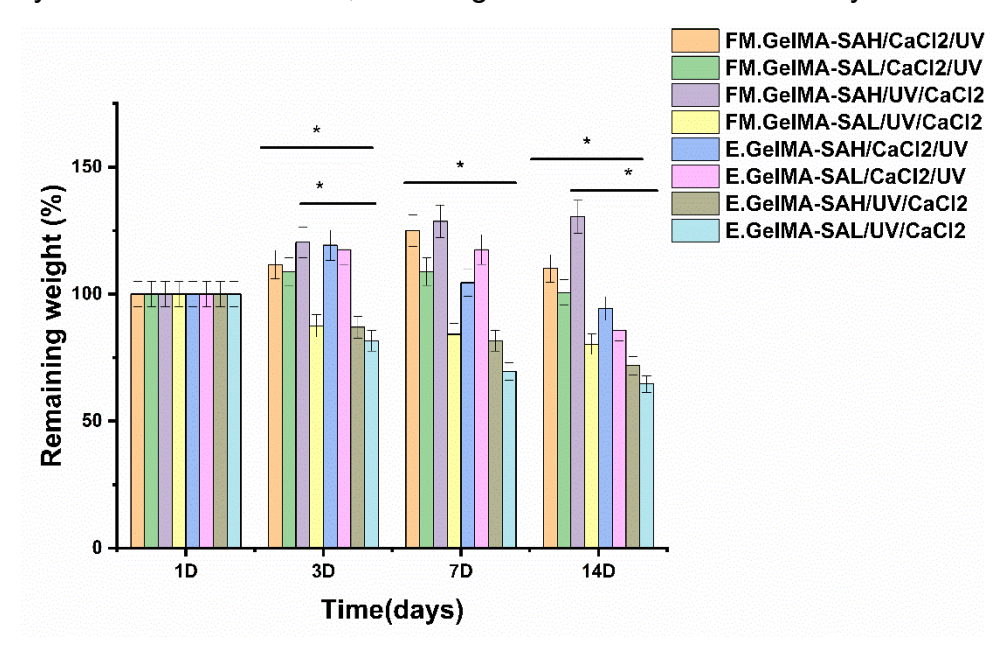


Figure 7.13. Remaining weight of FM.GelMA-SAH/CaCl $_2$ /UV, FM.GelMA-SAL/CaCl $_2$ /UV, FM.GelMA-SAH/UV/CaCl $_2$, FM.GelMA-SAL/UV/CaCl $_2$, E.GelMA-SAH/CaCl $_2$ /UV, E.GelMA-SAH/UV/CaCl $_2$, E.GelMA-SAL/UV/CaCl $_2$, hydrogel samples after 14 days of incubations in PBS at 37 °C (n = 3).FM and E refer to filtration and ethanol sterilization methods, respectively. * p < 0.05.

7.3.2. Material biological and cell viability characterisation

Figures 7.14 presented the metabolic activity and cytotoxicity data of seeded cells in 3D cultures using the hydrogel samples mentioned above as substrates. These assessments were performed on days 1, 3, 7, and 14. These assessments were performed on days 1, 3, 7, and 14. Additionally, confocal imaging with live/dead staining was conducted to evaluate the viability and cytotoxicity of cells within the hydrogel samples. The results showed that metabolic activity significantly (p<0.05, increased after three days of culture in hydrogel samples sterilized using the filtration method, continuing to rise until day 14. In contrast, hydrogels sterilized with ethanol exhibited a steady decline in metabolic activity, reaching the lowest values at the end of the 14-day period. Among the hydrogel samples, FM.GelMA-SAH/CaCl₂/UV,

FM.GelMA-SAH/UV/CaCl₂, and FM.GelMA-SAL/UV/CaCl₂ demonstrated the highest metabolic activity on day 14 compared to other samples (Fig. 7.14A and B).

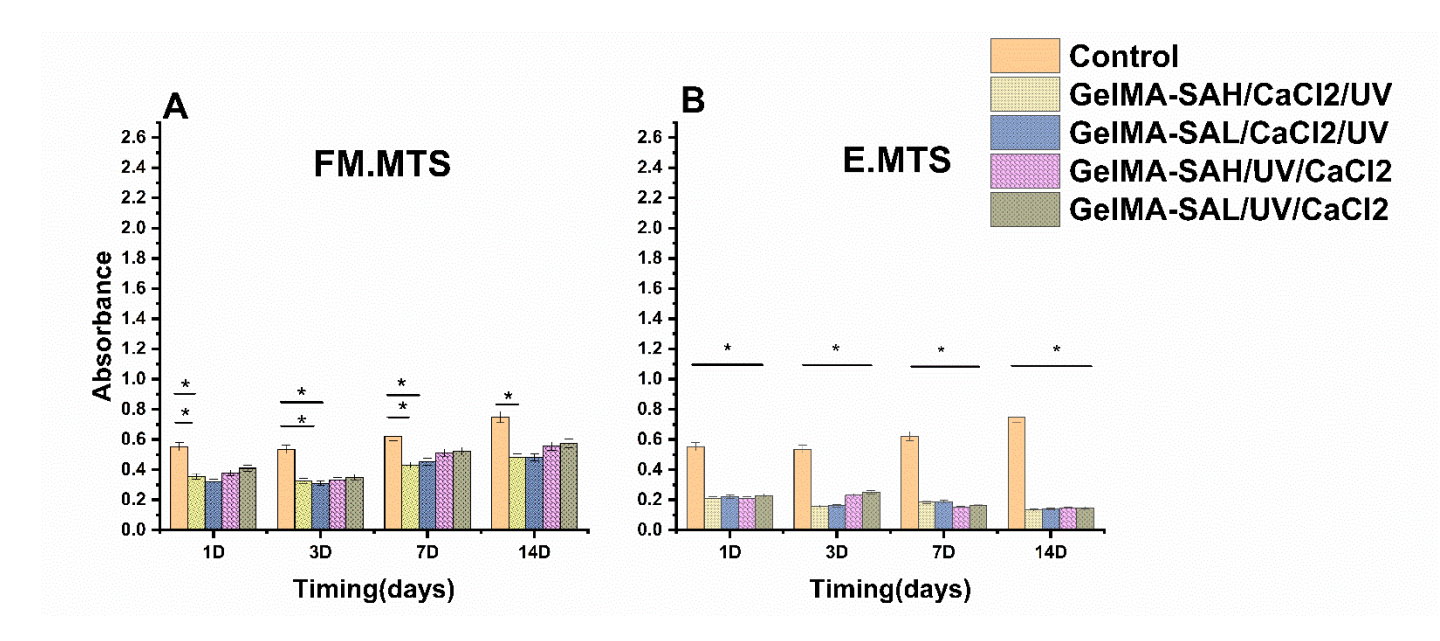


Figure 7.14. Cell viability (A & B) and metabolic activity of 3D cell culture of hydrogel samples sterilized using filtration or ethanol technique. Samples are GelMA-SAH/CaCl $_2$ /UV, GelMA-SAH/UV/CaCl $_2$, and GelMA-SAL/UV/CaCl $_2$. * p < 0.05.

Lactate dehydrogenase (LDH) release, an indicator of cytotoxicity, exceeded 30% in hydrogel samples sterilized with ethanol, with further increases observed by day 14. In contrast, LDH release in hydrogels sterilized via filtration remained around 30% throughout the study (Fig.7.15).

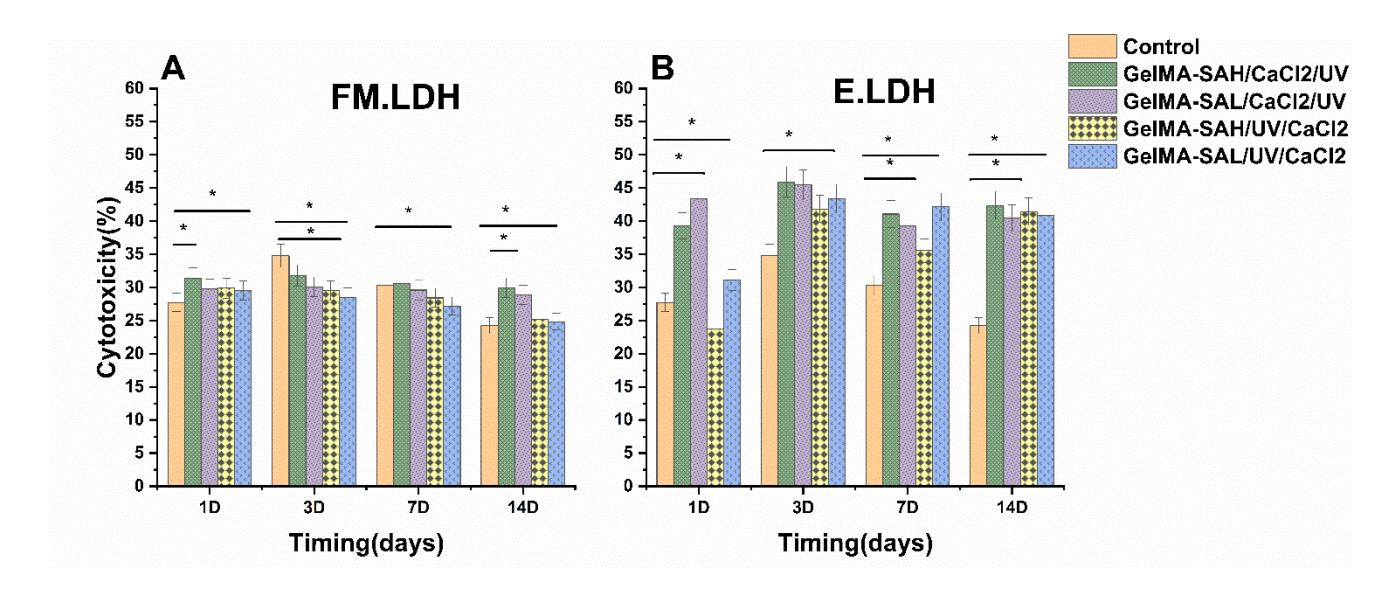


Figure 7.15. Cell cytotoxicity with LDH release of 3D cell culture of hydrogel samples sterilized using (A)filtration, and (B)ethanol techniques. Samples are: FM.GelMA-SAH/CaCl₂/UV, FM.GelMA-SAH/UV/CaCl₂, FM.GelMA-SAH/UV/CaCl₂, FM.GelMA-SAL/UV/CaCl₂, E.GelMA-SAH/CaCl₂/UV, E.GelMA-SAL/CaCl₂/UV, E.GelMA-SAH/UV/CaCl₂, and E.GelMA-SAL/UV/CaCl₂. FM and E refer to filtration and ethanol sterilization methods, respectively. * p < 0.05.

To further assess metabolic activity and cytotoxicity, confocal imaging was conducted using the live/dead staining method, as shown in Figures 7.16 and 7.17. Fluorescence microscopy images were captured on days 1, 3, 7, and 14 to evaluate cell viability within the hydrogel samples. As illustrated in the figures, cell viability increased progressively over time. Notably, hydrogels sterilized using the filtration method exhibited the highest viability on day 7 across all samples, and on day 14 for the GelMA-SAL/UV/CaCl₂ group. In contrast, the ethanol sterilized hydrogels exhibited lower cell viability, which declined noticeably over time, reaching the lowest levels by day 14.

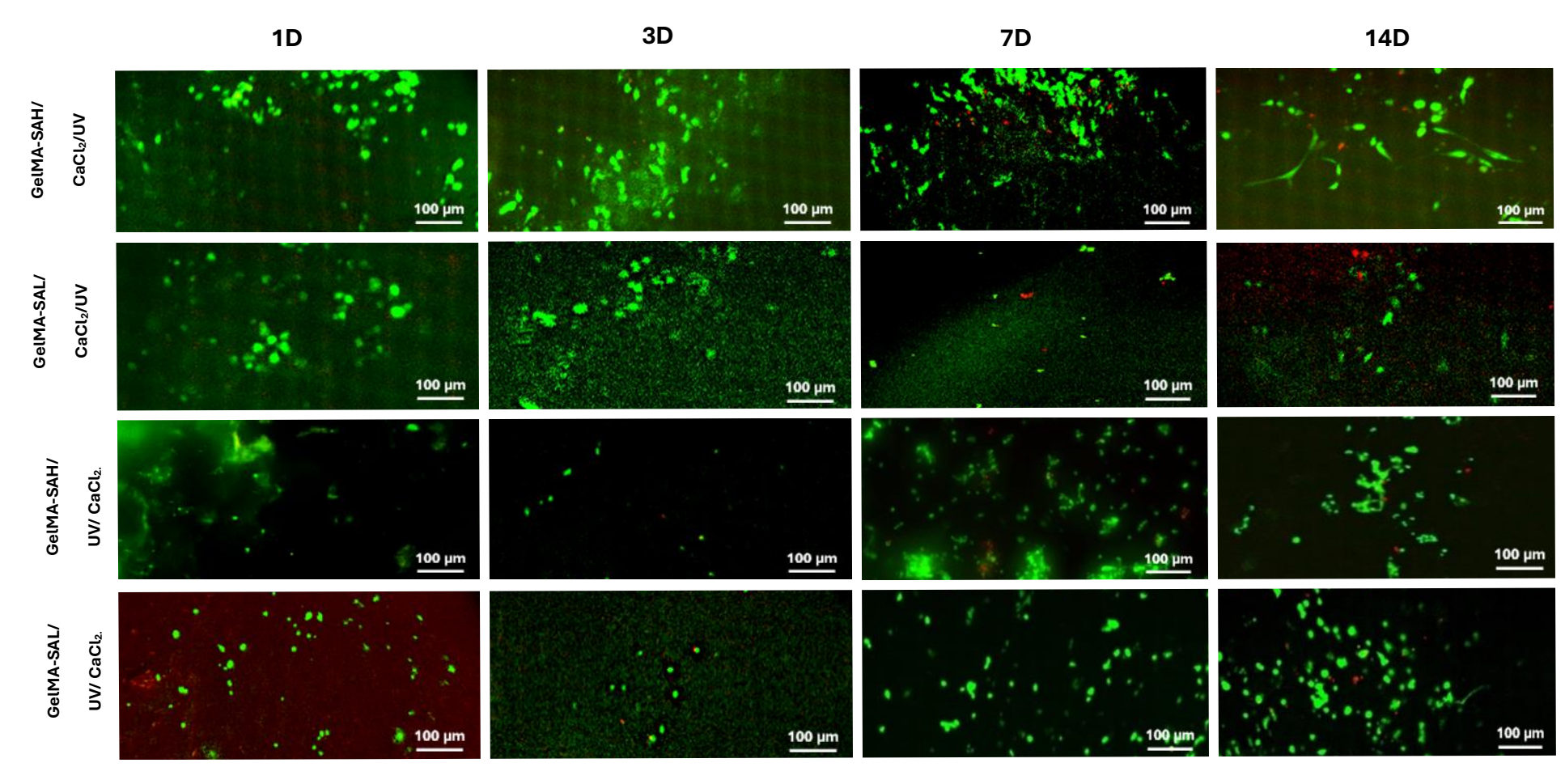


Figure 7.16. Live/dead images of hydrogel samples subjected to sterilization by filtration method. Samples are GelMA-SAH/CaCl₂/UV, GelMA-SAL/CaCl₂/UV, GelMA-SAH/UV/CaCl₂, and GelMA-SAL/UV/CaCl₂, on days, 1, 3, 7, and 12, using flurecent microscope, indicating living cells (green) and dead cells (red). Scale bar: 100 μm.

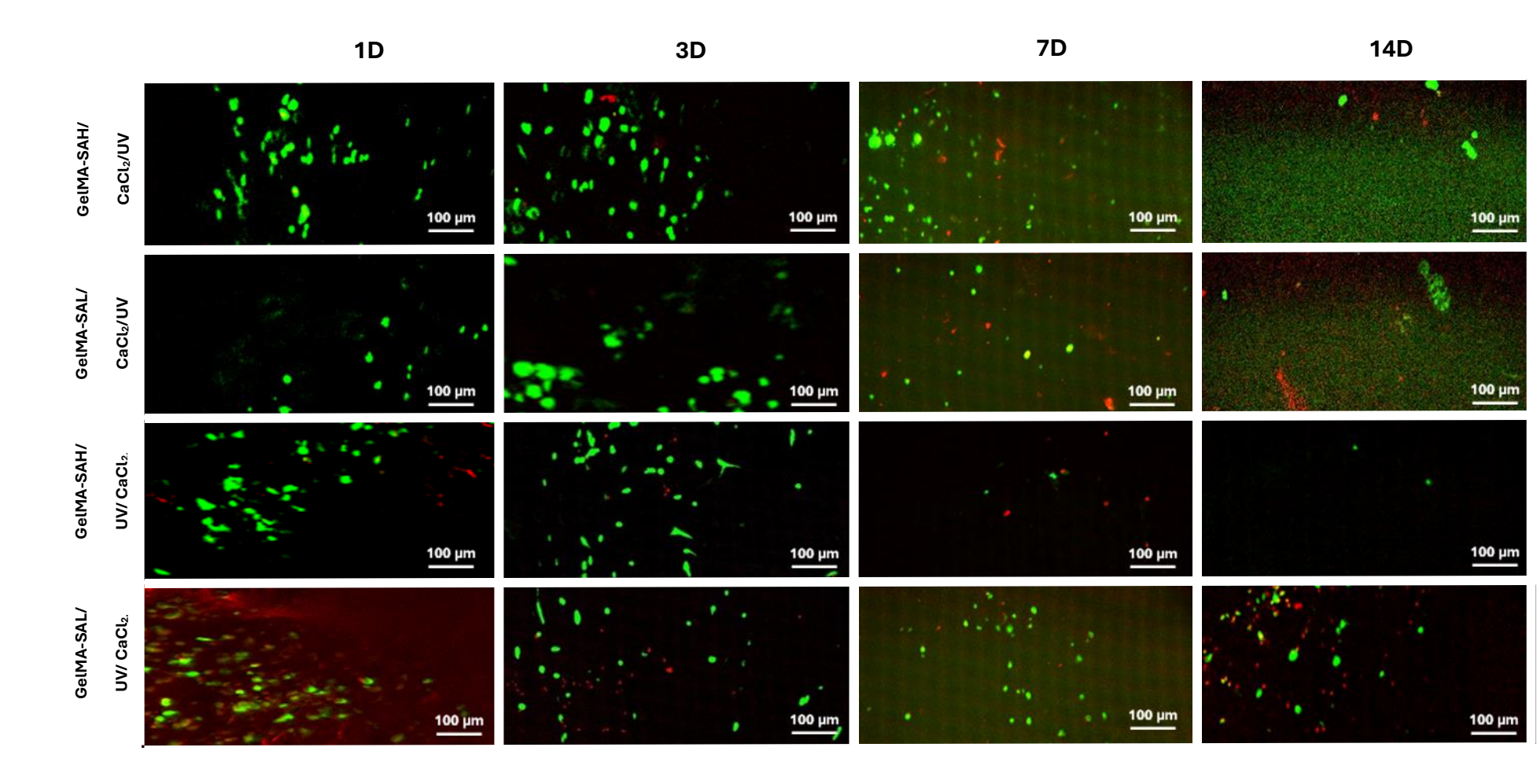


Figure 7.17. Live/dead images of hydrogel samples subjected to sterilization by ethanol method. Samples are GelMA-SAH/CaCl $_2$ /UV, GelMA-SAL/CaCl $_2$ /UV, GelMA-SAH/UV/CaCl $_2$, and GelMA-SAL/UV/CaCl $_2$, on days, 1, 3, 7, and 12, using flurecent microscope, indicating living cells (green) and dead cells (red). Scale bar: 100 μ m.

Using similar methods to test metabolic activity and cytotoxicity, the performance of HGE cells seeded into 3D cultures was evaluated using the same hydrogel samples subjected to sterilization by filtration method, except for GelMA-SAL/CaCl2/UV hydrogel sample. The hydrogel samples were GelMA-SAH/CaCl2/UV, GelMA-SAH/UV/CaCl2, and GelMA-SAL/UV/CaCl2, in addition to R collagen and GelMA hydrogel samples.



Figure 7.18. Microscopy images of human gingival epithelium cells (HGE, MOE1 cell line). Scale bar: 100 µm. Magnification: 10×.

Human gingival epithelium cells (HGE) were cultured and examined under microscopy to assess their morphology and growth characteristics (Fig 7.18). Figure.7.19A and B, presented the results of metabolic activity and cytotoxicity respectively, for HGE cells seeded into these hydrogels, respectively. The metabolic activity of the GelMA-SAH/CaCl₂/UV hydrogel was higher than that of the other samples on day 3. Additionally, when comparing all hydrogel samples, the GelMA-SAH/UV/CaCl₂ and GelMA-SAL/UV/CaCl₂ hydrogels showed higher metabolic activity on day 14.

For cytotoxicity, the results indicated that LDH values began to decrease by day 3 in the GelMA-SAH/UV/CaCl₂ and GelMA-SAL/UV/CaCl₂ samples. These decreases continued through day 14, demonstrating lower cytotoxicity compared with other hydrogel samples. Notably, LDH values across all hydrogel samples decreased by day 14 compared with day 1.

Figure 7.20 also demonstrated confocal images of HGE cells seeded within the aforementioned hydrogels, in addition to R collagen and GelMA hydrogel samples. These images showed that cell viability increased over time in the GelMA-SAH composites, outperforming both R collagen and GelMA hydrogel samples.

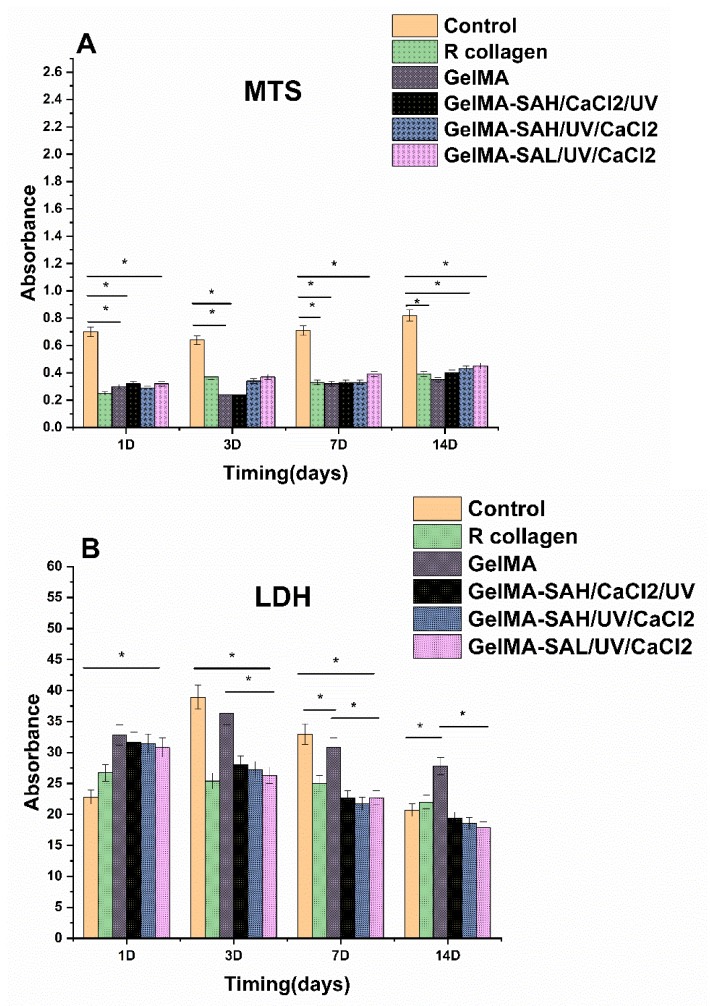


Figure 7.19. Metabolic activity and cytotoxicity of HGE cells using 3D culturing using different hydrogel samples, R collagen, GelMA, GelMA-SAH/CaCl₂/UV, GelMA-SAH/UV/CaCl₂, and GelMA-SAL/UV/CaCl₂, on days 1, 3,7 and 14 days. A, metabolic activity of HGE cells. B, LDH release of HGE cells. Data representing mean \pm SD(n=3). Sample is significantly different with * p < 0.05.

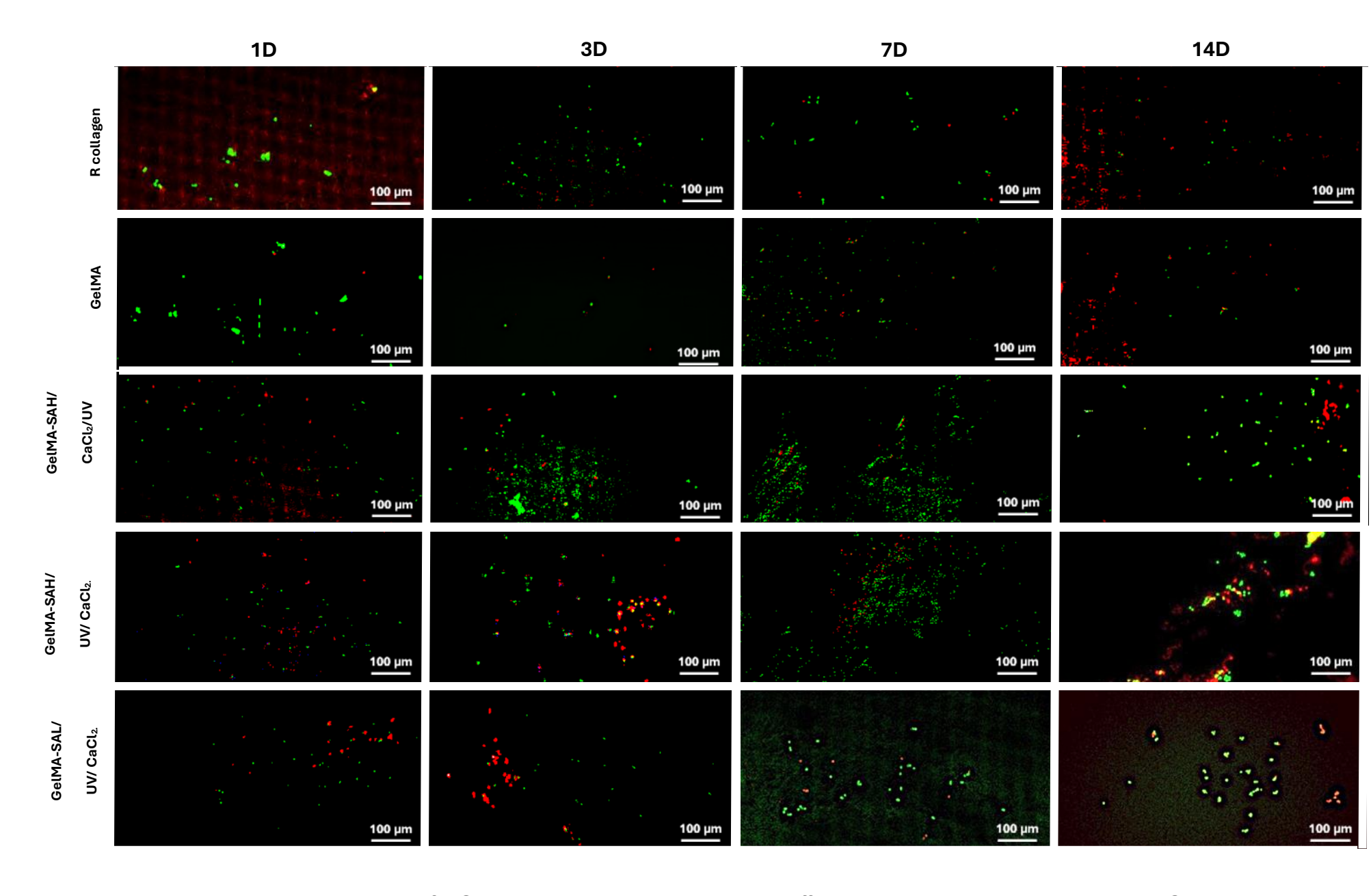


Figure 7.20. Viability and cytotoxicity of HGE cells using 3D culturing using different hydrogel samples, R collagen, GelMA, GelMA-SAH/CaCl₂/UV, GelMA-SAH/UV/CaCl₂, and GelMA-SAL/UV/CaCl₂, on days 1, 3,7 and 14 days, using flurecent microscope, indicating living cells (green) and dead cells (red). Scale bar: 100 µm

7.3.3. Engineered 3D gingival tissue (3DGT)

In this study, the metabolic activities of five hydrogel samples, used to construct 3DGT models in 96 well plates or cell culture inserts, were evaluated. These hydrogel samples were R collagen, GelMA, GelMA-SAH/CaCl₂/UV, GelMA-SAH/UV/CaCl₂, and GelMA-SAL/UV/CaCl₂.

Along with metabolic activity, cytotoxicity was assessed, with results supported by Live/Dead images. For the 3DGT model constructed in well plates, the results demonstrated that metabolic activity was highest when the hydrogel samples were submerged in a 50:50 mixture of HGFs medium and HGEs medium, compared to other ratios (100:0, 75:25, 25:75, or 0:100) (Fig. 7.21). Similarly, cytotoxicity evaluation showed lower LDH values for the 50:50 ratio, indicating reduced cytotoxicity compared to the other ratios (Fig.7.22). These lower LDH values persisted through day 14, confirming the 50:50 ratio's reduced cytotoxicity. Notably, LDH values for all hydrogel samples decreased by day 14.

These findings on metabolic activity and cytotoxicity were further supported by Live/Dead images, which displayed improved cell viability in all hydrogel samples when submerged in the 50:50 ratio. Based on the results of metabolic activity, cytotoxicity, and Live/Dead images, the 3DGT models were constructed in 96-well plates using the 50:50 medium mixture (Fig.7.23, see the Appendix G).

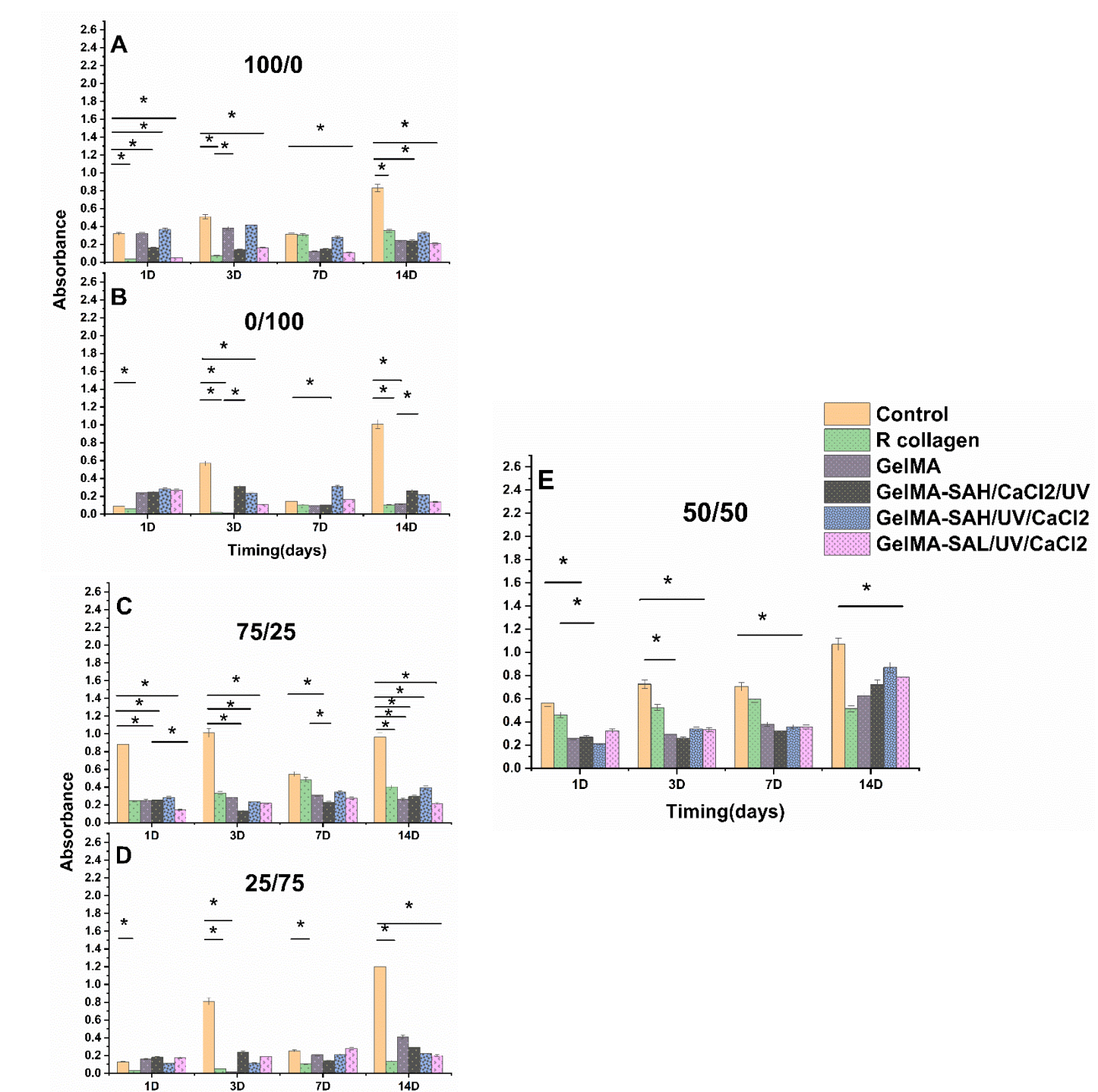
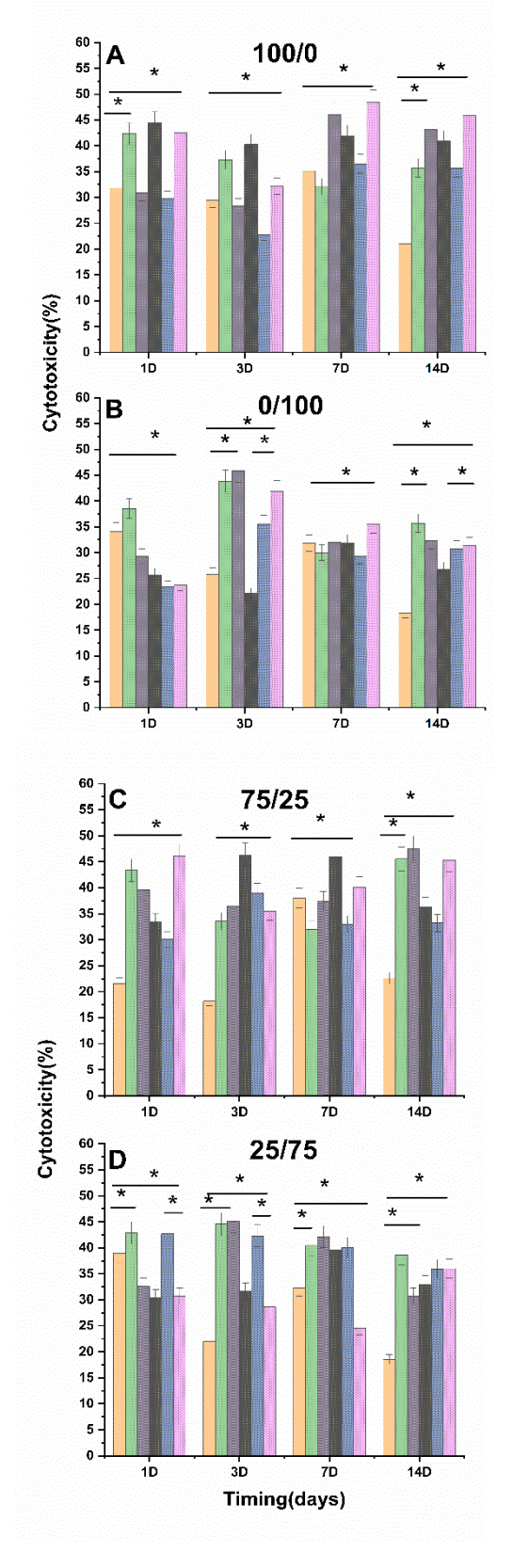


Figure 7.21. Metabolic activity of engineered 3DGT model constructed in well plates, using different hydrogel samples, R collagen, GelMA, GelMA-SAH/CaCl₂/UV, GelMA-SAH/UV/CaCl₂, and GelMA-SAL/UV/CaCl₂, on days 1, 3,7 and 14 days. Hydrogel samples were submerged in a different ratios of mixture of HGFs medium and HGEs medium for A-E with percentages:100:0, 0:100, 75:25, 25:75, and 50:50, respectively. Data representing mean \pm SD(n=3). * p < 0.05.

Timing(days)



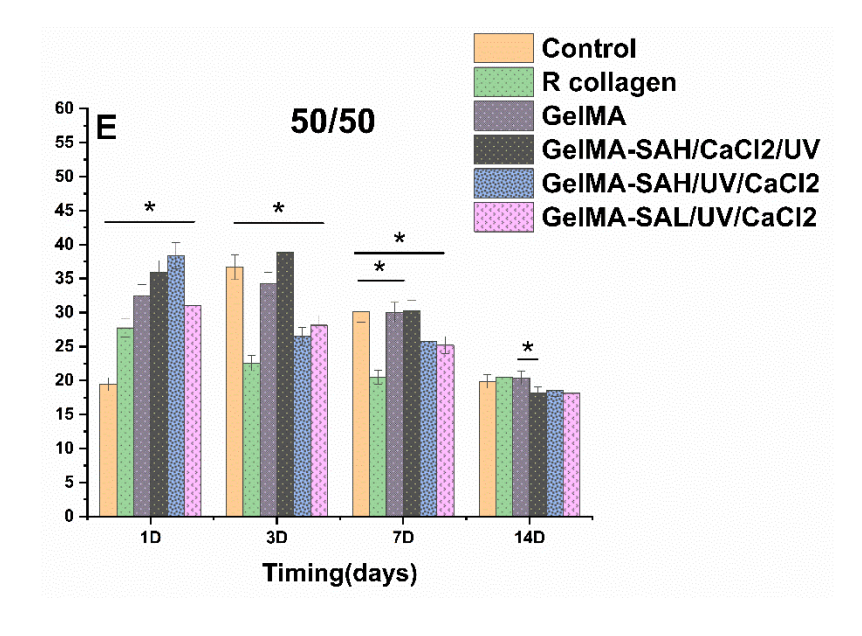


Figure 7.22. Cytotoxicity of engineered 3DGT model constructed in well plates, using different hydrogel samples, R collagen, GelMA, GelMA-SAH/CaCl₂/UV, GelMA-SAH/UV/CaCl₂, and GelMA-SAL/UV/CaCl₂, on days 1, 3,7 and 14 days. Hydrogel samples were submerged in a different ratio of mixture of HGFs medium and HGEs medium for A-E with percentages: 100:0, 0:100, 75:25, 25:75, and 50:50, respectively. Data representing mean \pm SD(n=3). * p < 0.05.

The developed 3DGT I models were successfully cultured within 13 mm Millicell® inserts placed in a 12 well plate format (Fig 7.24). The constructs demonstrated uniform gel formation within the inserts and consistent placement across all wells, confirming the reproducibility of the fabrication process. To promote stratification of the engineered 3DGT and simulate the physiological conditions of gingival tissues, the models were lifted to the air-liquid interface (ALI) on day 4 and maintained for 14 days. Live/Dead confocal images taken for each sample at day 14 revealed a higher density of dead cells compared to live cells at this stage (Fig.7.25 A, B, C, D, and E).

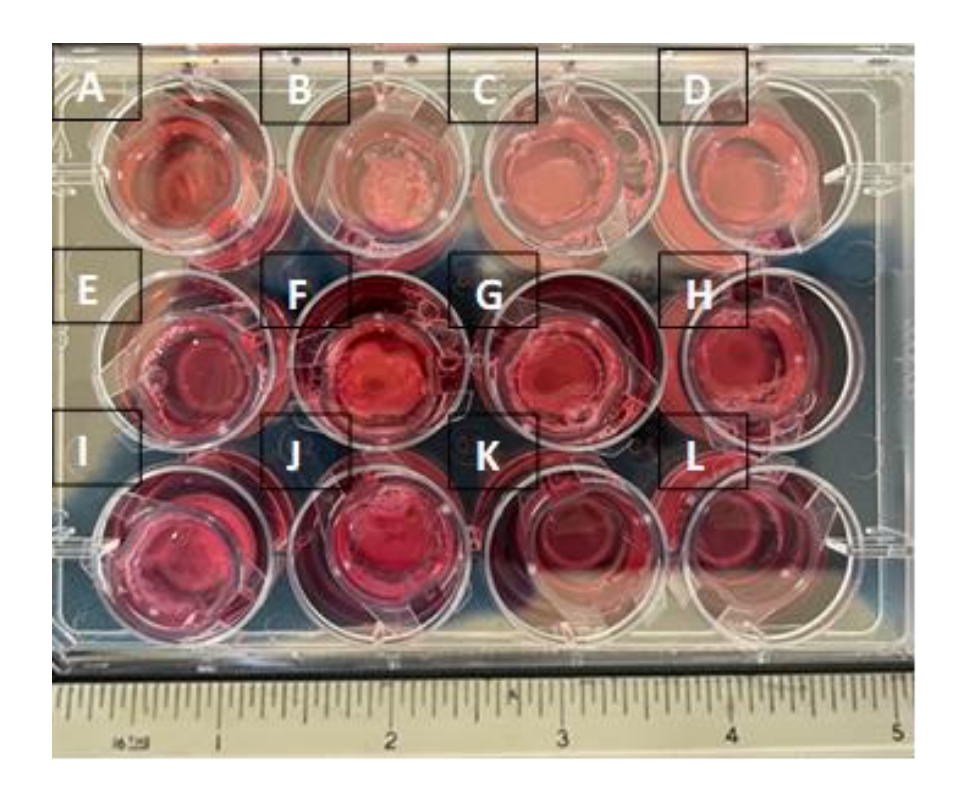
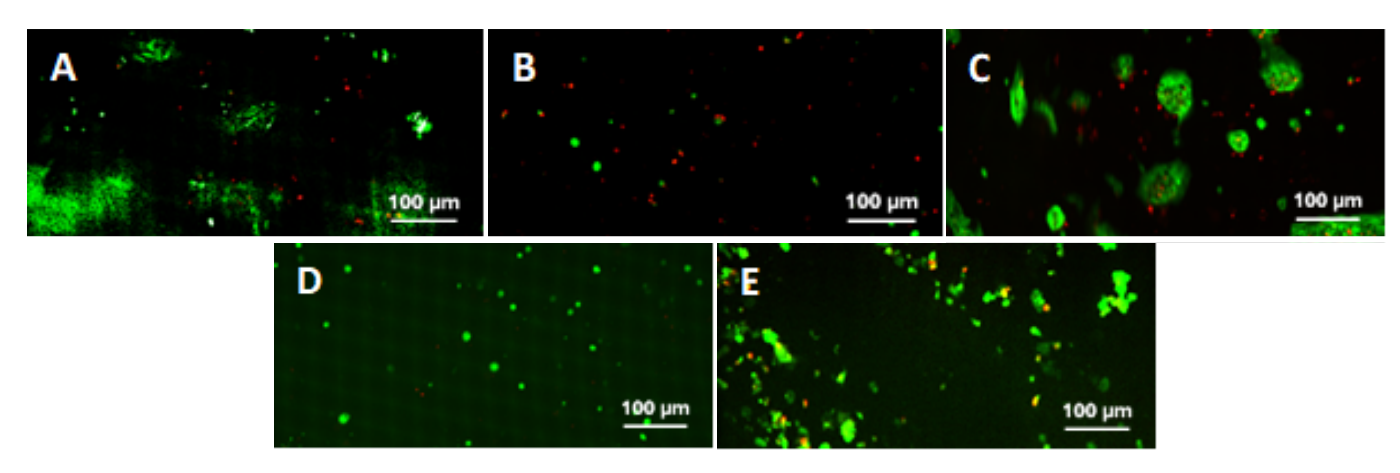


Figure 7.24. Image of 3D gingival tissue models cultured in 13 mm Millicell® inserts within a 12-well plate. Each insert contains a hydrogel-based construct seeded with cells images at day 14 after culturing and ready for lifting to ALI. The hydrogel samples are: (A&E) GelMA-SAH/CaCl₂/UV,(B,F,C,&G) GelMA-SAH/UV/CaCl₂, (D&H) GelMA-SAL/UV/CaCl₂, (I&J) R collagen, and (K&L) GelMA hydrogel samples.

7.3.4. Histological images of 3DGT models

Unfortunately, the 3DGT models constructed using GelMA or R collagen hydrogel samples were structurally compromised during histological processing. These samples degraded or lost integrity when exposed to the high temperatures involved in paraffin embedding, likely due to the thermal sensitivity of the hydrogel materials.

Figure 7.25F, G, and H, showed a histological expressive section images of three 3DGT models constructed using with GelMA-SA composites, stained with hematoxylin and eosin. The images revealed that HGF cells were evenly distributed throughout the 3D culture. However, these cells did not exhibit the typical cytoplasmic projections seen in normal gingival tissue. While the cells adhered to the dermal surface, only a few showed migratory behavior, penetrating the dermal matrices. These images also showed that the HGE cells formed a multilayered regenerated epithelium with no obvious keratinizing superficial layer on the surface, which is similar to the non-keratinized oral epithelia such as junctional epithelium in vivo. The greatest number of epithelial layers observed in models constructed with GelMA-SAL/UV/CaCl₂, compared to those made with GelMA-SAH/CaCl₂/UV and GelMA-SAH/UV/CaCl₂ hydrogel samples. However, the epithelial layer showed poor differentiation of oral keratinocytes, and the transition from cuboidal to squamous cells was unclear.



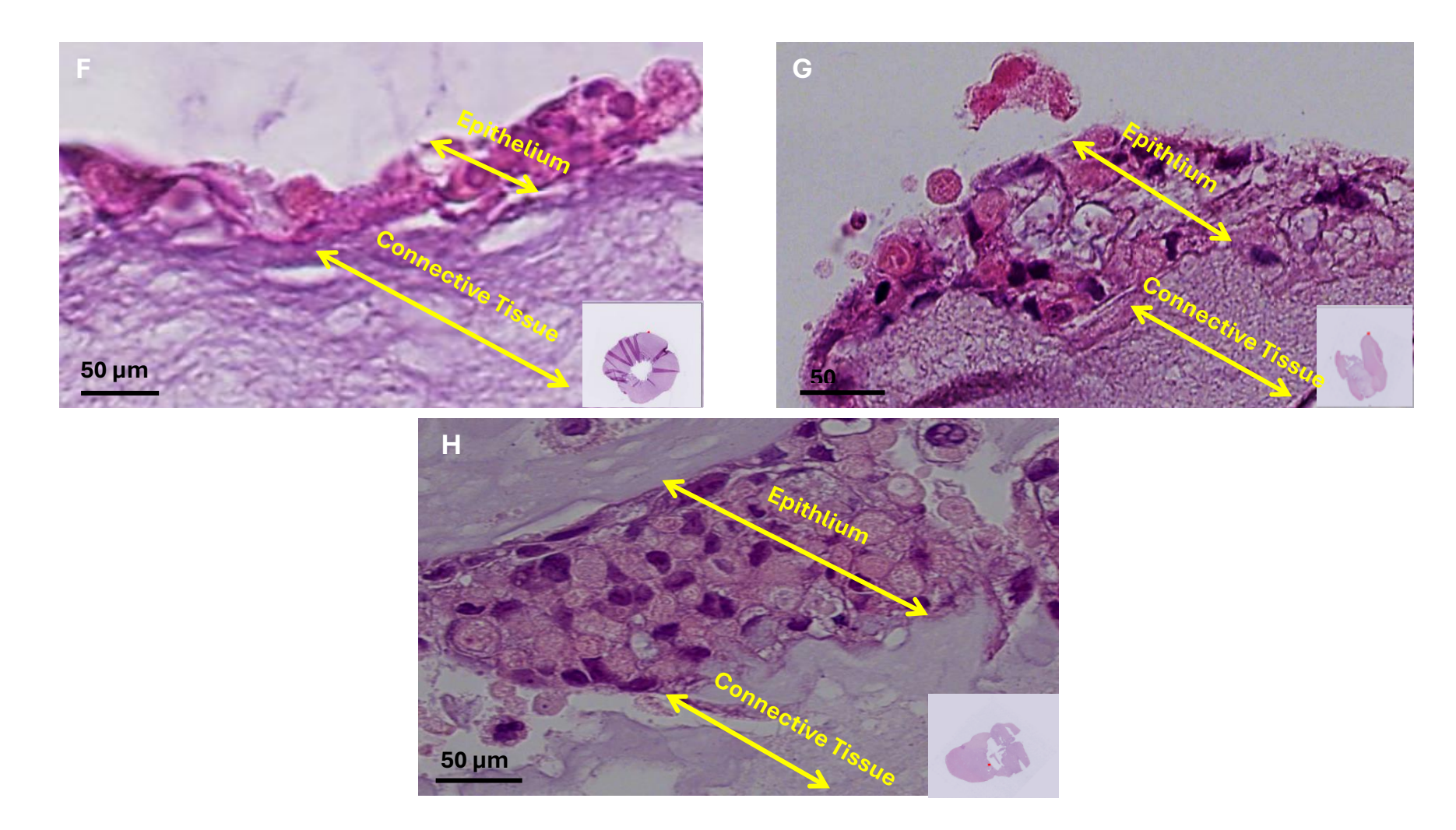


Figure 7.25. (A, B,C,D, and E) Live/dead confocal images at day 14 of lifting 3DGT model to ALI, using R collagen, GelMA. GelMA-SAH/CaCl₂/UV, GelMA-SAH/UV/CaCl₂, and GelMA-SAL/UV/CaCl₂, respectively. Confocal images captured using flurecent microscope, indicating living cells (green) and dead cell(red). Scale bar: 100 μm. (F, G,and H) H&E stained histological section images showing epithelial layer, and underlying connective tissue. Arrows indicate the distinct tissue layers, (Scale bar: 50 μm) at day 14 of lifting 3DGT model to ALI, using GelMA-SAH/CaCl₂/UV, GelMA-SAH/UV/CaCl₂, and GelMA-SAL/UV/CaCl₂, respectively.

7.4. Discussion

Sterilization methods play a crucial role in the development of hydrogel biomaterials for various tissue engineering applications, including drug delivery, wound healing, and tissue regeneration. Selecting an effective sterilization method is essential to preserve the biomechanical properties of hydrogel biomaterials. Therefore, evaluated two sterilization techniques were evaluated filtration and ethanol treatment for their effectiveness in sterilizing GelMA-SA composite hydrogels. Findings from previous chapter, highlighted that GelMA-SA composite hydrogels are considered potential candidates for fabricating HGF cell-populated hydrogel biomaterials, designed to mimic the native ECM of human gingival tissue. Following sterilization, the GelMA-SA composite hydrogel samples were subjected to crosslinking. The mechanical and biological properties of the samples were analysed and compared based on the sterilization methods used, as well as the crosslinking techniques employed. This comparison provides insights into how sterilization impacts the functionality and suitability of GelMA-SA hydrogels for tissue engineering applications.

Porosity is a critical factor in evaluating scaffold structures, as it influences nutrient transport, cell adhesion, proliferation, and overall tissue regeneration. Pore size, in particular, plays a key role in supporting cell migration and proliferation, as well as facilitating nutrient diffusion and waste removal (334).. Human gingival connective tissue is composed of a dense extracellular matrix (ECM) rich in collagen fibers, fibroblasts, and a well-organized vascular network. It typically contains rounded or elliptical pores formed by the arrangement of collagen and ground substance, which create a porous microenvironment conducive to cell infiltration and tissue remodelling. According to Le et al. (2018), the native gingival connective tissue exhibits pore sizes ranging from 30 to 80 μ m, which are considered optimal for supporting fibroblast migration and maintaining physiological function (354).

In this study, SEM analysis revealed that low-concentration hydrogel samples had larger pore sizes than high-concentration ones, suggesting reduced

mechanical integrity in the former. Additionally, samples sterilized using ethanol showed smaller pore sizes compared to those sterilized via filtration. Notably, the pore sizes observed in the GelMA-SA composite hydrogels fell within the 30–80 µm range, aligning with the native gingival architecture described by Le et al. (2018). This morphological similarity suggests that the composite hydrogels may provide a supportive environment for gingival cell attachment and function, making them promising candidates for soft tissue engineering applications.

Biochemical properties were analysed using FT-IR. One of the primary advantages of FTIR imaging is its ability to provide a biochemical fingerprint, offering detailed information on the content, structure, and chemical modifications of key biomolecules in the sample (355). High-concentration hydrogels exhibited increased peak intensities compared to low-concentration ones, indicating stronger intermolecular interactions between SA and GelMA chains. Furthermore, hydrogels sterilized using the filtration method demonstrated higher peak intensities compared to those sterilized with ethanol.

Notably, similar amide I spectra and biochemical characteristics to healthy human oral tissue have been reported by Naurecka et al., where the peak maximum of the C=O stretching band was observed at 1650 cm⁻¹(357). For amide II, Fukuyama et al. identified the peak maximum around 1550 cm⁻¹ in normal human oral connective tissue. Hydrogel samples sterilized via filtration and ethanol, mean values of amide II intensity align closely with those reported by Fukuyama et al., suggesting that these hydrogel samples share significant biochemical similarities with human gingival tissue.

Water contact angle measurement is a critical physicochemical property for evaluating the surface characteristics of biomaterials. When a material is exposed to body fluids or culture media, protein adsorption significantly influences initial cell attachment (333). The results indicated that GelMA-SAH and GelMA-SAL hydrogels, when crosslinked using UV/CaCl₂ methods with both ethanol and filtration sterilization, exhibited a hydrophobic nature. In contrast, the other hydrogel samples demonstrated a hydrophilic nature. These findings highlight the influence of UV crosslinking followed by ionic crosslinking with CaCl₂ on the

surface properties of GelMA-SA composite hydrogels. Comparable results were observed in a study by Van der Mei, White, and Busscher (2004), which reported the hydrophobic nature of gingival surfaces among 10 volunteers. Intra-oral water contact angles were measured under various conditions, including in the morning before brushing, immediately after brushing, and before and after lunch. The study found that gingival surfaces were hydrophobic, with water contact angles ranging from 72° to 79° (334). Our observations of increased hydrophobicity in UV/CaCl₂-crosslinked GelMA-SA composites are supported by prior work. For example, in corneal engineering studies, increasing GelMA concentration resulted in increased contact angle values (i.e. more hydrophobic surfaces) at higher polymer content (396).

DSC analysis was used to investigate the thermal properties of the samples, as it is a suitable method for assessing protein thermal stability and conformational changes (345). The melting point values were higher in high-concentration hydrogel samples compared to low-concentration ones, indicating stronger intermolecular bonds in the high-concentration hydrogels. Additionally, the results showed that hydrogels sterilized using the ethanol method exhibited higher melting temperatures than those sterilized with the filtration method. The melting points of the hydrogel samples were approximately 155°C, consistent with values reported by González-Masís et al (346). Furthermore, samples crosslinked with CaCl₂/UV showed higher melting point values compared to those crosslinked with UV/CaCl₂, highlighting the influence of crosslinking sequence on the thermal properties of GelMA-SA composites. The melting points of the hydrogel samples, being considerably higher than tissue denaturation values which reported by Samouillan et al, reflected the inherent thermal stability of the polymer network rather than protein unfolding. This high thermal stability is advantageous as it ensures that the hydrogels maintain structural integrity during common handling procedures, sterilization, and storage. Moreover, it suggests that the scaffolds can withstand physiological conditions without premature degradation or softening, supporting their suitability for applications in gingival tissue engineering.

In this study the results revealed that viscosity decreased with increasing shear rate, demonstrating the shear-thinning behavior of the hydrogels. Additionally, viscosity increased as the temperature decreased, emphasizing the influence of temperature on the viscous properties of the hydrogel samples. In oscillatory rheology and frequency tests, G' values of all hydrogel samples increased as the temperature decreased, emphasizing once more, the influence of temperature on the viscoelastic properties of the hydrogel samples. As anticipated, hydrogel samples sterilized using the ethanol method exhibited higher viscoelastic values than those sterilized via filtration. Moreover, these viscoelastic properties increased as the temperature decreased, further underscoring the significant impact of temperature on the viscoelastic behavior of the hydrogels.

In another investigation for the viscoelastic properties of hydrogel samples was measuring the storage modulus (E') and loss modulus (E"), as well as stiffness values, using DMA-uniaxial compression. The results demonstrated that E' values were consistently higher than E" for all hydrogel samples. However, these values were higher in hydrogel samples which were sterilized using ethanol compared with filtration method. These results indicated a predominantly elastic behavior rather than viscous behavior within the hydrogel structure (334). These findings underscore the critical influence of the sterilization method on the mechanical properties of hydrogel samples, highlighting its importance in optimizing hydrogel performance. In Chapter 6, the mechanical characterisation of the GelMA-SA hydrogels demonstrated that formulations with higher SA content and sequential crosslinking (UV/CaCl₂) achieved elastic moduli closely matching those of native gingival and oral mucosal tissues in both human and animal models. This prior finding is particularly relevant to the current investigation, as it establishes a mechanical foundation compatible with gingival fibroblast culture and tissue regeneration. Similarly, the sterilisation method was found to influence the mechanical properties of the hydrogel samples, as evidenced by the higher Young's modulus values in the ethanol-sterilised group compared with the filtration-sterilised group. This suggests that ethanol treatment may enhance network density or promote additional crosslinking, thereby

increasing stiffness. Interestingly, the effect of crosslinking sequence varied between sterilisation methods. In the filtration-sterilised samples, the UV/CaCl₂ sequence produced higher Young's modulus values than the CaCl₂/UV sequence, potentially due to more efficient initial covalent crosslinking followed by ionic reinforcement. Conversely, in the ethanol-sterilised group, the CaCl₂/UV sequence resulted in greater stiffness than UV/CaCl₂, indicating that ethanol may interact with the ionic crosslinking step to strengthen the hydrogel network. These findings highlight the combined influence of sterilisation method and crosslinking sequence on the mechanical performance of GelMA–SA composites, with potential implications for optimising hydrogel preparation in tissue engineering applications. Furthermore, double crosslinked systems such as GelMA/κ-carrageenan have been shown to yield higher Young's modulus and stiffer networks when compared to single crosslinking strategies (397).

Biodegradation is a critical property when selecting suitable biomaterials for biomedical applications (348). Biodegradable materials are widely employed in the biomedical field due to their tunable nature. The chemical and biological breakdown of these materials can lead to weight loss (a physical process), molecular weight changes (both chemical and physical), and alterations in mechanical properties (349, 350). Measuring weight loss is a common physical approach to assess the degradation rate of biomaterials (351). Interestingly, during the first three days, the E.GelMA-SAH/UV/CaCl₂ and E.GelMA-SAL/UV/CaCl₂ samples exhibited an initial increase in weight, followed by a steady decrease. In contrast, most hydrogels sterilized using the filtration method (except FM.GelMA-SAL/CaCl₂/UV) continued to swell, showing an increase in remaining weight until day 7, after which the weight began to decline. These findings highlight the significant influence of hydrogel concentration, crosslinking, and sterilization methods on their biodegradation properties. The results underscore the importance of optimizing these parameters for tailored biomedical applications.

In this study, metabolic activity values were higher for hydrogel samples sterilized via filtration compared to those sterilized with ethanol. Additionally, LDH release

in filtration-sterilized hydrogels remained around 30% throughout, indicating lower cytotoxicity. The enhanced biological performance of filtration-sterilized hydrogels can be explained by the gentle, non-destructive nature of this method, which avoids exposure to heat or solvents. Filtration does not alter the hydrogel's chemical or mechanical properties and does not introduce harmful residues, thereby better supporting cell adhesion, proliferation, and metabolic activity. This is consistent with reports in the literature that highlight the variability and potential detrimental effects of ethanol sterilization on hydrogels particularly regarding changes in gene expression and structural integrity even when cell viability appears unchanged (as reported in GelMA-based systems (393). Furthermore, studies on alginate hydrogels demonstrate that ethanol sterilization can effectively eliminate microbial contaminants while preserving mechanical strength and hydration, but this method is still less ideal than filtration because it carries a risk of altering scaffold morphology and pore structure, which can affect downstream cellular responses (394).

Therefore, the superior metabolic activity and lower LDH release observed with filtration-sterilized hydrogels align with findings from previous studies and underscore the importance of careful selection of sterilization protocols to maintain both structural integrity and biocompatibility.

Confocal images from live/dead staining of seeding HGF cells within the hydrogel samples demonstrated increasing cell viability over time in hydrogel samples sterilized with the filtration method, whereas cell viability declined in those sterilized with ethanol. These findings further validate the superior efficacy of filtration sterilization in maintaining the biological activity and viability of hydrogel samples during 3D culture with HGFs.

These findings emphasized the biocompatibility of hydrogel samples tested using a single cell type which was HGFs. These findings highlight the influence of sterilization, hydrogel concentration, and crosslinking on the structural, mechanical, and biological properties of GelMA-SA hydrogels, essential for optimizing their application in gingival tissue engineering.

Moreover, the results revealed that hydrogels sterilized using the ethanol method exhibited superior mechanical properties compared to those sterilized via filtration. Additionally, hydrogels crosslinked with CaCl₂ followed by UV irradiation demonstrated enhanced mechanical properties compared to those crosslinked in the reverse order (UV followed by CaCl₂), highlighting the significant impact of both sterilization techniques and crosslinking sequences on the material's properties. However, HGFs displayed higher viability when seeded in filtered hydrogels compared to ethanol-sterilized samples. These findings underscore the importance of optimizing both sterilization methods and crosslinking strategies to improve the suitability of GelMA-SA hydrogels for supporting human gingival cell growth, ultimately contributing to the development of advanced 3D human gingival cell cultures.

Similarly, the biocompatibility of the GelMA-SA composite hydrogels was tested and compared to R collagen and GelMA hydrogel samples using HGE cells. All GelMA-SA composite hydrogel samples were included in this investigation, except for the GelMA-SAL/CaCl₂/UV hydrogel. This particular sample exhibited significantly lower biological properties, rapid degradation, and inferior mechanical properties compared to the GelMA-SAH/CaCl₂/UV hydrogel. These limitations indicated its unsuitability for periodontal and soft tissue regeneration. Consequently, this sample was excluded from further investigations to focus on materials better aligned with the functional requirements of the intended application.

Biological properties of GelMA-SA composite hydrogel samples were investigated and compared to R collagen and GelMA hydrogel samples using HGE cells. The results indicated reduced metabolic activity of HGE cells cultured within GelMA and R collagen hydrogels compared to those cultured in GelMA-SAH composite hydrogels. However, metabolic activity decreased in HGE cells cultured within GelMA-SAH/CaCl₂/UV hydrogels compared to those in GelMA-SAH/UV/CaCl₂ and GelMA-SAL/UV/CaCl₂ hydrogels. This reduction may be attributed to the higher biodegradation rate of the GelMA-SAH/CaCl₂/UV hydrogel.

The LDH assay revealed higher release values from R collagen and GelMA samples compared to other hydrogel samples. These findings were corroborated by confocal microscopy images of live and dead cells. By day 14, confocal images demonstrated a greater intensity of live HGE cells within GelMA-SAH/UV/CaCl₂ and GelMA-SAL/UV/CaCl₂ hydrogels compared to the other hydrogels tested.

The GelMA-SA composite hydrogels demonstrated excellent biocompatibility, with both HGF, and HE cells viability over a 14-day culture period, as confirmed by live/dead staining and MTS assays. These results align with previous studies reporting high cell compatibility for GelMA-based hydrogels (e.g., Aljaber et al., 2023, Keskin-Erdogan et al., 2021), but the addition of SA hydrogel appeared to further stabilize the structure without compromising cell survival. Moreover, the compressive modulus of the optimized composite as mentioned above was comparable to native gingival connective tissue, supporting its mechanical suitability for gingival tissue engineering. Alongside their favorable mechanical properties of GelMA-SA composite hydrogels, making them highly suitable for 3D cell culture applications. Considering the sequence of the crosslinking method used to fabricate the GelMA-SA composites, the findings demonstrate that these hydrogels exhibit tunable degradation rates, as well as mechanical and biocompatible properties conducive to supporting the survival of human gingival fibroblasts. These attributes position the GelMA-SA composite as a promising candidate for periodontal and soft tissue regeneration, as well as drug delivery applications aimed at enhancing tissue regeneration.

To decipher the pathologies of periodontal diseases, it is important to establish in vitro models that mimic the mechanisms taking place within the gingival tissue. In this study, we construct 3DGT model as an invitro tool, by seeding HGF cells in engineered GelMA-SA composites to represent connective tissue. It has long been known that connective tissue underlying epithelia not only supports growth but also regulates differentiation of the epithelia (376). Therefore, such models should consist of both epithelium and connective tissue. For the generating such a model, we added HGE cells over the fibroblasts populated hydrogel samples. In this study we constructed this model in two different ways. The first way is by

keeping the model inside well plate and submersed by mixture of HGF and HGE cells medium. This method is considering the easier for crosslinking of hydrogel samples, at the same time ensure keeping medium arrived the cells.

The second method of constructing 3DGT model by using cell culture insert, followed by lifting the last model in ALI for 14 days. For both methods, we assessed the suitability of the 3DGT as an invitro model to evaluate biological characterization of GelMA-SA composites, and at histological level with the later method. We focused on model structures of generated epithelial layer and their associated underlying fibroblasts populated matrix.

The findings of this study highlighted critical challenges in the fabrication of 3DGT models using different hydrogel compositions. The results of this study suggested that the use of cell culture inserts may have influenced the structural integrity and cellular behavior within the engineered 3DGT models (377, 378). Constructs made with GelMA or R collagen hydrogels experienced melting, which may be attributed to suboptimal mechanical support provided by the inserts. Unlike well plates, which offer a stable and non-porous surface, inserts contain a permeable membrane that may have affected the gel's attachment, crosslinking efficiency, and overall stability. This could have impacted the ability of the hydrogel to maintain its 3D structure, affecting subsequent cellular interactions (379). Histological analysis of the GelMA-SA composite-based 3DGT models, stained with hematoxylin and eosin (H&E), demonstrated a uniform distribution of HGF cells within the 3D structure. However, the lack of characteristic cytoplasmic projections observed in normal gingival tissue suggests potential limitations in cell-matrix interactions or insufficient matrix stiffness to promote proper cellular morphology (380-382). While some fibroblasts adhered to the dermal surface, only a few exhibited migratory behavior, indicating that the scaffold composition and crosslinking strategy may influence cell motility and matrix penetration (382). The epithelial layer formation within the GelMA-SA composite models revealed a multilayered regenerated epithelium, which resembled the non-keratinized junctional epithelium found in vivo. However, the absence of a keratinized superficial layer suggests that the differentiation of oral keratinocytes within the

construct was suboptimal (383). Among the different GelMA-SA composite formulations, GelMA-SAL/UV/CaCl₂ demonstrated the highest number of epithelial layers compared to GelMA-SAH/CaCl₂/UV and GelMA-SAH/UV/CaCl₂ models. This indicates that the incorporation of sodium alginate (SAL) and the specific crosslinking approach may contribute to improved epithelial stratification. Furthermore, lifting the insert to establish an ALI may have contributed to variations in epithelial layer formation (149, 383). In this study, and while ALI conditions are known to promote epithelial differentiation, the histological findings revealed poor adhesion and differentiation of oral keratinocytes. This suggests that either the GelMA-SA hydrogel system was not fully compatible with the insert-based ALI approach, or the transition from submerged to ALI culture affected cell behavior due to mechanical stress or inadequate matrix support. The poor transition from cuboidal to squamous epithelial cells observed in these models may be linked to insufficient attachment of the hydrogel to the insert membrane, resulting in reduced stability and altered epithelial-mesenchymal interactions (384).

In contrast to previous studies (385-387), our observations indicated that constructing the 3D gingival tissue (3DGT) model using well plates instead of transwell inserts may provide a more stable environment for GelMA-SA hydrogels. These findings significantly contribute to the optimisation of the 3DGT model by demonstrating how culture platform architecture influences hydrogel performance and epithelial stratification. Specifically, this study compared the conventional transwell insert system with air liquid interface (ALI) culture to a simplified well plate based submerged system using a mixture of fibroblast and epithelial medium. While the ALI model produced superior epithelial stratification and structural organisation, closely resembling native gingival tissue, the submerged model in standard well plates proved to be a more cost effective and technically feasible alternative. The absence of specialised inserts or permeable membranes in the well plate method improved hydrogel adhesion and handling during fabrication. This comparison highlights the trade-offs between biological fidelity and experimental practicality and provides a framework for selecting

culture methods tailored to specific research objectives. Ultimately, these findings broaden the utility of the 3DGT model by offering an accessible and scalable platform for studying periodontal regeneration, drug delivery, and host–pathogen interactions.

CHAPTER 8

8. GENERAL DISCUSSION

The preceding chapters in this thesis have presented the results of five pieces of research. These five projects were collectively designed to investigate the possibilities of constructing a developed 3D gingival model. Developed 3D gingival model could recapitulate the microenvironment of human gingival tissue within two different conditions, healthy or diseased.

Chapters 1 of this thesis have presented the study hypotheses and research questions. The hypothesis proposed in this thesis was that "the possibility to construct a developed 3D gingival model as an advanced in-vitro tool. In addition, research hypothesis and questions have been formulated to address the knowledge gaps identified in the review of the literature.

In Chapter 3, which was the systematic review aimed to appraise current available 3D in vitro gingival models. At the same time, we had to determine the available substrates that are used successfully in reconstruction of this model. This systematic review presented the research conducted to answer the research question. This review analysed 37 different 3D gingival and peri-implant models from 22 studies. Twelve models showed good cell proliferation (Ki67 marker) in basal and suprabasal layers, and most demonstrated epithelial cell differentiation (various CK markers). However, no single model emerged as the best for studying 3D gingival or peri-implant tissues. This systematic review identified various gingival models which have been developed using primary cells, immortalized cell lines, or both. Models derived from primary cells formed the most epithelial layers, whereas those using H357 and OSCC cell lines lacked well-differentiated epithelium. One study successfully created a multi-layered model from immortalized primary human gingival cells (E6/E7 HPV-induced), suggesting that not all cell lines are suitable for model construction. Additionally,

greater clarity is needed when reporting cell-line-based models, as these cells inherit traits from their parent tissues but may not fully replicate normal epithelial behavior.

Substrate selection is crucial for gingival model construction, requiring biocompatibility, porosity, and mechanical stability. Ten different substrates were reviewed, with most being animal derived. Rat tail collagen type I was the most used, supporting epithelial stratification but prone to shrinkage, high cost, and structural differences from human ECM. Crosslinking with genipin/cytochalasin D improved shrinkage resistance and cell survival. Other animal-based substrates, including bovine and porcine collagen, showed promise but lacked resemblance to native gingival connective tissue. Dermal substrates (acellular cadaveric dermis, decellularized dermis, and bovine, porcine, and human-derived matrices) supported keratinocyte proliferation and fibroblast distribution but were limited in availability. DRT, a crosslinked bovine tendon collagen matrix, produced thicker tissue layers and better cell proliferation than equine and synthetic alternatives. Electrospun crosslinked bovine collagen was also used for a peri-implant gingival model, reducing tissue contraction. However, all substrates exhibited limitations in replicating native gingival properties.

Overall, the evidence highlighted high heterogeneity, and lack of standardized fabrication and characterization protocols for the creation of a valid 3D gingival or peri-implant model. We, therefore, propose a new framework for future characterization and construction of a 3D gingival model. The first step should include histological confirmation that the new model results in well-defined stratified epithelium layers with equal or more than four cell layers, and fibroblasts embedded and distributed homogenously in a well-structured substrate. Secondly well differentiated tissue layers should be confirmed via specific markers expression for each cell or layer regions, as following:

- Ki67 for cell proliferation near basal epithelial layer
- CK14 and CK5 for early differentiation in the basal layer and CK4 or CK13 in the suprabasal layer.

- CK16, CK18, CK19 and CK17 in different epithelial layers as late differentiation markers
- Involucrin as terminal differentiation marker for keratinocytes within the upper two third of the epithelium
- CK10 marker to confirm the presence of cornifying stratified epithelia as well as in proliferating epithelia
- Collagen IV and Laminin expression for the basement membrane
- CD90 and Collagen (I and II) in ECM
- Vimentin expression to confirm development of fibroblasts.

Thirdly an ideal 3D gingival model to use for different dental applications will need a well-developed vascular structure including capillary vessels, epithelial and stromal cells as well as immune, neural and bone cells

Future research should aim at resolving the current challenges of construction a developed vascularized 3D gingival model mimic native human gingival tissue by engineering a new substrate with a high remodeling activity and suitable microenvironment for seeding human gingival cells. The result from this systematic review showed that rat tail collagen type I is considered a more frequent substrate used for 3D gingival mode construction. However, this substrate has several disadvantages, for example, this substrate is expensive, and isolated rat tail collagen is invariably fragmented in addition to difficult manipulation in the lab (305). Therefore, it's important to prepare an alternative suitable substrate for 3D gingival model construction that recapitulates native human ECM. Moreover, the alternative substrate should be cost-effective and easily scalable from laboratory production.

Therefore, and for engineering a novel substrate, additional projects should be contributed for reaching our goals. Chapters 5, 6 and 7 presented projects that provided a result of investigation of several candidate hydrogel biomaterials.

Starting with Chapter 4, which has provided some novel insight into the characterization and molecular mechanisms of gingival tissues and suggest that the onset of periodontists may have a bias through non-hereditary pathways. In conclusion, this study compared gene expression profiles between diseased and healthy tissues from human gingiva. The two types of tissue expressed the same specific genes related to their functions with non-significant differences. In addition to provide the potential molecular mechanisms concerning periodontal tissue wound healing and regeneration. The knowledge generated from this study demonstrated some novel insight into the characterization gingival tissues for both healthy and pathological situations. Results from this project provide evidence to support our hypothesis, which based on possibility to developed 3D gingival model, which could be used to describe native human gingival structures in both conditions, healthy and diseased. Such a model could serve as a valuable platform for studying disease mechanisms, testing novel therapeutic strategies, and evaluating biomaterials in a physiologically relevant environment, thereby reducing reliance on animal models and improving the translational relevance of research findings.

The development of a physiologically relevant 3D gingival model forms the foundation for advancing our understanding of gingival biology and pathology. To achieve a model that accurately mimics native tissue structure and function, the selection of an appropriate biomaterial is essential. Therefore, in Chapter 5 the subsequent phase of this research a range of hydrogels with diverse biochemical and mechanical properties was investigated to identify those capable of supporting cell viability, tissue organisation, and extracellular matrix deposition. This systematic evaluation formed the basis for selecting the most suitable hydrogels for incorporation into the 3D gingival construct, ensuring its relevance for studying both healthy and diseased conditions. The findings included an investigation of candidate hydrogel biomaterials, where H-NMR analysis confirmed successful GelMA synthesis from bovine origin gelatin, with chemical variations influenced by the gelatin species origin source. The candidate hydrogel biomaterials were with different concentrations, and these were Gel, GelMAc,

GelMA, SA, in addition to R collagen. Results of investigation revealing that increased concentration reduced pore size but weakened mechanical strength, affecting cell behaviours. FTIR analysis showed weak intermolecular interactions in low-concentration samples, influenced by solvent type. Water contact angle measurements confirmed their hydrophilic nature, with low values compared to commercial tissue culture materials. DSC analysis indicated that solvent type and gelatin source affected melting points, impacting hydrogel stability. The melting point value of porcine origin gelatin, GelMAc was high compared with GelMA which were from bovine origin gelatin. However, this result confirmed the effect of gelatin source on the strength of GelMA hydrogel structure (342, 343). Rheological tests demonstrated higher viscosity and elastic modulus in highconcentration samples, confirming stronger network structures. However, hydrogel mechanical properties were lower than native gingival tissue, making them unsuitable for 3D gingival models. As a systematic review highlighted rat tail collagen as a common but costly and impractical substrate, emphasizing the need for alternatives. To enhance hydrogel suitability, mechanical properties must be tuned through crosslinking methods such as UV or thermal treatment, or by adding an aqueous solution of Ca2+ using calcium chloride to improve cell interactions and scaffold strength.

According to the results from the previous project, an additional project should be done to achieve our goals in construct a novel substrate. These results attributed to the presence of gap or missing information about the characterization of hydrogel biomaterial samples. Therefore, additional project had been established and all detailed have been in Chapter 6. We hypothesized that the mechanical and biological properties of GelMA-SA composite hydrogels could be tuned using single or double crosslinking methods. Due to ethical and practical challenges in obtaining human gingival tissue, we compared our novel composite with animal gingival samples. Our findings suggest these composites can regulate human gingival fibroblast behavior within a 3D gingival model.

SEM analysis revealed collagen fiber networks in animal samples and rat tail hydrogel after overnight incubation, highlighting the importance of incubation time

for complete gelation. Pore size analysis showed lower mechanical properties in low-concentration samples, with GelMA-SA hydrogel pore sizes aligning with those of human gingival tissue.

FT-IR spectroscopy indicated strong SA-GelMA interactions, with higher concentrations showing increased peak intensities. Spectral differences in animal tissues suggested higher protein content in sheep gingiva compared to porcine tissue, closely resembling human gingival tissue characteristics.

Water contact angle measurements demonstrated hydrophobicity in GelMA and GelMA-SA hydrogels crosslinked via UV, whereas others were hydrophilic. Animal gingival samples were hydrophilic due to epithelial layer removal. These findings emphasize the role of crosslinking in modifying hydrogel surface properties for tissue compatibility.

DSC analysis revealed higher melting points in hydrogels compared to rat tail collagen, with higher concentrations exhibiting stronger intermolecular bonds. Double crosslinking reduced water retention, enhancing mechanical stability. Among methods, CaCl₂/UV crosslinking provided greater thermal stability, making it suitable for applications requiring structural integrity.

Rheological studies confirmed that increased alginate concentration enhanced hydrogel viscosity, with double crosslinking forming a stronger network. Mechanical properties of GelMA-SA hydrogels aligned with those of animal gingival tissues, with SA concentration and crosslinking sequence influencing viscoelastic behavior. The mechanical properties of the developed GelMA-SA hydrogels were comparable to those of native gingival and mucosal tissues, underscoring their potential suitability for oral tissue engineering applications. Variations in elastic modulus among formulations reflected the influence of SA concentration and crosslinking sequence, with double UV/CaCl₂ crosslinking producing stiffer, more structurally stable composites. These findings highlight the importance of optimising both material composition and fabrication strategy to achieve physiologically relevant mechanical characteristics in 3D gingival models.

Biodegradability assessment showed higher degradation rates for CaCl₂/UV crosslinked hydrogels after day 7, whereas UV/CaCl2 crosslinked samples remained stable for the day 14. This highlights the tunable degradation properties of GelMA-SA composites, making them viable for applications requiring controlled biodegradability in tissue engineering. The biodegradability results further emphasized the significant influence of the crosslinking sequence on the stability of the fabricated composite hydrogels. Notably, the UV/CaCl₂ crosslinking approach improved the stability of the GelMA-SA composite hydrogel, facilitating its fabrication into predesigned structures. This feature is particularly essential in tissue engineering, where maintaining a balance between biomaterial degradation and tissue regeneration remains a critical challenge (388, 389). Furthermore, the degradability of biomaterials can be modulated to align with the remodeling rate of the target tissue, ensuring optimal integration and function (388, 390). These findings highlight that the GelMA-SA composite hydrogel exhibits tunable degradation properties, making it a promising candidate for applications requiring customized degradation periods specific to different tissues (375).

The results highlight the biocompatibility and favorable mechanical properties of GelMA-SA hydrogels, making them ideal for 3D cell culture. Their tunable degradation rates and ability to support HGF cell survival suggest their potential for periodontal and soft tissue regeneration as well as drug delivery applications. Building on the findings from the Chapter 6, where individual hydrogels and GelMA-SA composite hydrogels crosslinked using a single technique were evaluated and found to possess suboptimal mechanical and biocompatible properties for supporting a 3D gingival tissue model. Therefore, in Chapter 7, GelMA-SA composite hydrogels prepared using a double crosslinking technique for further investigation. In this chapter, we hypothesized that the properties of GelMA-SA composite hydrogels fabricated using a double crosslinking method could be further optimized by selecting an appropriate sterilization technique. This project was focused on fabricated and characterized a GelMA-SA composite hydrogel (GelMA-SAH/UV/CaCl₂, GelMA-SAL/UV/CaCl₂, GelMA-SAH/CaCl₂/UV,

and GelMA-SAL/CaCl₂/UV), and its mechanical properties and biocompatibility. Sterilization plays a crucial role in hydrogel biomaterials for tissue engineering, affecting biomechanical properties. This study evaluates filtration and ethanol sterilization methods on GelMA-SA hydrogels, which mimic the ECM of gingival tissue.

SEM imaging showed larger pore sizes in low-concentration hydrogels and smaller pores in ethanol-sterilized samples. The pore sizes of GelMA-SA hydrogels fell within the 30–80 µm range, aligning with human gingival tissue.

FT-IR analysis indicated stronger intermolecular interactions in high-concentration hydrogels, with filtration-sterilized samples showing higher peak intensities. Spectral analysis revealed biochemical similarities between sterilized hydrogels and human oral tissue. Water contact angle measurements showed UV/CaCl2-crosslinked hydrogels exhibited hydrophobicity, similar to gingival surfaces. DSC analysis demonstrated higher melting points in high-concentration hydrogels and ethanol-sterilized samples, emphasizing the impact of crosslinking and sterilization on thermal properties.

Rheological tests confirmed shear-thinning behavior, with increased viscosity at lower temperatures. Ethanol-sterilized hydrogels exhibited higher viscoelastic values, highlighting the sterilization method's effect on mechanical properties. DMA analysis showed predominantly elastic behavior, with ethanol-sterilized samples having higher stiffness values. Biodegradation studies indicated weight loss variations based on concentration, crosslinking, and sterilization. Filtration-sterilized hydrogels maintained higher metabolic activity and lower LDH release, preserving biological functionality better than ethanol-sterilized samples. Confocal imaging confirmed higher cell viability in filtration-sterilized hydrogels during 3D culture, underscoring its efficacy in maintaining biological activity.

Moreover, the findings emphasized the biocompatibility of hydrogel samples tested using a single cell type, HGFs. However, to develop an engineered scaffold suitable for constructing a 3D gingival model, the novel composite hydrogel must demonstrate biocompatibility with all types of human gingival cells, such as

human gingival epithelial and endothelial cells. Therefore, for our future studies, we will further investigate the properties of GelMA, SA, and GelMA-SA hydrogels in greater detail, employing filtration as a sterilization technique. This approach aims to confirm the suitability of the novel GelMA-SA composite hydrogel for supporting human gingival cells and its potential for constructing a 3D gingival model.

These findings highlight the influence of sterilization, hydrogel concentration, and crosslinking on the structural, mechanical, and biological properties of GelMA-SA hydrogels, essential for optimizing their application in gingival tissue engineering. In a conclusion, the results revealed that hydrogels sterilized using the ethanol method exhibited superior mechanical properties compared to those sterilized via filtration. Additionally, hydrogels crosslinked with CaCl₂ followed by UV irradiation demonstrated enhanced mechanical properties compared to those crosslinked in the reverse order (UV followed by CaCl₂), highlighting the significant impact of both sterilization techniques and crosslinking sequences on the material's properties. However, HGFs displayed higher viability when seeded in filtered hydrogels compared to ethanol-sterilized samples. These findings underscore the importance of optimizing both sterilization methods and crosslinking strategies to improve the suitability of GelMA-SA hydrogels for supporting human gingival cell growth, ultimately contributing to the development of advanced 3D human gingival cell cultures.

Following the selection of filtration as the preferred sterilization method for the GelMA-SA composite hydrogels, we proceeded to assess their potential as a novel carrier for human gingival epithelial cell seeding

In this chapter also, we discussed the biocompatibility of the GelMA-SA composite hydrogels in comparison to R collagen and GelMA hydrogel samples using human gingival epithelial (HGE) cells. All GelMA-SA composite hydrogel formulations were included in this investigation, except for the GelMA-SAL/CaCl₂/UV sample. This particular formulation demonstrated significantly reduced biological performance, rapid degradation, and inferior mechanical

properties when compared to the GelMA-SAH/CaCl₂/UV hydrogel. These limitations underscored its unsuitability for periodontal and soft tissue regeneration applications. Therefore, it was excluded from subsequent analyses to allow a focused evaluation of materials that better meet the functional requirements of the intended 3D gingival tissue model. The results demonstrated that HGE cells exhibited reduced metabolic activity when cultured within GelMA and R collagen hydrogels compared to those cultured in GelMA-SAH composite hydrogels. However, a decline in metabolic activity was observed in HGE cells within the GelMA-SAH/CaCl₂/UV hydrogels relative to those in GelMA-SAH/UV/CaCl₂ and GelMA-SAL/UV/CaCl₂ hydrogels. This reduction may be attributed to the higher biodegradation rate associated with the GelMA-SAH/CaCl₂/UV formulation.

As discussed in a later stage of this study, the GelMA-SA composite hydrogels demonstrated excellent biocompatibility, supporting the viability of both HGFs and HGE cells over a 14-day culture period, as confirmed by live/dead staining and MTS assays. These findings are consistent with previous reports highlighting the high cell compatibility of GelMA-based hydrogels (200, 203). Notably, the incorporation of SA appeared to enhance the structural stability of the hydrogel without negatively impacting cell survival. Additionally, the elastic modulus of the optimized GelMA-SA composite was comparable to that of native gingival connective tissue, supporting its mechanical suitability for gingival tissue engineering applications. The favorable mechanical properties, combined with the ability to support 3D cell culture, underscore the potential of these composites in regenerative dentistry. Furthermore, depending on the sequence of the double crosslinking approach used during fabrication, the hydrogels exhibited tunable degradation rates along with modifiable mechanical and biocompatibility characteristics. These results position the GelMA-SA composite hydrogels as strong candidates for periodontal and soft tissue regeneration, as well as for drug delivery systems designed to enhance tissue repair.

Building on these findings, the next phase of the study focused on constructing and evaluating a 3D gingival tissue model using the optimized GelMA-SA

composites as a scaffold for co-culturing human gingival fibroblasts and epithelial cells, aiming to replicate the structural and functional features of native gingival tissue. Moreover, understanding periodontal disease pathology requires in vitro models that replicate gingival tissue mechanisms. Therefore, in this study, we developed a 3DGT model by seeding HGF cells in GelMA-SA composites to simulate connective tissue, followed by the addition of HGE cells to mimic the epithelial layer. Two approaches were used: (1) submerged culture in well plates and (2) an air-liquid interface (ALI) setup using cell culture inserts.

Our findings highlight key challenges in 3DGT model fabrication. Constructs in cell culture inserts showed compromised stability, with GelMA and R collagen hydrogels experiencing melting, likely due to inadequate mechanical support. Unlike well plates, inserts have a permeable membrane, which may have disrupted gel attachment, crosslinking, and structural integrity, affecting cellular interactions.

Histological analysis of GelMA-SA-based 3DGT models (H&E staining) revealed uniform HGF distribution but limited cell-matrix interactions, indicated by the absence of cytoplasmic projections. While some fibroblasts adhered to the surface, cell migration and matrix penetration were minimal, suggesting that hydrogel composition and crosslinking strategy influence cellular behavior. The epithelial layer formed in GelMA-SA composite models resembled non-keratinized junctional epithelium, but the absence of a keratinized superficial layer suggests suboptimal keratinocyte differentiation. Among the different formulations, GelMA-SAL/UV/CaCl₂ exhibited the highest epithelial stratification, indicating that SAL incorporation and double crosslinking may enhance epithelial development. However, ALI conditions led to poor epithelial adhesion and differentiation, possibly due to mechanical stress or inadequate matrix support. The limited transition from cuboidal to squamous epithelial cells suggests that hydrogel-insert attachment issues may have impacted epithelial-mesenchymal interactions.

Our results suggest that well plates provide a more stable environment for GelMA-SA hydrogels, likely due to improved adhesion, crosslinking, and

mechanical stability, supporting better epithelial layer formation. Future studies should explore alternative culture methods, insert modifications, or optimized hydrogel formulations to improve 3DGT model development under ALI conditions. In a conclusion, these results demonstrate that the GelMA-sodium alginate (GelMA-SAH/UV/CaCl₂, GelMA-SAL/UV/CaCl₂, GelMA-SAH/CaCl₂/UV, and GelMA-SAL/CaCl₂/UV) composite scaffolds exhibit mechanical properties comparable to those of human gingival tissue. The biocompatibility of these hydrogels was confirmed through cell culture experiments, taking into account the concentration of sodium alginate (SA) in the formulation of the GelMA-SA composites. These biomechanical properties are well-suited to support the survival of human gingival fibroblasts and human gingival epithelial cells by providing a microenvironment that closely mimics the native extracellular matrix of human gingival tissue. Consequently, GelMA-SA composites are anticipated to serve as a promising new scaffold material in the field of 3D periodontal tissue engineering. While the GelMA-SA composites provided a more stable scaffold for 3DGT models compared to GelMA or R collagen hydrogels, limitations in fibroblast migration, epithelial adhesion, and differentiation remain key challenges.

Conclusion, Limitations, and Future Directions

This thesis investigated the development and characterization of 3D gingival tissue (3DGT) models using GelMA-SA composite hydrogels, with the aim of reproducing key structural and functional features of native gingiva. The study demonstrated that hydrogel concentration, crosslinking strategy, and sterilisation method significantly influenced scaffold physicochemical properties, mechanical behaviour, and cell compatibility. Spatial transcriptomic analysis further provided insights into the molecular profiles of healthy and diseased gingival tissues, identifying potential targets for improving tissue-engineered models. Collectively, these findings establish a foundation for designing hydrogels with tunable properties for application in gingival tissue engineering and periodontal research.

Despite the promising outcomes, this study has several limitations that should be acknowledged. First, the 3DGT models lack vasculature, which is a critical component of native gingival tissue for nutrient delivery, waste removal, and regulation of inflammatory responses. Without a vascular network, the model may not fully recapitulate physiological gradients or the dynamic cell–cell interactions present in vivo. Second, immune components such as resident immune cells and infiltrating leukocytes are absent, limiting the model's ability to mimic host–microbe interactions and the complex immune response characteristic of periodontal disease. Third, the study was limited to short- and mid-term assessments, whereas long-term stability, degradation, and functional performance of the scaffolds under physiologic conditions remain untested.

Addressing these limitations in future work by incorporating vascularization strategies, co-cultures with immune cells, and extended culture or implantation studies will be essential to develop models that more closely replicate the native gingival microenvironment. Moreover, future optimization efforts should focus on improving hydrogel mechanical properties, enhancing bioactivity, and integrating more physiologically relevant culture conditions to achieve a fully functional 3DGT model that constructed using cell culture insert. The next step for future study, is constructing 3D gingival model using GelMA-SA composite based on well plate rather than cell culture insert. This method will enable getting proper and easier way to crosslinking GelMA-SA composite scaffolds. This could offer construction developed 3D gingival model.

REFERENCES:-

- 1. Garant PR, Garant P. Oral cells and tissues: Quintessence Publishing Company Chicago, IL, USA:; 2003.
- 2. Lang NP, Berglundh T, Giannobile WV, Sanz M. Lindhe's clinical periodontology and implant dentistry: John Wiley & Sons; 2021.
- 3. Kabakov L, Nemcovsky CE, Plasmanik-Chor M, Meir H, Bar DZ, Weinberg E. Fibroblasts from the oral masticatory and lining mucosa have different gene expression profiles and proliferation rates. J Clin Periodontol. 2021 Oct;48(10):1393-1401. doi: 10.1111/jcpe.13532. Epub 2021 Aug 23. PMID: 34409631.
- 4. Chen Y, Gao B, Cai W, Lai J, Lai K, Wang Y. Oral mucosa: anti-inflammatory function, mechanisms, and applications. J Mater Chem B. 2025 Mar 26;13(13):4059-4072. doi: 10.1039/d4tb02845g. PMID: 40062381.
- 5. Duan Y, Liang Y, Yang F, Ma Y. Neural Regulations in Tooth Development and Tooth-Periodontium Complex Homeostasis: A Literature Review. Int J Mol Sci. 2022 Nov 16;23(22):14150. doi: 10.3390/ijms232214150. PMID: 36430624; PMCID: PMC9698398.
- 6. Carvalho BAS, Duarte CAB, Silva JF, Batista WWDS, Douglas-de-Oliveira DW, de Oliveira ES, Soares LG, Galvão EL, Rocha-Gomes G, Glória JCR, Gonçalves PF, Flecha OD. Clinical and radiographic evaluation of the Periodontium with biologic width invasion. BMC Oral Health. 2020 Apr 16;20(1):116. doi: 10.1186/s12903-020-01101-x. PMID: 32299404; PMCID: PMC7164352.
- 7. Ibáñez-Cortés M, Martín-Piedra MÁ, Blanco-Elices C, García-García ÓD, España-López A, Fernández-Valadés R, Sánchez-Quevedo MDC, Alaminos M, Chato-Astrain J, Garzón I. Histological characterization of the human masticatory oral mucosa. A histochemical and immunohistochemical study. Microsc Res Tech. 2023 Dec;86(12):1712-1724. doi: 10.1002/jemt.24398. Epub 2023 Aug 31. PMID: 37650503.
- 8. Garrod D, Chidgey M. Desmosome structure, composition and function. Biochim Biophys Acta. 2008 Mar;1778(3):572-87. doi: 10.1016/j.bbamem.2007.07.014. Epub 2007 Aug 9. PMID: 17854763.
- 9. Groeger SE, Meyle J. Epithelial barrier and oral bacterial infection. Periodontol 2000. 2015 Oct;69(1):46-67. doi: 10.1111/prd.12094. PMID: 26252401.
- 10. Francis DL, Reddy SSP, Yadalam PK. Reconceptualizing gingival keratinization: from epithelial autonomy to artificial intelligence-driven therapeutic planning. Odontology. 2025 Sep 13. doi: 10.1007/s10266-025-01197-z. Epub ahead of print. PMID: 40940557.
- 11. Newman MG, Takei H, Klokkevold PR, Carranza FA. Newman and Carranza's Clinical Periodontology E-Book: Newman and Carranza's Clinical Periodontology E-Book: Elsevier Health Sciences; 2018.
- 12. Nakamura M. Histological and immunological characteristics of the junctional epithelium. Jpn Dent Sci Rev. 2018 May;54(2):59-65. doi:

- 10.1016/j.jdsr.2017.11.004. Epub 2017 Dec 7. PMID: 29755616; PMCID: PMC5944073.
- 13. Lodish HF, Berk A, Kaiser C, Krieger M, Bretscher A, Ploegh HL, et al. Molecular cell biology: WH Freeman New York; 2021.
- 14. Li A, Chen Y, Schuller AA, van Der Sluis LW, Tjakkes GHE. Dietary inflammatory potential is associated with poor periodontal health: A population-based study. Journal of Clinical Periodontology. 2021;48(7):907-18.
- 15. Sandros J, Papapanou P, Nannmark U, Dahlen G. Porphyromonas gingivalis invades human pocket epithelium in vitro. Journal of periodontal research. 1994;29(1):62-9.
- 16. Belibasakis GN, Meier A, Guggenheim B, Bostanci N. The RANKL-OPG system is differentially regulated by supragingival and subgingival biofilm supernatants. Cytokine. 2011;55(1):98-103.
- 17. Nakamura M. Histological and immunological characteristics of the junctional epithelium. Japanese Dental Science Review. 2018;54(2):59-65.
- 18. Li LT, Jiang G, Chen Q, Zheng JN. Ki67 is a promising molecular target in the diagnosis of cancer. Molecular medicine reports. 2015;11(3):1566-72.
- 19. Lu EM-C, Ratnayake J, Rich AM. Assessment of proliferating cell nuclear antigen (PCNA) expression at the invading front of oral squamous cell carcinoma. BMC oral health. 2019;19:1-7.
- 20. Arun R, Hemalatha R, Arun K, Kumar T. E-cadherin and CD1a expression in gingival epithelium in periodontal health, disease and post-treatment. Indian Journal of Dental Research. 2010;21(3):396.
- 21. Moll R, Divo M, Langbein L. The human keratins: biology and pathology. Histochemistry and cell biology. 2008;129:705-33.
- 22. Bosch FX, Ouhayoun J-P, Bader BL, Collin C, Grund C, Lee I, Franke WW. Extensive changes in cytokeratin expression patterns in pathologically affected human gingiva. Virchows Archiv B. 1989;58:59-77.
- 23. Pöllänen MT, Salonen JI, Uitto VJ. Structure and function of the tooth–epithelial interface in health and disease. Periodontology 2000. 2003;31(1):12-31.
- 24. Alam H, Sehgal L, Kundu ST, Dalal SN, Vaidya MM. Novel function of keratins 5 and 14 in proliferation and differentiation of stratified epithelial cells. Molecular biology of the cell. 2011;22(21):4068-78.
- 25. Groeger S, Meyle J. Oral mucosal epithelial cells. Frontiers in immunology. 2019;10:208.
- 26. Jiang Q, Yu Y, Ruan H, Luo Y, Guo X. Morphological and functional characteristics of human gingival junctional epithelium. BMC Oral Health. 2014 Apr 3;14:30. doi: 10.1186/1472-6831-14-30. PMID: 24708739; PMCID: PMC4234347.
- 27. Furue M. Regulation of filaggrin, loricrin, and involucrin by IL-4, IL-13, IL-17A, IL-22, AHR, and NRF2: pathogenic implications in atopic dermatitis. International journal of molecular sciences. 2020;21(15):5382.
- 28. El Ghalbzouri A, Ponec M. Diffusible factors released by fibroblasts support epidermal morphogenesis and deposition of basement membrane components. Wound repair and regeneration. 2004;12(3):359-67.

- 29. Kandikonda S, Oda D, Niederman R, Sorkin BC. Cadherin-mediated adhesion is required for normal growth regulation of human gingival epithelial cells. Cell Adhesion and Communication. 1996;4(1):13-24.
- 30. Hatakeyama S, Yaegashi T, Oikawa Y, Fujiwara H, Mikami T, Takeda Y, Satoh M. Expression pattern of adhesion molecules in junctional epithelium differs from that in other gingival epithelia. Journal of periodontal research. 2006;41(4):322-8.
- 31. Thacher SM, Rice RH. Keratinocyte-specific transglutaminase of cultured human epidermal cells: relation to cross-linked envelope formation and terminal differentiation. Cell. 1985;40(3):685-95.
- 32. Ta BM, Gallagher GT, Chakravarty R, Rice RH. Keratinocyte transglutaminase in human skin and oral mucosa: cytoplasmic localization and uncoupling of differentiation markers. Journal of Cell Science. 1990;95(4):631-8.
- 33. Smith SA, Dale BA. Immunologic localization of filaggrin in human oral epithelia and correlation with keratinization. Journal of investigative dermatology. 1986;86(2):168-72.
- 34. Kantarci A, Nseir Z, Kim Y-S, Sume S, Trackman P. Loss of basement membrane integrity in human gingival overgrowth. Journal of dental research. 2011;90(7):887-93.
- 35. Holle J, Kunstfeld R. The influence of fibroblasts on the differentiation of cultured epithelial cells in vitro. Plastic and reconstructive surgery. 2004;114(2):599.
- 36. Ivaska J, Pallari H-M, Nevo J, Eriksson JE. Novel functions of vimentin in cell adhesion, migration, and signaling. Experimental cell research. 2007;313(10):2050-62.
- 37. Alberts B. Molecular biology of the cell: Garland science; 2017.
- 38. Häkkinen L, Larjava H, Fournier BP. Distinct phenotype and therapeutic potential of gingival fibroblasts. Cytotherapy. 2014;16(9):1171-86.
- 39. Bartold PM, Walsh LJ, Narayanan AS. Molecular and cell biology of the gingiva. Periodontology 2000. 2000;24(1):28-55.
- 40. Birkedal-Hansen H. Role of matrix metalloproteinases in human periodontal diseases. Journal of periodontology. 1993;64:474-84.
- 41. Moharamzadeh K, Brook I, Van Noort R, Scutt A, Smith K, Thornhill M. Development, optimization and characterization of a full-thickness tissue engineered human oral mucosal model for biological assessment of dental biomaterials. Journal of Materials Science: Materials in Medicine. 2008;19:1793-801.
- 42. Ramamoorthi M, Bakkar M, Jordan J, Tran SD. Osteogenic potential of dental mesenchymal stem cells in preclinical studies: a systematic review using modified ARRIVE and CONSORT guidelines. Stem cells international. 2015;2015.
- 43. Nanci, A. and Causa, H. (2018) Ten Cate's Oral Histology Development, Structure, and Function. 9th Edition, Elsevier, St. Louis.
- 44. Lang, Niklaus P., and Jan Lindhe, eds. *Clinical periodontology and implant dentistry, 2 Volume Set.* John Wiley & Sons, 2015.
- 45. Saffar JL, Lasfargues JJ, Cherruau M. Alveolar bone and the alveolar process: the socket that is never stable. Periodontol 2000. 1997;13:76-90.

- 46. Sokos D, Everts V, de Vries TJ. Role of periodontal ligament fibroblasts in osteoclastogenesis: a review. J Periodontal Res. 2015;50(2):152-9.
- 47. Bosshardt DD, Stadlinger B, Terheyden H. Cell-to-cell communication-periodontal regeneration. Clin Oral Implants Res. 2015;26(3):229-39.
- 48. Nanci A, Bosshardt DD. Structure of periodontal tissues in health and disease. Periodontol 2000. 2006;40:11-28.
- 49. Foster BL, Soenjaya Y, Nociti FH, Jr., Holm E, Zerfas PM, Wimer HF, et al. Deficiency in acellular cementum and periodontal attachment in bsp null mice. J Dent Res. 2013;92(2):166-72.
- 50. Suzuki M, Matsuzaka K, Yamada S, Shimono M, Abiko Y, Inoue T. Morphology of Malassez's epithelial rest-like cells in the cementum: transmission electron microscopy, immunohistochemical, and TdT-mediated dUTP-biotin nick end labeling studies. J Periodontal Res. 2006;41(4):280-7.
- 51. Finn R. Oral anatomy, histology and embryology, 6th edition. Br Dent J. 2024;237(11):834.
- 52. Li J, Parada C, Chai Y. Cellular and molecular mechanisms of tooth root development. Development. 2017;144(3):374-84.
- 53. Frost HM. Wolff's Law and bone's structural adaptations to mechanical usage: an overview for clinicians. Angle Orthod. 1994;64(3):175-88.
- 54. Zhao YQ, Zhou YH, Zhao J, Feng Y, Gao ZR, Ye Q, et al. Sex Variations in the Oral Microbiomes of Youths with Severe Periodontitis. Journal of Immunology Research. 2021;2021.
- 55. Rams TE, Listgarten MA, Slots J. Radiographic alveolar bone morphology and progressive periodontitis. Journal of Periodontology. 2018;89(4):424-30.
- 56. Albandar JM. Underestimation of periodontitis in NHANES surveys. Journal of periodontology. 2011;82(3):337-41.
- 57. Pihlstrom BL, Michalowicz BS, Johnson NW. Periodontal diseases. Lancet. 2005;366(9499):1809-20.
- 58. Kinane DF, Stathopoulou PG, Papapanou PN. Periodontal diseases. Nat Rev Dis Primers. 2017;3:17038.
- 59. Highfield J. Diagnosis and classification of periodontal disease. Aust Dent J. 2009;54 Suppl 1:S11-26.
- 60. Ohlrich E, Cullinan M, Seymour G. The immunopathogenesis of periodontal disease. Australian dental journal. 2009;54:S2-S10.
- 61. Kebschull M, Demmer R, Papapanou P. "Gum bug, leave my heart alone!"—epidemiologic and mechanistic evidence linking periodontal infections and atherosclerosis. Journal of dental research. 2010;89(9):879-902.
- 62. Belibasakis GN, Bostanci N. Inflammatory and bone remodeling responses to the cytolethal distending toxins. Cells. 2014;3(2):236-46.
- 63. West N, Chapple I, Claydon N, D'Aiuto F, Donos N, Ide M, et al. BSP implementation of European S3 level evidence-based treatment guidelines for stage I-III periodontitis in UK clinical practice. Journal of Dentistry. 2021;106:103562.
- 64. Chapple ILC, Mealey BL, Van Dyke TE, Bartold PM, Dommisch H, Eickholz P, et al. Periodontal health and gingival diseases and conditions on an intact and a reduced periodontium: Consensus report of workgroup 1 of the 2017 World

- Workshop on the Classification of Periodontal and Peri-Implant Diseases and Conditions. J Periodontol. 2018;89 Suppl 1:S74-s84.
- 65. Papapanou PN, Sanz M, Buduneli N, Dietrich T, Feres M, Fine DH, et al. Periodontitis: Consensus report of workgroup 2 of the 2017 World Workshop on the Classification of Periodontal and Peri-Implant Diseases and Conditions. Journal of Periodontology. 2018;89:S173-S82.
- 66. Caton JG, Armitage G, Berglundh T, Chapple ILC, Jepsen S, Kornman KS, et al. A new classification scheme for periodontal and peri-implant diseases and conditions Introduction and key changes from the 1999 classification. J Clin Periodontol. 2018;45 Suppl 20:S1-s8.
- 67. Tonetti MS, Greenwell H, Kornman KS. Staging and grading of periodontitis: Framework and proposal of a new classification and case definition. J Periodontol. 2018;89 Suppl 1:S159-s72.
- 68. Ridgeway EE. Periodontal disease: diagnosis and management. J Am Acad Nurse Pract. 2000;12(3):79-84.
- 69. Nazir MA. Prevalence of periodontal disease, its association with systemic diseases and prevention. Int J Health Sci (Qassim). 2017;11(2):72-80.
- 70. Albandar JM. Global risk factors and risk indicators for periodontal diseases. Periodontol 2000. 2002;29:177-206.
- 71. Brodzikowska A, Górski B. Polymorphisms in Genes Involved in Inflammation and Periodontitis: A Narrative Review. Biomolecules. 2022;12(4).
- 72. Graves D. Cytokines that promote periodontal tissue destruction. J Periodontol. 2008;79(8 Suppl):1585-91.
- 73. Van Dyke TE. Pro-resolving mediators in the regulation of periodontal disease. Mol Aspects Med. 2017;58:21-36.
- 74. Yucel-Lindberg T, Båge T. Inflammatory mediators in the pathogenesis of periodontitis. Expert Rev Mol Med. 2013;15:e7.
- 75. Abrahamian L, Pascual-LaRocca A, Barallat L, Valles C, Herrera D, Sanz M, et al. Intra- and inter-examiner reliability in classifying periodontitis according to the 2018 classification of periodontal diseases. J Clin Periodontol. 2022;49(8):732-9.
- 76. West N, Chapple I, Claydon N, D'Aiuto F, Donos N, Ide M, Needleman I, Kebschull M; British Society of Periodontology and Implant Dentistry Guideline Group Participants. BSP implementation of European S3 level evidence-based treatment guidelines for stage I-III periodontitis in UK clinical practice. J Dent. 2021 Mar;106:103562. doi: 10.1016/j.jdent.2020.103562. Epub 2021 Feb 8. PMID: 33573801.
- 77. Oh SL, Yang JS, Kim YJ. Discrepancies in periodontitis classification among dental practitioners with different educational backgrounds. BMC Oral Health. 2021;21(1):39.
- 78. Becker ST, Beck-Broichsitter BE, Graetz C, Dörfer CE, Wiltfang J, Häsler R. Peri-implantitis versus periodontitis: functional differences indicated by transcriptome profiling. Clin Implant Dent Relat Res. 2014;16(3):401-11.
- 79. Davanian H, Stranneheim H, Båge T, Lagervall M, Jansson L, Lundeberg J, Yucel-Lindberg T. Gene expression profiles in paired gingival biopsies from periodontitis-affected and healthy tissues revealed by massively parallel sequencing. PLoS One. 2012;7(9):e46440.

- 80. Demmer RT, Behle JH, Wolf DL, Handfield M, Kebschull M, Celenti R, et al. Transcriptomes in healthy and diseased gingival tissues. J Periodontol. 2008;79(11):2112-24.
- 81. Kim YG, Kim M, Kang JH, Kim HJ, Park JW, Lee JM, et al. Transcriptome sequencing of gingival biopsies from chronic periodontitis patients reveals novel gene expression and splicing patterns. Hum Genomics. 2016;10(1):28.
- 82. Lundmark A, Davanian H, Båge T, Johannsen G, Koro C, Lundeberg J, Yucel-Lindberg T. Transcriptome analysis reveals mucin 4 to be highly associated with periodontitis and identifies pleckstrin as a link to systemic diseases. Sci Rep. 2015;5:18475.
- 83. Lander ES, Weinberg RA. Genomics: journey to the center of biology. Science. 2000;287(5459):1777-82.
- 84. Mattick J, Amaral P. RNA, the Epicenter of Genetic Information: A new understanding of molecular biology. Abingdon (UK): CRC Press
- © 2023 John Mattick and Paulo Amaral.; 2022.
- 85. Moore PB. Structural motifs in RNA. Annu Rev Biochem. 1999;68:287-300.
- 86. Villarreal L, Witzany G. Self-empowerment of life through RNA networks, cells and viruses. F1000Res. 2023;12:138.
- 87. Cobb M. 60 years ago, Francis Crick changed the logic of biology. PLoS Biol. 2017;15(9):e2003243.
- 88. Crick F. Central dogma of molecular biology. Nature. 1970;227(5258):561-3.
- 89. Crick FH, editor On protein synthesis. Symp Soc Exp Biol; 1958.
- 90. Crick FH, Barnett L, Brenner S, Watts-Tobin RJ. General nature of the genetic code for proteins. Nature. 1961;192:1227-32.
- 91. Minchin S, Lodge J. Understanding biochemistry: structure and function of nucleic acids. Essays Biochem. 2019;63(4):433-56.
- 92. Raina M, Ibba M. tRNAs as regulators of biological processes. Front Genet. 2014;5:171.
- 93. Van Lint S, Heirman C, Thielemans K, Breckpot K. mRNA: From a chemical blueprint for protein production to an off-the-shelf therapeutic. Hum Vaccin Immunother. 2013;9(2):265-74.
- 94. Yum K, Wang ET, Kalsotra A. Myotonic dystrophy: disease repeat range, penetrance, age of onset, and relationship between repeat size and phenotypes. Curr Opin Genet Dev. 2017;44:30-7.
- 95. Papatheodorou I, Oellrich A, Smedley D. Linking gene expression to phenotypes via pathway information. J Biomed Semantics. 2015;6:17.
- 96. Colgan AM, Cameron AD, Kröger C. If it transcribes, we can sequence it: mining the complexities of host-pathogen-environment interactions using RNA-seq. Curr Opin Microbiol. 2017;36:37-46.
- 97. Conway T, Creecy JP, Maddox SM, Grissom JE, Conkle TL, Shadid TM, et al. Unprecedented high-resolution view of bacterial operon architecture revealed by RNA sequencing. mBio. 2014;5(4):e01442-14.
- 98. Hör J, Gorski SA, Vogel J. Bacterial RNA Biology on a Genome Scale. Mol Cell. 2018;70(5):785-99.

- 99. Mortazavi A, Williams BA, McCue K, Schaeffer L, Wold B. Mapping and quantifying mammalian transcriptomes by RNA-Seq. Nat Methods. 2008;5(7):621-8.
- 100. Velculescu VE, Zhang L, Vogelstein B, Kinzler KW. Serial analysis of gene expression. Science. 1995;270(5235):484-7.
- 101. Stark R, Grzelak M, Hadfield J. RNA sequencing: the teenage years. Nat Rev Genet. 2019;20(11):631-56.
- 102. Wang Z, Gerstein M, Snyder M. RNA-Seq: a revolutionary tool for transcriptomics. Nat Rev Genet. 2009;10(1):57-63.
- 103. Schena M, Shalon D, Davis RW, Brown PO. Quantitative monitoring of gene expression patterns with a complementary DNA microarray. Science. 1995;270(5235):467-70.
- 104. Jiménez-Chillarón JC, Díaz R, Ramón-Krauel M. Chapter 4 Omics Tools for the Genome-Wide Analysis of Methylation and Histone Modifications. In: Simó C, Cifuentes A, García-Cañas V, editors. Comprehensive Analytical Chemistry. 63: Elsevier; 2014. p. 81-110.
- 105. Sidova M, Tomankova S, Abaffy P, Kubista M, Sindelka R. Effects of postmortem and physical degradation on RNA integrity and quality. Biomol Detect Quantif. 2015;5:3-9.
- 106. Alvarez ML, Nourbakhsh M. RNA mapping protocols: northern blot and amplification of cDNA ends. Disease Gene Identification: Methods and Protocols. 2011:199-220.
- 107. Sterling CH, Veksler-Lublinsky I, Ambros V. An efficient and sensitive method for preparing cDNA libraries from scarce biological samples. Nucleic Acids Res. 2015;43(1):e1.
- 108. Kukurba KR, Montgomery SB. RNA Sequencing and Analysis. Cold Spring Harb Protoc. 2015;2015(11):951-69.
- 109. Hesse M, Zimek A, Weber K, Magin TM. Comprehensive analysis of keratin gene clusters in humans and rodents. Eur J Cell Biol. 2004;83(1):19-26.
- 110. Costa LA, da Silva ICB, Mariz B, da Silva MB, Freitas-Ribeiro GM, de Oliveira NFP. Influence of smoking on methylation and hydroxymethylation levels in global DNA and specific sites of KRT14, KRT19, MIR-9-3 and MIR-137 genes of oral mucosa. Arch Oral Biol. 2016;72:56-65.
- 111. Cabral A, Voskamp P, Cleton-Jansen AM, South A, Nizetic D, Backendorf C. Structural organization and regulation of the small proline-rich family of cornified envelope precursors suggest a role in adaptive barrier function. J Biol Chem. 2001;276(22):19231-7.
- 112. Lohman FP, Medema JK, Gibbs S, Ponec M, van de Putte P, Backendorf C. Expression of the SPRR cornification genes is differentially affected by carcinogenic transformation. Exp Cell Res. 1997;231(1):141-8.
- 113. Hohl D, de Viragh PA, Amiguet-Barras F, Gibbs S, Backendorf C, Huber M. The small proline-rich proteins constitute a multigene family of differentially regulated cornified cell envelope precursor proteins. J Invest Dermatol. 1995;104(6):902-9.
- 114. Kartasova T, van Muijen GN, van Pelt-Heerschap H, van de Putte P. Novel protein in human epidermal keratinocytes: regulation of expression during differentiation. Mol Cell Biol. 1988;8(5):2204-10.

- 115. Zhu G, Cai H, Ye L, Mo Y, Zhu M, Zeng Y, et al. Small Proline-Rich Protein 3 Regulates IL-33/ILC2 Axis to Promote Allergic Airway Inflammation. Front Immunol. 2021;12:758829.
- 116. Gibbs S, Lohman F, Teubel W, van de Putte P, Backendorf C. Characterization of the human spr2 promoter: induction after UV irradiation or TPA treatment and regulation during differentiation of cultured primary keratinocytes. Nucleic Acids Res. 1990;18(15):4401-7.
- 117. Ricard-Blum S. The collagen family. Cold Spring Harb Perspect Biol. 2011;3(1):a004978.
- 118. Gordon MK, Hahn RA. Collagens. Cell Tissue Res. 2010;339(1):247-57.
- 119. Zachariadou C, Hart T, Hooper D, Mariotti A. Molecular characteristics of periodontal health: Collagens: Defining the healthy human gingival collagen transcriptome: Defining the healthy human gingival collagen transcriptome. J Periodontol. 2023;94(5):606-15.
- 120. Butler GS, Overall CM. Matrix metalloproteinase processing of signaling molecules to regulate inflammation. Periodontol 2000. 2013;63(1):123-48.
- 121. Folgueras AR, Pendás AM, Sánchez LM, López-Otín C. Matrix metalloproteinases in cancer: from new functions to improved inhibition strategies. Int J Dev Biol. 2004;48(5-6):411-24.
- 122. Ihrie RA, Reczek E, Horner JS, Khachatrian L, Sage J, Jacks T, Attardi LD. Perp is a mediator of p53-dependent apoptosis in diverse cell types. Curr Biol. 2003;13(22):1985-90.
- 123. Riley T, Sontag E, Chen P, Levine A. Transcriptional control of human p53-regulated genes. Nat Rev Mol Cell Biol. 2008;9(5):402-12.
- 124. Ang YS, Rivas RN, Ribeiro AJS, Srivas R, Rivera J, Stone NR, et al. Disease Model of GATA4 Mutation Reveals Transcription Factor Cooperativity in Human Cardiogenesis. Cell. 2016;167(7):1734-49.e22.
- 125. He JG, Li HR, Han JX, Li BB, Yan D, Li HY, et al. GATA-4-expressing mouse bone marrow mesenchymal stem cells improve cardiac function after myocardial infarction via secreted exosomes. Sci Rep. 2018;8(1):9047.
- 126. Guo S, Zhang Y, Zhou T, Wang D, Weng Y, Wang L, Ma J. Role of GATA binding protein 4 (GATA4) in the regulation of tooth development via GNAI3. Sci Rep. 2017;7(1):1534.
- 127. Mattuella LG, Bernardi L, Zambra FMB, Campagnaro MB, Oppermann RV, Xavier LL, et al. Human leukocyte antigen-G polymorphisms in periodontitis. Acta Odontol Scand. 2020;78(2):141-5.
- 128. Stein GS, Lian JB, van Wijnen AJ, Stein JL, Montecino M, Javed A, et al. Runx2 control of organization, assembly and activity of the regulatory machinery for skeletal gene expression. Oncogene. 2004;23(24):4315-29.
- 129. Linqing Z, Guohua J, Haoming L, Xuelei T, Jianbing Q, Meiling T. Runx1t1 regulates the neuronal differentiation of radial glial cells from the rat hippocampus. Stem Cells Transl Med. 2015;4(1):110-6.
- 130. Kelwick R, Desanlis I, Wheeler GN, Edwards DR. The ADAMTS (A Disintegrin and Metalloproteinase with Thrombospondin motifs) family. Genome Biol. 2015;16(1):113.

- 131. Martina E, Degen M, Rüegg C, Merlo A, Lino MM, Chiquet-Ehrismann R, Brellier F. Tenascin-W is a specific marker of glioma-associated blood vessels and stimulates angiogenesis in vitro. Faseb j. 2010;24(3):778-87.
- 132. Li Y, Zhang M, Chen H, Dong Z, Ganapathy V, Thangaraju M, Huang S. Ratio of miR-196s to HOXC8 messenger RNA correlates with breast cancer cell migration and metastasis. Cancer Res. 2010;70(20):7894-904.
- 133. Asli NS, Kessel M. Spatiotemporally restricted regulation of generic motor neuron programs by miR-196-mediated repression of Hoxb8. Dev Biol. 2010;344(2):857-68.
- 134. Braig S, Mueller DW, Rothhammer T, Bosserhoff AK. MicroRNA miR-196a is a central regulator of HOX-B7 and BMP4 expression in malignant melanoma. Cell Mol Life Sci. 2010;67(20):3535-48.
- 135. Liu XH, Lu KH, Wang KM, Sun M, Zhang EB, Yang JS, et al. MicroRNA-196a promotes non-small cell lung cancer cell proliferation and invasion through targeting HOXA5. BMC Cancer. 2012;12:348.
- 136. Shah N, Sukumar S. The Hox genes and their roles in oncogenesis. Nat Rev Cancer. 2010;10(5):361-71.
- 137. Petersen PE, Ogawa H. The global burden of periodontal disease: towards integration with chronic disease prevention and control. Periodontology 2000. 2012;60(1):15-39.
- 138. Caton J, Nyman S, Zander H. Histometric evaluation of periodontal surgery II. Connective tissue attachment levels after four regenerative procedures. Journal of Clinical Periodontology. 1980;7(3):224-31.
- 139. Sanz M, Herrera D, Kebschull M, Chapple I, Jepsen S, Beglundh T, et al. Treatment of stage I-III periodontitis-The EFP S3 level clinical practice guideline. J Clin Periodontol. 2020;47 Suppl 22(Suppl 22):4-60.
- 140. Khan S, Khalid T, Bettiol S, Crocombe LA. Non-surgical periodontal therapy effectively improves patient-reported outcomes: A systematic review. Int J Dent Hyg. 2021;19(1):18-28.
- 141. Boehm TK, Kim CS. Overview of Periodontal Surgical Procedures. StatPearls. Treasure Island (FL): StatPearls Publishing

Copyright © 2025, StatPearls Publishing LLC.; 2025.

- 142. Herrera D, Berglundh T, Schwarz F, Chapple I, Jepsen S, Sculean A, Kebschull M, Papapanou PN, Tonetti MS, Sanz M; EFP workshop participants and methodological consultant. Prevention and treatment of peri-implant diseases—The EFP S3 level clinical practice guideline. J Clin Periodontol. 2023 Jun;50 Suppl 26:4-76.
- 143. Manresa C, Sanz-Miralles EC, Twigg J, Bravo M. Supportive periodontal therapy (SPT) for maintaining the dentition in adults treated for periodontitis. Cochrane Database Syst Rev. 2018;1(1):Cd009376.
- 144. Charbonneau AM, Roy S, Tran SD. Oral-Facial Tissue Reconstruction in the Regenerative Axolotl. J Exp Zool B Mol Dev Evol. 2016;326(8):489-502.
- 145. Upadhyay A, Pillai S, Khayambashi P, Sabri H, Lee KT, Tarar M, et al. Biomimetic Aspects of Oral and Dentofacial Regeneration. Biomimetics (Basel). 2020;5(4).

- 146. Steinberg T, Dieterle MP, Tomakidi P. Molecular Research on Oral Diseases and Related Biomaterials: A Journey from Oral Cell Models to Advanced Regenerative Perspectives. Int J Mol Sci. 2022;23(9).
- 147. Upadhyay A, Pillai S, Khayambashi P, Sabri H, Lee KT, Tarar M, et al. Biomimetic aspects of oral and dentofacial regeneration. Biomimetics. 2020;5(4):51.
- 148. Nguyen TT, Mui B, Mehrabzadeh M, Chea Y, Chaudhry Z, Chaudhry K, Tran SD. Regeneration of tissues of the oral complex: Current. J Can Dent Assoc. 2013;79:d1.
- 149. AlFatlawi Z, Huang M, Chau DYS, D'Aiuto F. Three dimensional (3D) gingival models in periodontal research: a systematic review. J Mater Sci Mater Med. 2023;34(11):58.
- 150. Charbonier F, Indana D, Chaudhuri O. Tuning Viscoelasticity in Alginate Hydrogels for 3D Cell Culture Studies. Curr Protoc. 2021;1(5):e124.
- 151. Langer R. VacantiJP: Tissue engineering. Science. 1993;260(5110):920-6.
- 152. Kumar A, Mukhtar-Un-Nisar S, Zia A. Tissue engineering-the promise of regenerative dentistry. Biol Med. 2011;3(2):108-13.
- 153. Chen F-M, Jin Y. Periodontal tissue engineering and regeneration: current approaches and expanding opportunities. Tissue Engineering Part B: Reviews. 2010;16(2):219-55.
- 154. Moysidou C-M, Barberio C, Owens RM. Advances in engineering human tissue models. Frontiers in bioengineering and biotechnology. 2021;8:620962.
- 155. Taylor MW, Taylor MW. A history of cell culture. Viruses and man: a history of interactions. 2014:41-52.
- 156. Breslin S, O'Driscoll L. Three-dimensional cell culture: the missing link in drug discovery. Drug discovery today. 2013;18(5-6):240-9.
- 157. Bates AM, Fischer CL, Abhyankar VP, Johnson GK, Guthmiller JM, Progulske-Fox A, Brogden KA. Matrix metalloproteinase response of dendritic cell, gingival epithelial keratinocyte, and T-cell transwell co-cultures treated with Porphyromonas gingivalis hemagglutinin-B. International journal of molecular sciences. 2018;19(12):3923.
- 158. Sancilio S, di Giacomo V, Di Giulio M, Gallorini M, Marsich E, Travan A, et al. Biological responses of human gingival fibroblasts (HGFs) in an innovative co-culture model with Streptococcus mitis to thermosets coated with a silver polysaccharide antimicrobial system. PLoS One. 2014;9(5):e96520.
- 159. Rheinwatd JG, Green H. Seria cultivation of strains of human epidemal keratinocytes: the formation keratinizin colonies from single cell is. Cell. 1975;6(3):331-43.
- 160. Arenholt-Bindslev D, Jepsen A, MacCallum DK, Lillie JH. The growth and structure of human oral keratinocytes in culture. Journal of investigative dermatology. 1987;88(3):314-9.
- 161. Lauer G. Autografting of feeder-cell free cultured gingival epithelium: method and clinical application. Journal of Cranio-Maxillofacial Surgery. 1994;22(1):18-22.
- 162. Radyuk SN, Mericko PA, Popova TG, Grene E, Alibek K. In vitro-generated respiratory mucosa: a new tool to study inhalational anthrax. Biochemical and biophysical research communications. 2003;305(3):624-32.

- 163. Duval K, Grover H, Han L-H, Mou Y, Pegoraro AF, Fredberg J, Chen Z. Modeling physiological events in 2D vs. 3D cell culture. Physiology. 2017;32(4):266-77.
- 164. Fitzgerald KA, Malhotra M, Curtin CM, O'Brien FJ, O'Driscoll CM. Life in 3D is never flat: 3D models to optimise drug delivery. Journal of Controlled Release. 2015;215:39-54.
- 165. Kapałczyńska M, Kolenda T, Przybyła W, Zajączkowska M, Teresiak A, Filas V, et al. 2D and 3D cell cultures–a comparison of different types of cancer cell cultures. Archives of Medical Science. 2018;14(4):910-9.
- 166. Huh D, Hamilton GA, Ingber DE. From 3D cell culture to organs-on-chips. Trends in cell biology. 2011;21(12):745-54.
- 167. Shamir ER, Ewald AJ. Three-dimensional organotypic culture: experimental models of mammalian biology and disease. Nature reviews Molecular cell biology. 2014;15(10):647-64.
- 168. Dvir T, Timko BP, Kohane DS, Langer R. Nanotechnological strategies for engineering complex tissues. Nat Nanotechnol. 2011;6(1):13-22.
- 169. Ramseier CA, Rasperini G, Batia S, Giannobile WV. Advanced reconstructive technologies for periodontal tissue repair. Periodontology 2000. 2012;59(1):185-202.
- 170. Moharamzadeh K, Franklin KL, Brook IM, van Noort R. Biologic assessment of antiseptic mouthwashes using a three-dimensional human oral mucosal model. Journal of periodontology. 2009;80(5):769-75.
- 171. Moyes DL, Runglall M, Murciano C, Shen C, Nayar D, Thavaraj S, et al. A biphasic innate immune MAPK response discriminates between the yeast and hyphal forms of Candida albicans in epithelial cells. Cell host & microbe. 2010;8(3):225-35.
- 172. Samaranayake Y, Dassanayake R, Cheung B, Jayatilake J, Yeung K, Yau J, Samaranayake L. Differential phospholipase gene expression by Candida albicans in artificial media and cultured human oral epithelium. Apmis. 2006;114(12):857-66.
- 173. Schaller M, Boeld U, Oberbauer S, Hamm G, Hube B, Korting HC. Polymorphonuclear leukocytes (PMNs) induce protective Th1-type cytokine epithelial responses in an in vitro model of oral candidosis. Microbiology. 2004;150(9):2807-13.
- 174. Takeda K, Gosiewska A, Peterkofsky B. Similar, but not identical, modulation of expression of extracellular matrix components during in vitro and in vivo aging of human skin fibroblasts. Journal of cellular physiology. 1992;153(3):450-9.
- 175. VON F. BIOCHEMIE UND FUNKTION DER GLYKOSAMINOGLYKANE DER HAUT. 1976.
- 176. Ma L, Gao C, Mao Z, Zhou J, Shen J, Hu X, Han C. Collagen/chitosan porous scaffolds with improved biostability for skin tissue engineering. Biomaterials. 2003;24(26):4833-41.
- 177. Moharamzadeh K, Colley H, Murdoch C, Hearnden V, Chai WL, Brook IM, et al. Tissue-engineered Oral Mucosa. Journal of Dental Research. 2012;91(7):642-50.

- 178. Basso FG, Pansani TN, Marcelo CL, de Souza Costa CA, Hebling J, Feinberg SE. Phenotypic markers of oral keratinocytes seeded on two distinct 3D oral mucosa models. Toxicology in Vitro. 2018;51:34-9.
- 179. Sobue T, Bertolini M, Thompson A, Peterson DE, Diaz PI, Dongari-Bagtzoglou A. Chemotherapy-induced oral mucositis and associated infections in a novel organotypic model. Molecular oral microbiology. 2018;33(3):212-23.
- 180. Dias KD, de Sousa DL, Barbugli PA, Cerri PS, Salih VM, Vergani CE. Development and characterization of a 3D oral mucosa model as a tool for host-pathogen interactions. Journal of Microbiological Methods. 2018;152:52-60.
- 181. Tigani EK, Skrtic D, Valerio MS, Kaufman G. Assessing the effect of triethyleneglycol dimethacrylate on tissue repair in 3D organotypic cultures. Journal of Applied Toxicology. 2019;39(2):247-59.
- 182. Chen J, Ahmad R, Li W, Swain M, Li Q. Biomechanics of oral mucosa. Journal of The Royal Society Interface. 2015;12(109):20150325.
- 183. Tomakidi P, Fusenig NE, Kohl A, Komposch G. Histomorphological and biochemical differentiation capacity in organotypic co-cultures of primary gingival cells. Journal of Periodontal Research. 1997;32(4):388-400.
- 184. Dabija-Wolter G, Sapkota D, Cimpan MR, Neppelberg E, Bakken V, Costea DE. Limited in-depth invasion of Fusobacterium nucleatum into in vitro reconstructed human gingiva. Archives of Oral Biology. 2012;57(4):344-51.
- 185. Golinski PA, Groger S, Herrmann JM, Bernd A, Meyle J. Oral mucosa model based on a collagen-elastin matrix. Journal of Periodontal Research. 2011;46(6):704-11.
- 186. Kriegebaum U, Mildenberger M, Mueller-Richter UDA, Klammert U, Kuebler AC, Reuther T. Tissue engineering of human oral mucosa on different scaffolds: in vitro experiments as a basis for clinical applications. Oral Surgery, Oral Medicine, Oral Pathology & Oral Radiology. 2012;114(s5):S190-S8.
- 187. Buskermolen JK, Reijnders CM, Spiekstra SW, Steinberg T, Kleverlaan CJ, Feilzer AJ, et al. Development of a Full-Thickness Human Gingiva Equivalent Constructed from Immortalized Keratinocytes and Fibroblasts. Tissue Engineering Part C: Methods. 2016;22(8):781-91.
- 188. Dongari-Bagtzoglou A, Kashleva H. Development of a novel three-dimensional in vitro model of oral Candida infection. Microbial Pathogenesis. 2006;40(6):271-8.
- 189. Razali M, Ngeow WC, Omar RA, Chai WL. An In-Vitro Analysis of Peri-Implant Mucosal Seal Following Photofunctionalization of Zirconia Abutment Materials. Biomedicines. 2021;9(1).
- 190. Benam KH, Dauth S, Hassell B, Herland A, Jain A, Jang K-J, et al. Engineered in vitro disease models. Annual Review of Pathology: Mechanisms of Disease. 2015;10:195-262.
- 191. Caddeo S, Boffito M, Sartori S. Tissue engineering approaches in the design of healthy and pathological in vitro tissue models. Frontiers in bioengineering and biotechnology. 2017;5:40.
- 192. Carter M, Shieh JC. Guide to research techniques in neuroscience: Academic Press; 2015.

- 193. Bao K, Akguel B, Bostanci N. Establishment and Characterization of Immortalized Gingival Epithelial and Fibroblastic Cell Lines for the Development of Organotypic Cultures. Cells Tissues Organs. 2014;199(4):228-37.
- 194. Bao K, Papadimitropoulos A, Akgül B, Belibasakis GN, Bostanci N. Establishment of an oral infection model resembling the periodontal pocket in a perfusion bioreactor system. Virulence. 2015;6(3):265-73.
- 195. Ferra-Canellas MD, Munar-Bestard M, Garcia-Sureda L, Lejeune B, Ramis JM, Monjo M. BMP4 micro-immunotherapy increases collagen deposition and reduces PGE2 release in human gingival fibroblasts and increases tissue viability of engineered 3D gingiva under inflammatory conditions. Journal of Periodontology.
- 196. Buskermolen JK, Janus MM, Roffel S, Krom BP, Gibbs S. Saliva-Derived Commensal and Pathogenic Biofilms in a Human Gingiva Model. Journal of Dental Research. 2018;97(2):201-8.
- 197. Shang L, Deng D, Buskermolen JK, Janus MM, Krom BP, Roffel S, et al. Multi-species oral biofilm promotes reconstructed human gingiva epithelial barrier function. Scientific Reports. 2018;8(1):16061.
- 198. Roffel S, Wu G, Nedeljkovic I, Meyer M, Razafiarison T, Gibbs S. Evaluation of a novel oral mucosa in vitro implantation model for analysis of molecular interactions with dental abutment surfaces. Clinical Implant Dentistry & Related Research. 2019;21 Suppl 1:25-33.
- 199. Ingendoh-Tsakmakidis A, Mikolai C, Winkel A, Szafranski SP, Flak CS, Rossi A, et al. Commensal and pathogenic biofilms differently modulate perimplant oral mucosa in an organotypic model. Cellular Microbiology. 2019;21(10).
- 200. Jennings LR, Colley HE, Ong J, Panagakos F, Masters JG, Trivedi HM, et al. Development and Characterization of In Vitro Human Oral Mucosal Equivalents Derived from Immortalized Oral Keratinocytes. Tissue Engineering Part C: Methods. 2016;22(12):1108-17.
- 201. Chai WL, Brook IM, Palmquist A, van Noort R, Moharamzadeh K. The biological seal of the implant-soft tissue interface evaluated in a tissue-engineered oral mucosal model. Journal of the Royal Society Interface. 2012;9(77):3528-38.
- 202. Andersen T, Auk-Emblem P, Dornish M. 3D cell culture in alginate hydrogels. Microarrays. 2015;4(2):133-61.
- 203. Troy E, Tilbury MA, Power AM, Wall JG. Nature-based biomaterials and their application in biomedicine. Polymers. 2021;13(19):3321.
- 204. Seyedmahmoud R, Çelebi-Saltik B, Barros N, Nasiri R, Banton E, Shamloo A, et al. Three-dimensional bioprinting of functional skeletal muscle tissue using gelatin methacryloyl-alginate bioinks. Micromachines. 2019;10(10):679.
- 205. Keskin-Erdogan Z, Patel KD, Chau DY, Day RM, Kim HW, Knowles JC. Utilization of GelMA with phosphate glass fibers for glial cell alignment. Journal of Biomedical Materials Research Part A. 2021;109(11):2212-24.
- 206. Wang H, Wan J, Zhang Z, Hou R. Recent advances on 3D-bioprinted gelatin methacrylate hydrogels for tissue engineering in wound healing: A review of current applications and future prospects. Int Wound J. 2024;21(4):e14533.

- 207. Liu W, Zhong Z, Hu N, Zhou Y, Maggio L, Miri AK, et al. Coaxial extrusion bioprinting of 3D microfibrous constructs with cell-favorable gelatin methacryloyl microenvironments. Biofabrication. 2018;10(2):024102.
- 208. Lambert BJ, Mendelson TA, Craven MD. Radiation and ethylene oxide terminal sterilization experiences with drug eluting stent products. AAPS PharmSciTech. 2011;12(4):1116-26.
- 209. Zhao Y, Zhu B, Wang Y, Liu C, Shen C. Effect of different sterilization methods on the properties of commercial biodegradable polyesters for single-use, disposable medical devices. Mater Sci Eng C Mater Biol Appl. 2019;105:110041.
- 210. Valente TA, Silva DM, Gomes PS, Fernandes MH, Santos JD, Sencadas V. Effect of Sterilization Methods on Electrospun Poly(lactic acid) (PLA) Fiber Alignment for Biomedical Applications. ACS Appl Mater Interfaces. 2016;8(5):3241-9.
- 211. Benyathiar P, Selke SE, Harte BR, Mishra DK. The effect of irradiation sterilization on poly (lactic) acid films. Journal of Polymers and the Environment. 2021;29:460-71.
- 212. Zhang F, Scull G, Gluck JM, Brown AC, King MW. Effects of sterilization methods on gelatin methacryloyl hydrogel properties and macrophage gene expressionin vitro. Biomed Mater. 2022;18(1).
- 213. Aljaber MB, Verisqa F, Keskin-Erdogan Z, Patel KD, Chau DYS, Knowles JC. Influence of Gelatin Source and Bloom Number on Gelatin Methacryloyl Hydrogels Mechanical and Biological Properties for Muscle Regeneration. Biomolecules. 2023;13(5).
- 214. Rizwan M, Chan SW, Comeau PA, Willett TL, Yim EKF. Effect of sterilization treatment on mechanical properties, biodegradation, bioactivity and printability of GelMA hydrogels. Biomed Mater. 2020;15(6):065017.
- 215. Sun M, Sun X, Wang Z, Guo S, Yu G, Yang H. Synthesis and Properties of Gelatin Methacryloyl (GelMA) Hydrogels and Their Recent Applications in Load-Bearing Tissue. Polymers (Basel). 2018;10(11).
- 216. Keskin-Erdogan Z, Patel KD, Chau DYS, Day RM, Kim HW, Knowles JC. Utilization of GelMA with phosphate glass fibers for glial cell alignment. J Biomed Mater Res A. 2021;109(11):2212-24.
- 217. Lytle RB. Soft tissue displacement beneath removable partial and complete dentures. Journal of Prosthetic Dentistry. 1962;12(1):34-43.
- 218. Choi JJE, Zwirner J, Ramani RS, Ma S, Hussaini HM, Waddell JN, Hammer N. Mechanical properties of human oral mucosa tissues are site dependent: A combined biomechanical, histological and ultrastructural approach. Clinical and experimental dental research. 2020;6(6):602-11.
- 219. Dabija-Wolter G, Bakken V, Cimpan MR, Johannessen AC, Costea DE. In vitro reconstruction of human junctional and sulcular epithelium. Journal of Oral Pathology & Medicine. 2013;42(5):396-404.
- 220. Golinski PA, Gröger S, Herrmann JM, Bernd A, Meyle J. Oral mucosa model based on a collagen-elastin matrix. Journal of Periodontal Research. 2011;46(6):704-11.
- 221. Jennings LR, Colley HE, Ong J, Panagakos F, Masters JG, Trivedi HM, et al. Development and characterization of in vitro human oral mucosal equivalents

- derived from immortalized oral keratinocytes. Tissue Engineering Part C: Methods. 2016;22(12):1108-17.
- 222. Koskinen Holm C, Qu C. Engineering a 3D In Vitro Model of Human Gingival Tissue Equivalent with Genipin/Cytochalasin D. International Journal of Molecular Sciences. 2022;23(13):03.
- 223. Sakulpaptong W, Clairmonte IA, Blackstone BN, Leblebicioglu B, Powell HM. 3D engineered human gingiva fabricated with electrospun collagen scaffolds provides a platform for in vitro analysis of gingival seal to abutment materials. Plos one. 2022;17(2):e0263083.
- 224. Dabija-Wolter G, Sapkota D, Cimpan MR, Neppelberg E, Bakken V, Costea DE. Limited in-depth invasion of Fusobacterium nucleatum into in vitro reconstructed human gingiva. Archives of Oral Biology. 2012;57(4):344-51.
- 225. de Carvalho Dias K, de Sousa DL, Barbugli PA, Cerri PS, Salih VM, Vergani CE. Development and characterization of a 3D oral mucosa model as a tool for host-pathogen interactions. Journal of Microbiological Methods. 2018;152:52-60.
- 226. Kriegebaum U, Mildenberger M, Mueller-Richter UD, Klammert U, Kuebler AC, Reuther T. Tissue engineering of human oral mucosa on different scaffolds: in vitro experiments as a basis for clinical applications. Oral Surgery, Oral Medicine, Oral Pathology and Oral Radiology. 2012;114(5 Suppl):S190-8.
- 227. Roffel S, Wu G, Nedeljkovic I, Meyer M, Razafiarison T, Gibbs S. Evaluation of a novel oral mucosa in vitro implantation model for analysis of molecular interactions with dental abutment surfaces. Clinical Implant Dentistry and Related Research. 2019;21:25-33.
- 228. Zhu M, Wang Y, Ferracci G, Zheng J, Cho N-J, Lee BH. Gelatin methacryloyl and its hydrogels with an exceptional degree of controllability and batch-to-batch consistency. Scientific reports. 2019;9(1):6863.
- 229. Zhou F, Hong Y, Liang R, Zhang X, Liao Y, Jiang D, et al. Rapid printing of bioinspired 3D tissue constructs for skin regeneration. Biomaterials. 2020;258:120287.
- 230. Wu Z, Xie S, Kang Y, Shan X, Li Q, Cai Z. Biocompatibility evaluation of a 3D-bioprinted alginate-GelMA-bacteria nanocellulose (BNC) scaffold laden with oriented-growth RSC96 cells. Materials Science and Engineering: C. 2021;129:112393.
- 231. O'Connell CD, Onofrillo C, Duchi S, Li X, Zhang Y, Tian P, et al. Evaluation of sterilisation methods for bio-ink components: gelatin, gelatin methacryloyl, hyaluronic acid and hyaluronic acid methacryloyl. Biofabrication. 2019;11(3):035003.
- 232. Stoppel WL, White JC, Horava SD, Henry AC, Roberts SC, Bhatia SR. Terminal sterilization of alginate hydrogels: efficacy and impact on mechanical properties. J Biomed Mater Res B Appl Biomater. 2014;102(4):877-84.
- 233. Moghimi N, Kamaraj M, Zehtabi F, Amin Yavari S, Kohandel M, Khademhosseini A, John JV. Development of bioactive short fiber-reinforced printable hydrogels with tunable mechanical and osteogenic properties for bone repair. J Mater Chem B. 2024 Mar 13;12(11):2818-2830. doi: 10.1039/d3tb02924g. PMID: 38411556.
- 234. Basara G, Yue X, Zorlutuna P. Dual crosslinked gelatin methacryloyl hydrogels for photolithography and 3D printing. Gels. 2019;5(3):34.

- 235. Qian SJ, Huang QR, Chen RY, Mo JJ, Zhou LY, Zhao Y, et al. Single-Cell RNA Sequencing Identifies New Inflammation-Promoting Cell Subsets in Asian Patients With Chronic Periodontitis. Front Immunol. 2021;12:711337.
- 236. Zhou HL, Chen DH, Xie GF, Li JJ, Tang JJ, Tang L. LncRNA-mediated ceRNA network was identified as a crucial determinant of differential effects in periodontitis and periimplantitis by high-throughput sequencing. Clinical Implant Dentistry and Related Research. 2020;22(3):424-50.
- 237. Lundmark A, Gerasimcik N, Bage T, Jemt A, Mollbrink A, Salmen F, et al. Gene expression profiling of periodontitis-affected gingival tissue by spatial transcriptomics. Scientific Reports. 2018;8.
- 238. Reddy SSP, Manohar B. Histological and whole-genome sequencing analysis of coronally advanced flap with connective tissue graft for the treatment of gingival recession-A case study. Clin Adv Periodontics. 2024;14(3):192-200.
- 239. Reddy SSP, Manohar B. Histological and whole-genome sequencing analysis of coronally advanced flap with connective tissue graft for the treatment of gingival recession-A case study. Clin Adv Periodontics. 2023.
- 240. Lundmark A, Gerasimcik N, Båge T, Jemt A, Mollbrink A, Salmén F, et al. Gene expression profiling of periodontitis-affected gingival tissue by spatial transcriptomics. Sci Rep. 2018;8(1):9370.
- 241. Huang DW, Sherman BT, Tan Q, Kir J, Liu D, Bryant D, et al. DAVID Bioinformatics Resources: expanded annotation database and novel algorithms to better extract biology from large gene lists. Nucleic Acids Res. 2007;35(Web Server issue):W169-75.
- 242. Wang J, Duncan D, Shi Z, Zhang B. WEB-based GEne SeT AnaLysis Toolkit (WebGestalt): update 2013. Nucleic Acids Res. 2013;41(Web Server issue):W77-83.
- 243. Zhang B, Kirov S, Snoddy J. WebGestalt: an integrated system for exploring gene sets in various biological contexts. Nucleic Acids Res. 2005;33(Web Server issue):W741-8.
- 244. Li H, Zhen Y, Geng Y, Feng J, Wang J, Zhang H. Exploring the Molecular Mechanism of Thoracic Aortic Aneurysm via Bioinformatics Analysis. Med Sci Monit. 2018;24:1533-9.
- 245. Shetty S. Keratinization and its disorders. Oman Med J. 2012;27(5):348-57.
- 246. Marcushamer M, King DL, McGuff S. White sponge nevus: case report. Pediatr Dent. 1995;17(7):458-9.
- 247. Scully C, Challacombe SJ. Pemphigus vulgaris: update on etiopathogenesis, oral manifestations, and management. Crit Rev Oral Biol Med. 2002;13(5):397-408.
- 248. Black M, Mignogna MD, Scully C. Number II. Pemphigus vulgaris. Oral Dis. 2005;11(3):119-30.
- 249. Lane EB, McLean WH. Keratins and skin disorders. J Pathol. 2004;204(4):355-66.
- 250. McLean WH, Irvine AD. Disorders of keratinisation: from rare to common genetic diseases of skin and other epithelial tissues. Ulster Med J. 2007;76(2):72-82.
- 251. Uitto J, Richard G, McGrath JA. Diseases of epidermal keratins and their linker proteins. Exp Cell Res. 2007;313(10):1995-2009.

- 252. Gibbs S, Fijneman R, Wiegant J, van Kessel AG, van De Putte P, Backendorf C. Molecular characterization and evolution of the SPRR family of keratinocyte differentiation markers encoding small proline-rich proteins. Genomics. 1993;16(3):630-7.
- 253. Zimmermann N, Doepker MP, Witte DP, Stringer KF, Fulkerson PC, Pope SM, et al. Expression and regulation of small proline-rich protein 2 in allergic inflammation. Am J Respir Cell Mol Biol. 2005;32(5):428-35.
- 254. Mariotti A. The extracellular matrix of the periodontium: dynamic and interactive tissues. Periodontol 2000. 1993;3:39-63.
- 255. Zhang J, Lu S, Lu T, Han D, Zhang K, Gan L, et al. Single-cell analysis reveals the COL11A1(+) fibroblasts are cancer-specific fibroblasts that promote tumor progression. Front Pharmacol. 2023;14:1121586.
- 256. Sorsa T, Mäntylä P, Tervahartiala T, Pussinen PJ, Gamonal J, Hernandez M. MMP activation in diagnostics of periodontitis and systemic inflammation. J Clin Periodontol. 2011;38(9):817-9.
- 257. Murphy G, Nagase H. Progress in matrix metalloproteinase research. Mol Aspects Med. 2008;29(5):290-308.
- 258. Fine N, Hassanpour S, Borenstein A, Sima C, Oveisi M, Scholey J, et al. Distinct Oral Neutrophil Subsets Define Health and Periodontal Disease States. J Dent Res. 2016;95(8):931-8.
- 259. Van Dyke TE, Serhan CN. Resolution of inflammation: a new paradigm for the pathogenesis of periodontal diseases. J Dent Res. 2003;82(2):82-90.
- 260. Bickel M. The role of interleukin-8 in inflammation and mechanisms of regulation. J Periodontol. 1993;64(5 Suppl):456-60.
- 261. Rey I, Effendi-Ys R, Sukatendel K. The Comparison of Serum Interleukin-8 Levels Based on Severity of Liver Cirrhosis. Med Arch. 2024;78(2):92-4.
- 262. Ng MY, Lin T, Chen SH, Liao YW, Liu CM, Yu CC. Er:YAG laser suppresses pro-inflammatory cytokines expression and inflammasome in human periodontal ligament fibroblasts with Porphyromonas gingivalis-lipopolysaccharide stimulation. J Dent Sci. 2024;19(2):1135-42.
- 263. Finoti LS, Nepomuceno R, Pigossi SC, Corbi SC, Secolin R, Scarel-Caminaga RM. Association between interleukin-8 levels and chronic periodontal disease: A PRISMA-compliant systematic review and meta-analysis. Medicine (Baltimore). 2017;96(22):e6932.
- 264. Ni XB, Jia C, Yu HD, Li YQ, Zeng XT, Leng WD. Comprehensive analysis of interleukin-8 gene polymorphisms and periodontitis susceptibility. Oncotarget. 2017;8(30):48996-9004.
- 265. Yang ZJ, Tang XP, Lai QG, Ci JB, Yuan KF. Interleukin-8 -251A/T polymorphism and periodontitis susceptibility: a meta-analysis. Genet Mol Res. 2016;15(4).
- 266. Wang L, Tanaka S, Ramirez F. GATA-4 binds to an upstream element of the human alpha2(I) collagen gene (COL1A2) and inhibits transcription in fibroblasts. Matrix Biol. 2005;24(5):333-40.
- 267. Zhu N, Zheng X, Qiao W, Huang W, Li R, Song Y. Activation of GATA-binding protein 4 regulates monocyte chemoattractant protein-1 and chemotaxis in periodontal ligament cells. J Periodontal Res. 2022;57(1):195-204.

- 268. Baines M, Ebringer A. HLA and disease. Mol Aspects Med. 1992;13(4):263-378.
- 269. Zinkernagel RM, Doherty PC. The discovery of MHC restriction. Immunol Today. 1997;18(1):14-7.
- 270. Sone S, Nakamura M, Maruya Y, Takahashi I, Mizoguchi I, Mayanagi H, Sasano Y. Expression of versican and ADAMTS during rat tooth eruption. J Mol Histol. 2005;36(4):281-8.
- 271. Stanton H, Melrose J, Little CB, Fosang AJ. Proteoglycan degradation by the ADAMTS family of proteinases. Biochim Biophys Acta. 2011;1812(12):1616-29.
- 272. Vázquez F, Hastings G, Ortega MA, Lane TF, Oikemus S, Lombardo M, Iruela-Arispe ML. METH-1, a human ortholog of ADAMTS-1, and METH-2 are members of a new family of proteins with angio-inhibitory activity. J Biol Chem. 1999;274(33):23349-57.
- 273. Chiquet-Ehrismann R, Tucker RP. Tenascins and the importance of adhesion modulation. Cold Spring Harb Perspect Biol. 2011;3(5).
- 274. Brellier F, Tucker RP, Chiquet-Ehrismann R. Tenascins and their implications in diseases and tissue mechanics. Scand J Med Sci Sports. 2009;19(4):511-9.
- 275. Ning LJ, Zhang YJ, Zhang YJ, Zhu M, Ding W, Jiang YL, et al. Enhancement of Migration and Tenogenic Differentiation of Macaca Mulatta Tendon-Derived Stem Cells by Decellularized Tendon Hydrogel. Front Cell Dev Biol. 2021;9:651583.
- 276. Tucker RP, Degen M. The Expression and Possible Functions of Tenascin-W During Development and Disease. Front Cell Dev Biol. 2019;7:53.
- 277. Hosiriluck N, Kashio H, Takada A, Mizuguchi I, Arakawa T. The profiling and analysis of gene expression in human periodontal ligament tissue and fibroblasts. Clin Exp Dent Res. 2022;8(3):658-72.
- 278. Darda L, Hakami F, Morgan R, Murdoch C, Lambert DW, Hunter KD. The role of HOXB9 and miR-196a in head and neck squamous cell carcinoma. PLoS One. 2015;10(4):e0122285.
- 279. Tsai KW, Liao YL, Wu CW, Hu LY, Li SC, Chan WC, et al. Aberrant expression of miR-196a in gastric cancers and correlation with recurrence. Genes Chromosomes Cancer. 2012;51(4):394-401.
- 280. Maru DM, Singh RR, Hannah C, Albarracin CT, Li YX, Abraham R, et al. MicroRNA-196a is a potential marker of progression during Barrett's metaplasia-dysplasia-invasive adenocarcinoma sequence in esophagus. Am J Pathol. 2009;174(5):1940-8.
- 281. Hui AB, Shi W, Boutros PC, Miller N, Pintilie M, Fyles T, et al. Robust global micro-RNA profiling with formalin-fixed paraffin-embedded breast cancer tissues. Lab Invest. 2009;89(5):597-606.
- 282. Mueller DW, Bosserhoff AK. MicroRNA miR-196a controls melanoma-associated genes by regulating HOX-C8 expression. Int J Cancer. 2011;129(5):1064-74.
- 283. Rinn JL, Bondre C, Gladstone HB, Brown PO, Chang HY. Anatomic demarcation by positional variation in fibroblast gene expression programs. PLoS Genet. 2006;2(7):e119.
- 284. Van Dyke TE, van Winkelhoff AJ. Infection and inflammatory mechanisms. J Clin Periodontol. 2013;40 Suppl 14:S1-7.

- 285. Gursoy UK, Könönen E. Understanding the roles of gingival beta-defensins. J Oral Microbiol. 2012;4.
- 286. Moharamzadeh K, Brook IM, Van Noort R, Scutt AM, Smith KG, Thornhill MH. Development, optimization and characterization of a full-thickness tissue engineered human oral mucosal model for biological assessment of dental biomaterials. Journal of Materials Science-Materials in Medicine. 2008;19(4):1793-801.
- 287. Carter SD, Costa PF, Vaquette C, Ivanovski S, Hutmacher DW, Malda J. Additive Biomanufacturing: An Advanced Approach for Periodontal Tissue Regeneration. Ann Biomed Eng. 2017;45(1):12-22.
- 288. Nesic D, Schaefer BM, Sun Y, Saulacic N, Sailer I. 3D Printing Approach in Dentistry: The Future for Personalized Oral Soft Tissue Regeneration. J Clin Med. 2020;9(7).
- 289. Ivanovski S, Vaquette C, Gronthos S, Hutmacher DW, Bartold PM. Multiphasic scaffolds for periodontal tissue engineering. J Dent Res. 2014;93(12):1212-21.
- 290. Binlateh T, Thammanichanon P, Rittipakorn P, Thinsathid N, Jitprasertwong P. Collagen-Based Biomaterials in Periodontal Regeneration: Current Applications and Future Perspectives of Plant-Based Collagen. Biomimetics (Basel). 2022;7(2).
- 291. Muniraj G, Tan RHS, Dai Y, Wu R, Alberti M, Sriram G. Microphysiological Modeling of Gingival Tissues and Host-Material Interactions Using Gingiva-on-Chip. Adv Healthc Mater. 2023;12(32):e2301472.
- 292. Woo HN, Cho YJ, Tarafder S, Lee CH. The recent advances in scaffolds for integrated periodontal regeneration. Bioact Mater. 2021;6(10):3328-42.
- 293. Moher D, Liberati A, Tetzlaff J, Altman DG. Preferred reporting items for systematic reviews and meta-analyses: the PRISMA statement. J Clin Epidemiol. 2009;62(10):1006-12.
- 294. Hooijmans CR, Rovers MM, de Vries R, Leenaars M, Ritskes-Hoitinga M, Langendam MW. SYRCLE's risk of bias tool for animal studies. BMC medical research methodology. 2014;14(1):1-9.
- 295. Shang L, Deng D, Roffel S, Gibbs S. Differential influence of Streptococcus mitis on host response to metals in reconstructed human skin and oral mucosa. Contact Dermatitis. 2020;83(5):347-60.
- 296. Shang L, Deng DM, Buskermolen JK, Janus MM, Krom BP, Roffel S, et al. Multi-species oral biofilm promotes reconstructed human gingiva epithelial barrier function. Scientific Reports. 2018;8.
- 297. Bao K, Papadimitropoulos A, Akgul B, Belibasakis GN, Bostanci N. Establishment of an oral infection model resembling the periodontal pocket in a perfusion bioreactor system. Virulence. 2015;6(3):265-73.
- 298. Ferrà-Cañellas MdM, Munar-Bestard M, Garcia-Sureda L, Lejeune B, Ramis JM, Monjo M, et al. BMP4 micro-immunotherapy increases collagen deposition and reduces PGE2 release in human gingival fibroblasts and increases tissue viability of engineered 3D gingiva under inflammatory conditions. Journal of Periodontology. 2021;92(10):1448-59.

- 299. Bao K, Akguel B, Bostanci N. Establishment and characterization of immortalized gingival epithelial and fibroblastic cell lines for the development of organotypic cultures. Cells Tissues Organs. 2014;199(4):228-37.
- 300. Casella JF, Flanagan MD, Lin S. Cytochalasin D inhibits actin polymerization and induces depolymerization of actin filaments formed during platelet shape change. Nature. 1981;293(5830):302-5.
- 301. Hwang YJ, Larsen J, Krasieva TB, Lyubovitsky JG. Effect of genipin crosslinking on the optical spectral properties and structures of collagen hydrogels. ACS Appl Mater Interfaces. 2011;3(7):2579-84.
- 302. Li S, Ge S, Yang P. Expression of cytokeratins in enamel organ, junctional epithelium and epithelial cell rests of Malassez. Journal of periodontal research. 2015;50(6):846-54.
- 303. Suhadi Pasaribu R, Ibrahim Auerkari E, Winoto Suhartono A. Histogical changes in oral mucosa (gingiva) as a method for estimating post-mortem interval: A literature review. Saudi Dent J. 2024 Jul;36(7):980-983. doi: 10.1016/j.sdentj.2024.05.002. Epub 2024 May 7. PMID: 39035559; PMCID: PMC11255919.
- 304. Ng Y-Z, South AP. Tissue engineering of tumor stromal microenvironment with application to cancer cell invasion. JoVE (Journal of Visualized Experiments). 2014(85):e51321.
- 305. Ng YZ, South AP. Tissue engineering of tumor stromal microenvironment with application to cancer cell invasion. J Vis Exp. 2014(85).
- 306. Heinrich MA, Liu W, Jimenez A, Yang J, Akpek A, Liu X, et al. 3D bioprinting: from benches to translational applications. Small. 2019;15(23):1805510.
- 307. Joseph P, Prabhakar P, Holtfreter B, Pink C, Suvan J, Kocher T, Pitchika V. Systematic review and meta-analysis of randomized controlled trials evaluating the efficacy of non-surgical periodontal treatment in patients with concurrent systemic conditions. Clin Oral Investig. 2023;28(1):21.
- 308. Song R, Murphy M, Li C, Ting K, Soo C, Zheng Z. Current development of biodegradable polymeric materials for biomedical applications. Drug design, development and therapy. 2018:3117-45.
- 309. Zhao Y, Yao R, Ouyang L, Ding H, Zhang T, Zhang K, et al. Three-dimensional printing of Hela cells for cervical tumor model in vitro. Biofabrication. 2014; 6: 035001.
- 310. Gopinathan J, Noh I. Recent trends in bioinks for 3D printing. Biomaterials research. 2018;22:1-15.
- 311. Mondal A, Gebeyehu A, Miranda M, Bahadur D, Patel N, Ramakrishnan S, et al. Characterization and printability of Sodium alginate-Gelatin hydrogel for bioprinting NSCLC co-culture. Scientific reports. 2019;9(1):19914.
- 312. Troy E, Tilbury MA, Power AM, Wall JG. Nature-Based Biomaterials and Their Application in Biomedicine. Polymers (Basel). 2021;13(19).
- 313. Song R, Murphy M, Li C, Ting K, Soo C, Zheng Z. Current development of biodegradable polymeric materials for biomedical applications. Drug Des Devel Ther. 2018;12:3117-45.
- 314. Lynn A, Yannas I, Bonfield W. Antigenicity and immunogenicity of collagen. Journal of Biomedical Materials Research Part B: Applied Biomaterials: An Official Journal of The Society for Biomaterials, The Japanese Society for Biomaterials,

- and The Australian Society for Biomaterials and the Korean Society for Biomaterials. 2004;71(2):343-54.
- 315. Moharamzadeh K, Colley H, Murdoch C, Hearnden V, Chai W, Brook I, et al. Tissue-engineered oral mucosa. Journal of dental research. 2012;91(7):642-50.
- 316. Paige KT, Cima LG, Yaremchuk MJ, Schloo BL, Vacanti JP, Vacanti CA. De novo cartilage generation using calcium alginate-chondrocyte constructs. Plastic and reconstructive surgery. 1996;97(1):168-78.
- 317. Masuda K, Sah RL, Hejna MJ, Thonar EJM. A novel two-step method for the formation of tissue-engineered cartilage by mature bovine chondrocytes: the alginate-recovered-chondrocyte (ARC) method. Journal of Orthopaedic Research. 2003;21(1):139-48.
- 318. Augst AD, Kong HJ, Mooney DJ. Alginate hydrogels as biomaterials. Macromol Biosci. 2006;6(8):623-33.
- 319. Zhang YS, Khademhosseini A. Advances in engineering hydrogels. Science. 2017;356(6337).
- 320. Davidenko N, Schuster CF, Bax DV, Farndale RW, Hamaia S, Best SM, Cameron RE. Evaluation of cell binding to collagen and gelatin: a study of the effect of 2D and 3D architecture and surface chemistry. Journal of Materials Science: Materials in Medicine. 2016;27:1-14.
- 321. Bello AB, Kim D, Kim D, Park H, Lee S-H. Engineering and functionalization of gelatin biomaterials: From cell culture to medical applications. Tissue Engineering Part B: Reviews. 2020;26(2):164-80.
- 322. Jaipan P, Nguyen A, Narayan RJ. Gelatin-based hydrogels for biomedical applications. Mrs Communications. 2017;7(3):416-26.
- 323. Grundy H, Reece P, Buckley M, Solazzo C, Dowle A, Ashford D, et al. A mass spectrometry method for the determination of the species of origin of gelatine in foods and pharmaceutical products. Food Chemistry. 2016;190:276-84.
- 324. Benton JA, DeForest CA, Vivekanandan V, Anseth KS. Photocrosslinking of gelatin macromers to synthesize porous hydrogels that promote valvular interstitial cell function. Tissue Engineering Part A. 2009;15(11):3221-30.
- 325. Van Den Bulcke AI, Bogdanov B, De Rooze N, Schacht EH, Cornelissen M, Berghmans H. Structural and rheological properties of methacrylamide modified gelatin hydrogels. Biomacromolecules. 2000;1(1):31-8.
- 326. Yu H, Luo X, Li Y, Shao L, Yang F, Pang Q, et al. Advanced Hybrid Strategies of GelMA Composite Hydrogels in Bone Defect Repair. Polymers (Basel). 2024;16(21).
- 327. Pepelanova I, Kruppa K, Scheper T, Lavrentieva A. Gelatin-Methacryloyl (GelMA) Hydrogels with Defined Degree of Functionalization as a Versatile Toolkit for 3D Cell Culture and Extrusion Bioprinting. Bioengineering (Basel). 2018;5(3).
- 328. Gray VP, Amelung CD, Duti IJ, Laudermilch EG, Letteri RA, Lampe KJ. Biomaterials via peptide assembly: Design, characterization, and application in tissue engineering. Acta Biomater. 2022;140:43-75.
- 329. Benton JA, DeForest CA, Vivekanandan V, Anseth KS. Photocrosslinking of gelatin macromers to synthesize porous hydrogels that promote valvular interstitial cell function. Tissue Eng Part A. 2009;15(11):3221-30.

- 330. Prakash Parthiban S, Rana D, Jabbari E, Benkirane-Jessel N, Ramalingam M. Covalently immobilized VEGF-mimicking peptide with gelatin methacrylate enhances microvascularization of endothelial cells. Acta Biomater. 2017;51:330-40.
- 331. Agten H, Van Hoven I, Van Hoorick J, Van Vlierberghe S, Luyten FP, Bloemen V. In vitro and in vivo evaluation of periosteum-derived cells and iPSC-derived chondrocytes encapsulated in GelMA for osteochondral tissue engineering. Front Bioeng Biotechnol. 2024;12:1386692.
- 332. Das S, Valoor R, Jegadeesan JT, Basu B. 3D bioprinted GelMA scaffolds for clinical applications: promise and challenges. Bioprinting. 2024:e00365.
- 333. Zhao X, Sun X, Yildirimer L, Lang Q, Lin ZYW, Zheng R, et al. Cell infiltrative hydrogel fibrous scaffolds for accelerated wound healing. Acta Biomater. 2017;49:66-77.
- 334. Ansari S, Pouraghaei Sevari S, Chen C, Sarrion P, Moshaverinia A. RGD-Modified Alginate-GelMA Hydrogel Sheet Containing Gingival Mesenchymal Stem Cells: A Unique Platform for Wound Healing and Soft Tissue Regeneration. ACS Biomater Sci Eng. 2021;7(8):3774-82.
- 335. Zhu K, Shin SR, van Kempen T, Li YC, Ponraj V, Nasajpour A, et al. Gold Nanocomposite Bioink for Printing 3D Cardiac Constructs. Adv Funct Mater. 2017;27(12).
- 336. Seyedmahmoud R, Çelebi-Saltik B, Barros N, Nasiri R, Banton E, Shamloo A, et al. Three-Dimensional Bioprinting of Functional Skeletal Muscle Tissue Using GelatinMethacryloyl-Alginate Bioinks. Micromachines (Basel). 2019;10(10).
- 337. Chiu Y-C, Cheng M-H, Engel H, Kao S-W, Larson JC, Gupta S, Brey EM. The role of pore size on vascularization and tissue remodeling in PEG hydrogels. Biomaterials. 2011;32(26):6045-51.
- 338. Derkach SR, Voron'ko NG, Sokolan NI, Kolotova DS, Kuchina YA. Interactions between gelatin and sodium alginate: UV and FTIR studies. Journal of Dispersion Science and Technology. 2020;41(5):690-8.
- 339. Huang R, Pal R, Moon G. Characteristics of sodium alginate membranes for the pervaporation dehydration of ethanol–water and isopropanol–water mixtures. Journal of Membrane Science. 1999;160(1):101-13.
- 340. Sun H, Wang Y, Zhang K, Zhong Y, Lin L, Zhou H, et al. Hydrophilic and hydrophobic poly (l-lactic acid) films by building porous topological surfaces. Journal of Applied Polymer Science. 2017;134(10).
- 341. Tzoneva R, Faucheux N, Groth T. Wettability of substrata controls cell-substrate and cell-cell adhesions. Biochimica et Biophysica Acta (BBA)-General Subjects. 2007;1770(11):1538-47.
- 342. De Carvalho R, Grosso C. Characterization of gelatin based films modified with transglutaminase, glyoxal and formaldehyde. Food hydrocolloids. 2004;18(5):717-26.
- 343. Rahman MS, Al-Saidi GS, Guizani N. Thermal characterisation of gelatin extracted from yellowfin tuna skin and commercial mammalian gelatin. Food Chemistry. 2008;108(2):472-81.
- 344. Rasoulianboroujeni M, Kiaie N, Tabatabaei FS, Yadegari A, Fahimipour F, Khoshroo K, Tayebi L. Dual Porosity Protein-based Scaffolds with Enhanced Cell Infiltration and Proliferation. Sci Rep. 2018;8(1):14889.

- 345. Maeda Y, Wood WW. Finite Element Method Simulation of Bone Resorption Beneath a Complete Denture. Journal of Dental Research. 1989;68(9):1370-3.
- 346. González-Masís J, Cubero-Sesin JM, Guerrero S, González-Camacho S, Corrales-Ureña YR, Redondo-Gómez C, et al. Self-assembly study of type I collagen extracted from male Wistar Hannover rat tail tendons. Biomaterials Research. 2020;24:1-11.
- 347. Józefowicz W. [Results of studies on elasticity moduli of the soft tissues of the denture-bearing area]. Protet Stomatol. 1970;20(3):171-6.
- 348. Margesin R, Schinner F. Biodegradation and bioremediation of hydrocarbons in extreme environments. Appl Microbiol Biotechnol. 2001;56(5-6):650-63.
- 349. Bartnikowski M, Dargaville TR, Ivanovski S, Hutmacher DW. Degradation mechanisms of polycaprolactone in the context of chemistry, geometry and environment. Progress in Polymer Science. 2019;96:1-20.
- 350. Basu A, Domb AJ. Recent Advances in Polyanhydride Based Biomaterials. Adv Mater. 2018;30(41):e1706815.
- 351. Mndlovu H, Kumar P, du Toit LC, Choonara YE. A review of bio material degradation assessment approaches employed in the biomedical field. npj Materials Degradation. 2024;8(1):66.
- 352. O'Connell CD, Zhang B, Onofrillo C, Duchi S, Blanchard R, Quigley A, et al. Tailoring the mechanical properties of gelatin methacryloyl hydrogels through manipulation of the photocrosslinking conditions. Soft matter. 2018;14(11):2142-51.
- 353. Yannas I, Lee E, Orgill DP, Skrabut E, Murphy GF. Synthesis and characterization of a model extracellular matrix that induces partial regeneration of adult mammalian skin. Proceedings of the National Academy of Sciences. 1989;86(3):933-7.
- 354. Le NM, Song S, Zhou H, Xu J, Li Y, Sung CE, et al. A noninvasive imaging and measurement using optical coherence tomography angiography for the assessment of gingiva: An in vivo study. Journal of Biophotonics. 2018;11(12):e201800242.
- 355. Kendall C, Isabelle M, Bazant-Hegemark F, Hutchings J, Orr L, Babrah J, et al. Vibrational spectroscopy: a clinical tool for cancer diagnostics. Analyst. 2009;134(6):1029-45.
- 356. Ouellet G, Dubé J, Gauvin R, Laterreur V, Bouhout S, Bolduc S. Production of an optimized tissue-engineered pig connective tissue for the reconstruction of the urinary tract. Tissue Engineering Part A. 2011;17(11-12):1625-33.
- 357. Naurecka ML, Sierakowski BM, Kasprzycka W, Dojs A, Dojs M, Suszyński Z, Kwaśny M. FTIR-ATR and FT-Raman spectroscopy for biochemical changes in oral tissue. American Journal of Analytical Chemistry. 2017;8(03).
- 358. Fukuyama Y, Yoshida S, Yanagisawa S, Shimizu M. A study on the differences between oral squamous cell carcinomas and normal oral mucosas measured by Fourier transform infrared spectroscopy. Biospectroscopy. 1999;5(2):117-26.
- 359. Tabatabaei F, Moharamzadeh K, Tayebi L. Fibroblast encapsulation in gelatin methacryloyl (GelMA) versus collagen hydrogel as substrates for oral

- mucosa tissue engineering. Journal of Oral Biology & Craniofacial Research. 2020;10(4):573-7.
- 360. Wei J, Igarashi T, Okumori N, Igarashi T, Maetani T, Liu B, Yoshinari M. Influence of surface wettability on competitive protein adsorption and initial attachment of osteoblasts. Biomedical materials. 2009;4(4):045002.
- 361. van der Mei HC, White DJ, Busscher HJ. On the wettability of soft tissues in the human oral cavity. Archives of Oral Biology. 2004;49(8):671-3.
- 362. Elworthy A, Greenman J, Doherty F, Newcombe R, Addy M. The substantivity of a number of oral hygiene products determined by the duration of effects on salivary bacteria. Journal of periodontology. 1996;67(6):572-6.
- 363. Miles CA, Burjanadze TV, Bailey AJ. The kinetics of the thermal denaturation of collagen in unrestrained rat tail tendon determined by differential scanning calorimetry. Journal of molecular biology. 1995;245(4):437-46.
- 364. Han C, Zhang H, Wu Y, He X, Chen X. Dual-crosslinked hyaluronan hydrogels with rapid gelation and high injectability for stem cell protection. Sci Rep. 2020;10(1):14997.
- 365. Mihajlovic M, Rikkers M, Mihajlovic M, Viola M, Schuiringa G, Ilochonwu BC, et al. Viscoelastic Chondroitin Sulfate and Hyaluronic Acid Double-Network Hydrogels with Reversible Cross-Links. Biomacromolecules. 2022;23(3):1350-65.
- 366. Tang R, Samouillan V, Dandurand J, Lacabanne C, Lacoste-Ferre MH, Bogdanowicz P, et al. Identification of ageing biomarkers in human dermis biopsies by thermal analysis (DSC) combined with Fourier transform infrared spectroscopy (FTIR/ATR). Skin Research and Technology. 2017;23(4):573-80.
- 367. Goktas S, Dmytryk JJ, McFetridge PS. Biomechanical behavior of oral soft tissues. Journal of periodontology. 2011;82(8):1178-86.
- 368. Tomlin H, Wilson H. The measurement of thickness and hardness of oral soft tissues. British Dental Journal. 1968;124(1):22-7.
- 369. Inoue K, Arikawa H, Fujii K, Shinohara N, Kawahata N. Viscoelastic properties of oral soft tissue 1. A method of determining elastic modulus of oral soft tissue. Dental materials journal. 1985;4(1):47-53,121.
- 370. Kydd WL, Mandley J. The stiffness of palatal mucoperiosteum. The Journal of Prosthetic Dentistry. 1967;18(2):116-21.
- 371. Nokubi T, Tsutsumi S, Yamaga T, Okuno T, Ida K. Finite element stress analysis of tooth, periodontal membrane and alveolar bone. J Jpn Res Soc Dental Mater Appl. 1976;33:369-78.
- 372. Józefowicz W. Results of studies on elasticity moduli of the soft tissues of the denture-bearing area. Protetyka stomatologiczna. 1970;20(3):171-6.
- 373. Aljaber MB, Verisqa F, Keskin-Erdogan Z, Patel KD, Chau DY, Knowles JC. Influence of Gelatin Source and Bloom Number on Gelatin Methacryloyl Hydrogels Mechanical and Biological Properties for Muscle Regeneration. Biomolecules. 2023;13(5):811.
- 374. Zhu J, Marchant RE. Design properties of hydrogel tissue-engineering scaffolds. Expert Rev Med Devices. 2011;8(5):607-26.
- 375. Tan SH, Chua DAC, Tang JRJ, Bonnard C, Leavesley D, Liang K. Design of hydrogel-based scaffolds for in vitro three-dimensional human skin model reconstruction. Acta Biomater. 2022;153:13-37.

- 376. Karring T, Lang NP, Löe H. The role of gingival connective tissue in determining epithelial differentiation. J Periodontal Res. 1975;10(1):1-11.
- 377. Abuwatfa WH, Pitt WG, Husseini GA. Scaffold-based 3D cell culture models in cancer research. Journal of Biomedical Science. 2024;31(1):7.
- 378. Edmondson R, Broglie JJ, Adcock AF, Yang L. Three-dimensional cell culture systems and their applications in drug discovery and cell-based biosensors. Assay Drug Dev Technol. 2014;12(4):207-18.
- 379. Bauer M, Metzger M, Corea M, Schädl B, Grillari J, Dungel P. Novel 3D-Printed Cell Culture Inserts for Air-Liquid Interface Cell Culture. Life (Basel). 2022;12(8).
- 380. Xia J, Liu ZY, Han ZY, Yuan Y, Shao Y, Feng XQ, Weitz DA. Regulation of cell attachment, spreading, and migration by hydrogel substrates with independently tunable mesh size. Acta Biomater. 2022;141:178-89.
- 381. D'Urso M, Kurniawan NA. Mechanical and Physical Regulation of Fibroblast-Myofibroblast Transition: From Cellular Mechanoresponse to Tissue Pathology. Front Bioeng Biotechnol. 2020;8:609653.
- 382. Luo T, Tan B, Zhu L, Wang Y, Liao J. A Review on the Design of Hydrogels With Different Stiffness and Their Effects on Tissue Repair. Front Bioeng Biotechnol. 2022;10:817391.
- 383. Rusu D, Calenic B, Greabu M, Kralev A, Boariu M, Bojin F, et al. Evaluation of oral keratinocyte progenitor and T-lymphocite cells response during early healing after augmentation of keratinized gingiva with a 3D collagen matrix a pilot study. BMC Oral Health. 2016;17(1):9.
- 384. Kalluri R, Weinberg RA. The basics of epithelial-mesenchymal transition. J Clin Invest. 2009;119(6):1420-8.
- 385. Roffel S, Wu G, Nedeljkovic I, Meyer M, Razafiarison T, Gibbs S. Evaluation of a novel oral mucosa in vitro implantation model for analysis of molecular interactions with dental abutment surfaces. Clin Implant Dent Relat Res. 2019;21 Suppl 1(Suppl Suppl 1):25-33.
- 386. Ingendoh-Tsakmakidis A, Mikolai C, Winkel A, Szafrański SP, Falk CS, Rossi A, et al. Commensal and pathogenic biofilms differently modulate perimplant oral mucosa in an organotypic model. Cell Microbiol. 2019;21(10):e13078.
- 387. Koskinen Holm C, Qu C. Engineering a 3D In Vitro Model of Human Gingival Tissue Equivalent with Genipin/Cytochalasin D. Int J Mol Sci. 2022;23(13).
- 388. Drury JL, Mooney DJ. Hydrogels for tissue engineering: scaffold design variables and applications. Biomaterials. 2003;24(24):4337-51.
- 389. Akdag Z, Ulag S, Kalaskar DM, Duta L, Gunduz O. Advanced Applications of Silk-Based Hydrogels for Tissue Engineering: A Short Review. Biomimetics (Basel). 2023;8(8).
- 390. Li X, Sun Q, Li Q, Kawazoe N, Chen G. Functional hydrogels with tunable structures and properties for tissue engineering applications. Frontiers in chemistry. 2018;6:499.
- 391. Cuomo F, Cofelice M, Lopez F. Rheological Characterization of Hydrogels from Alginate-Based Nanodispersion. Polymers (Basel). 2019 Feb 3;11(2):259. doi: 10.3390/polym11020259. PMID: 30960242; PMCID: PMC6419013.

- 392. Freeman FE, Kelly DJ. Tuning Alginate Bioink Stiffness and Composition for Controlled Growth Factor Delivery and to Spatially Direct MSC Fate within Bioprinted Tissues. Sci Rep. 2017 Dec 6;7(1):17042. doi: 10.1038/s41598-017-17286-1. PMID: 29213126; PMCID: PMC5719090.
- 393. Zhang F, Scull G, Gluck JM, Brown AC, King MW. Effects of sterilization methods on gelatin methacryloyl hydrogel properties and macrophage gene expression*in vitro*. Biomed Mater. 2022 Dec 7;18(1):10.1088/1748-605X/aca4b2. doi: 10.1088/1748-605X/aca4b2. PMID: 36410038; PMCID: PMC10038140.
- 394. Stoppel WL, White JC, Horava SD, Henry AC, Roberts SC, Bhatia SR. Terminal sterilization of alginate hydrogels: efficacy and impact on mechanical properties. J Biomed Mater Res B Appl Biomater. 2014 May;102(4):877-84. doi: 10.1002/jbm.b.33070. Epub 2013 Nov 21. PMID: 24259507; PMCID: PMC8218599
- 395. Samouillan V, Ober C, Lacoste-Ferré MH. Impact of Aging and Pathologies on Human Oral Mucosa: Preliminary Investigation of Biophysical Markers from Thermal and Vibrational Analyses. Biomolecules. 2025 Jul 8;15(7):978. doi: 10.3390/biom15070978. PMID: 40723850; PMCID: PMC12292607.
- 396. Yan Y, Cao Y, Cheng R, Shen Z, Zhao Y, Zhang Y, Zhou G, Sang S. Preparation and In Vitro Characterization of Gelatin Methacrylate for Corneal Tissue Engineering. Tissue Eng Regen Med. 2022 Feb;19(1):59-72. doi: 10.1007/s13770-021-00393-6. Epub 2021 Oct 19. PMID: 34665455; PMCID: PMC8782967.
- 397. Gan X, Li C, Sun J, Zhang X, Zhou M, Deng Y, Xiao A. GelMA/κ-carrageenan double-network hydrogels with superior mechanics and biocompatibility. RSC Adv. 2023 Jan 6;13(3):1558-1566. doi: 10.1039/d2ra06101e. PMID: 36688070; PMCID: PMC9817081.
- 398. Yan Y, Cao Y, Cheng R, Shen Z, Zhao Y, Zhang Y, Zhou G, Sang S. Preparation and In Vitro Characterization of Gelatin Methacrylate for Corneal Tissue Engineering. Tissue Eng Regen Med. 2022 Feb;19(1):59-72. doi: 10.1007/s13770-021-00393-6. Epub 2021 Oct 19. PMID: 34665455; PMCID: PMC8782967.
- 399. Gan X, Li C, Sun J, Zhang X, Zhou M, Deng Y, Xiao A. GelMA/κ-carrageenan double-network hydrogels with superior mechanics and biocompatibility. RSC Adv. 2023 Jan 6;13(3):1558-1566. doi: 10.1039/d2ra06101e. PMID: 36688070; PMCID: PMC9817081.
- 400. Jiang Q, Yu Y, Ruan H, Luo Y, Guo X. Morphological and functional characteristics of human gingival junctional epithelium. BMC Oral Health. 2014 Apr 3;14:30. doi: 10.1186/1472-6831-14-30. PMID: 24708739; PMCID: PMC4234347.

Appendix A-

Chapter 1. Supplementary Components of the Periodontal Disease Classification. And Supplementary Cell Types Used for Human Gingival Cell Expansion and Seeding.

Components of the Periodontal Disease Classification

Periodontal health and gingival/diseased Conditions

Periodontal health and gingival health

A.Clinical health on an intact periodontium

B.Clinical health on a reduced periodontium

stable periodontitis patient

Non-periodontitis patient

Gingivitis Biofilm Induced

A. Associated with biofilm alone

B. Gingivitis Mediated by either Systemic Risk Factors or Local Risk Factors

a.Systemic Risk Factors (modifying factors)

Smoking

Hyperglycemia

Nutritional factors

Pharmacological factors

Sex

steroids hormones (Puberty, menstrual cycle, pregnancy, oral contraceptives)

Hematological conditions

b. Local Risk Factors (predisposing factors)

Dental plaque biofilm retaining factors

Oral dryness

C. Drug-influenced gingival enlargement

Gingival Diseases Non-biofilm Induced

A. Genetic/developmental disorders

i. Hereditary gingival fibromatosisa

B. Specific infections

- i. Bacterial origin
- a. Neisseria gonorrhoeaea
- b. Treponema palliduma
- c. Mycobacterium tuberculosisa
- d. Streptococcal gingivitis
 - ii. Viral origin
 - a. Coxsackie virus (hand-foot-and-mouth disease)a
 - b. Herpes simplex I & II (primary or recurrent)a
 - c. Varicella zoster (chicken pox & shingles V nerve)a
 - d. Molluscum contagiosuma
- e. Human papilloma virus (squamous cell papilloma; condyloma acuminatum; verruca vulgaris; focal epithelial hyperplasia)
 - iii. Fungal origin
- a. Candidosis
- b.Other mycoses, e.g., histoplasmosis, aspergillosis

C. Inflammatory and immune conditions

i. Hypersensitivity reactions

- a. Contact allergya
- b. Plasma cell gingivitisa
- c. Erythema multiformea
- ii. Autoimmune diseases of skin and mucous membranes
- a. Pemphigus vulgarisa
- b. Pemphigoida
- c. Lichen planusa
- d. Lupus erythematosusa Systemic lupus erythematosis Discoid lupus erythematosis
- iii. Granulomatous inflammatory lesions (orofacial granulomatoses)
- a. Crohn's diseasea
- b. Sarcoidosisa

D. Reactive processes

- i. Epulides
- a. Fibrous epulis
- b. Calcifying fibroblastic granuloma
- c. Vascular epulis (pyogenic granuloma)
- d. Peripheral giant cell granulomaa

E. Neoplasms

- i. Premalignancy
- a. Leukoplakia
- b. Erythroplakia
- ii. Malignancy
- a. Squamous cell carcinoma
- b. Leukemic cell infiltrationa
- c. Lymphomaa Hodgkin Non-Hodgki

F. Endocrine, nutritional & metabolic diseases

i. Vitamin deficienciesa

- a. Vitamin C deficiency (scurvy)
- G. Traumatic lesions
- i. Physical/mechanical trauma
- a. Frictional keratosis
- b. Mechanically induced gingival ulceration
- c. Factitious injury (self-harm)
- ii. Chemical (toxic) burn
- iii. Thermal insults
- a.Burns to gingiva

H. Gingival pigmentation

- i. Melanoplakiaa
- ii. Smoker's melanosis
- iii. Drug-induced pigmentation (antimalarials, minocycline)
- iv. Amalgam tattoo

Forms of periodontitis

A.Necrotizing Periodontal Diseases

Necrotizing gingivitis

Necrotizing periodontitis

Necrotizing stomatitis

- B. Periodontitis Associated with Systemic Diseases
- B1.Systemic disorders that have a major impact on the loss of periodontal tissues by influencing periodontal inflammation
 - i.Genetic disorders

Diseases associated with immunologic disorders

Down syndrome

Leukocyte adhesion deficiency syndromes

Papillon-Lefèvre syndrome

Haim-Munk syndrome

Chediak-Higashi syndrome

Severe neutropenia– Congenital neutropenia (Kostmann syndrome)

Cyclic neutropenia

Primary immunodeficiency diseases

- Chronic granulomatous disease

Hyperimmunoglobulin E syndromes

Cohen syndrome

Diseases affecting the oral mucosa and gingival tissue

Epidermolysis bullosa

- Dystrophic epidermolysis bullosa
- Kindler syndrome

Plasminogen deficiency

Diseases affecting the connective tissues

Ehlers-Danlos syndromes (types IV, VIII)

Angioedema (C1-inhibitor deficiency)

Systemic lupus erythematosus

Metabolic and endocrine disorders

Glycogen storage disease

Gaucher disease

Hypophosphatasia

Hypophosphatemic rickets

Hajdu-Cheney syndrome

ii.Acquired immunodeficiency diseases

Acquired neutropenia

HIV infection

iii.Inflammatory diseases

Epidermolysis bullosa acquisita

Inflammatory bowel disease

Other systemic disorders that influence the pathogenesis of periodontal diseases

Diabetes mellitus

Obesity

Osteoporosis

Arthritis (rheumatoid arthritis, osteoarthritis)

Emotional stress and depression

Smoking (nicotine dependence)

Medications

Systemic disorders that can result in loss of periodontal tissues independent of periodontitis

Neoplasms

Primary neoplastic diseases of the periodontal tissues

Oral squamous cell carcinoma

Odontogenic tumors

Other primary neoplasms of the periodontal tissues

Secondary metastatic neoplasms of the periodontal tissues

Other disorders that may affect the periodontal tissues

Granulomatosis with polyangiitis Langerhans cell histiocytosis

Giant cell granulomas

Hyperparathyroidism

Systemic sclerosis (scleroderma)

Vanishing bone disease (Gorham-Stout syndrome)

Periodontitis

- a. Stages: Based on severity and complexity of management
- i. Stage I: initial periodontitis.
- ii. Stage II: moderate periodontitis with potential for additional tooth loss.
- iii. Stage III: sever periodontitis with potential for loss of dentition.
- b. Extend and distribution: localized, generalized, molar- incisor distribution.
- c. Grade: evidence or risk of rapid progression, anticipated treatment response.
- i. Grade A: slow rate of progression.
- ii. Grade B: moderate rate of progression.
- iii. Grade C: rapid rate of progression.

Periodontal manifestations of systemic diseases and development and acquired conditions

- a. Systemic diseases or conditions affecting the periodontal supporting tissues
- b.Other periodontal conditions
- a.Periodontal abcesses
- b.Endodontic-periodontal lesion
- c.Mucogingival deformities and conditions around teeth
- a.Gingival phenotype
- b.Gingival/soft tissue recession
- c. Lack of gingiva
- d. Decreased vestibular depth.

- e.Aberrant frenum/muscle position.
- f. Gingival excess.
- G. Abnormal color
- h. Condition of exposed root surface.

d.Traumatic occlusal force

- a.Primary occlusal trauma
- b.Secondary occlusal trauma
- c.Orthodontic forces
- e.Prosthesis- and tooth-related factors that modify or predispose to plaque-induced gingival diseases/periodontitis
- a.Localized tooth-related factors
- b.Localized dental prostheses-related factors

Peri-implantitis diseases and conditions

- a.Peri-implant health
- b.Peri-implant mucositis
- c.Peri-implantitis
- d.Peri-implant soft and hard tissue deficiencies

Appendix B-

Chapter 2.

1.Primary Human Gingival Fibroblasts (HGF)

Source: Normal, Human, Adult - PCS-201-018

Primary gingival fibroblast was isolated from the gingiva. The cell has applications in human gingival fibroblasts (hGF) and could potentially be an alternative source of mesenchymal stem cells (MSC) for regenerative medicine studies as they share similar morphology, CD markers, and differentiation lineage.

Product category Human cells

Product type Primary cell

Organism Homo sapiens, human

Cell type fibroblast

Morphology spindle-shaped; cells are bipolar and refractile

Tissue Gingiva

Applications 3D cell culture; Stem cell research

Product format Frozen

Storage conditions Vapor phase of liquid nitrogen

2.Cell line Human Gingival Epithelial Cells (HGE)

Source: Normal, Human, Adult

Cell Line Data Sheet

Kagoshima University

MOE1a, MOE1b Cell Name : Animal Human

[Basic Characteristics]

Genus Homo Species sapiens Sex Male Age 28-year old

Tissue origin mouth (gingival epithelium)

Life span infinite

Morphology small polygonal cells

[Culture information]

Passage number more than 50

Defined K-SFM (gibco) Medium catalog No. 10744-019

Temperature 37 degrees Celsius 5% CO2

Cell density /Passage : 70% confluent

Methods of passages: Rinse with PBS twice. Treat with 0.25% trypsin(W/V) and 0.02% EDTA (WV) in PBS for 10~15min at 37 degree celcius. In case of sticky adhesion, expand trypsinization upto 20 min, or use sterile rubber policeman.(* see caution described below)

Antibiotics used PenicilinG + streptomycin

Doubling time 1 week

Caution for Passages: Do not use the medium containing serum. Do NOT use serum for inactivating trypsin. Remove media and rinse with PBS(-) twice. Treat cells with 0.25% trypsin(W/V) and 0.02% EDTA (W/V) in PBS for 5~20 minutes at room temperature. Suspend and collect cells with 2:1 mixture of (PBS(-) and DKSFM). Centrifuge them (approx 1000 rpm 10 min), discard supernatant, resuspend with 2:1 mixture of (PBS(-) and DKSFM). Recentrifuge, remove supernatant, and suspend cells with K-SFM, and plate MOE1 cells onto tissue-culture

We found that maintaining MOE1 with serum containing medium causes apparent morphological changes. We have treated MOE1 cells for 7days with MC210 to remove potential mycoplasma contamination. If necessary, repeat this procedure.

Treat MOE1a cells as well as MOE1b cells. Ref: Oral sci Int 8 (2011) 20-28. Kibe et al.

Correspondence:

Shosei Kishida (shosei@m2.kufm.kagoshima-u.ac.jp)
Dept Biochem Genet. Kagoshima Univ Grad Sch Med Dent (Jan 07 2018)

Appendix C

Chapter 3. Supplemental Data 2. Categories used for quality assessment and risk of bias (modified from the ARRIVE and CONSORT guidelines) (Ramamoorthi, Bakkar, Jordan, & Tran, 2015).

Items	Description	Grade
1	Title	(0) Inaccurate/no concise
		(1) Concise/adequate
2	Abstract: either a structured	(1) Clearly inadequate
	summary of background, research	(2) Possibly accurate
	objectives, key experiment methods,	(3) Clearly accurate
	principal findings, and conclusion of	
	the study or self-contained (should	
	contain enough information to enable a good understanding of the	
	rationale for the approach)	
3	Introduction: background,	(1) Insufficient
9	experimental approach, and	(2) Possibly sufficient/some
	explanation of rationale/hypothesis	information
	, , , , , , , , , , , , , , , , , , ,	(3) Clearly meets/sufficient
4	Introduction: preprimary and	(1) Not clearly stated
	secondary objectives for the	(2) Clearly stated
	experiments (specific	
_	primary/secondary objectives)	
5	Methods: study design explained	(1) Clearly insufficient
	number of experimental and control	(2) Possibly sufficient
	groups, steps to reduce bias (demonstrating the consistency of	(3) Clearly sufficient
	the experiment (done more than	
	once), sufficient detail for replication,	
	blinding in evaluation, etc.)	
6	Methods: precise details of	(1) Clearly insufficient
	experimental procedure (i.e., how,	(2) Possibly sufficient
	when, where, and why)	(3) Clearly sufficient
7	Methods: How sample size was	(1) No
	determined (details of control and	(2) Unclear/not complete
	experimental group) and sample	(3) Adequate/clear
8	size calculation. Methods: Details of statistical	(1) No
0	methods and analysis (statistical	(1) No (2) Unclear/not complete
	methods used to compare groups)	(3) Adequate/clear
9	Results: explanation for any	(1) No
-	excluded data, results of each	(2) Unclear/not complete
	analysis with a measure of precision	(3) Adequate/clear
	as standard deviation or standard	
	error or confidence interval	
10	Discussion: interpretation/scientific	(0) Clearly inadequate
	implication, limitations, and	(1) Possibly accurate
	generalizability/translation	(2) Clearly accurate

11	Statement of potential conflicts and	(0) No
	funding disclosure	(1) Yes
12	Publication in a peer-review journal	(0) No
	•	(1) Yes

Appendix D

Chapter 4

In this study, and for the diseased tissue samples, there were non-significant upregulate expression of KRT16, KRT14, KRT12, KRT24, and KRTDAP, beside down-regulation of KRT1, KRT5, KRT76, and KRT6A genes compared with healthy gingival tissue samples. The results also revealed upregulated expression of SPRR2B, Collagen type XI alpha 1 chain (COL11A1), MMP2 and MMP9 genes in diseased compared with healthy tissue samples. In addition, there was upregulated expression of, the inflammatory gene, C-X-C motif chemokine ligand 8(CXCL8) gene in the diseased tissues compared with healthy tissue samples. Moreover, the results showed an upregulated expression of the P53 apoptosis effector related to PMP22 (PERP), and the GATA4 genes- which have implications for apoptosis- between the diseased compared with healthy tissue samples. On the other hand, there were downregulationin the diseased tissues compared with healthy tissue samples with the HLA-DRA (Major Histocompatibility Complex, Class II, DR Alpha), RUNX1 partner transcriptional co-repressor 1(RUNX1T1), ADAM metallopeptidase with thrombospondin type 1 motif 20(ADAMTS20), Tenascin N gene (TNN), and Homeobox B9 (HOXB9) genes.

Appendix E

Chapter 5. Table.5.1. Outcome of hydrogels sample investigations.

	(FTIR) Region Band in cm- ¹ Amide /Saccharide		DSC, Melt Peak Temperature (°C) Mean±SD	Viscosity(Pas) Mean±SD		
	I	II		37 °C	20 °C	4 °C
GelH	1633±0.2	1519±0.3	131.18±0.7	0.015±0.001	10.7±43.7	1123.5±4746 .9
GelL	1636±1.4	1548±0.9	146.51±12.5	0.004±0.001	1.7±7.4	0.7±0.7
SAH	1602±0.13	1411±0.01	137.1±1.5	0.12±0.01	0.17±0.02	0.25±0.04
SAL	1600±0.4	1410±2.1	144.45±23.95	0.05±0.003	0.03±0.003	0.13±0.02
GelMAcH	1627±2.4	1523±0.5	156±1.9	0.1±0.001	1.1±1.7	0.6±2.4
GelMAcL	1629±2.01	1520±0.3	124.7±0.18	0.004±0.001	0.005±0.001	0.22±0.2
GelMA-UCLH	1632±0.41	1521±3.1	143.6±8.002	0.02±0.7	1.3±5.9	0.03±0.0001
GelMA-UCLL	1634±0.24	1530±0.02	151.8±8.4	0.002±4.1	0.004±0.001	0.02±0.002

Shear stress(Pas) Mean±SD

Flow point (Pa) Mean±SD

	37 °C	20 °C	4 °C	37 °C	20 °C	4 °C
GelH	11.48±6.6	1486.38.0 4±3.4	11726.04± 13.2	6.6±2.1	354.5±4.7	2887.7±2.4
GelL	3.6±2.7	15.3±8.4	349.4±18.1	2.14±0. 3	7.52±8.01	126.5±10.2
SAH	90.3±45.4	128.9±63. 1	178.6±82.7	6.1±5.8	7.1±81.3	7.52±15.6
SAL	41.2±21.8	27.3±13.8	95.4±46.8	3.2±0.6	3.4±8.3	5.4±7.3
GelMAcH	7.7±4.6	450.1±17. 7	51.2±18.8	7.9±5.1	117.94±2.3	904.4±2.06
GelMAcL	3.21±2.4	4.04±2.9	108.9±17.3	5.45±1 2.8	5.3±15.6	17.17±21.2
GelMA- UCLH	8.9±1.8	4.04±2.9	0.21±0.14	1.3±11. 9	3.6±7.12	127.6±11.8
GelMA- UCLL	1.9±1.4	3.2±2.3	1.5±9.2	3.2±5.1 2	2.7±13.8	29.5±14.1

Amplitude sweeps G', G" (Pa) Mean±SD

frequency sweeps G',G" (Pa)

	37 °C	20 °C	4 °C	37 °C	20 °C	4 °C
GelH	3.15±4.7,	369.7±279.6,	3738.5±33.4,	496.5±13.4,	1466.1±13.8,	8929.5±15.6,
	1.5±2.1	68.7±10.6	596.5±10.9	234.1±18.7	187.97±11	425.8±14.5
GelL	2.8±4.1,	6.4±5.4,	151.4±122.1,	377.6±12.3,	443.06±18.4,	852.41±16.5,
GeiL						
	1.9±2.	2.9±1.8	32.2±19.4	98.7±14.9	179.7±16	340.4±16.8
SAH	2.5±3.6,	2.4±3.4,	2.5±3.6,	449.2±15.2,	598.19,	686.29±26.9,
	2.1±1.9	2.6±2.2	3.2±2.3	221.9±14.2	280.8±39.1	366.28±18.2
SAL	2.8±4.03,	2.9±4.1,	2.5±3.5,	472.4±10.8,	560.6±28.7,	275.9±14.9,
	2.2±2.6	2.3±2.8	2.7±2.6	206.9±15.9	261.3±10.0	67.9±14.2

GelMAcH	2.3±3.1,	184.7±141.8, 26.9±3.30	1826.6±15.2,	476.5±12.5,	1095.5±12.6,	7700.1±10.8,
	2.1±2.5		209.5±19.9	251.6±16.3	407.3±17.2	744.3±14.9
GelMAcL	3.1±4.4,	2.8±4.01,	20.3±17.5	2820.04±19.2	2818.9±12.7	275.96±16.9
	2.1±2.8	2.1±2.8	4.9±5.	36.0±15	47.7±14.4	67.9±14.2
GelMAH	3.5±4.8,	3.2±4.6,	284.6±228.9,	298.1±13.003,	280.5±13,	230.4±12.5,
	1.6±2.3	1.7±2.1	32.5±12.3	111.5±16.7	94.5±22.6	21.9±25.9
GelMAL	3.4±4.8,	2.6±3.8,	26.6±21.1,	311.25±13.2,	496.5±15.3,	227.9±10.4,
	1.7±2.3	1.8±2.4	6.5±7.6	122.7±14.7	246.8±17.1	38±16.7

Appendix F

Chapter 6 . Supplementary Figures and table

- 1-Figure 6.16
- 2-Figure 6.22
- 3-Figure 6.23
- 4-Figure 6.24
- 5-Figure 6.25
- 6-Table 6.2

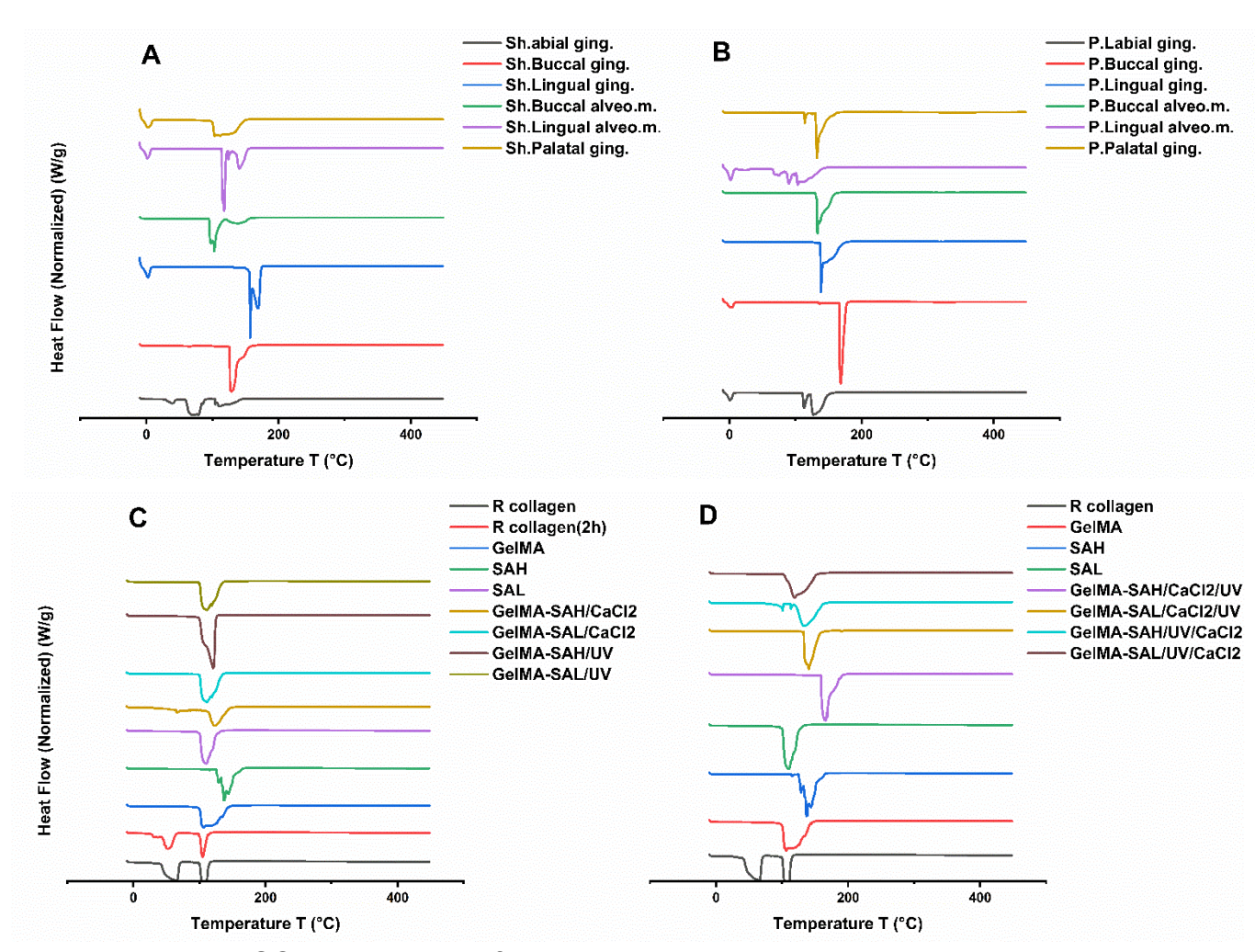


Figure 6.16. DSC thermograms for samples which were examined under a continuous flowrate of nitrogen gas with the following conditions: equilibrate (-10 °C), isothermal (1 min), and ramp (10 °C/min to 450 °C/min). (A), sheep

labial, buccal, and lingual gingival tissue samples(Sh.Labial ging., Sh.Buccal ging., Sh.Lingual ging.), sheep buccal, and lingual oral alveolar mucosal tissue samples(Sh.Buccal alveo.m., and Sh.Lingual alveo.m.), and sheep palatal gingival tissue sample (Sh.Palatal ging.). Porcine labial, buccal, and lingual gingival tissue samples(P.Labial ging., P.Buccal ging., and Lingual ging.), porcine buccal, and lingual oral alveolar mucosal tissue samples(P.Buccal alveo.m., and P.Lingual alveo.m.), and porcine palatal gingival tissue sample (P.Palatal ging.). (B), hydrogel samples are R collagen, R collagen(2h), GelMA, SAH, SAL, GelMA-SAH/CaCl₂, GelMA-SAL/CaCl₂, GelMA-SAH/UV, and GelMA-SAL/UV. (C), hydrogel samples are R collagen, GelMA, SAH, SAL, GelMA-SAH/CaCl₂/UV, GelMA-SAL/CaCl₂/UV, GelMA-SAH/UV/CaCl₂, and GelMA-SAL/UV/CaCl₂.

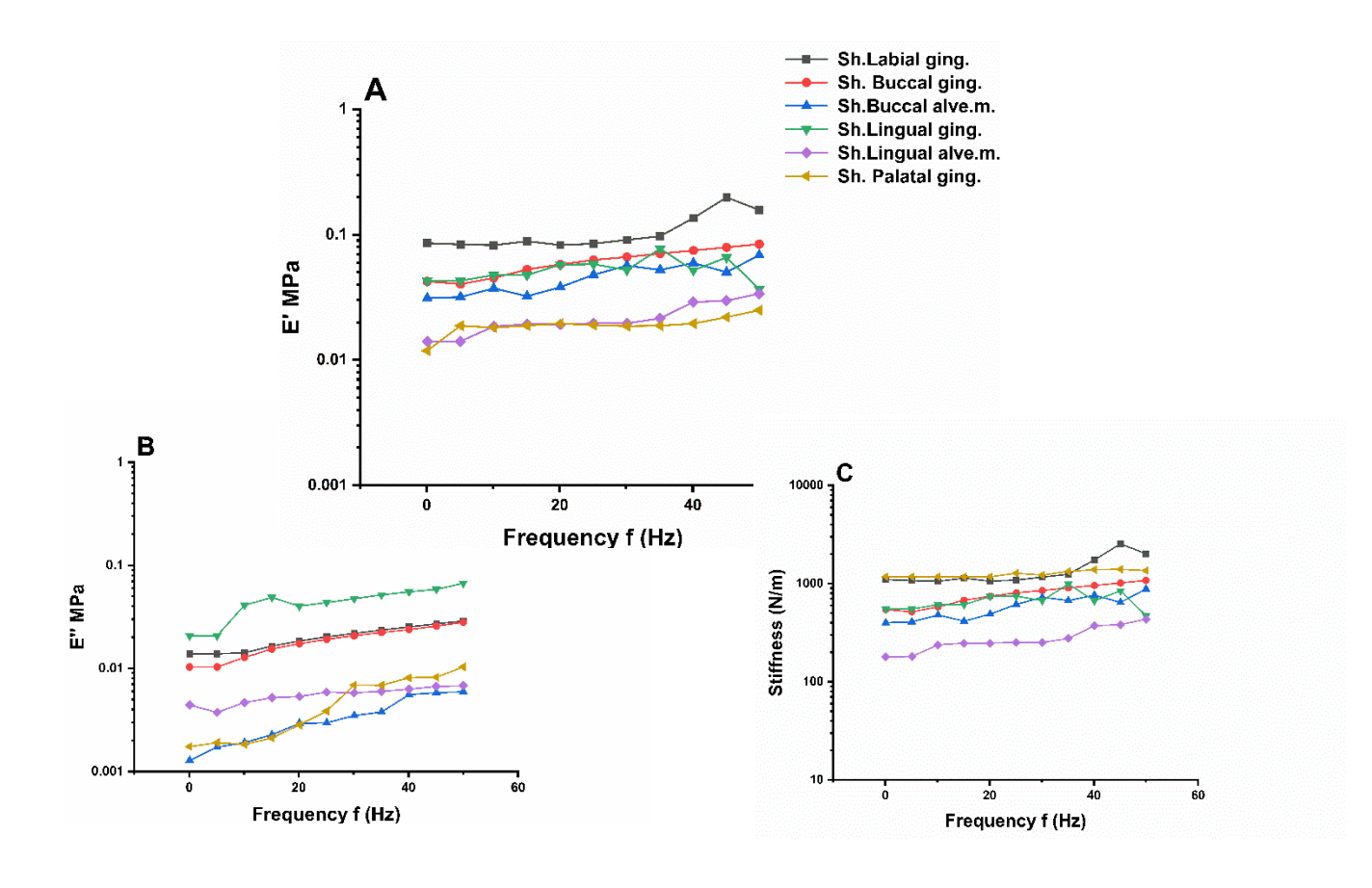


Figure 6.23. Elastic modulus E'(A), loss modulus E"(B), and stiffness (C), as a function of frequency oscillations ranging from 0.1 to 50 Hz at 5 Hz intervals for each sample. Samples were pre-loaded with a force of 0.001 N and dynamically tested at low deformation (0.25% strain), taken at the temperature of 37 °C. Samples are sheep oral mucosal tissue samples for labial, buccal, and lingual gingival tissue samples (Sh.Labial ging., Sh.Buccal ging., Sh.Lingual ging.), buccal, and lingual oral alveolar mucosal tissue samples (Sh.Buccal alveo.m., and Sh.Lingual alveo.m.), and palatal gingival tissue sample (Sh.Palatal ging.).

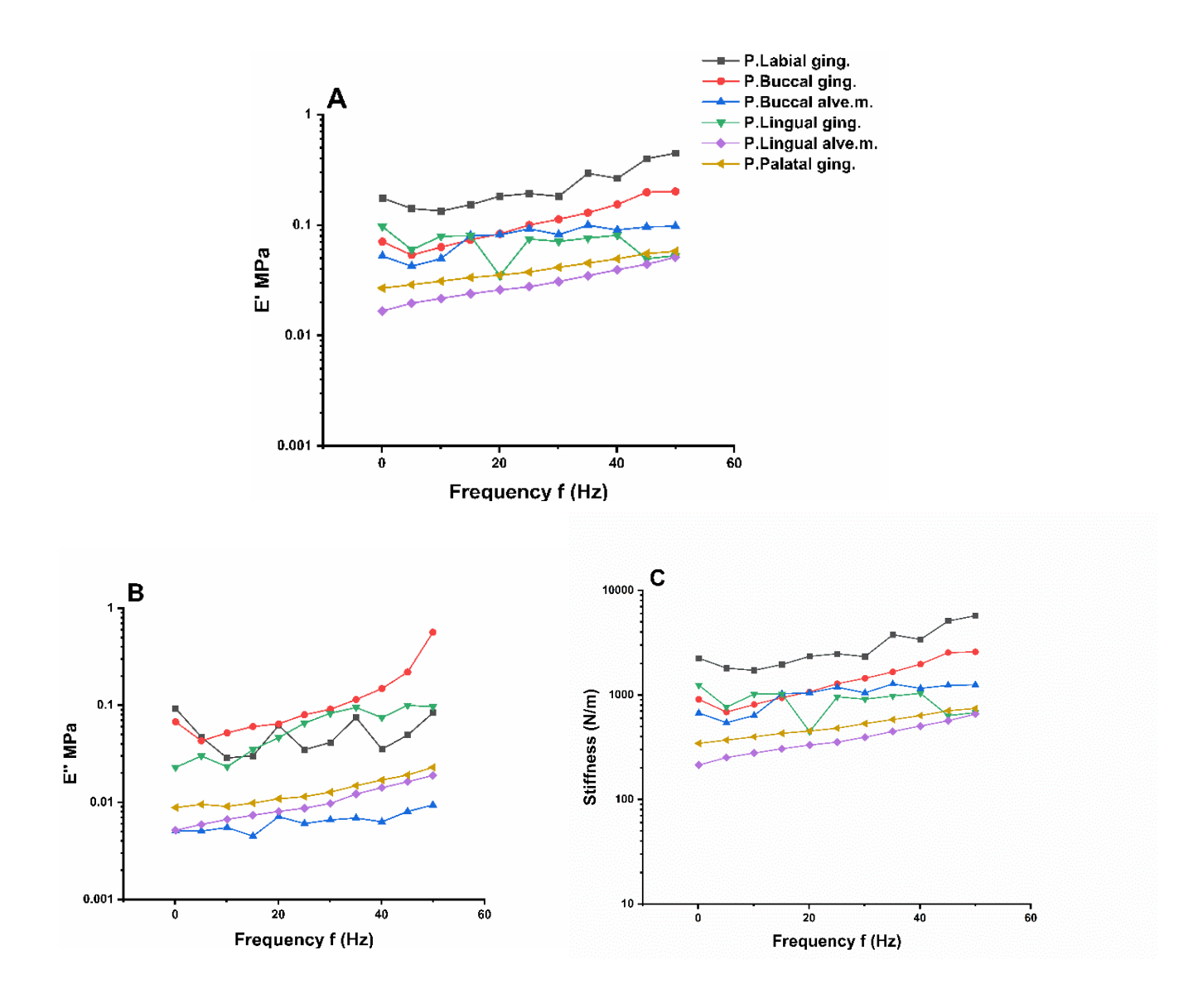
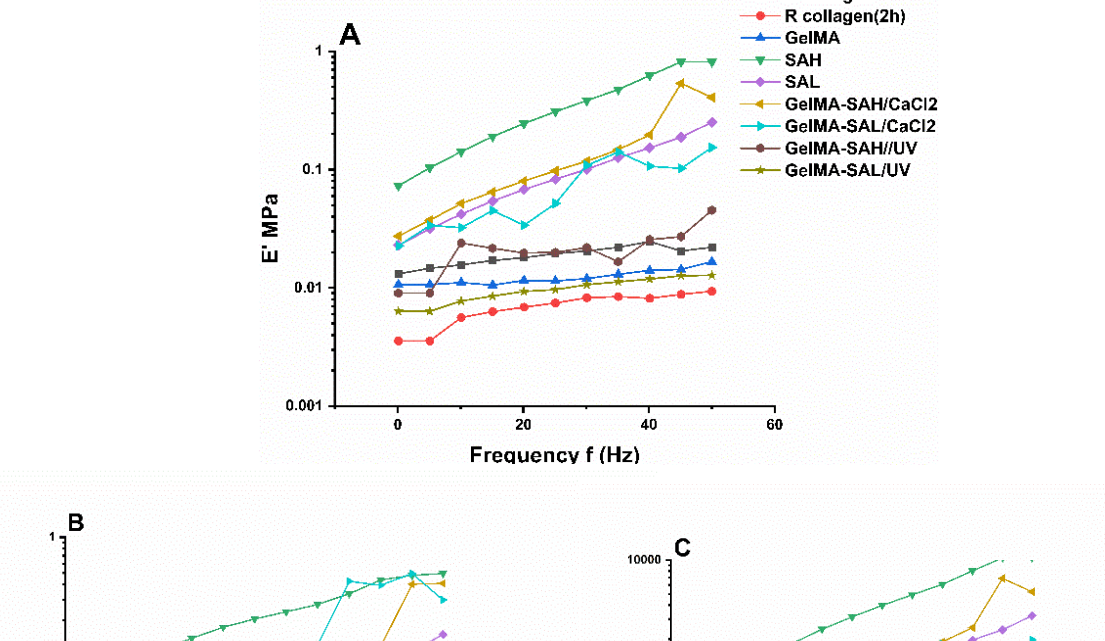


Figure 6.24. Elastic modulus E'(A), loss modulus E"(B), and stiffness (C), as a function of frequency oscillations ranging from 0.1 to 50 Hz at 5 Hz intervals for each sample. Samples were pre-loaded with a force of 0.001 N and dynamically tested at low deformation (0.25% strain), taken at the temperature of 37 °C. Samples are porcine oral mucosal tissue samples for labial, buccal, and lingual gingival tissue samples (P.Labial ging., P.Buccal ging., P.Lingual ging.), buccal, and lingual oral alveolar mucosal tissue samples (P.Buccal alveo.m., and P.Lingual alveo.m.), and palatal gingival tissue sample (P.Palatal ging.).



R collagen

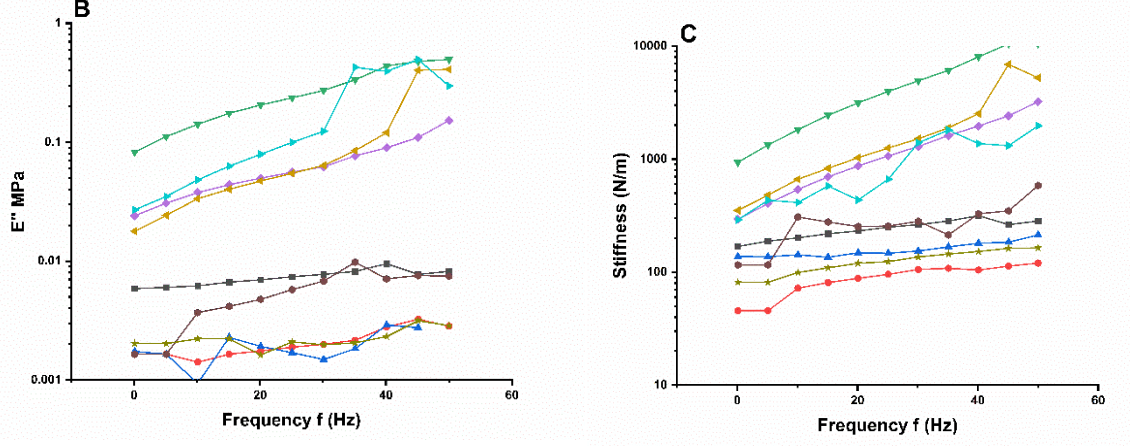


Figure 6.25. Elastic modulus E'(A), loss modulus E"(B), stiffness (C), as a function of frequency oscillations ranging from 0.1 to 50 Hz at 5 Hz intervals for each sample. Samples were pre-loaded with a force of 0.001 N and dynamically tested at low deformation (0.25% strain), taken at the temperature of 37 °C. Hydrogel samples are R collagen, R collagen(2h), GelMA, SAH, SAL, GelMA-SAH/CaCl₂, GelMA-SAL/CaCl₂, GelMA-SAH/UV, and GelMA-SAL/UV.

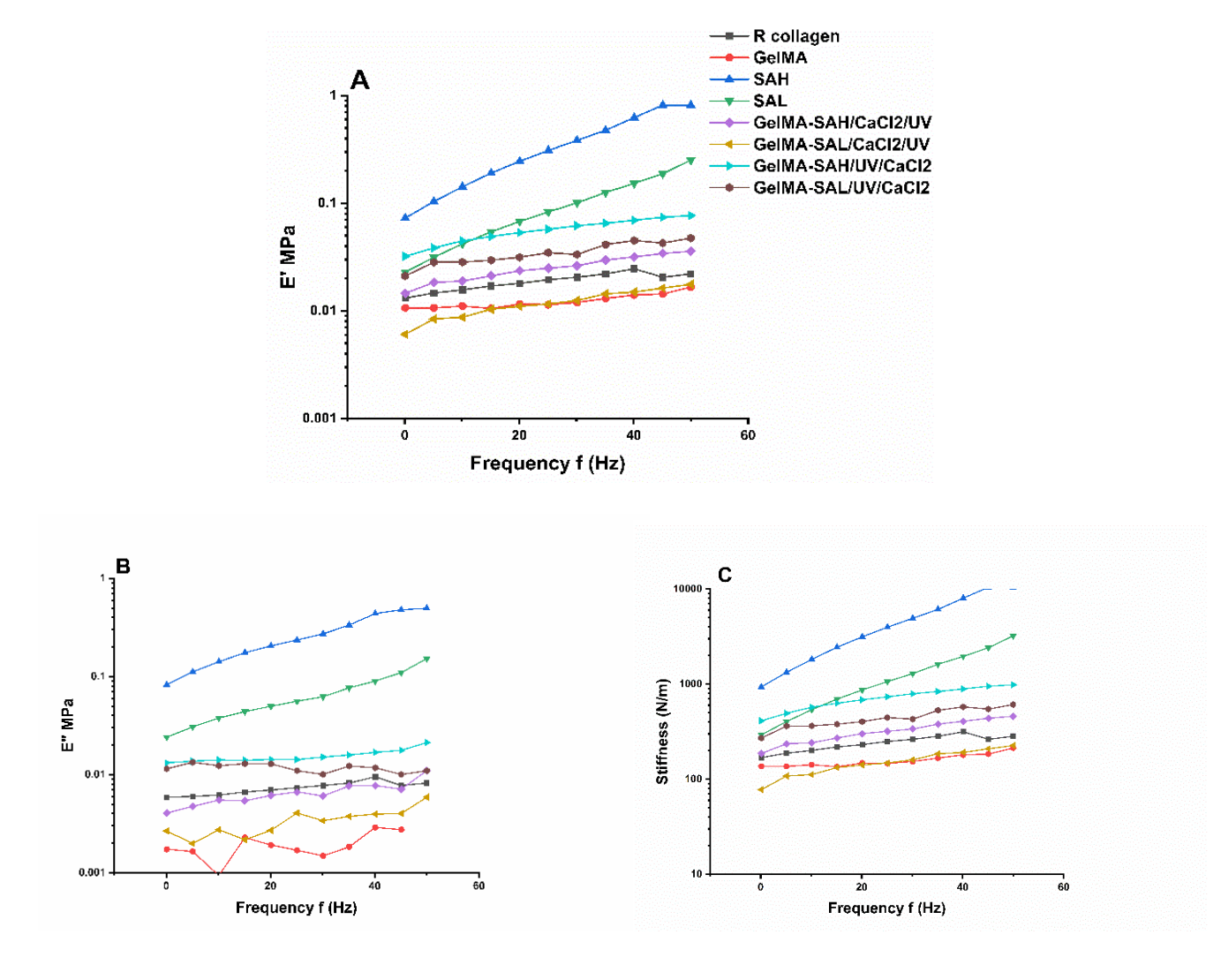


Figure 6.26. Elastic modulus E'(A), loss modulus E"(B), stiffness (C), as a function of frequency oscillations ranging from 0.1 to 50 Hz at 5 Hz intervals for each sample. Samples were pre-loaded with a force of 0.001 N and dynamically tested at low deformation (0.25% strain), taken at the temperature of 37 °C. Hydrogel samples are R collagen, GelMA, SAH, SAL, GelMA-SAH/CaCl₂/UV, GelMA-SAL/CaCl₂/UV, GelMA-SAH/UV/CaCl₂, and GelMA-SAL/UV/CaCl₂.

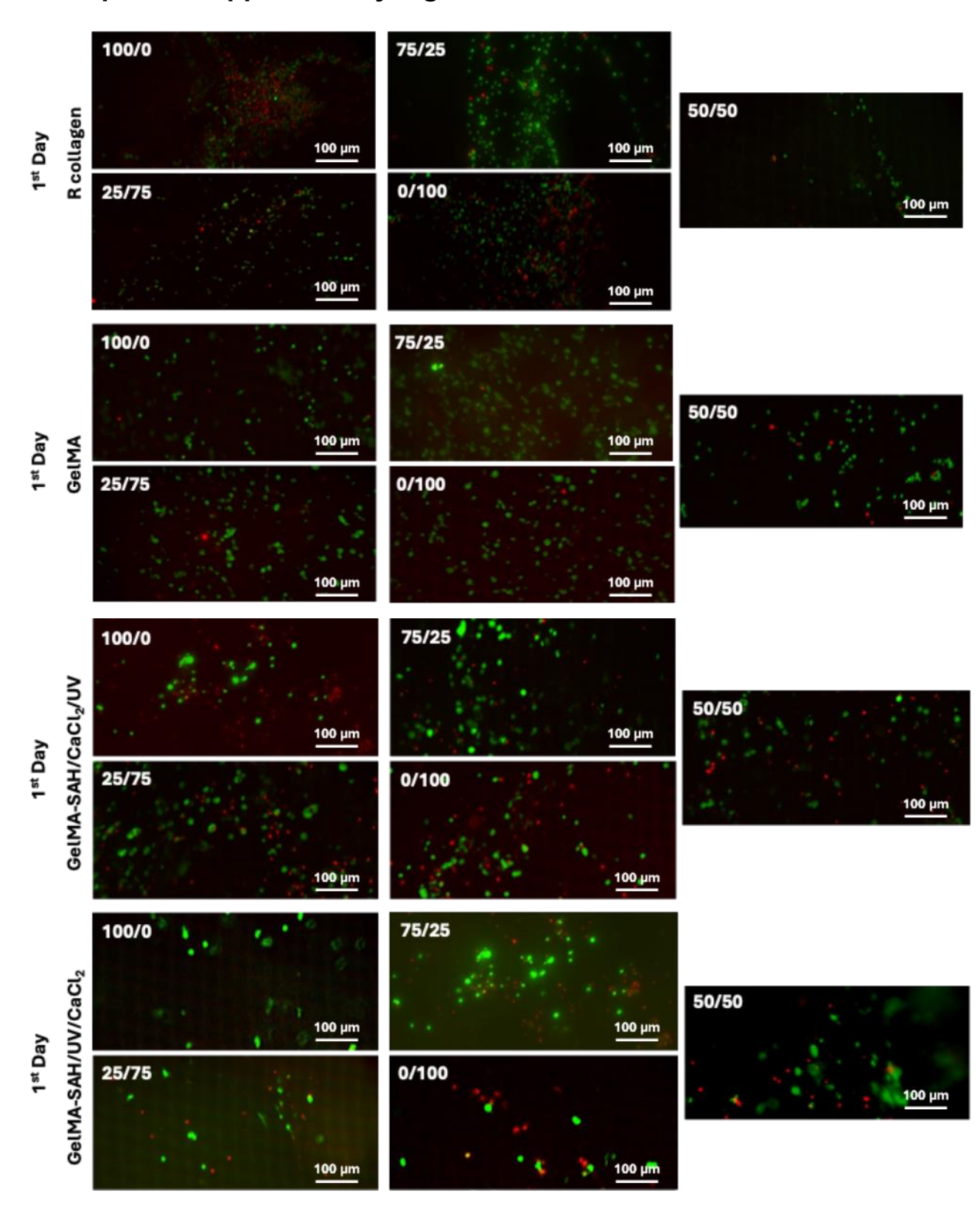
Table 6.2 presents the elastic modulus (E'), loss modulus (E"), stiffness, and the corresponding Young's modulus (E) as functions of oscillation frequency ranging from 0.1 to 50 Hz at 5 Hz intervals for each sample. Samples were pre-loaded with a force of 0.001 N and dynamically tested at low deformation (0.25% strain), taken at the temperature of 37 °C. Samples are animal sheep and porcine, and different hydrogel samples.

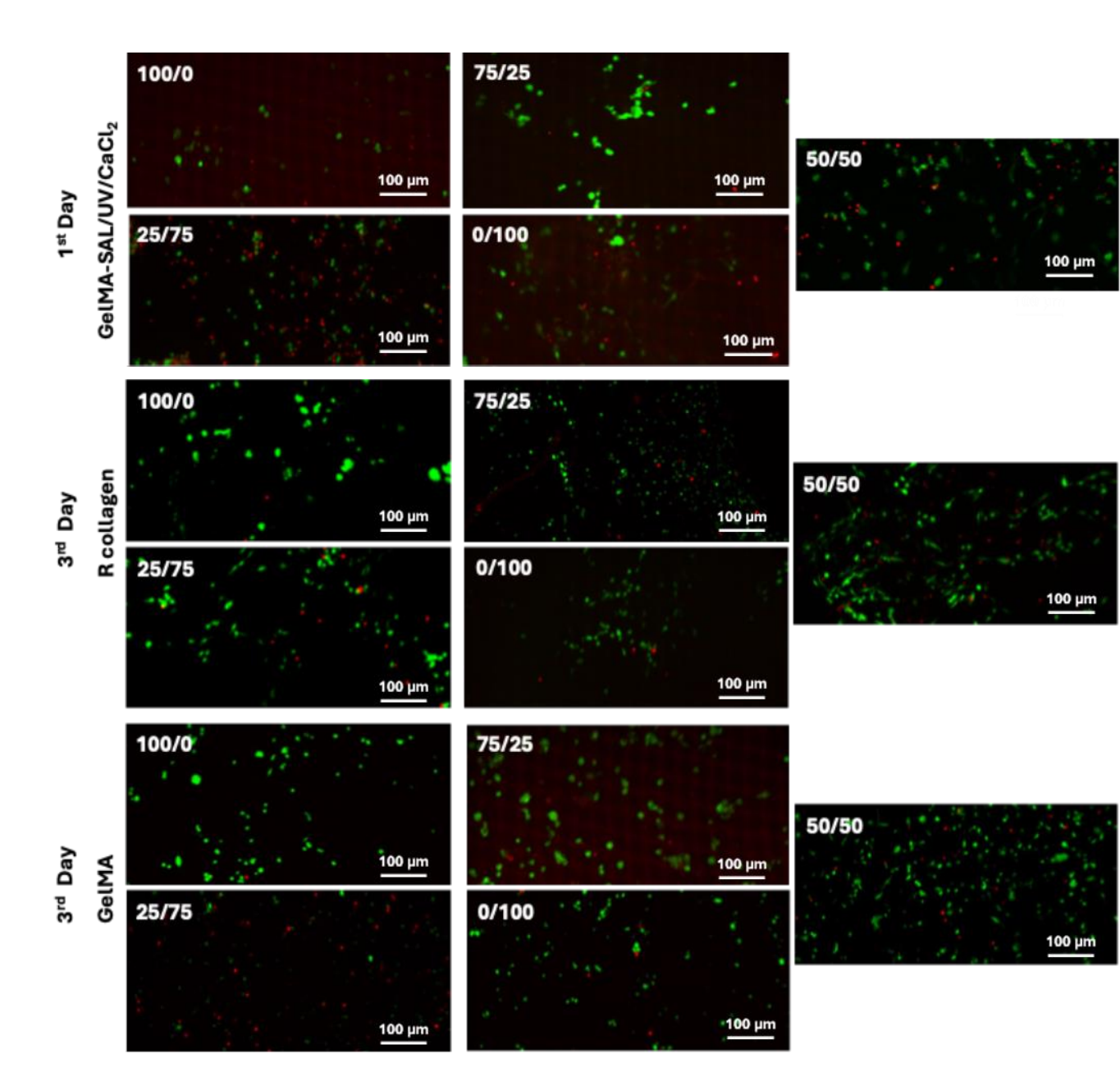
	MPa	MPa	N/m	MPa
Sh.labial	0.12 ± 0.0363	0.02 ± 0.005	1369 ± 660	0.2132 ± 0.07
Sh.buccal attach	0.06±0.02	0.02±0.006	788.1±146.6	0.16±0.03
Sh.lingual attach	0.053±0.012	0.045±0.01	676.84±145.27	0.16±0.03
Sh.buccal alveolar	0.046±0.013	0.003±0.002	589.53±128.21	0.12±0.03
Sh.lingual alveolar	0.022±0.006	0.006±0.001	278.27±34.81	0.05±0.01
Sh.palatal	0.019±0.003	0.005±0.003	244.84±31.94	0.05±0.01
P.labial	0.23±0.11	0.05±0.02	2986.08±639.46	0.54±0.15
P.buccal attach	0.11±0.05	0.14±0.15	1443.94±334.16	0.26±0.08
P.lingual attach	0.069±0.018	0.061±0.030	880.50±232.04	0.21±0.05
P.buccal alveolar	0.078±0.021	0.006±0.001	1006.495±273.487	0.217±0.064
P.lingual alveolar	0.010±0.002	0.002±0.0004	391.160±76.484	0.075±0.018
P.palatal	0.040±0.011	0.013±0.005	515.165±80.527	0.105±0.019
R collagen(2h)	0.007±0.002	0.002±0.001	89.005±24.483	0.019±0.006
R collagen	0.019±0.004	0.007± 0.001	242.235±39.002	0.053±0.009
GelMA	0.012±0.002	0.002±0.001	158.538±10.778	0.034±0.003
SAH	0.380±0.271	0.270±0.148	4873.365±1813.624	0.721±0.424
SAL	0.102±0.072	0.067± 0.038	1306.538±456.395	0.198±0.107
GelMA- SAH/CaCl₂	0.160±0.164	0.118±0.145	2058.385±528.888	0.234±0.124
GelMA- SAL/CaCl₂	0.076±0.048	0.190±0.177	970.270±547.378	0.176±0.128

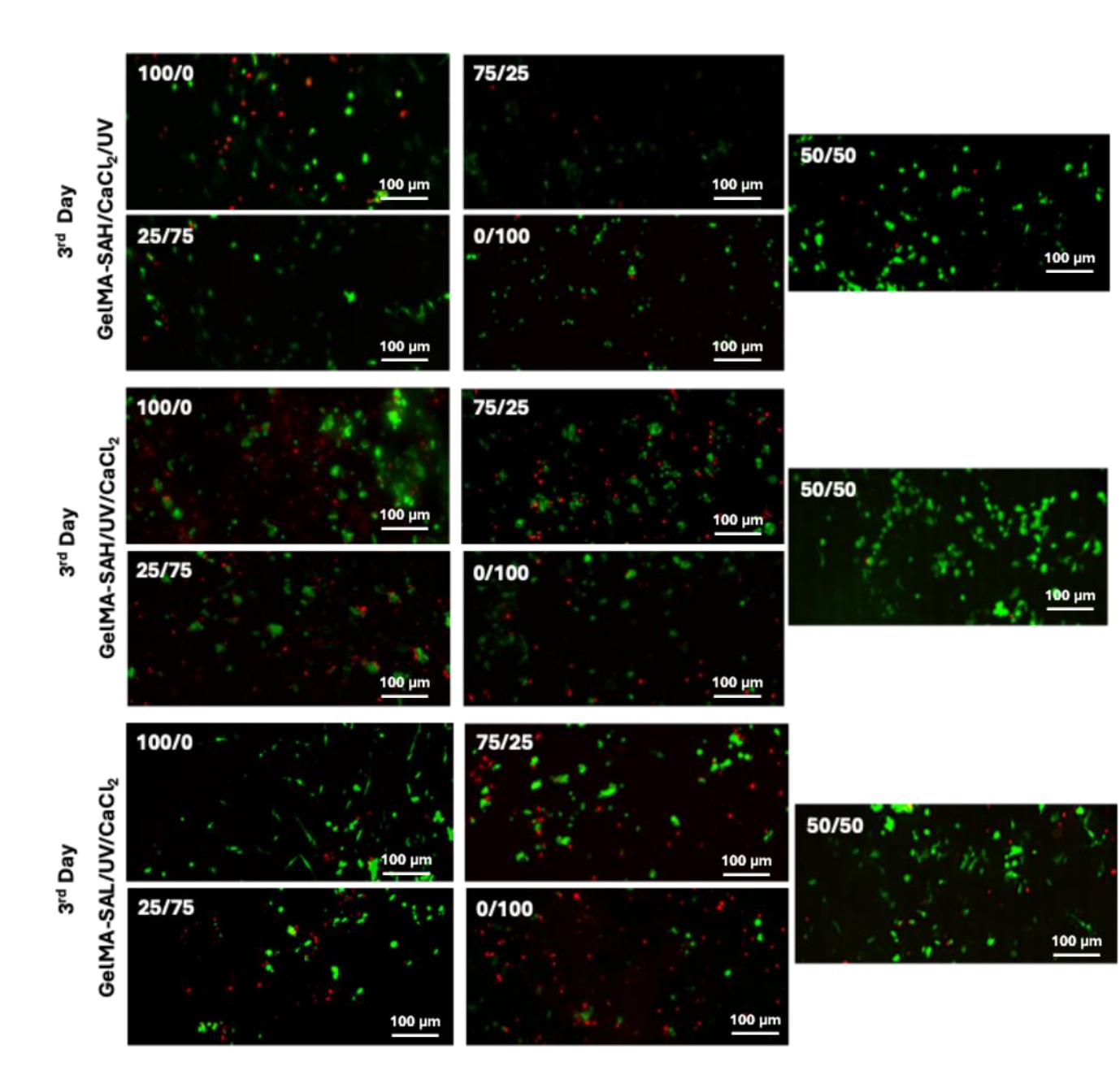
GelMA-SAH/UV	0.022±0.010	0.005±0.003	279.848±74.012	0.053±0.017
GelMA-SAL/UV	0.010±0.002	0.002±0.0004	124.845±23.606	0.026±0.006
GelMA- SAH/CaCl ₂ /UV	0.025±0.007	0.007±0.002	325.337±62.385	0.066±0.015
GelMA- SAL/CaCl₂/UV	0.012±0.004	0.003±0.001	153.872±33.489	0.031±0.008
GelMA- SAH/UV/CaCl ₂	0.057±0.015	0.015±0.002	725.66±146.83	0.15±0.03
GelMA- SAL/UV/CaCl₂	0.035±0.008	0.012±0.001	447.078±75.279	0.093±0.018
E.GeIMA- SAH/CaCl ₂ /UV	0.085±0.008	0.062±0.001	855.443±105.854	0.255±0.025
E.GelMA- SAL/CaCl₂/UV	0.107±0.015	0.065±0.002	1074.324±186.662	0.320±0.044
E.GelMA- SAH/UV/CaCl ₂	0.075±0.007	0.057±0.002	759.788±88.260	0.226±0.021
E.GelMA- SAL/UV/CaCl ₂	0.062±0.004	0.053±0.001	625.066±45.861	0.186±0.011

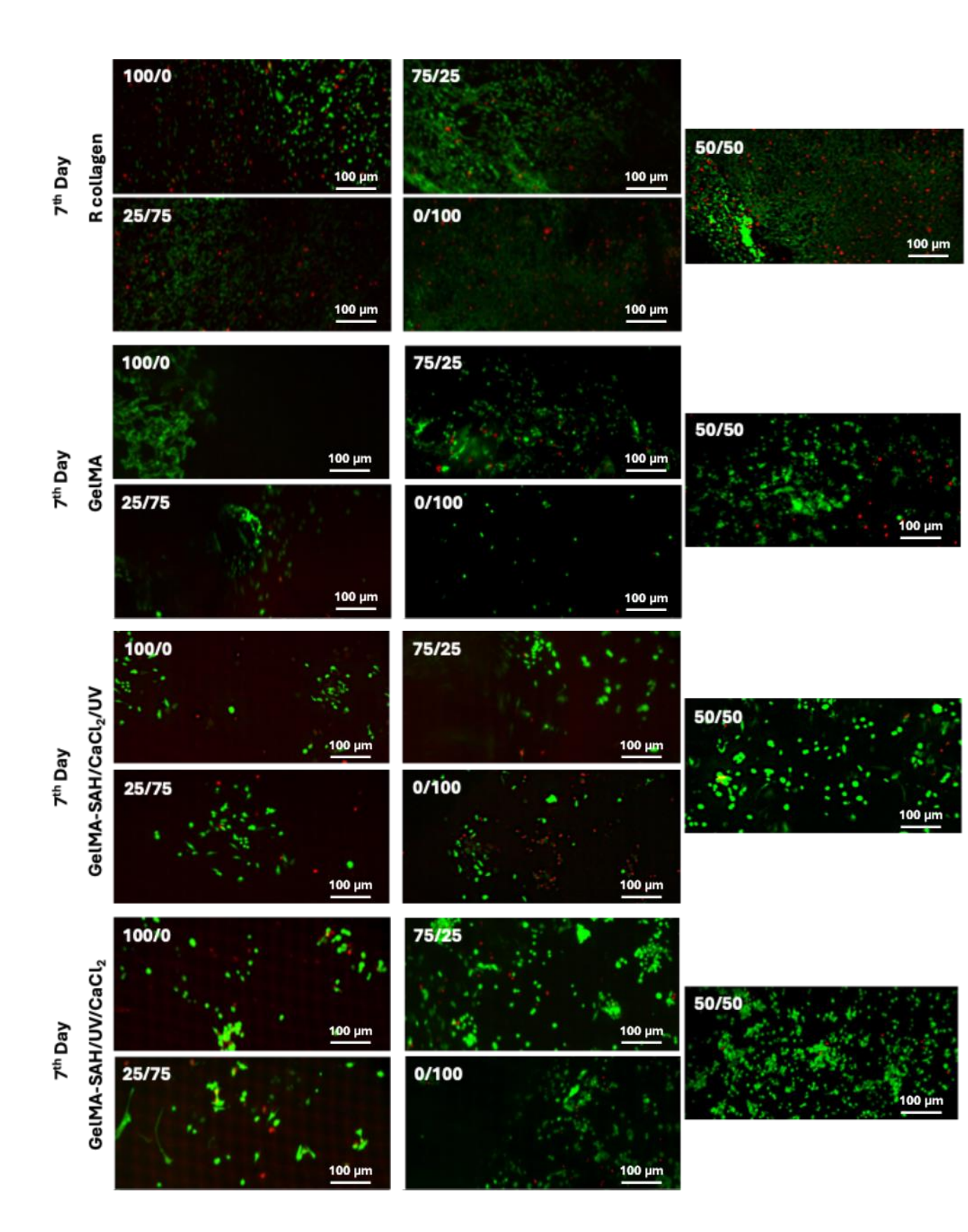
Appendix G

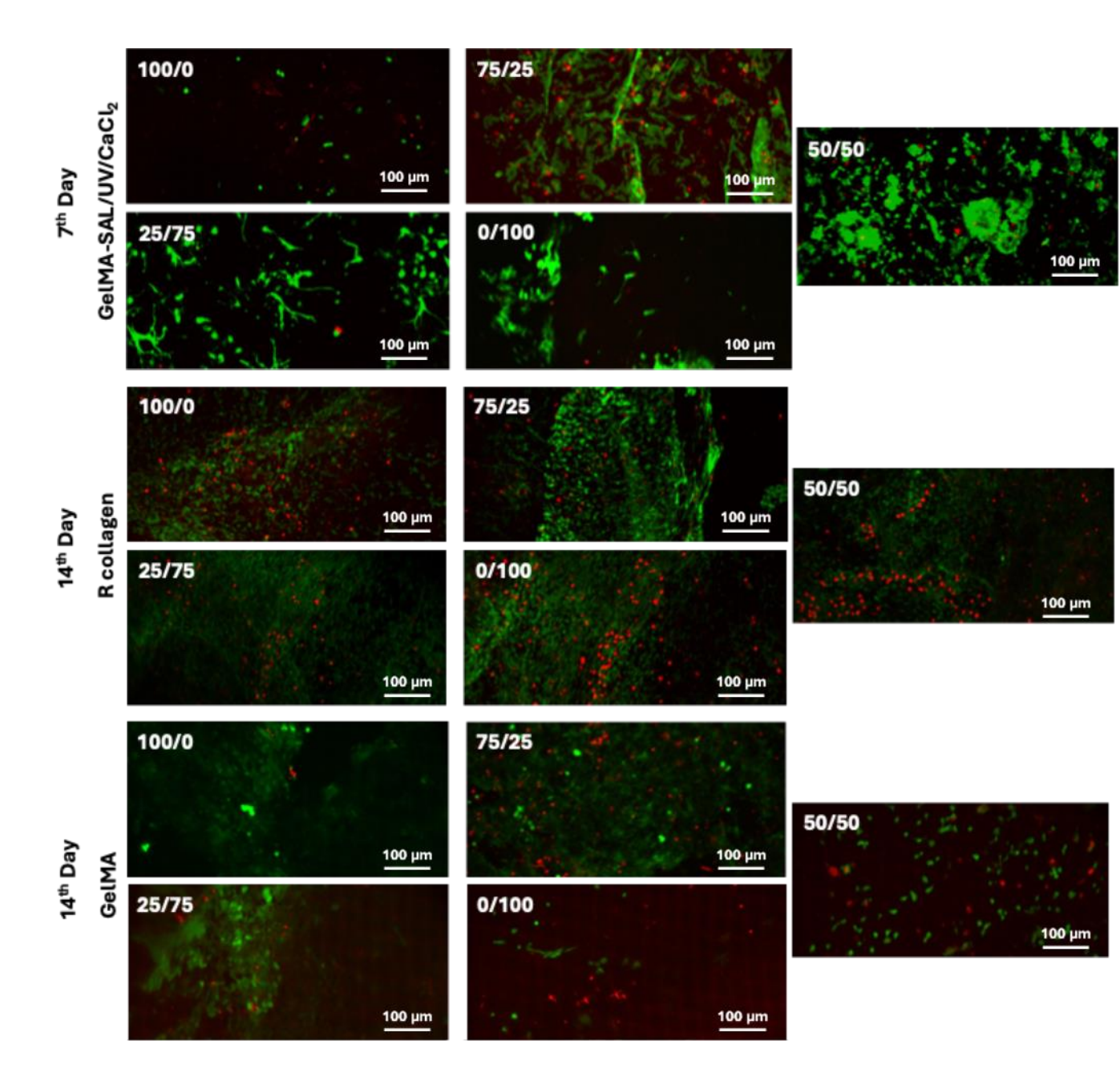
Chapter 7. Supplementary Figure 7.23.











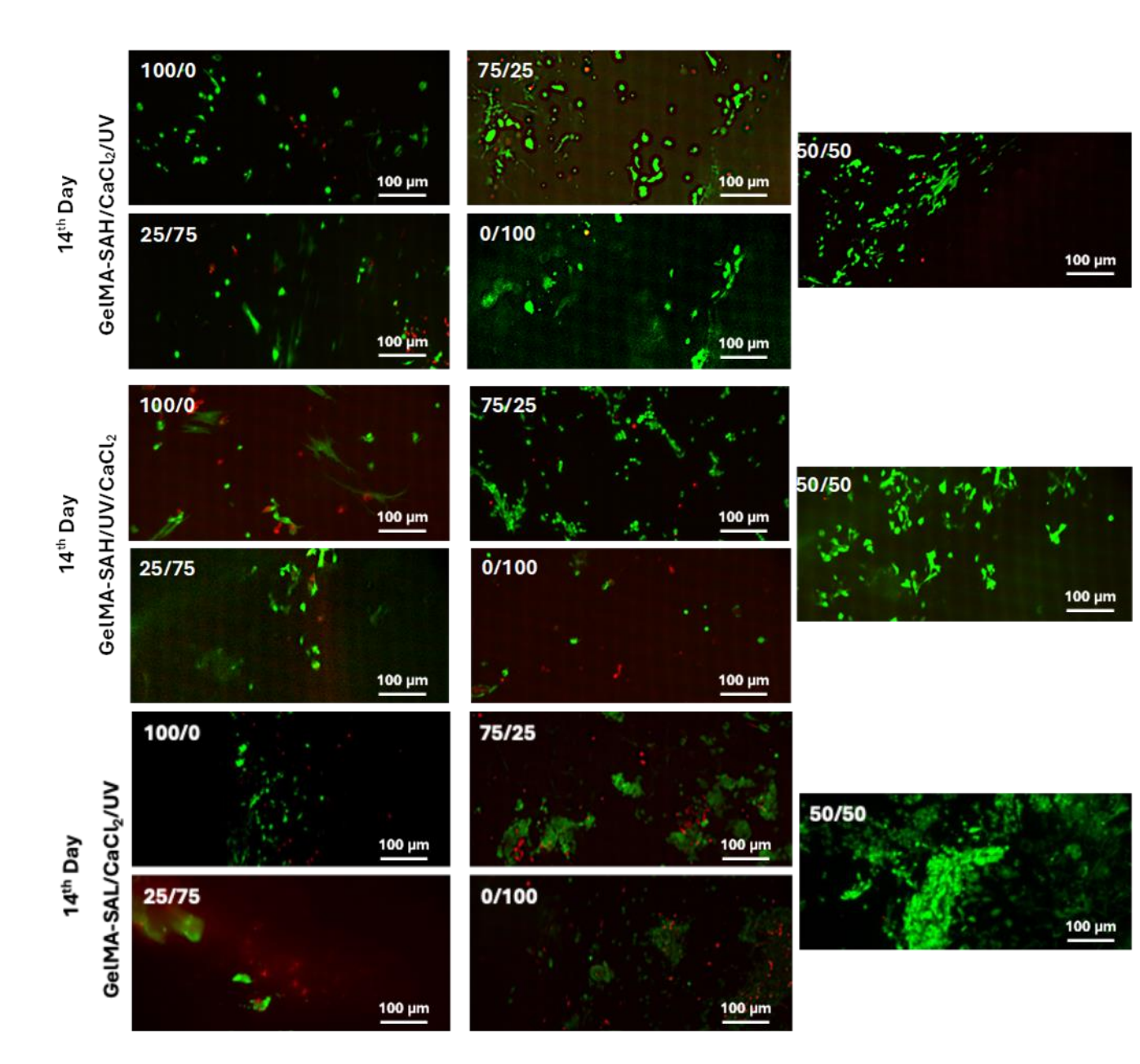


Figure 7.23. Live/dead confocal images of engineered 3DGT model constructed in well plates, using different hydrogel samples, R collagen, GelMA, GelMA-SAH/CaCl2/UV, GelMA-SAH/UV/CaCl2, and GelMA-SAL/UV/CaCl2, on days 1, 3,7 and 14 days. Hydrogel samples were submerged in a different ratios of mixture of HGFs medium and HGEs medium (100:0, 75:25, 50:50, 25:75, or 0:100). Data representing mean \pm SD(n=3). using fluorescent microscope, indicating living cells (green) and dead cells (red). Scale bar: 100 μm .